

UNIVERSITY OF OKLAHOMA

GRADUATE COLLEGE

PLEISTOCENE CORAL REEF DESTRUCTION IN THE FLORIDA KEYS:  
PALEOTEMPESTITE EVIDENCE FROM A HIGH RESOLUTION LIDAR XRF  
ANALYSIS OF WINDLEY KEY QUARRY, FL

A THESIS

SUBMITTED TO THE GRADUATE FACULTY

in partial fulfillment of the requirements for the

Degree of

MASTER OF SCIENCE

By

EMMA LYN GIDDENS

Norman, Oklahoma

2016

PLEISTOCENE CORAL REEF DESTRUCTION IN THE FLORIDA KEYS:  
PALEOTEMPESTITE EVIDENCE FROM A HIGH RESOLUTION LIDAR XRF  
ANALYSIS OF WINDLEY KEY QUARRY, FL

A THESIS APPROVED FOR THE  
CONOCOPHILLIPS SCHOOL OF GEOLOGY AND GEOPHYSICS

BY

---

Dr. John D. Pigott, Chair

---

Dr. Richard D. Elmore

---

Dr. Kulwadee L. Pigott

© Copyright by EMMA LYN GIDDENS 2016  
All Rights Reserved.

*I would like to dedicate this paper to my loving and supportive family. Thank you for all you have done for me; I would not be where I am today without each and every one of you.*

## **Acknowledgements**

I would like to greatly thank my thesis advisor Dr. John Pigott for all his support, encouragement, and knowledge he has given me during my time here at the University of Oklahoma. I would also like to appreciate my committee members, Dr. Richard Elmore and Dr. Kulwadee Pigott, for their time and help with my thesis project. I would also like to thank the ConocoPhillips School of Geology and Geophysics for providing me with ample resources and a superior education. Thank you to Tan Nyugen and the Riegl team for teaching me how to operate a LIDAR scanner and being available to answer any question no matter the time of day. Thank you to the Windley Key Quarry Florida State Park Rangers, especially manager Michael Guarino, for allowing me access to the park. I would like to acknowledge all the graduate students that assisted me, especially Brandon Swain and John Hornbuckle who traveled to Florida to help me collect data. Last but not least, I would like to thank my family for their continuous love and support.

# Table of Contents

Acknowledgements .....	iv
List of Tables .....	vii
List of Figures.....	viii
Abstract.....	xii
Chapter 1: Introduction.....	1
1.1 Statement of the Problem .....	1
1.2 Discontinuity Surfaces.....	2
1.3 Previous Work .....	6
Chapter 2: The Florida Keys .....	9
2.1 Physiography .....	9
2.2 Study Area .....	10
2.3 Geologic Setting .....	12
2.4 Key Largo Limestone .....	15
Chapter 3: Methods .....	21
3.1 LIDAR.....	21
3.1.1 LIDAR Theory .....	21
3.1.2 LIDAR Collection Mechanics.....	26
3.1.3 LIDAR Processing.....	29
3.2 XRF .....	38
3.2.1 XRF Collection.....	38
3.2.2. XRF Processing.....	39
Chapter 4: Observations/Interpretation .....	41

4.1 Combining LIDAR and XRF Data.....	41
4.2 Diagenesis.....	62
4.3 Evidence for Tempestite.....	64
4.4 Evidence of a Sea Level Fall .....	72
Chapter 5: Conclusion .....	76
5.1 Conclusions .....	76
5.2 Recommendations for Future Work .....	77
References .....	79
Appendix A: Windley Key Quarry Data Collection Permit.....	83
Appendix B: LIDAR Data Collection Controls .....	84
Appendix C: XRF Raw Scan Results .....	90
Appendix D: Windley Key Quarry XRF Station Photo's with Coral and Discontinuity Surface Identification .....	99
Appendix E: XRF Mineralogy Results.....	180
Appendix F: Solid Mineral Sample XRF Standards in Parts Per Million (ppm) .....	189

## **List of Tables**

Table 1: List of corals found in the Key Largo Limestone Formation inside Windley Key quarry. (Alive photos copied from google images) .....	19
Table 2: Table 1 cont. ....	20



## List of Figures

Figure 1: Upside down <i>M. annularis</i> .....	2
Figure 2: Bivalves and mollusks in coral rubble .....	2
Figure 3: More than one episode of <i>M. annularis</i> ' are growing on top of each other .....	3
Figure 4: Examples of different discontinuity surfaces marked by red arrows.....	5
Figure 5: The sketch below was made by Frujitier et al., 2000 to highlight the erosional surface and mark core locations. ....	8
Figure 6: The lower keys are perpendicular to the continental shelf, where the upper keys are parallel to the shelf edge.....	9
Figure 7: The photo on the right is of the Florida Keys and Islamorada is highlighted by the red box. ....	10
Figure 8: Windley Key Quarry .....	11
Figure 9: Red dust from Africa .....	12
Figure 10: Pleistocene global sea level curve with isotope stages 2-7.....	13
Figure 11: Stratigraphic column of Southern Florida.....	15
Figure 12: The Key Largo Limestone .....	17
Figure 13: <i>M. annularis</i> thrives off the shelf about 10m deep. ....	18
Figure 14: LIDAR mounted on a tripod in the field.....	21
Figure 15: LIDAR emits multiple light pulses and each pulse returns once it encounters an object.....	22
Figure 16: Target reflectance (%) vs maximum measurement range (m) of the two different scan settings .....	23

Figure 17: NASA JPL library spectroscopy solid sample data showing median (solid line) and quartiles (dashed lines) for shale and sandstone .....	25
Figure 18: Reigl VZ-400 with Nikon D800 camera mounted on top.....	26
Figure 19: Map of Windley Key Quarry .....	28
Figure 20: 360 degree initial scan, unprocessed and is displayed in ‘true color’ .....	30
Figure 21: Available attributes to view each scan.....	31
Figure 22: Raw scan data on the left and filtered data on the right.....	33
Figure 23: The parameters set to filter all raw data.....	34
Figure 24: Wall 5, scan position 13-1 and displayed in True Color.....	35
Figure 25: Reflectance of walls 2-5 on top and 5-9 on bottom.....	37
Figure 26: Windley Key Quarry map with XRF scan locations .....	40
Figure 27: The close look of this <i>Diploria labyrubthiformis</i> (iPhone image on top and reflectance below) demonstrates the power of a high resolution LIDAR scan .....	42
Figure 28: Reflectance of half of wall 2 with the XRF scan results.....	44
Figure 29: This <i>Diploria clivosa</i> likely was quickly buried in order to preserve its mineral composition. ....	45
Figure 30: Reflectance of the other half of wall 2 with XRF scan results .....	46
Figure 31: Reflectance of wall 3 with XRF scan results .....	47
Figure 32: It is not clear where to draw the white line indicating the discontinuity surface from the previous figure.....	48
Figure 33: Reflectance of wall 4 with XRF scan results.....	49
Figure 34: Reflectance of wall 5 with XRF scan results .....	50
Figure 35: Reflectance of wall 6 with XRF scan results .....	51

Figure 36: Reflectance of wall 7 with XRF scan results .....	52
Figure 37: Reflectance of wall 8 with XRF scan results .....	53
Figure 38: Reflectance of wall 9 with XRF scan results.....	54
Figure 39: <i>Diploria labyrinthiformis</i> surrounded by a high and low Mg calcite coating	55
Figure 40: Reflectance of half of wall 10 with XRF scan results .....	56
Figure 41: On top is a photo and the bottom is a LIDAR reflectance image .....	57
Figure 42: The photo on the left was taken with an iPhone and the image on the right is LIDAR reflectance .....	58
Figure 43: Reflectance of the other half of wall 10 with XRF scan results .....	59
Figure 44: Reflectance of wall 11 with XRF scan results .....	60
Figure 45: iPhoto image on the left and LIDAR reflectance on the right .....	61
Figure 46: Cartoon demonstrating the interaction of the meteoric vadose and phreatic zones with the marine zones.....	63
Figure 47: Stress-strain plots for <i>M. annularis</i> .....	65
Figure 48: This depression marks the location a coral colony used to thrive, but was dislodged during Hurricane Rita in 2005 .....	67
Figure 49: Sediment-scoured corals atop a large sand flat at the East Flower Garden Banks .....	67
Figure 50: <i>Diploria strigosa</i> gouged by waterbourne projectiles during Hurricane Rita	68
Figure 51: Fenestrae beds in an eolian dune in northern Bahamas .....	69
Figure 52: Fenestrae beds with a scoured base. ....	70
Figure 53: Global temperature curve during the last interglacial based on oxygen isotopes from a Greenland ice core .....	71

Figure 54: Diagram showing the U/Th ages of corals in relation to an erosional surface hypothesized to have formed during the mid-Sangamon from either a sea level lowstand or a massive storm .....	73
Figure 55: Truncated <i>M. annularis</i> and a lithophagid boring (red arrow) from the Bahamas .....	74
Figure 56: Sediment filled cave in the Bahamas. ....	75

## Abstract

Not all unconformities are alike, and for carbonates, their discrimination can be difficult. In this regard, one particular discontinuity surface, among many, which is exposed as a laterally persistent surface in the Pleistocene Key Largo Limestone of the classic Florida Windley Key Quarry outcrop is problematic. Attempts to date the surface have been inconclusive.  $U_{234}$ - $Th_{230}$  dating by previous researchers reveals older ages (130 ka) above the surface and younger (126 ka) below. Is this discontinuity surface allocyclic (eustatic sea level fall), autocyclic (biologic, climatic, or storm changes) or diagenetic (phreatic-vadose fluctuations)? In order to address this problem, a novel approach incorporating high resolution Light Detection and Ranging (LIDAR) and X-Ray Fluorescence (XRF) is employed on a cm scale. LIDAR reflectivity is correlated to XRF mineralogical constructed compositions and quantitatively mapped using color extraction, which highlights the amount of Aragonite, Calcite and Hi Mg Calcite. The precise location of the XRF scan is matched to the LIDAR high resolution reflectivity image and run through a color extraction algorithm. The colors are then correlated to the specific carbonate minerals.

Observations reveal the main reef builder to be massive colonies of *Montastraea annularis* accompanied by *Diploria labyrinthiformis*, *Diploria strigosa*, *Diploria clivosa*, *Porites astreoides*, *Porites porites*, *Montastraea cavernosa*, *Siderastrea radians* and *Siderastrea siderea*. Syndepositional porosity is common within the colonies from boring Pholads and Clionid sponges. In between the colonies are disarticulated mollusks, *Porites* sp., and abundant *Halimeda* flakes and carbonate mud. Examination of fossil coral-algal species above the discontinuity surface reveals post-mortem

dislocation and dislodgement of corals as well as occasional planar surfaces. While the corals are composed of various stages of aragonite inverting to calcite with low Mg calcite carbonate mud filled cavities, the undulating surface when cutting through corals is coated by Hi Mg calcite coralline algae. Repatriation/regrowth of *Montastraea annularis* above the surface on top of older *Montastraea annularis* is observed. The dislodgement, destruction and repatriation/regrowth of these colonies without significant differences in diagenesis above and below the discontinuity suggests a storm event of large magnitude rather than a sea level fall and subaerial exposure unconformity or groundwater fluctuations. To break a *Montastraea annularis* at depths of 10m, a maximum inferred depth for this Key Largo Pleistocene reef, takes considerable wave energy to fracture these massive corals (greater than 44 meganewtons/meters<sup>2</sup>), e.g. a hurricane or tsunami. Such an event would also allow the ripping up of older rocks and depositing them on top of and adjacent to younger rocks (e.g. the observed  $U_{234}$ - $Th_{230}$  vertical stratigraphic age inversion) and would be consistent with the observed cobble to boulder-sized allochem rubble above the discontinuity surface. These observations appear to support the hypothesis that this discontinuity surface represents the autocyclic paleotempestite signature of a Pleistocene hurricane or tsunami.

# Chapter 1: Introduction

## 1.1 Statement of the Problem

This paper will focus on identifying discontinuity surfaces inside Windley Key Quarry, FL using a detailed 3D mineralogic, XRF constrained, LIDAR reflectance map. Are the observed discontinuity surfaces within the Sangamon Key Largo Limestone a product of autocyclic or allocyclic processes? And how much time has passed,  $\sim a$  vs  $\sim ka$ , respectively?

Many have studied Windley Key Quarry to determine the physical and chemical properties, as well as the origin of the limestone. Others have noticed a few of the same discontinuity surfaces this paper will focus on. The surfaces are not linear; they are wavy and seem to, in some cases, cut across corals. Currently there is no universal agreement regarding the origin of the surface. Fruijtier, Elliot and Schlager (2000) believe the surface is a product of diagenesis. Harrison and Coniglio (1985) understand the unconformity to be evidence of a sea level fall. Until now, no one has considered the surface to be the result of a super storm. Evidence of coral rubble and broken, upside down and dislodged corals are commonly exposed in the quarry walls (Figures 1 and 2). A gradual sea level fall or diagenesis would not be capable of this coral destruction. Owing to much debate over the origin of the Key Largo Limestone and its discontinuity surfaces, previous work along with LIDAR and XRF scans of the quarry walls will be integrated to investigate the origin of the discontinuity surface.



**Figure 1: Upside down *M. annularis***



**Figure 2: Bivalves and mollusks in coral rubble**

### **1.2 Discontinuity Surfaces**

A discontinuity surface represents a break in the stratigraphic record owing to a hiatus in sedimentation and/or erosion of previously deposited material (Clari, Pierre and Martire, 1995). Discontinuity surfaces are important in carbonate diagenesis as they are able to act as either a barrier or migration pathway for fluids. Carbonate discontinuities are categorized as either an exposure, omission or erosional surfaces. Exposure surfaces are associated with subaerial exposure and alteration, usually marked by a karsted horizon and here, vadose-zone diagenesis is common (Hillgärtner, 1998). Omission surfaces are a product of a submarine sedimentary hiatus commonly evidenced by mineralization (e.g. submarine cementation) and/or biological activity (e.g. boring) during exposure on the sea floor. Erosional surfaces represent the removal of previously deposited material and show evidence of a change in hydrodynamic energy (Hillgärtner, 1998). Rip-up clasts, scours and a change in grain size or texture are common with a change in hydrodynamic energy. Two processes possibly responsible would be a tsunami or a large storm event both of which could deposit a



specific type of erosional surface: a tempestite surface. Such surfaces show evidence of an abrupt and short lived high energy event and a return to normal sedimentation. A discontinuity surface separates more than one growth episode of *M. annularis* and a



**Figure 3: More than one episode of *M. annularis*' are growing on top of each other**

jumbled mix of *M. annularis* inside the Windley Key Quarry (Figure 3). However, if the corals were only disturbed and not totally destroyed, they would commence to grow. A possible example is Figure 3. Coral species are selective to the amount of wave energy, sunlight, etc. so, a small disruption in sea level would force these corals to grow elsewhere. *M. annularis*, for example, thrives in low energy, clear, and warm marine environments; therefore, if the sea level were to change, *M. annularis* would no longer succeed in their current location on the shelf.

Windley Key Quarry contains a variety of discontinuity surfaces. Figure 4 has five pictures (A-E) showing the different discontinuities throughout Windley Key Quarry. A: There are a cluster of *M. annularis*' and two *Diploria*. There is a low Mg calcite surface surrounding and preserving *M. annularis* heads and a rubble filled karst omission surface separating two *Diploria* and surrounding all corals. B: The arrows are pointing to a rubble filled karst sediment chute that tore through a large *M. annularis* and others nearby. C and D: There is a low Mg calcite coating around the large corals and rubble cutting through them. E: High Mg calcite coating and erosional surface. This *M. annularis* has been torn apart and is laying sideways. An erosional surface, possibly from a large storm, separates the coral from rubble.



**Figure 4: Examples of different discontinuity surfaces marked by red arrows. A: Multiple growth episodes. B: Sediment chutes pointed out by red arrows. C & D: Low Mg calcite surface surrounding corals. E: High Mg calcite erosional surface.**

### 1.3 Previous Work

Much research has been devoted to the geology of the Florida Keys, the Key Largo Limestone formation, and even Windley Key Quarry. One common issue many have questioned is the type of carbonate reef the Pleistocene Key Largo Limestone developed. Was it a deep water reef, back reef, barrier reef or a cluster of patch reefs? Stanley (1966) concluded Key Largo formed as a deep water outer reef tract because of the abundance of the coral *Montastraea annularis*, which necessitates low wave energy. Hoffmeister and Multer (1968) rejected Stanley's (1966) hypothesis and instead proposed Key Largo formed in a back reef with possible structural tilting to lower the outer platform. Dodd, Hattin, and Liebe (1973) alternately concluded Key Largo is a complex of patch reefs and sand shoals that were initiated near the outer shelf edge, which migrated laterally as sea level rose. Currently, Harrison et al. (1985) conclusion regarding Key Largo's formation is the most widely accepted (Halley, Vacher, and Shinn, 1997). They surmise the Key Largo Limestone to be a complex of shallow-water shelf margin reefs (Harrison et al., 1985) as the Upper Florida Keys, which are the present geomorphic expression of these reefs, are too large and extensive to simply be patch reefs and they find no evidence of lagoons, which are associated with patch reefs.

Another perplexing issue is age. Fruijtier et al., (2000) observed the discontinuity surface inside Windley Key Quarry and conducted a mass-spectrometric  $^{234}\text{U}^{230}\text{Th}$  survey to determine the ages of a coral above and below the surface. They found the coral that was stratigraphically, only centimeters, above the surface to be older than the coral below the surface. Figure 5 shows a few of their sample locations. For example, their sample 222 from a *Siderastrea* below the surface dated 126 ka, where

Samples 224 I and II from a *Diploria* above the surface dated 130 ka. Fruijtier et al., (2000) suggested the cause of the inverse stratigraphy were the high temperatures and precipitation rates during the Sangamon in Florida which aided substantial weathering, specifically Uranium leakage, of the Key Largo Limestone. They believe the harsh environmental conditions enhanced diagenesis which altered the Uranium-Thorium data, for ages in excess of 5,000+ years. Thus the ages should be suspect. The coral above the surface probably did undergo Uranium leakage, but why did it alter more than the one below? Could instead ages be reliable, and a large storm capable of dislodging corals simply detach older corals and throw them on top of younger corals? This is the question this thesis attempts to answer.



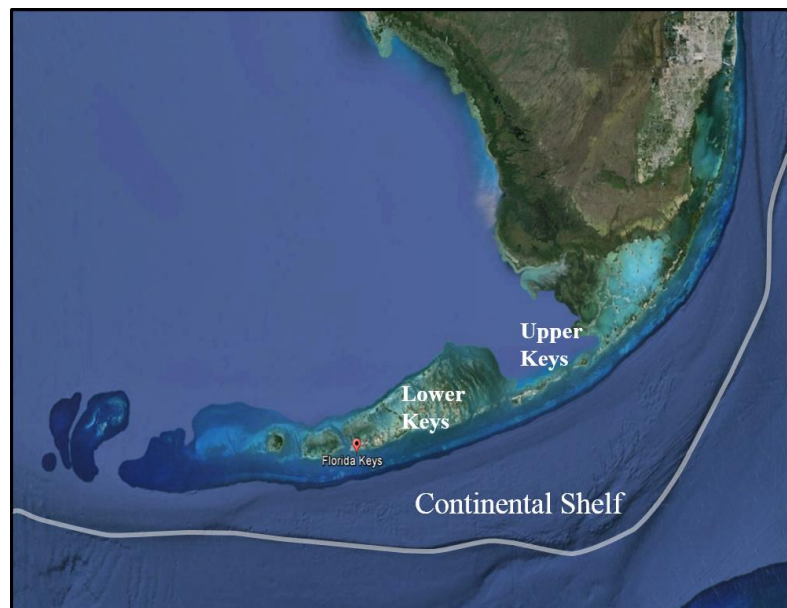
Courtesy of Frujittier, Elliot and Schlager (2000)

Figure 5: The sketch below was made by Frujittier et al., 2000 to highlight the erosional surface and mark core locations.

## Chapter 2: The Florida Keys

### 2.1 Physiography

The Florida Keys form a crescentic string of limestone islands that are connected by Highway US 1 (Hoffmeister et al., 1968). North is the Florida Bay and Gulf of Mexico, and south is the Atlantic Ocean. The keys are broken up into the Upper Keys and the Lower Keys, which lie upon continental crust and make up part of North America's Southern passive margin. The Miami Limestone (formation of interest) crops out throughout the Florida Keys, where the Miami Oolite Member makes up the Lower Florida Keys and the Key Largo Member the Upper Florida Keys. The lower keys trend NW and the upper keys trend NE. During formation and deposition, reefs orient themselves parallel to the shelf edge and tidal bars/channels orient themselves perpendicular to the shelf edge (Figure 6); therefore, the Upper Keys orientation is



**Figure 6: The lower keys are perpendicular to the continental shelf, where the upper keys are parallel to the shelf edge**

consistent with a reef environment, and the Lower Keys that of a tidal influenced oolitic environment.

## 2.2 Study Area

Windley Key Quarry is located within Islamorada, Florida (Figure 7).

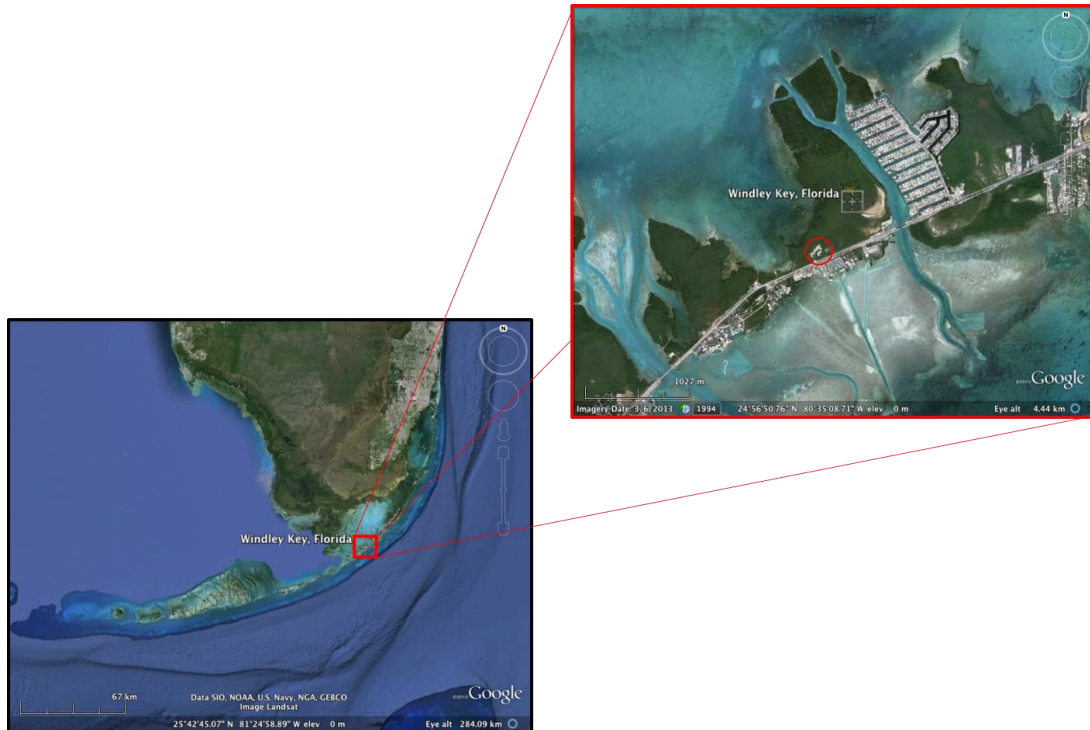


**Figure 7: The photo on the right is of the Florida Keys and Islamorada is highlighted by the red box. The photo on the right is a zoomed in view of the boxed area on the left. Windley Key Quarry is circled in red.**

Islamorada is one of the upper keys and is just south of Key Largo.

The quarry was active from 1912 through the 1960s providing rock to build roads, buildings and houses. The rock was also used as a decorative element. While being quarried, pilot holes were drilled through the limestone allowing a chisel machine to cut/quarry the rock. This process has left large, about 3 inch thick, fractures that run vertically down all the walls. Now, preserved as a geological treasure, the site is called



Windley Key Fossil Reef Geological State Park (Windley Key Quarry Brochure).



**Figure 8: Windley Key Quarry**

Windley Key Quarry contains three well exposed walls of the Key Largo Limestone: approximately West, North, and East facing (Figure 8). All of the walls are around 10 feet tall and have flat, laterally continuous tops. The walls are flat on top possibly because they were exposed, above the paleo water level, and were eroded.



**Figure 9: Red dust from Africa**

Enos (1977) believes the flat surface could be caused by erosion followed by a transgression during the Holocene. Some areas contain patchy, reddish, clay-rich soils. Robbin and Stipp (1979) and Muhs, Budahn, Prospero and Carey (2007) suggest the fine-grained particles in the soil crusts are likely derived from African dust (Figure 9).

### **2.3 Geologic Setting**

During the Pleistocene, a shallow marine embayment slowly separated the Keys from the mainland, then over time, sediment fill produced shallower and thus warmer seas where carbonate and plant growth flourished (Multer, Gischler, Lundberg,

Simmons and Shin, 2002). The Florida Keys contain two lithologic groups: the Key Largo Limestone and the Miami Limestone. The Key Largo Limestone is thought to lie stratigraphically beneath the Miami Limestone (Hoffmeister et al., 1968). Parker (1945) proved The Key Largo Limestone formed during the Sangamon Interglacial Stage 5e (Thorium-Uranium age dates of corals from Windley Key Quarry provided a range from 120,000 to 130,000 years ago) (Parker, 1945).

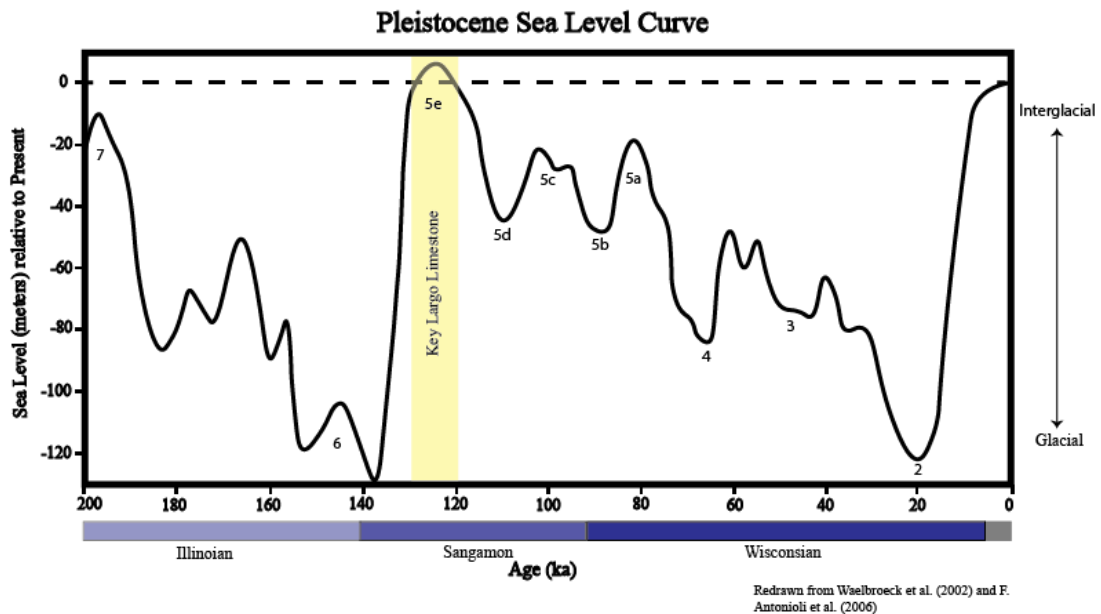
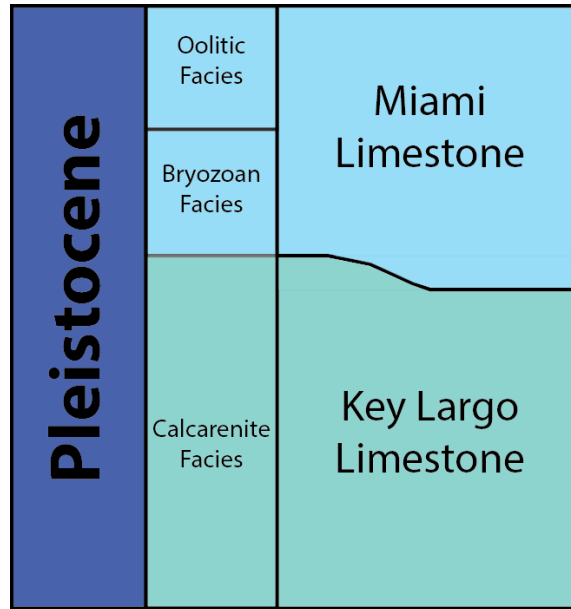


**Figure 10: Pleistocene global sea level curve with isotope stages 2-7.**

The transition from glacial Illinoian to interglacial Sangamon occurred approximately 125,000 years ago (Figure 10). Evidence from ice-core data, pollen studies of lake sediments, and data from benthic foraminifera and stable isotopes indicates that this last interglacial included one or more episodes of extreme climate fluctuation (White, 1998). Between 130 and 127 ka sea level rose to heights well above the current level, such that all of southern Florida was an epeiric sea. Thorium-Uranium

age dates of Pleistocene carbonate rocks in other parts of the world agree there was a worldwide sea level high-stand during this time (Kaufman and Broecker, 1965) and elevation measurements at Windley Key suggest sea level was around 6.6 meters higher than the present (Muhs, Simmons, Schumann, and Halley, 2011). During this rise in sea level, under semi-restricted conditions, is when the coral reefs of the Key Largo Formation developed. U-series isotope dating of corals at Windley Key Quarry suggest that the last interglacial sea-level high stand in the Florida Keys began 127 ka and lasted 9,000 years (Muhs et al., 2011). A rapid sea level fall around 126-125 ka interrupted coral growth and led to a period of erosion and freshwater diagenesis. Ice core data from Greenland explains this global sea level fall by proving during this time temperatures fell about 9°C (White, 1998). During the Wisconsinian stage, about 85,000 years ago, a glaciation began to lower sea level, killing the coral reef. The dying biota secreted acid into the water which began to erode and dissolve the reef.



Redrawn from Hoffmesiter, Stockman, and Mutler, 1967

**Figure 11: Stratigraphic column of Southern Florida. The Miami Limestone contains 2 facies: Oolitic and Bryozoan. The Key Largo Limestone is made up of a Calcarenite facies.**

The Key Largo Limestone underlies the upper Florida Keys, Soldier Key to Bahia Honda, and in some areas measures to as much as 145 feet (Hoffmeister, 1974). The stratigraphy of southern Florida is unclear. There are many varied opinions; therefore, a generalized stratigraphic column (Figure 11) compiles data from Hoffmesiter, Stockman, and Mutler (1967) and Berggren, Kent, Swisher, and Aubury (1995) to simply show the Key Largo Limestone Formation lies beneath the Miami Limestone formation. Today, Windley Key Quarry sits 18 feet above sea level, which is the highest natural elevation in the Florida Keys (State of Florida, 2012).

## 2.4 Key Largo Limestone

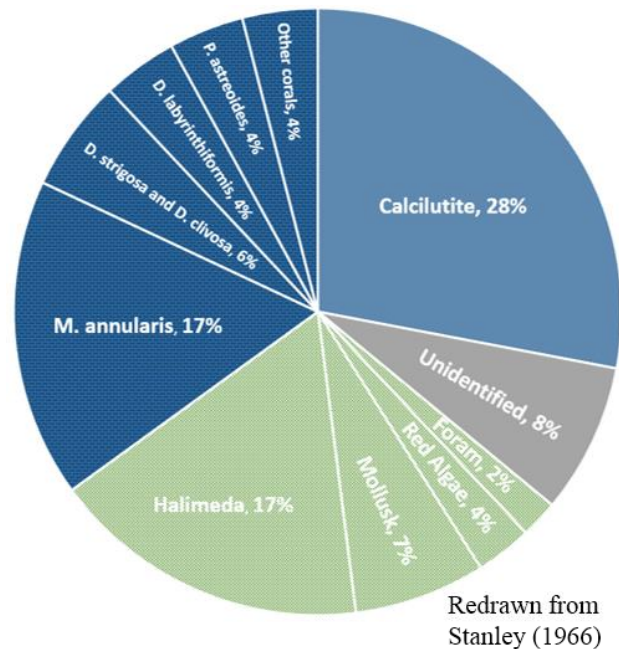
The Pleistocene Key Largo Limestone is a Boundstone/Biolithite (Dunham/Folk classification) with *Montastraea annularis* dominating more than half of the framework

(Stanley, 1966). It is a white to light grey, moderately to well indurated, fossiliferous, coralline limestone composed of coral heads encased in a calcarenitic matrix with little to no siliciclastic sediment (Florida Geological Survey, 2001). The coral species in the Key Largo Limestone are shown in Table 1. The Limestone Formation consists of an *in situ* organic framework formed by hermatypic corals and an interstitial calcarenite, all cemented and bounded together by crustose coralline algae and milleporid corals (Stanley, 1966). The calcarenite/packstones in between the corals are a product of winnowing wave action and micro-borers (Puri, Collier, 1967). Reef crests exposed to vigorous wave activity are often cemented by red coralline algae.

Puri et al. (1967) conducted an X-Ray diffraction analysis of a southern Floridan and Puerto Rican calcarenite, which concluded the matrix consists of secondary calcite after aragonite had been altered by solution-re precipitation and inversion. To determine where the aragonite was in the rock, Stanley (1966) stained thin sections of calcarenite with cobalt nitrate. He found that aragonite formed 75 percent and high-magnesium calcite formed 20 percent of the original calcarenite. This mineralogic composition shows that aragonite secreting organisms, such as *Halimeda* and hermatypic corals, and high Mg secreting coralline algae were dominant. Fossils that initially were high Mg calcite have been altered in place to low Mg calcite by meteoric zone diagenesis and fossils that were originally aragonite have been replaced by sparry calcite (Stanley, 1966).

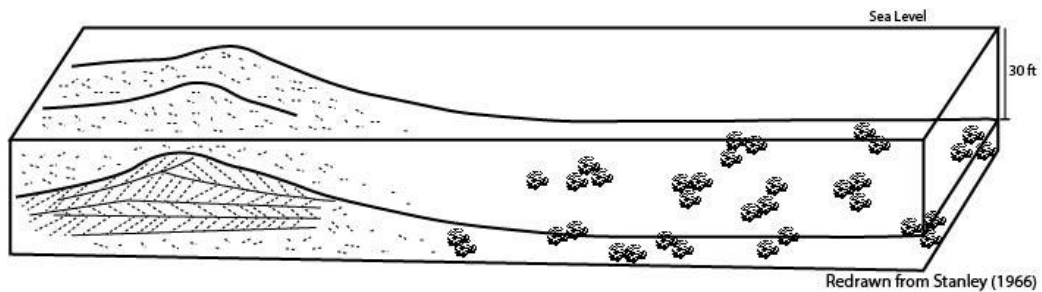
In Windley Key Quarry Stanley (1966) found corals comprise about 30% of the rock volume with *Montastraea annularis* making up half (Figure 12). *M. annularis* grow in different forms: smooth subhemispherical colonies, large multilobular heads,

and sheet-like masses (Hoffmeister, 1968). Within the quarry subhemispherical and multilobular heads dominate suggesting water depths less than 20m because, as water depth increases, *M. annularis* heads become less spherical and more sheet-like (Foster, 1983). The other principal corals are *Diploria strigosa*, *Diploria clivosa*, *Diploria labyrinthiformis*, and *Porites astreoides*. The most abundant type of skeletal material is the calcareous green algae, *Halimeda*, which in outcrop is a dark and flakey material. Other recognizable skeletal debris present are alcyonarian spicules, echinoid spines, bryozoans, and milleporids.



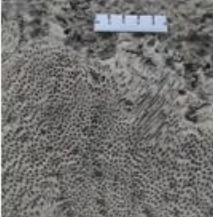









**Figure 12: The Key Largo Limestone**

The lack of *Acropora palmata* in the Key Largo Limestone is problematic. One possibility is that water depths were too great, as *A. palmata* only thrives in shallow water. Also, *M. annularis* is known to succeed only in quiet, low energy marine environments. Stanley (1966) believes the Key Largo reef grew in 10-20m of water (Figure 13). Precht and Miller (2007) on the other hand, suggest cold winters may have killed off the *A. palmata*.











**Figure 13: *M. annularis* thrives off the shelf about 10m deep.**



Scientific Name Common Name	Colony Size	Water Depth (ft.)	Description	Fossil	Alive
<i>Montastraea annularis</i> Boulder Star Coral	1-10 feet	20-75	<ul style="list-style-type: none"> <li>- Grow in clusters of long, thick columns with large, dome-like tops.</li> <li>- Surfaces are usually smooth with close, uniform and evenly extended corallites.</li> </ul>		
<i>Montastraea cavernosa</i> Great Star Coral	2-8 feet	2-8	<ul style="list-style-type: none"> <li>- Colonies form massive boulders and domes that can develop into plates or sheets in deep water.</li> <li>- Surface is covered with distinctive corallites.</li> </ul>		
<i>Porites porites</i> Finger Coral	1-4 feet	3-80	<ul style="list-style-type: none"> <li>- Has stout, irregular stubby branches with enlarged tips.</li> <li>- Most common on moderate to deeper reefs</li> </ul>		
<i>Porites astreoides</i> Mustard Hill Coral	6 inches – 2 feet	18-80	<ul style="list-style-type: none"> <li>- Colonies encrust in shallow waters forming rounded heads, boulders or domes.</li> <li>- Surface is lumpy and covered with small, closely set corallites that give a porous appearance.</li> <li>- Inhabit all reef environments</li> </ul>		
<i>Diploria clivosa</i> Knobby Brain Coral	6 inches – 4 feet	3-20	<ul style="list-style-type: none"> <li>- Form hemispherical domes</li> <li>- Surface has numerous irregular knobs</li> <li>- Inhabit shallow environments both seaward and lagoonal</li> </ul>		

**Table 1: List of corals found in the Key Largo Limestone Formation inside Windley Key quarry. (Alive photos copied from google images)**

<p><i>Diploria strigosa</i> Symmetrical Brain Coral</p>	<p>6 inches – 6 feet</p>	<p>20-40</p>	<ul style="list-style-type: none"> <li>- Form smooth contoured plates to domes</li> <li>- Long valleys are often connected and convoluted</li> <li>- Ridges are evenly rounded, usually without a top groove</li> <li>- Inhabit most marine environments</li> </ul>		
<p><i>Diploria labyrinthiformis</i> Grooved Brain Coral</p>	<p>1-4 feet</p>	<p>15-50</p>	<ul style="list-style-type: none"> <li>- Form hemispherical heads</li> <li>- Deep, often narrow, polyp bearing valleys are separated by broad ridges with wide grooves.</li> <li>- Valleys are highly convoluted and often interconnected</li> <li>- Inhabit seaward slope</li> </ul>		
<p><i>Siderastrea siderea</i> Massive Starlet Coral</p>	<p>1-6 feet</p>	<p>25-45</p>	<ul style="list-style-type: none"> <li>- Form rounded heads, boulders or domes.</li> <li>- Surface coated with small, symmetrical, pitted corallites.</li> <li>- Prefer clear shallow water in protected areas.</li> <li>- Also found in deep environments</li> </ul>		
<p><i>Siderastrea radians</i> Lesser Starlet Coral</p>	<p>4-12 inches</p>	<p>3-30</p>	<ul style="list-style-type: none"> <li>- Colonies form flat encrusting plates that can grow in small irregular rounded domes</li> <li>- In shallow water they roll freely across bottom surge</li> </ul>		

**Table 2: Table 1 cont.**

## Chapter 3: Methods

### 3.1 LIDAR

#### 3.1.1 LIDAR Theory

One of the major tools used in this investigation is a LIDAR. LIDAR (light detection and ranging) is a device that scans a terrestrial environment and produces a high-resolution image (Figure 14).

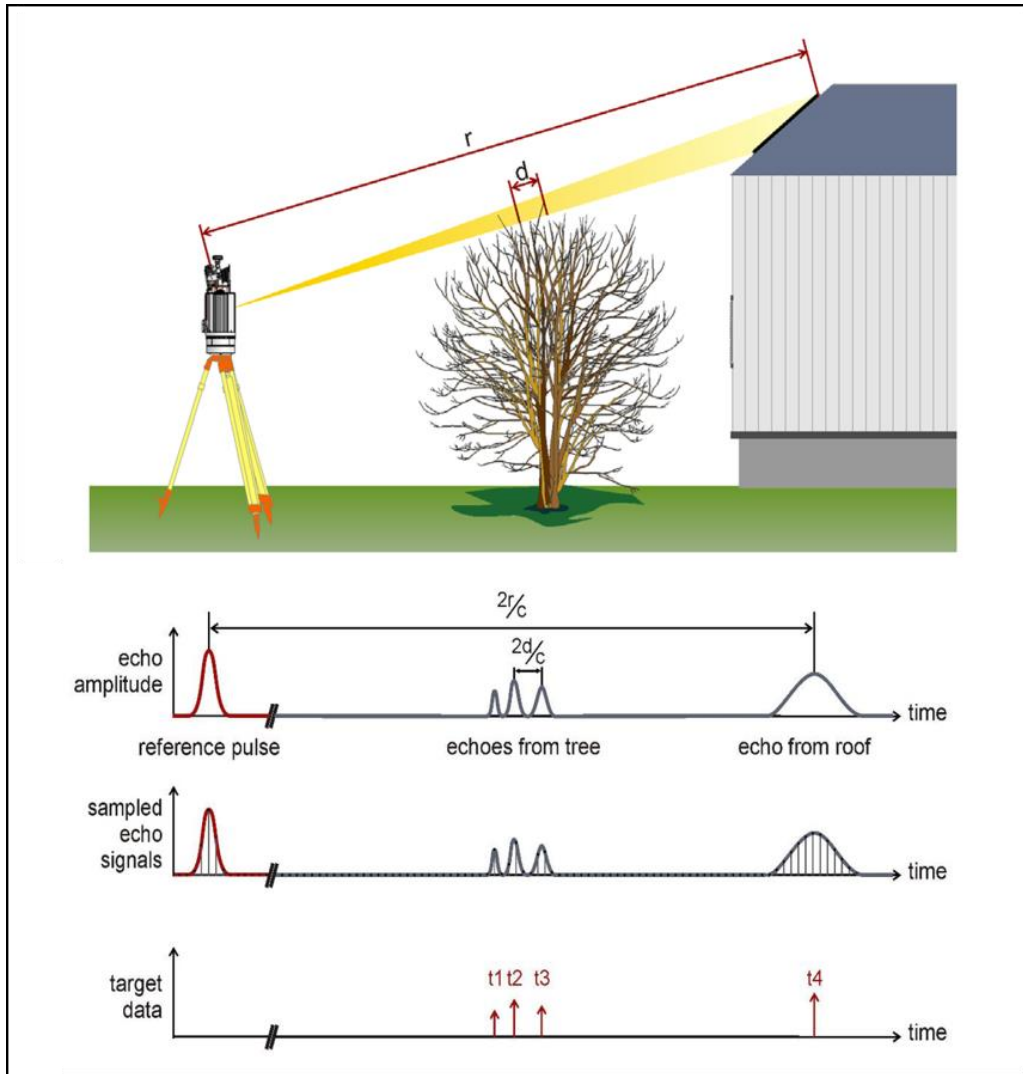


**Figure 14: LIDAR mounted on a tripod in the field**

This optical remote sensing device measures the distance to, and/or other properties of a target, by illuminating the target with light using pulses from a laser. These scanners can collect thousands of points per second, which are compiled as a “cloud” of points that approximate the target surface (RIEGL, 2012). When the light source encounters the granular surface, some photons are absorbed while some are scattered (RIEGL,

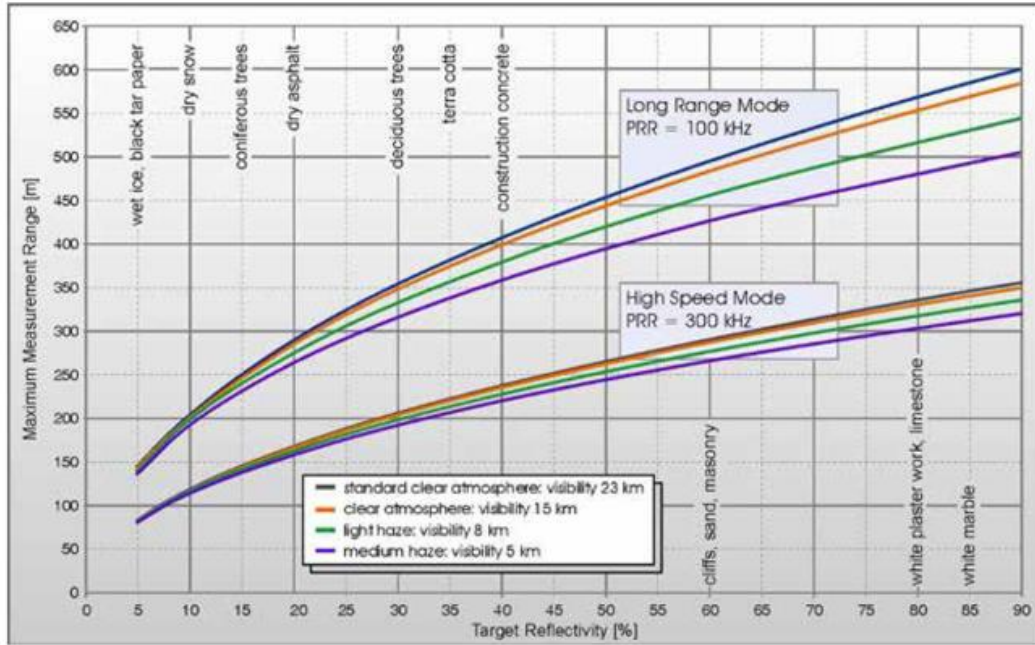
2012). LIDAR uses the time of flight and angle of emission to accurately (within cm) calculate the x, y, and z location of a point on a targeted surface (Burton, Dunlap, Wood and Flaig, 2011). LIDAR scanners collect intensity returns, which is the power returned/power emitted. In other words, intensity is the power of the backscattered signal relative to the power of the emitted signal. The strength of the reflected signal is related to the geometry between the laser emitter and the targeted surface, and the reflective character of the target at the wavelength of the laser (Burton et al., 2011).

As Figure 15 shows, LIDAR records the distance each light pulse traveled. In the example, the LIDAR detected 4 objects and labeled them t1-t4. Each reflectance, or intensity, point is mainly based on how quickly each pulse returns to the scanner. Intensity is also influenced by distance, target reflectivity, angle of incidence, roughness, and environmental conditions (Burton et al., 2011). Figure 16 shows how environmental conditions (ex: a foggy day) and the objects being scanned (ex: trees, white marble) affect the measurement range.



Riegl (2012)

**Figure 15: LIDAR emits multiple light pulses and each pulse returns once it encounters an object. The LIDAR records the distance each pulse traveled and labels them.**



Riegl (2012)

**Figure 16: Target reflectance (%) vs maximum measurement range (m) of the two different scan settings: Long range and high speed mode.**

The reflectance of a granular surface is controlled by the composition of individual grains, their weight fraction, and grain size (Burton et al., 2011). Although not quantitatively assessed, weathering and moisture also effect the intensity returns. Weathered surfaces, such as the presence of dust, mud cake, and lichen, diminish intensity returns. Since water is a strong absorber, water-saturated rock will also weaken intensity returns (Burton et al., 2011). After conducting a few experiments, Burton et al. (2011) were able to show a correlation between LIDAR intensity, weight percent clay, and weight percent combined quartz, K-spar, and plagioclase. Therefore, LIDAR intensity is sensitive to lithology in clastic outcrops that are lightly unweathered and dry. Figure 17 from Burton et al. (2011) correlates wavelength and reflectance in shales

and sandstones. Although these rock types are not of interest for this paper, it shows reflectance is dependent on lithology. We shall use this principal in a powerful way.

With LIDAR 3D models, geologists are able to simultaneously study the outcrop at a variety of scales and viewing angles in a virtual environment, which enables the

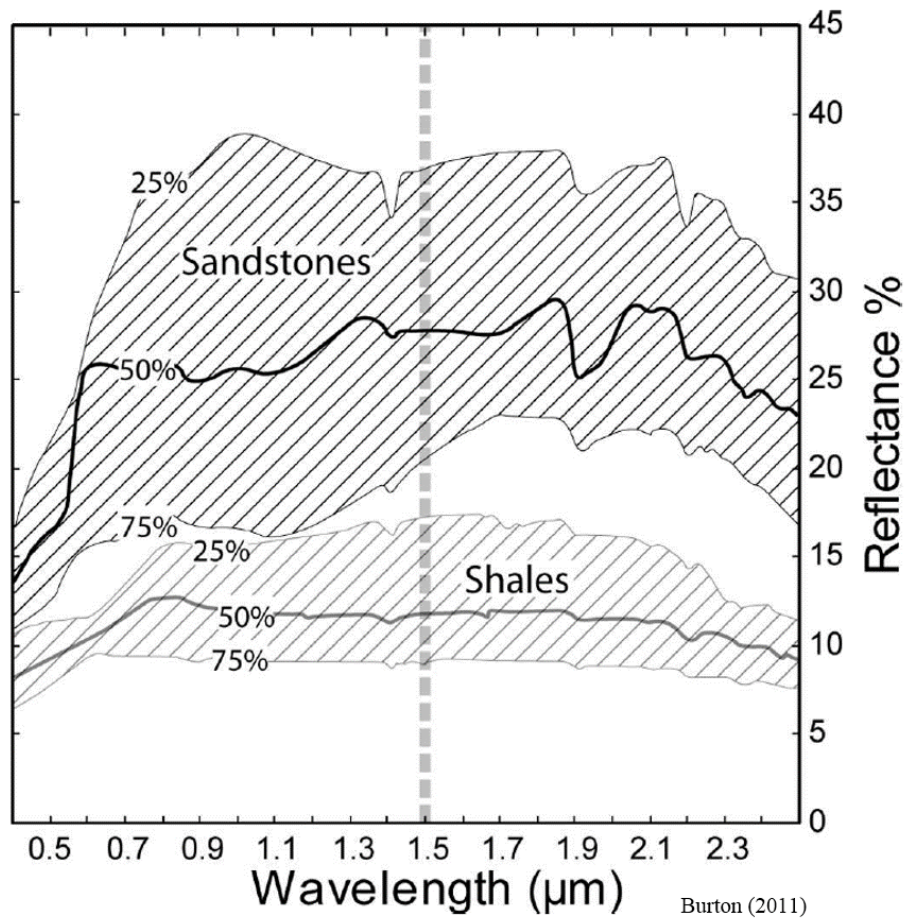


**Figure 17: NASA JPL library spectroscopy solid sample data showing median (solid line) and quartiles (dashed lines) for shale and sandstone. The central dashed line approximates the wavelength of terrestrial LIDAR (Burton et al., 2011).**

scientist to study the complex structure and stratigraphic features of an outcrop.

### 3.1.2 LIDAR Collection Mechanics

The LIDAR employed is a Laser Class 1 VZ-400 with a maximum range of 600 m, precision of 3 mm, and an accuracy of 5 mm. It also contains an internal GPS and Wi-Fi capability, so scan data is downloaded real time to an adjacent computer. A Nikon D800 camera is mounted on top of the LIDAR (Figure 18).

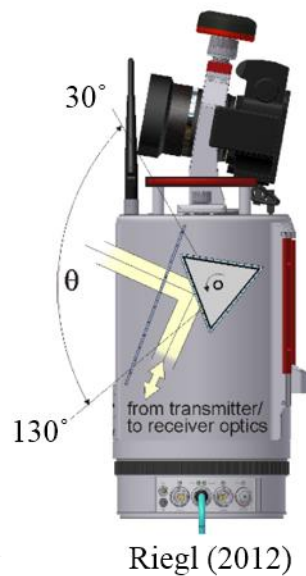


**Figure 18: Reigl VZ-400 with Nikon D800 camera mounted on top. The scanner is able to image anything between 30 and 130 degrees.**

The LIDAR is secured on a tripod which was moved to 16 different locations around the quarry always about 10 feet from the walls (Figure 19). These multiple scan positions are tied together by referencing common points. These ‘tie points’ are very reflective for quick identification on the scan image. Before scanning begins, one must forecast all scan positions and place the reflective stickers and cylinders in a place where they can be detected by most scans. The cylinders were placed on corners on top of the quarry walls and the flat reflectors were stuck directly on the quarry wall away



from any classifiable specimen. Each new scan needs at least 3 reflectors in common with all previous scans. Once set up, the LIDAR is initiated to complete a 360° scan from a computer nearby. Every 360° scan used 0.060 degree resolution, which took about 2 minutes. A resolution of 0.060 degree means that a point will be placed every 0.060 degrees. So a smaller number, like 0.005 degree, will contain more points, which will produce a higher resolution picture. Once the 360° scan is complete, the Nikon D800 will take seven pictures, each time rotating 51.43 degrees in order to image 360 degrees. The Nikon's shutter speed was set to 1/250s, the aperture to f/22.0 and the ISO to 400.

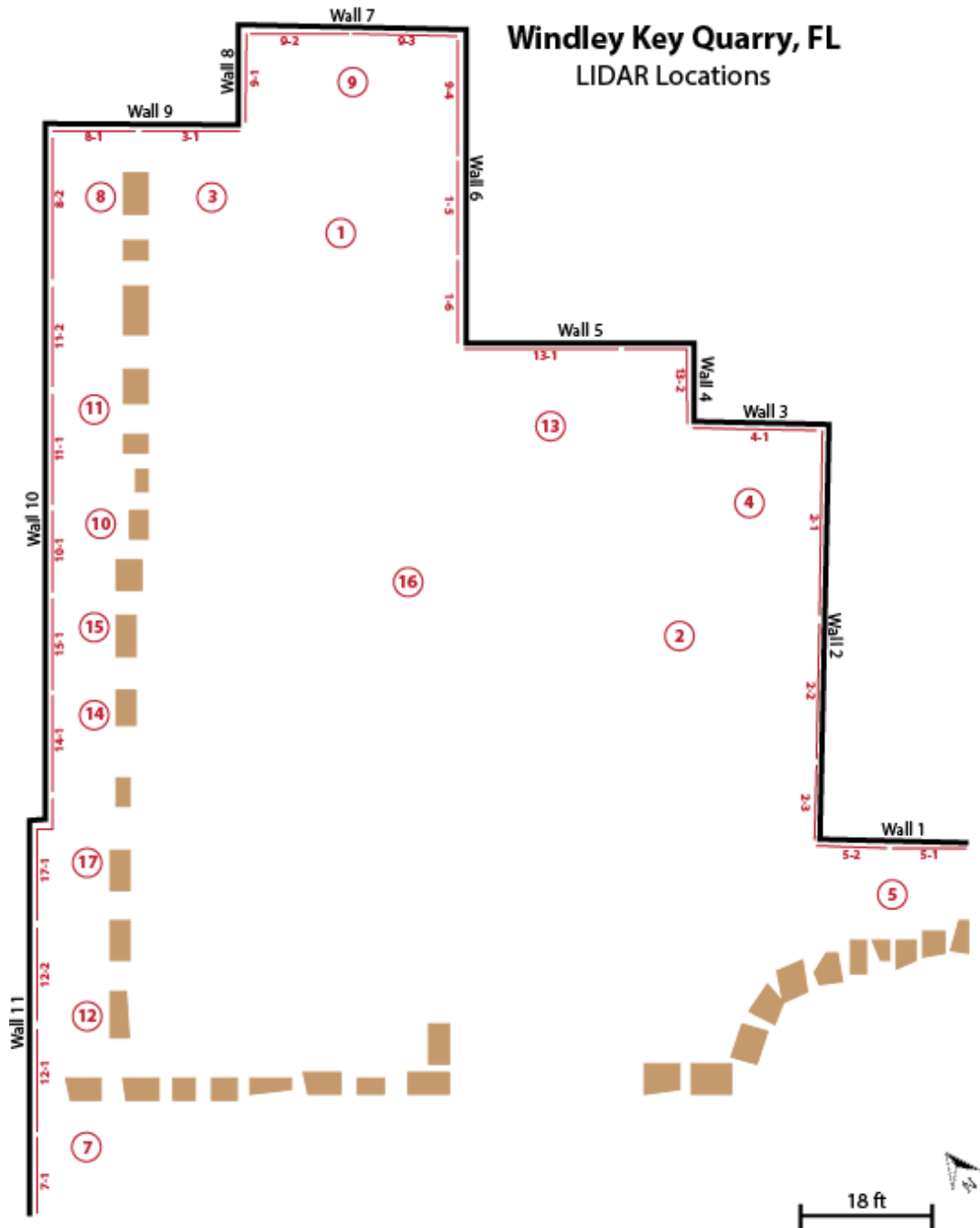


**Figure 19: Map of Windley Key Quarry. Each scan position is circled in red and their high resolution scans are numbered along the walls. 2-3 indicates scan position 2, high resolution scan 3. The brown blocks are large boulders.**

These pictures are later meshed with the point cloud data to view the scan's 'true color'. Next, each reflector is located and matched with their identical reflector from different scans. For example, reflector A from scan 1 is tied to reflector A from scan 2. This step allows all scans to be viewed/meshed together.

The super fine details of the quarry walls are imaged with a second, higher resolution (0.005 deg.), scan. These fine scans are selected by zooming in on the 360° scan data and outlining an area of interest. Here, only the quarry wall in front of the LIDAR was scanned, cropping out vegetation and limiting the scan from obscure angles. These scans usually took 45 minutes each.

In December 2014, a total of 69 scans were conducted in Windley Key Quarry. Of those 69, 21 were 360° scans and 48 were fine-scans. 23 reflectors were placed around the quarry: 8 cylinders and 15 flat reflectors. (See Appendix B for data collection statistics.) Temperatures ranged from 64°F to 77°F. Humidity ranged from 52% to 82%. Wind speeds ranged from 3-12 mph.

### *3.1.3 LIDAR Processing*

The computer program RiscanPro 2.0.1 is used to view, process, and interpret LIDAR data. The raw scan data is displayed by millions of points (all together called a 'point cloud'), which are unevenly distributed. Figure 20 is an example of a raw 360° scan displayed in 'true color'. Figure 21 shows the set parameters for Figure 20. Areas closer to the LIDAR are populated with more points than areas further away. A point cloud is a set of points with coordinate values in a well-defined coordinate system, in this case the scanner's own coordinate system (SOCS). Each point of the point cloud has valuable additional attributes, such as time stamp, amplitude, reflectance, and pulse



**Figure 20: 360 degree initial scan, unprocessed and is displayed in 'true color'. Each scan is 'colored' by the photos the Nikon D800 camera takes after each scan. The location of the scan is easily noticed by the white, or data less area. The area surrounding the LIDAR will not contain data points because, recall Figure 18, the first point will be at a 130 degrees. Notice there are more points closer to the scan position than further away.**

shape deviation (RIEGL, 2012). In Figure 20, notice how the boulders along the NW wall obstruct the scanners view. This is why scan positions 8, 10, 11, 12, 14, 15, and 17 were positioned in front of the boulders close to the wall. First, to preserve the raw data

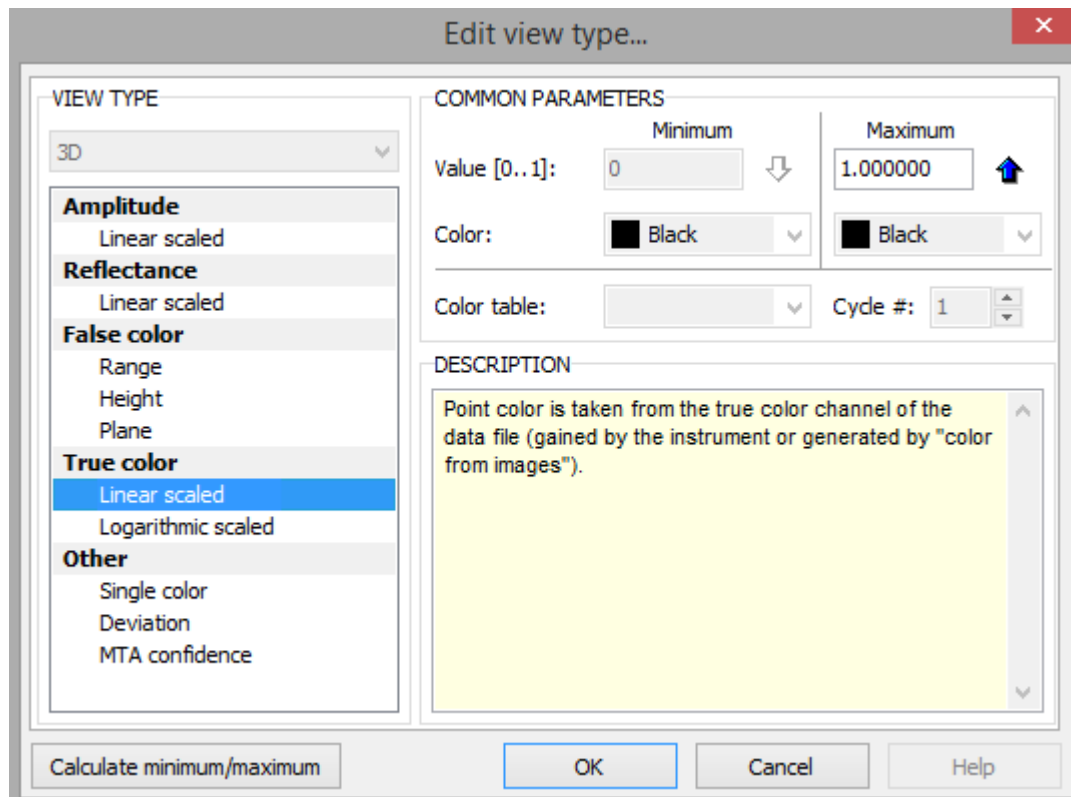


**Figure 21: The options on the left side are all the available attributes to view each scan. Figure 20 selected True Color. Other options are Amplitude, Reflectance, a single color, Range and Height. Range will assign colors based on the distance from the scanner and Height will assign colors based on the topography.**

all scans are converted to polydata. That way, if a processing mistake is made, one is able to start over with the raw data. To make the data more uniform, and easier to handle, points are deleted from the polydata and evenly distributed by running the Octree Filter. Figure 22 shows two images. The on the left is the original raw data and

on the right has been filtered. Figure 23 is a screenshot of the octree filter parameters. Clusters of, or unnecessary, points are deleted and empty, or point-less areas are filled in. Points are also distributed evenly (the filtered data looks more like a grid). As only the quarry walls are of interest, everything else (the ground, vegetation, the Visitor Center, etc.) are deleted, which also makes each data set more manageable. Once the data is cleaned of all noise, the points are triangulated to create a mesh (Figure 24). The mesh smooths out the points to create a more continuous image.

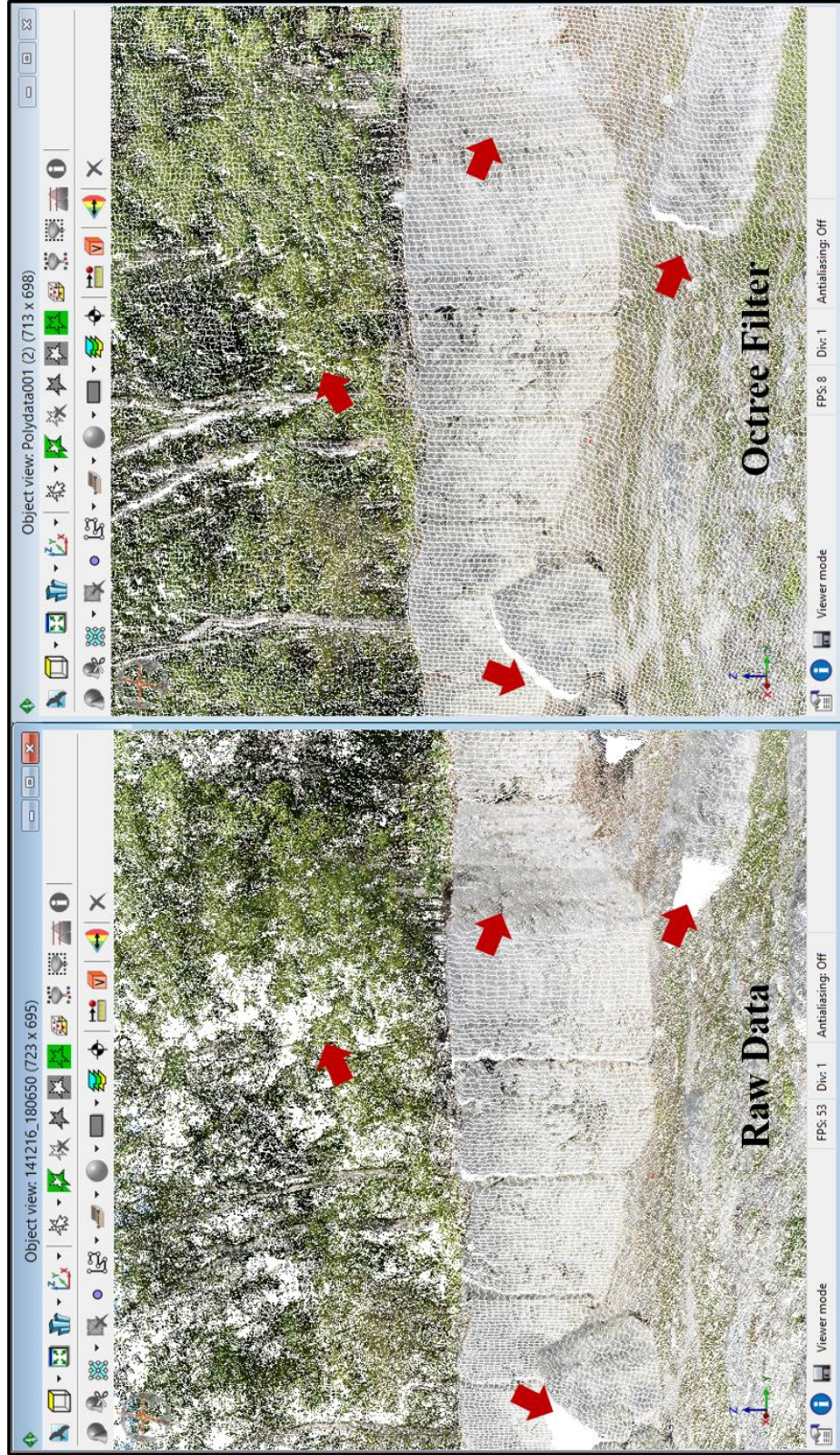


**Figure 22: Raw scan data on the left and filtered data on the right. The red arrows point to areas that the octree filter altered. These are scans of walls 8 and 9.**

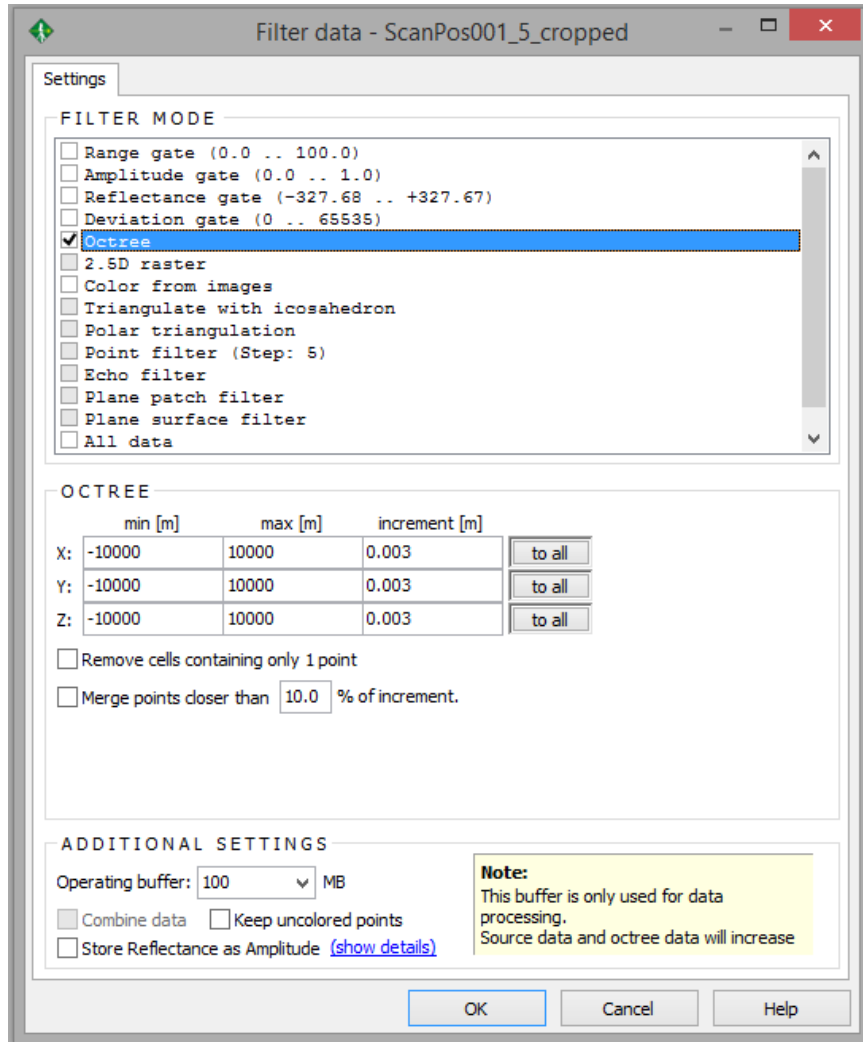


**Figure 23: The parameters set to filter all raw data. The min and max are insignificant but the increment is significant. An increment of 0.003m is the finest grid size my dataset could handle. If the increment was set to 0.005, each point would be further away, which would decrease the scan’s resolution. If the increment was set to 0.002, the filter process would fail.**

Amplitude, Reflectance, and True Color are the 3 most important attributes.

Amplitude is given relative to the amplitude of an echo signal at the detection threshold of the instrument; thus, the value of the amplitude reading is a ratio, given in the units



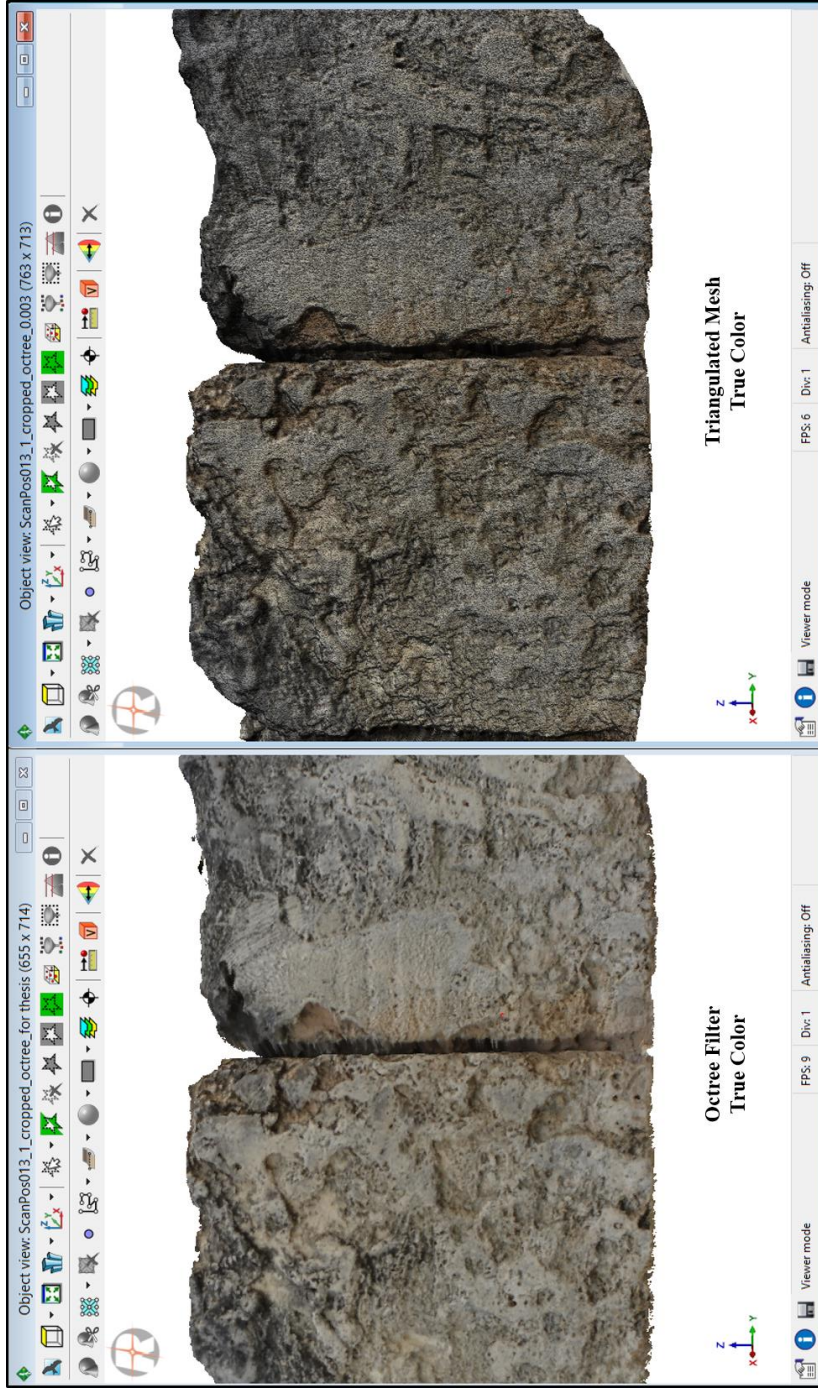


**Figure 24: Both images are of wall 5, scan position 13-1 and displayed in True Color. All vegetation has been deleted so only the quarry wall is visible. After the data has been run through the octree filter (image on the left), the points are triangulated to create a more continuous image.**

of decibel (dB). The Amplitude of the signal reaching the laser scanner depends on a number of parameters, such as the emitted laser pulse peak power, the receiver aperture, and the targets range (RIEGL, 2012). Since Amplitude is only valid for targets directly in front of the scanner, this attribute is disregarded. Reflectance, on the other hand, is reliable at any receiver aperture and range. It is a target property (also given in decibels (dB)) and refers to the fraction of incident optical power that is reflected by that target at a certain wavelength. The reflectance provided is a ratio of the actual amplitude of that target to the amplitude of a white flat target at the same range, oriented orthonormal to the beam axis, and with a size in excess of the laser footprint (RIEGL, 2012). Reflectance can be thought of as intensity, that is, the strength of the returning light pulse varies with the composition of the surface object reflecting the return. True Color is simply the original point cloud data colored by the images taken by the Nikon D800. Think of each point as a pixel of the image. Each pixel knows which point to color by linking the reflectors from the scans to the reflectors from the images.

The most useful attribute is reflectance owing to its independence of target angle. Each scan has a different minimum and maximum reflectance value. Viewing multiple scans with different minimum and maximum values would be inconclusive; therefore, the average min and the average max is a good starting point. From all 48 fine scans, the average min is 307 dB and the average max is 353 dB. With this large dB window it was hard to locate trends, so the scale was narrowed by locating where most data lies within the color bar. The optimal reflectance window to view carbonate material in Windley Key Quarry is between 325 and 328 dB. Using this as the standard

min and max value for all LIDAR scans will give conclusive data regarding the mineralogy and discontinuity trends. Figure 25 displays Reflectance of walls 2-9.

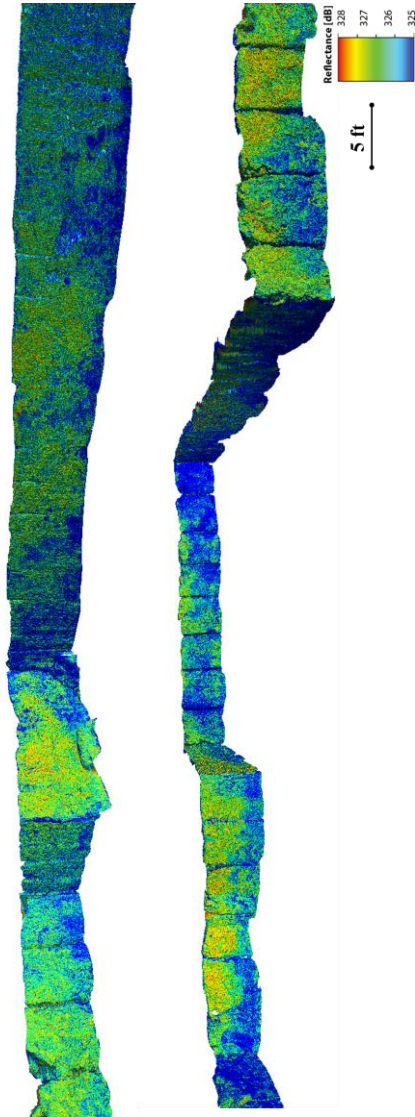


**Figure 25: Reflectance of walls 2-5 on top and 5-9 on bottom.**

## **3.2 XRF**

### *3.2.1 XRF Collection*

The second major tool integrated in this investigation is a portable XRF. A portable X-Ray Fluorescence (XRF) Thermo Scientific Niton XL3t Ultra was used inside Windley Key Quarry walls to detect the major and light elements. This machine is used throughout a variety of scientific disciplines due to its non-destructive characteristics, multi element capability, and the immediate availability of results following a measurement (Thermo Fisher Scientific, 2010). Geoscientists use an XRF on drilled core, for example, to identify sequence boundaries, unconformities, and depositional environments.

Measurements were taken every 5 feet (1.5 m) laterally and every 1 foot (0.3 m) vertically across and up the walls (Figure 26). Measurements were also collected at areas of interest that did not fall in the grid. The sample time for each measurement was 210 seconds and 412 measurements were taken in May, 2015 (Appendix C). During the 210 seconds three filters ran for 30 seconds each: Main, Low and High. “Main” searches for elements from manganese through bismuth, “Low” is best used to detect titanium through chromium, and “High” best identifies elements from silver to barium. Lastly, the “Light” filter ran for 60 seconds and searches for all other elements not detected (Thermo Fisher Scientific, 2010). Appendix D contains photographs of each XRF station with coral and discontinuity surface identification.

### *3.2.2. XRF Processing*

The list of all scans were transferred to an Excel spreadsheet for easy calculations and comparison. Once the scans in the field were complete the XRF was calibrated using a program (Pigott, personal communication), which incorporated pure mineral samples from the University of Oklahoma's mineral collection. The calibration output was transferred to the spreadsheet and the values taken from the field were reported. The elements of interest are iron (Fe), sulfur (S), magnesium (Mg), calcium (Ca), aluminum (Al), silicon (Si), and strontium (Sr). The measured standards of those elements were used to calculate the amount of pyrite, gypsum, aragonite, high Mg calcite, calcite, clay and quartz-chert present in each XRF measurement. The data are then displayed in excel graphs (Pigott, personal communication) and compared to processed LIDAR scans to identify lateral and vertical trends. Appendix E displays the mineralogy of each XRF scan and the table in Appendix F shows the mineral standards used to convert XRF elements to mineralogy.

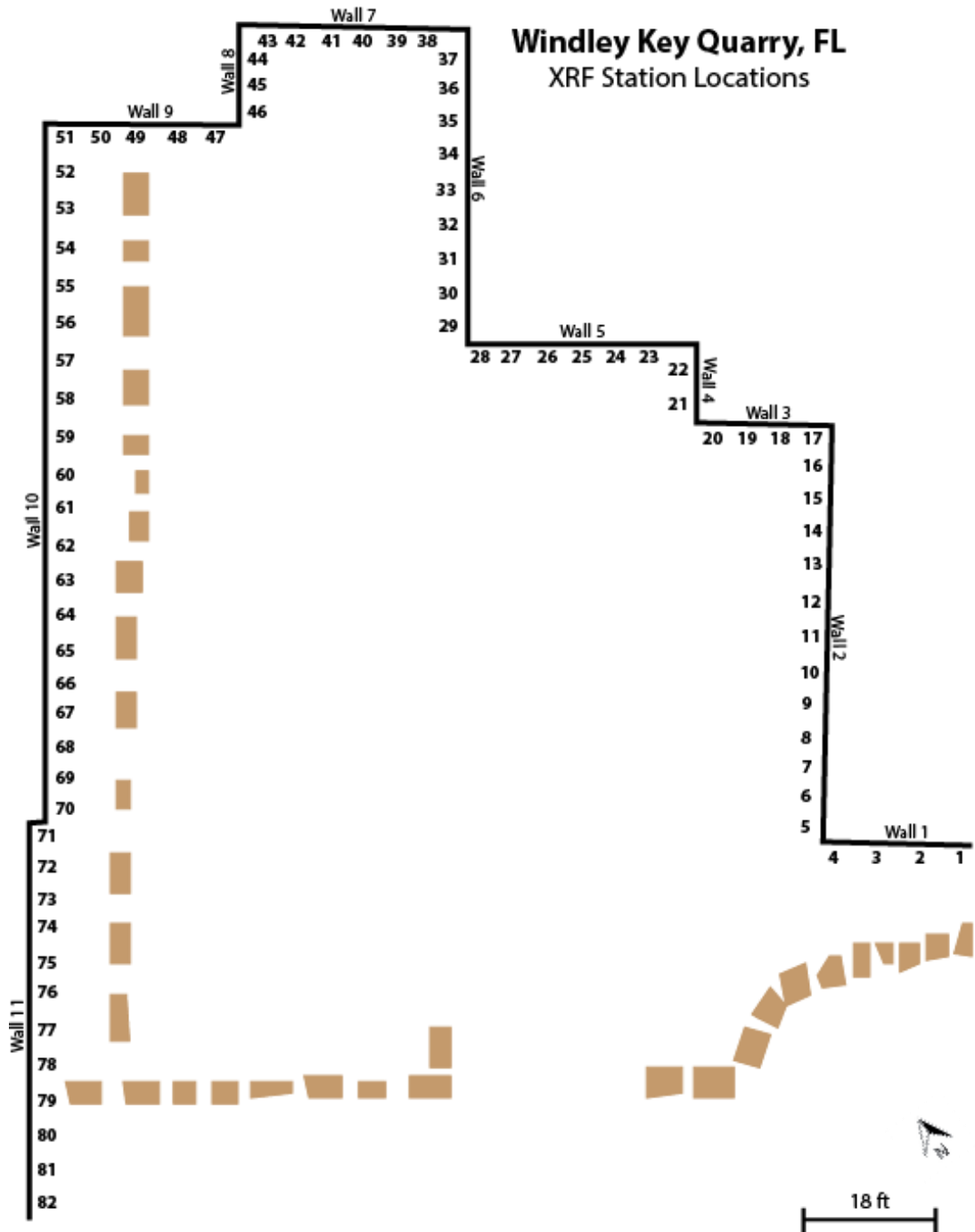
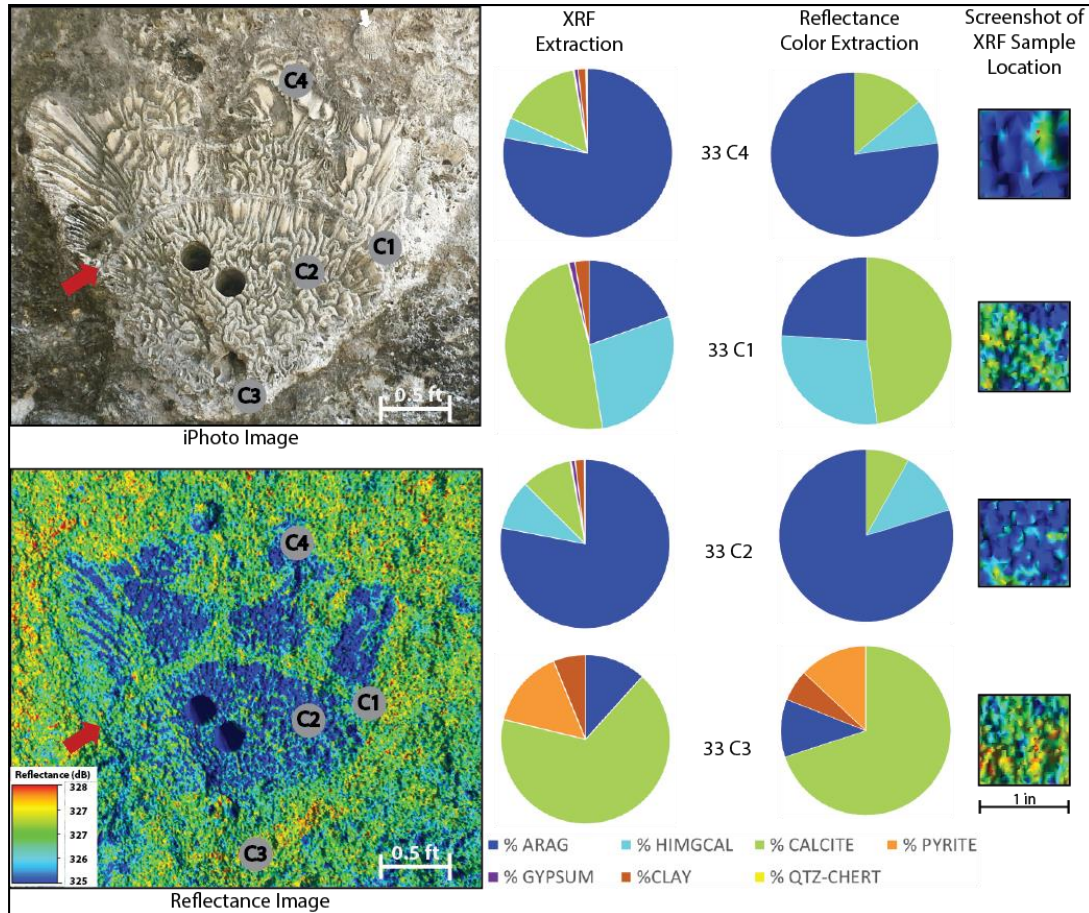


Figure 26: Windley Key Quarry map with XRF scan locations. The brown blocks are boulders.

## **Chapter 4: Observations/Interpretation**

### **4.1 Combining LIDAR and XRF Data**

As a novel technique, the XRF and LIDAR data were coupled in order to determine the mineralogy of the quarry walls. In order to assign a color to a mineral the XRF data needs is calibrated to the LIDAR data. To do this, three extra XRF scans (not in the 5x1 ft grid) were taken inside a small area (2x2 ft.) on wall 6 and named 33C1-33C4. Then, a screenshot of the exact XRF scan location on the LIDAR reflectance data was run through a basic color extraction computer algorithm (Pigott, personal communication). The results show the percentage of each color in the image. These results were then compared to the percentage of minerals in each XRF scan (Figure 27), where it was clear that reflectance is directly correlated to mineralogy.



**Figure 27: The close look of this *Diploria labyrinthiformis* (iPhone image on top and reflectance below) demonstrates the power of a high resolution LIDAR scan. C1-C4 mark the exact XRF scan positions. The first column of pie graphs show the percentage of each mineral detected by the XRF. The second column of pie graphs show the percentage of each color present in the image to the far right. The images in the third column are screenshots of the exact XRF scan location on the LIDAR reflectance scan. The red arrow marks another discontinuity surface and the small white arrow in the top right corner points to an upside down coral.**



Now as a whole, while looking at reflectance of the quarry wall's, one way then infer dark blue areas are aragonite rich, green/yellow areas are calcite rich and light blue areas are high Mg calcite rich. Pyrite, gypsum, clay, and quartz-chert are present in low quantities, if at all in same areas, their exact reflectance color was not able to be determined. Figures 28-45 show each quarry wall's reflectance with lines representing erosional surfaces. The undulating discontinuity surfaces are coated with high Mg calcite coralline algae, which would act as a fluid migration pathway not a seal (Pigott, 2013). Low Mg calcite carbonate mud fills cavities, burrows, or previous porous areas.

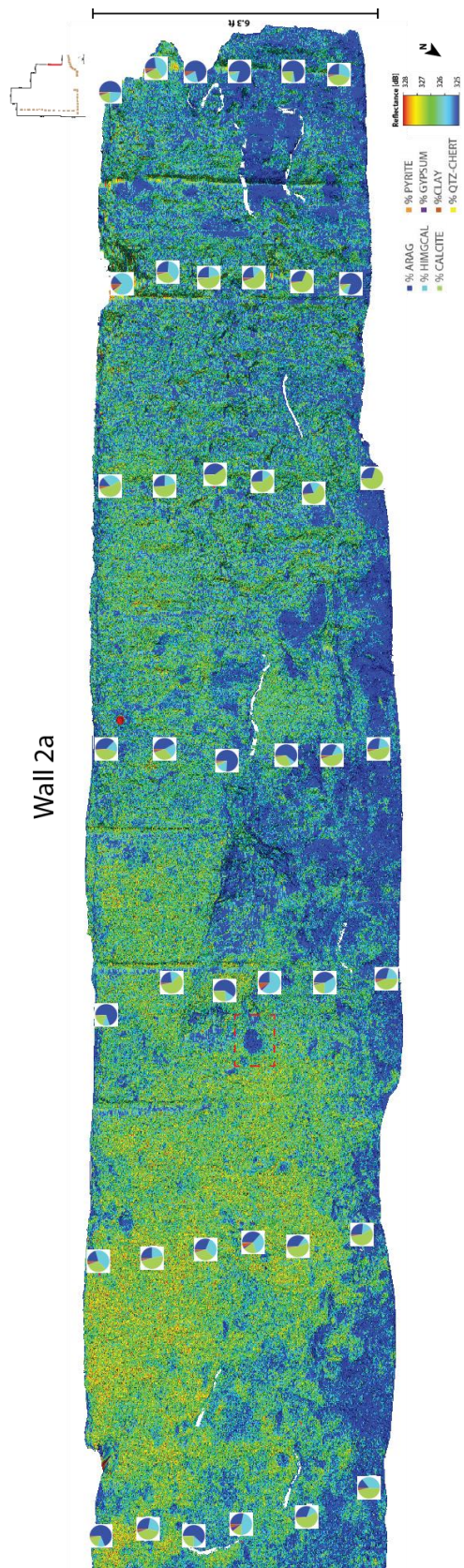


**Figure 28: Reflectance of half of wall 2 with the XRF scan results. The white lines trace over possible discontinuity surfaces. This wall contains more of the ‘non-core’ components (pyrite, gypsum, clay, quartz-chert) than other walls and the amounts of both low and high Mg calcite increase moving from right to left across the wall. The red dot at the top-middle of the wall is one of the reflective stickers used during the LIDAR scan. Well preserved corals are easily identified because they still contain close to 100% aragonite. For example, Figure 29 zooms in on the red boxed area.**



**Figure 29: This *Diploria clivosa* likely was quickly buried in order to preserve its mineral composition. It is surrounded by high Mg calcite mud, which sealed the coral and did not allow fluid penetration.**

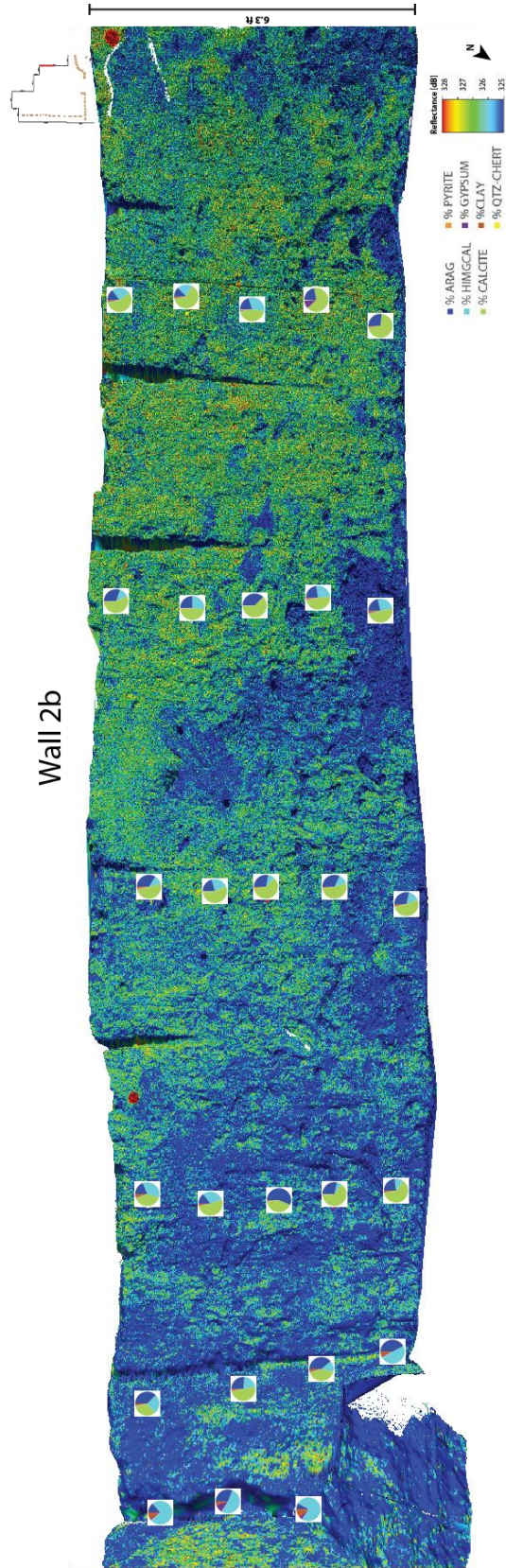


**Figure 30: Reflectance of the other half of wall 2 with XRF scan results. The white lines trace over possible discontinuity surfaces. This wall contains more of the 'non-core' components (pyrite, gypsum, clay, quartz-chert) than other walls and the amounts of both low and high Mg calcite increase moving from right to left across the wall. The red dots at the top and middle of the wall are a few of the reflective stickers used during the LIDAR scan. This wall does not have many well preserved corals, which suggests it all has been altered by meteoric water.**

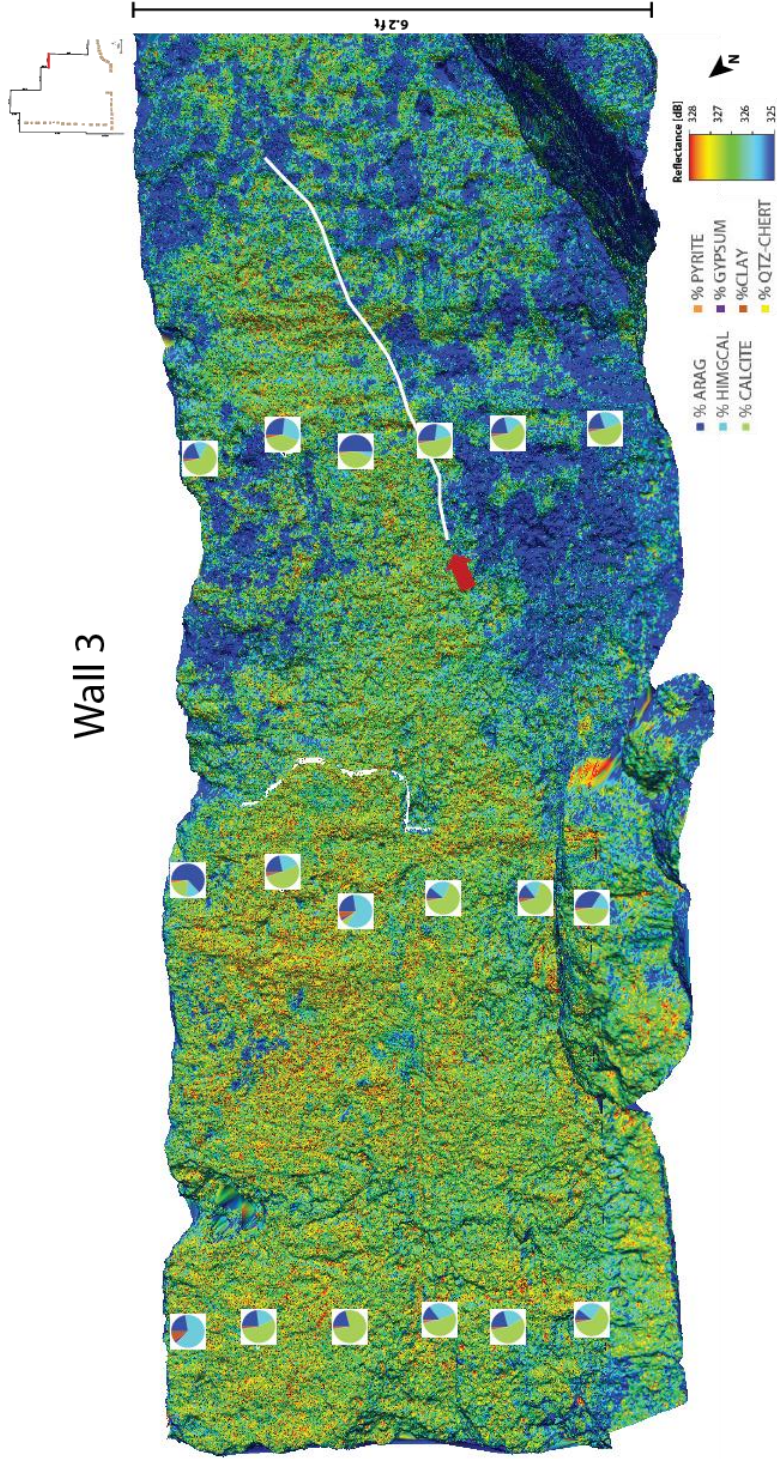


**Figure 31: Reflectance of wall 3 with XRF scan results. The white lines trace over possible discontinuity surfaces. This wall contains more of the 'non-core' components (pyrite, gypsum, clay, quartz-chert) than other walls. Corals seem to be imbricated below a possible surface pointed out by the red arrow. These corals are not easily identified with just a photo (Figure 32). LIDAR helps illuminate features that would not be recognized with the naked eye.**



**Figure 32: It is not clear where to draw the white line indicating the discontinuity surface from the previous figure. Also, note the lichen near the top of the wall. On the previous figure, this 'vegetation' is more reflective (red).**

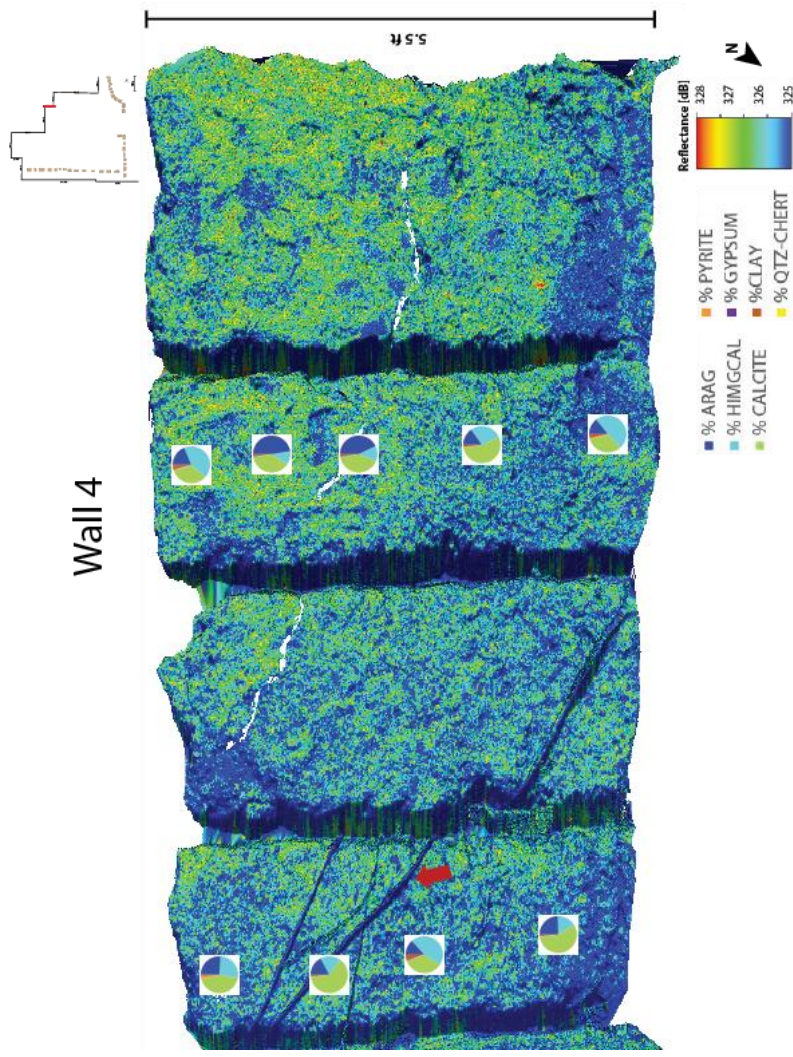


**Figure 33: Reflectance of wall 4 with XRF scan results. The white line traces over a possible discontinuity surface. This wall contains more of the 'non-core' components (pyrite, gypsum, clay, quartz-chert) than other walls. The linear features pointed out by the red arrow are tree roots that were edited out (area with no data), which is why they reflect blue.**

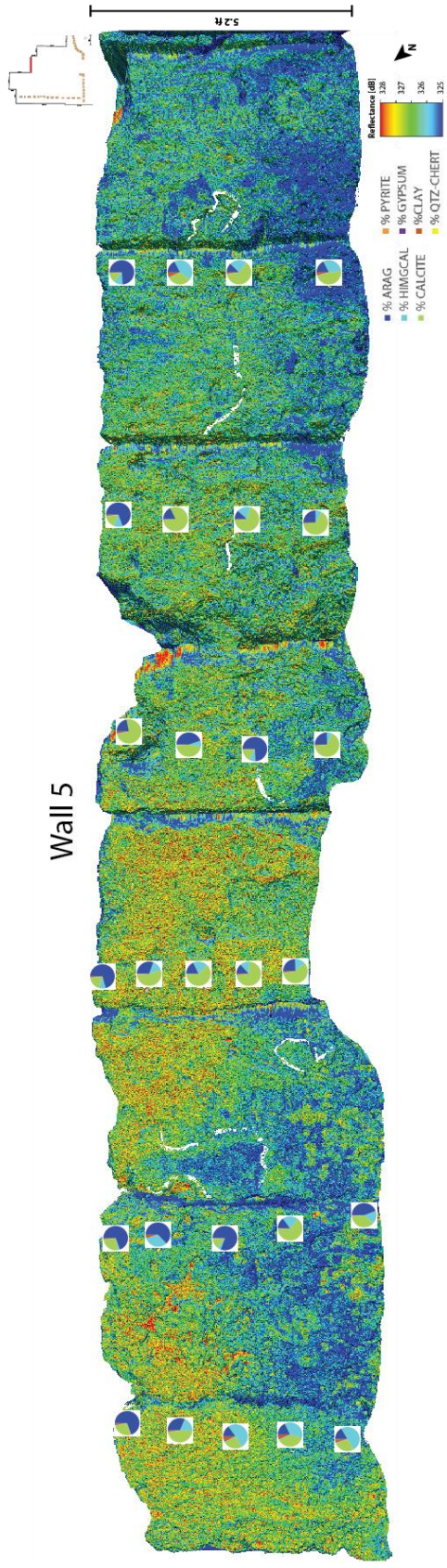


**Figure 34: Reflectance of wall 5 with XRF scan results. The white lines trace over possible discontinuity surfaces.**



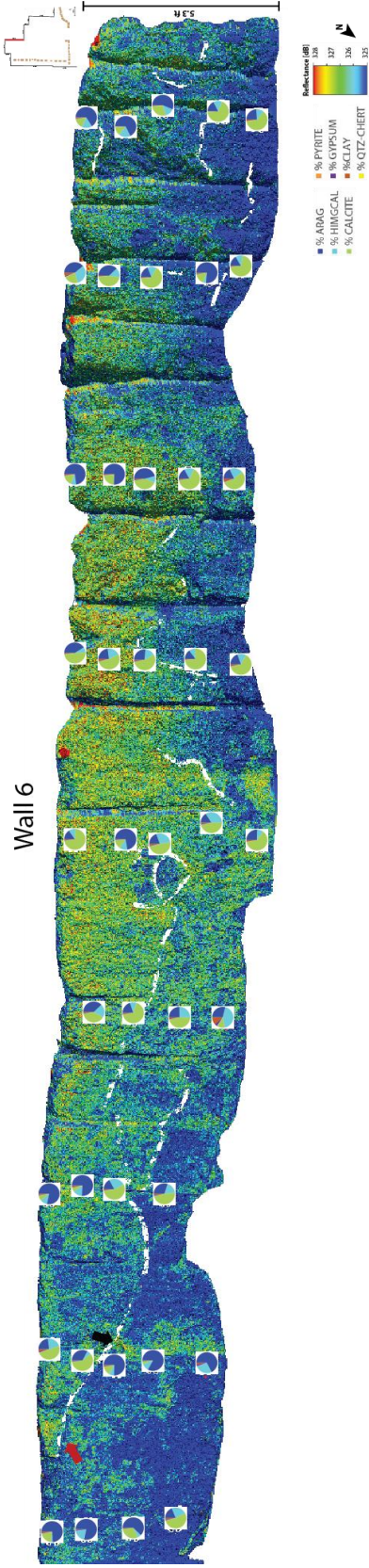


**Figure 35: Reflectance of wall 6 with XRF scan results. The white lines trace over possible discontinuity surfaces. The left half of this wall is the area Fruijtier et al. studied in 2000. The discontinuity surface pointed to by the red arrow is coated by high Mg calcite, which does not act as a seal. The surface looks to have been breached (black arrow) by fluids which seeped downwards. These fluids aided the inversion of aragonite to calcite.**

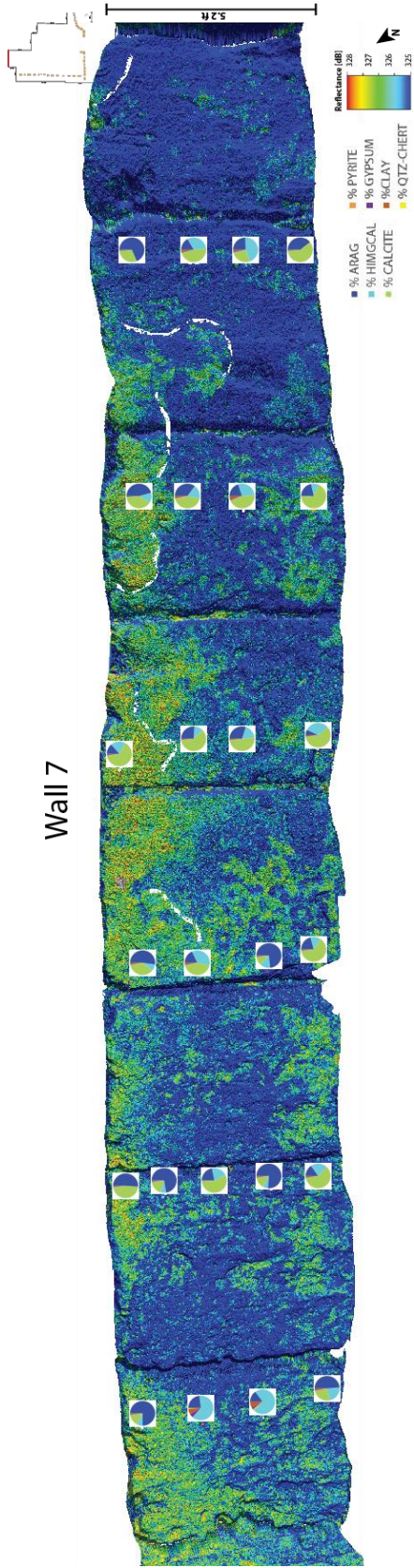


**Figure 36: Reflectance of wall 7 with XRF scan results. The white lines trace over possible discontinuity surfaces. There has been more diagenesis near the top and bottom of the wall due to the excess of low Mg calcite.**

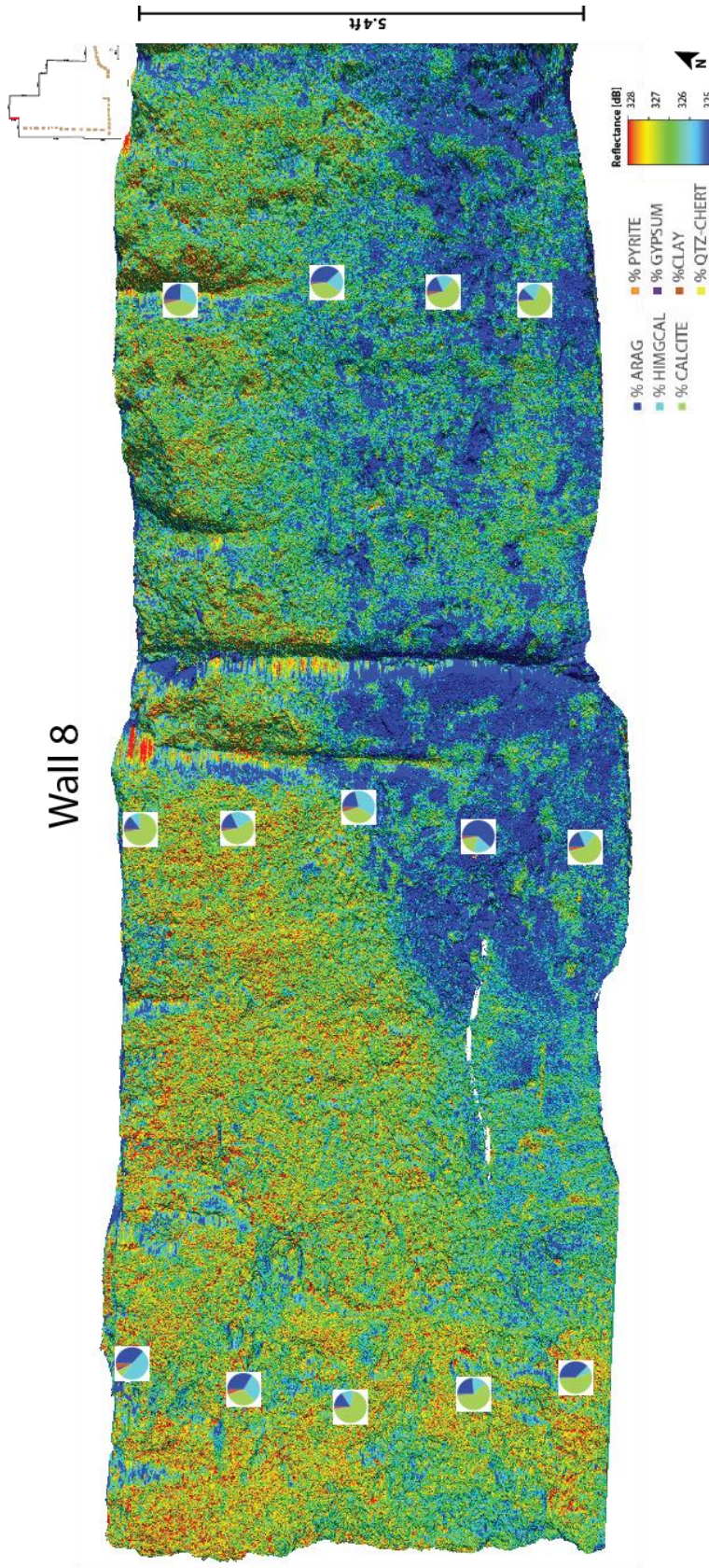


**Figure 37: Reflectance of wall 8 with XRF scan results. The white line traces over a possible discontinuity surface. In this case, the surface has planed off a colony of *M. annularis* (Figure 4D).**

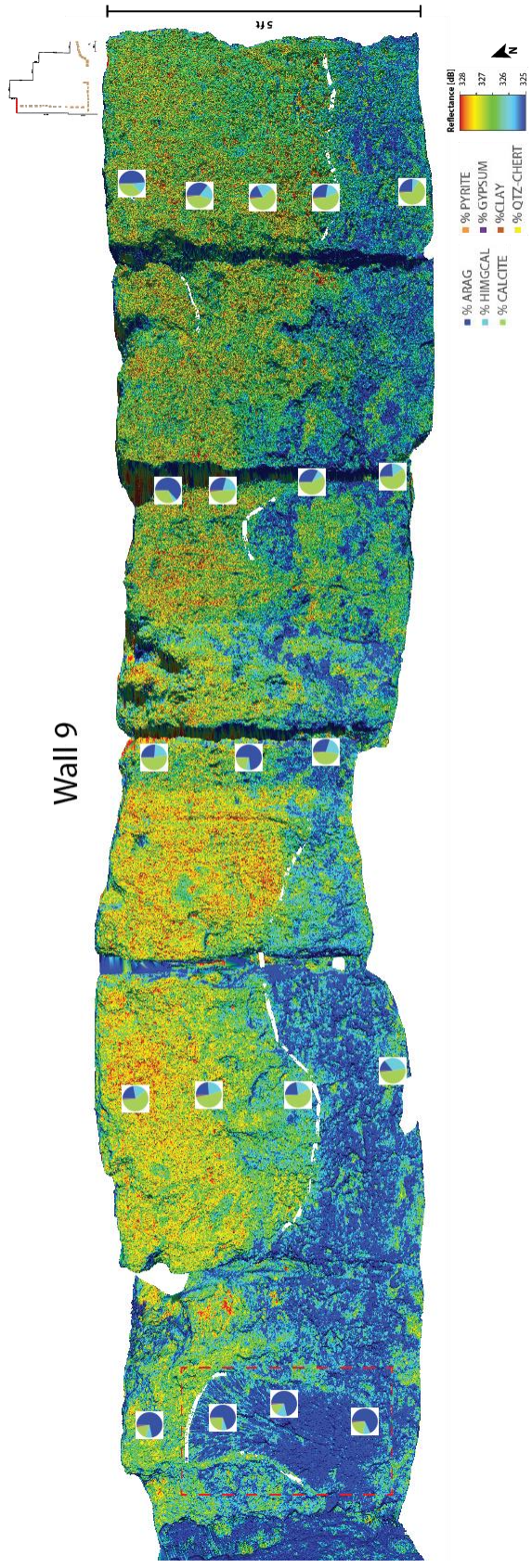


**Figure 38: Reflectance of wall 9 with XRF scan results. The white lines trace over possible discontinuity surfaces. The surfaces on this wall look similar to the surface through wall 6, which could be the result of a large storm event. Figure 39 zooms in on the large Diploria inside the red box.**

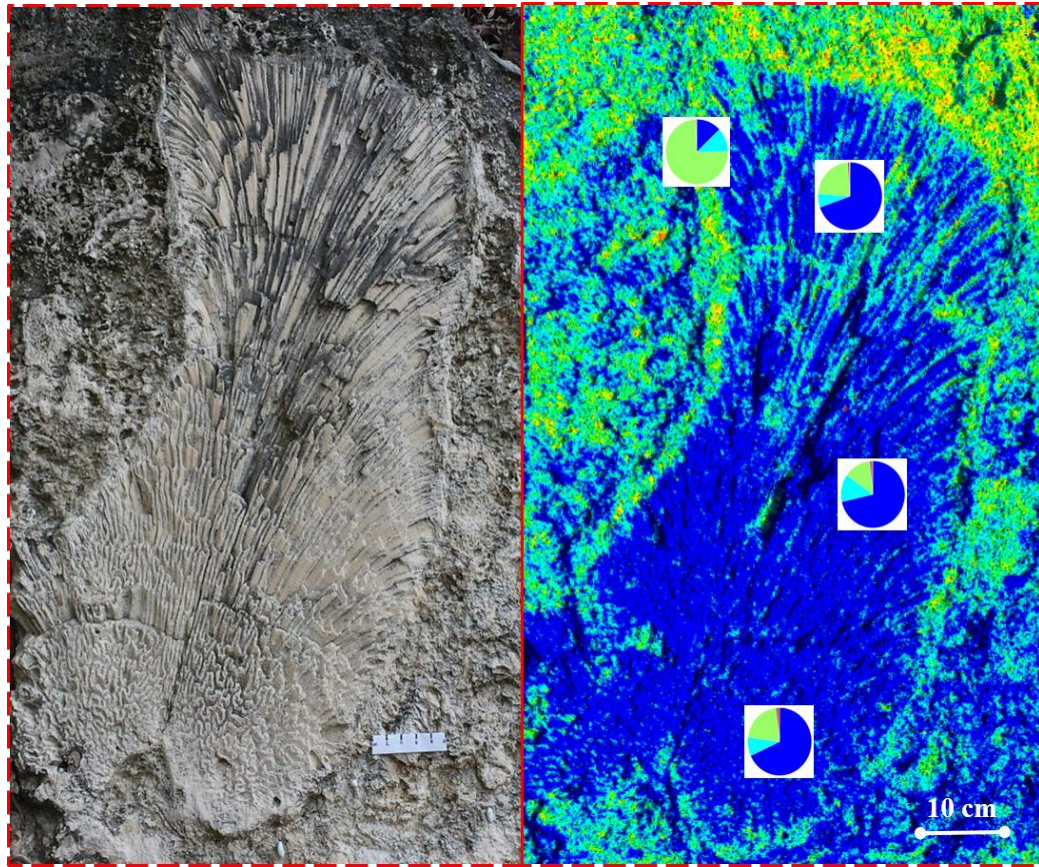


**Figure 39: *Diploria labyrinthiformis* surrounded by a high and low Mg calcite coating. This surface is not erosional, it is diagenetic. This type of surface is found coating most well preserved corals. The coral is surrounded by calcite mud and rubble, which is not a product of a long term sea level fall but more likely a product of a short term super storm. The top left XRF measurement is an extra scan taken to determine the mineralogy of the surface, which is mainly low Mg calcite (a seal).**

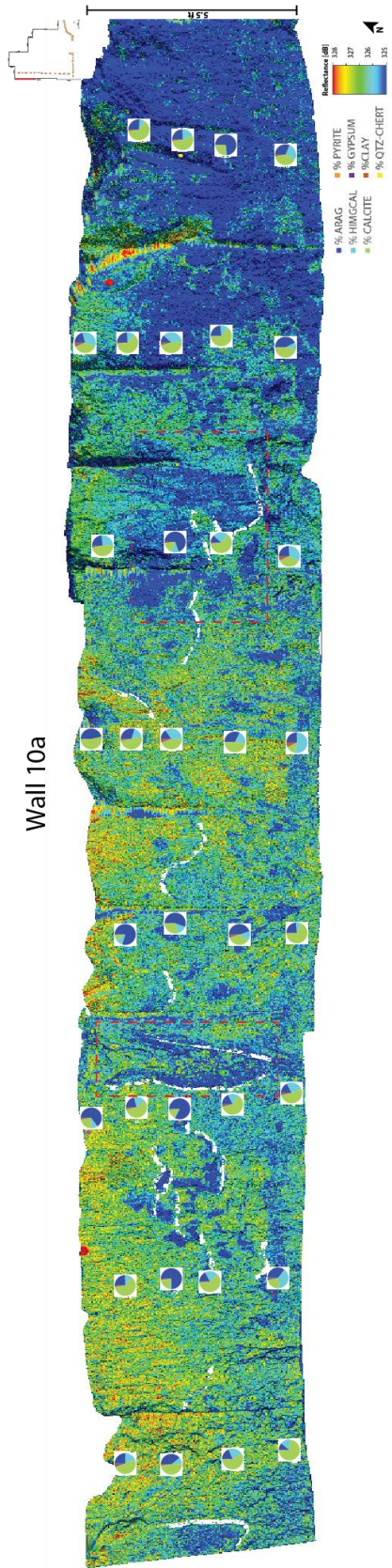


**Figure 40: Reflectance of half of wall 10 with XRF scan results. The white lines trace over possible discontinuity surfaces. Most of the surfaces are diagenetic as they are coating well preserved corals with low Mg calcite. There are two red boxed areas. The one on the right, Figure 41, zooms in on a possible sediment chute, or karst. The other, Figure 42, zooms in on another sediment chute or karst, but this chute or karst is filled with clastic and carbonate material.**

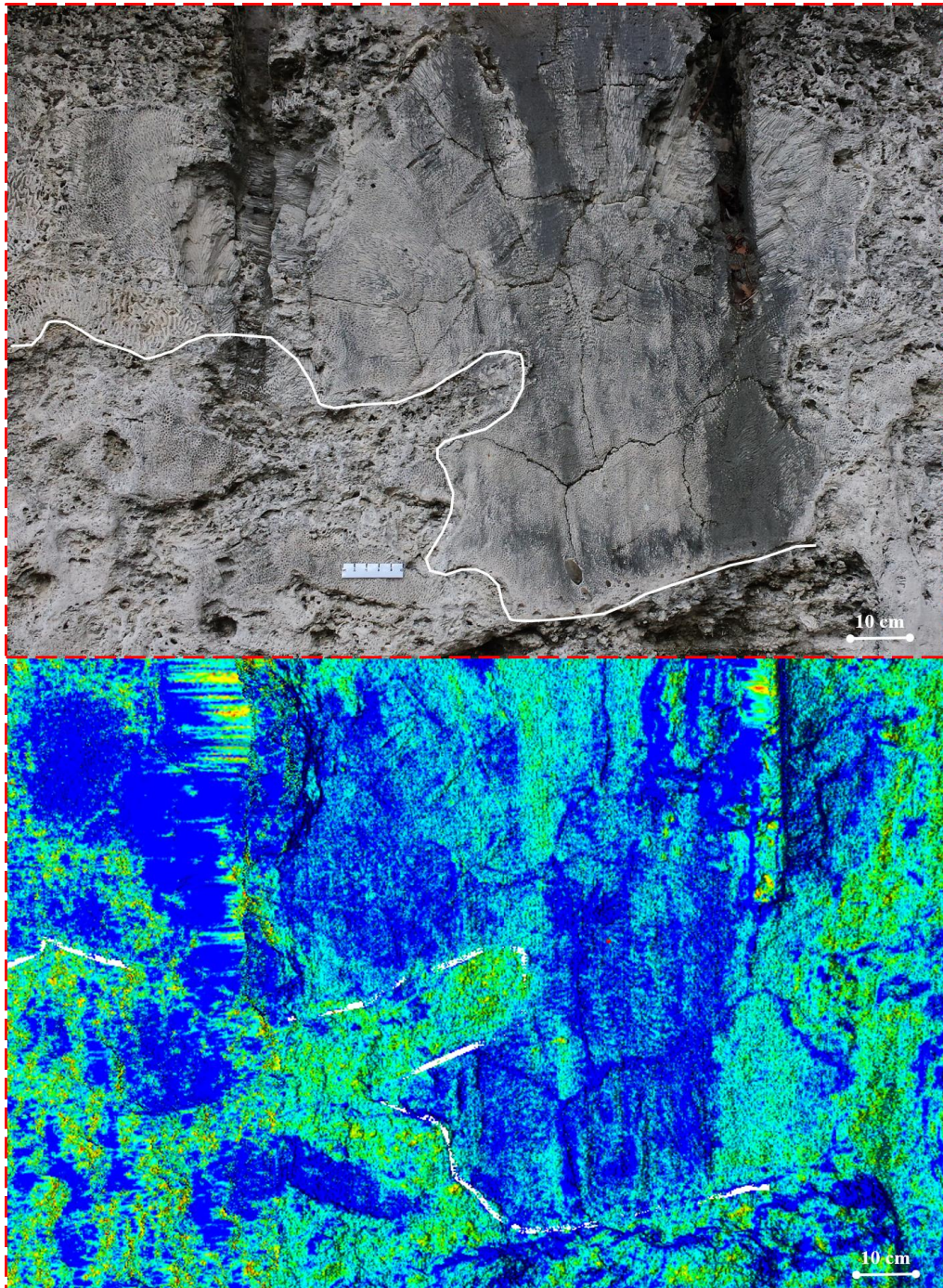


**Figure 41:** On top is a photo and the bottom is a LIDAR reflectance image. The sediment chute or karst is calcite rich and has eroded through a large *M. annularis*. To the left, the surface has also cut a *Diploria* in half.

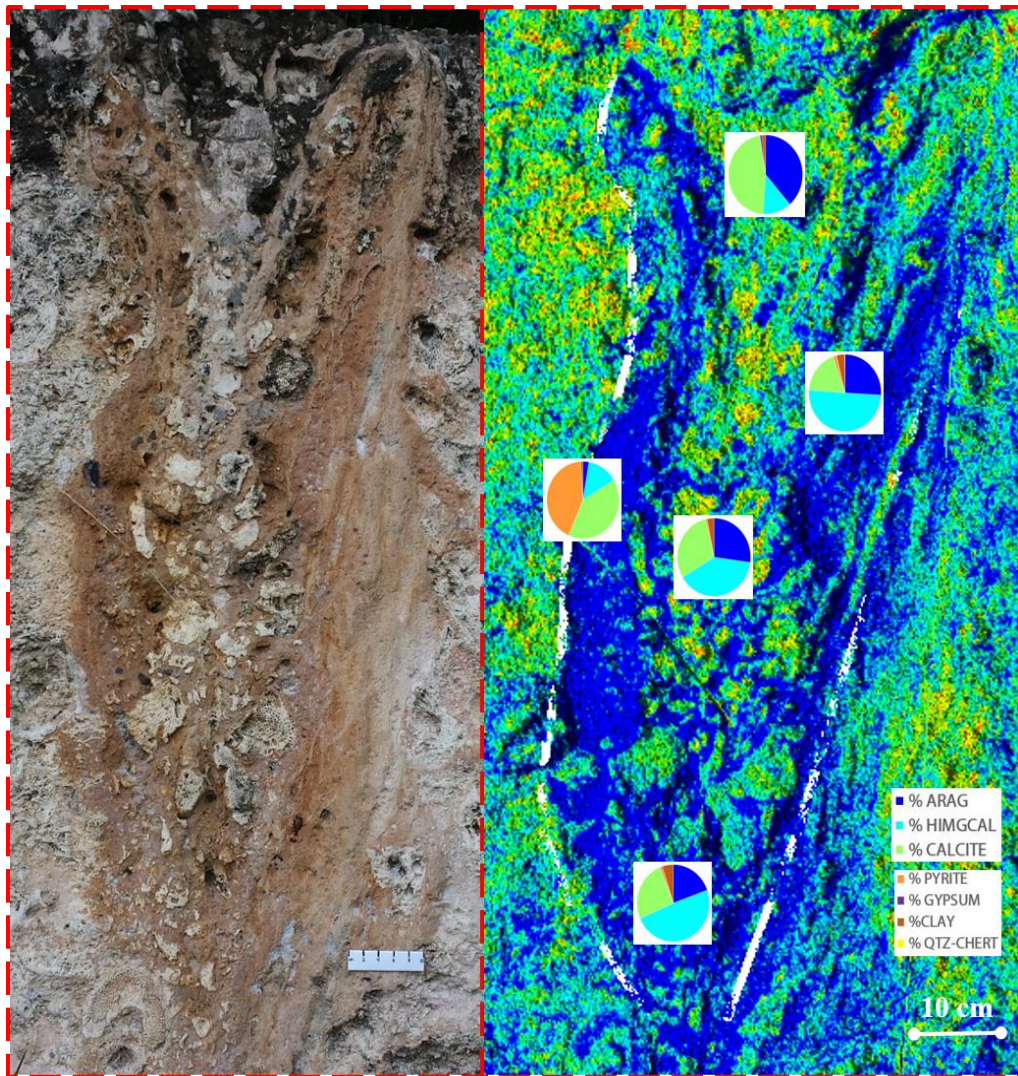


**Figure 42: The photo on the left was taken with an iPhone and the image on the right is LIDAR reflectance. This sediment chute or karst is filled with both clastic and carbonate material. There are large, well rounded, and angular clasts of chert and quartz, which suggests some sediments traveled further than others and not from the same source. A super storm would be capable of collecting materials originally from different environments and depositing them in the same place. The red material is fine loess from Africa.**



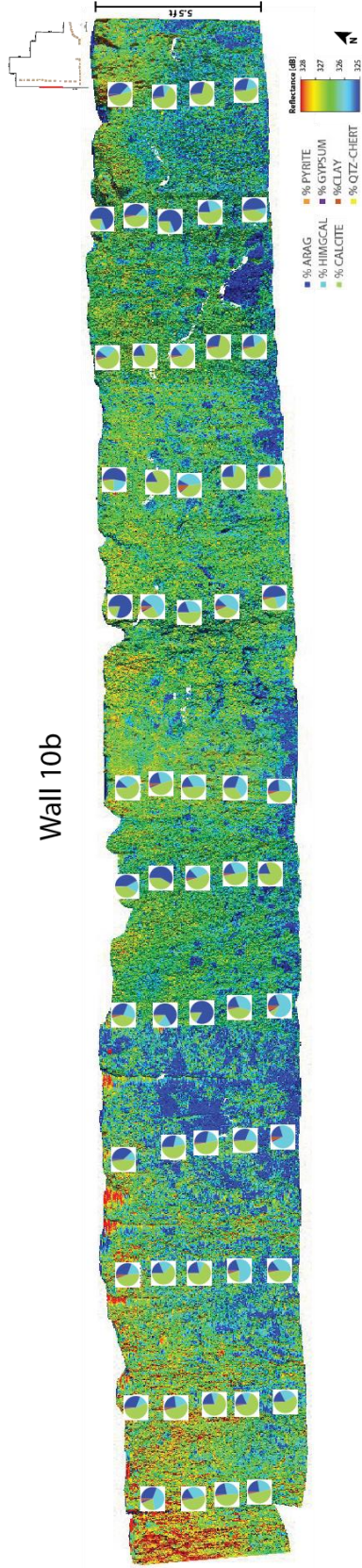


**Figure 43: Reflectance of the other half of wall 10 with XRF scan results. The white lines trace over possible discontinuity surfaces. Most are diagenetic surfaces coating well preserved corals. This wall contains more low Mg calcite than other walls, which infers this area was exposed to more meteoric fluids.**

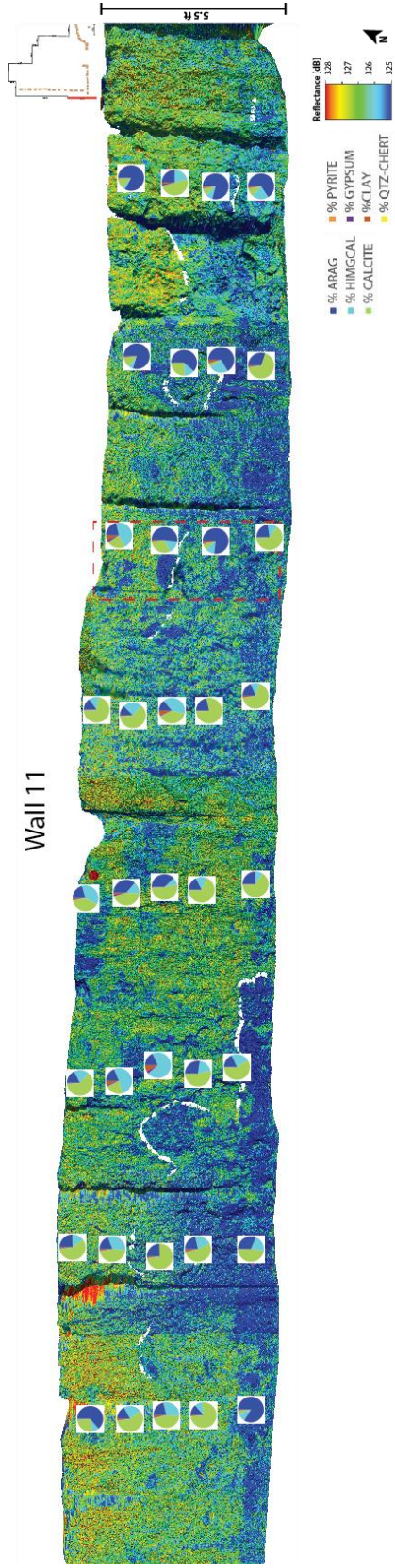


**Figure 44: Reflectance of wall 11 with XRF scan results. The white lines trace over possible discontinuity surfaces. Figure 45 shows an area where *M. annularis* appear both above and below a discontinuity surface.**

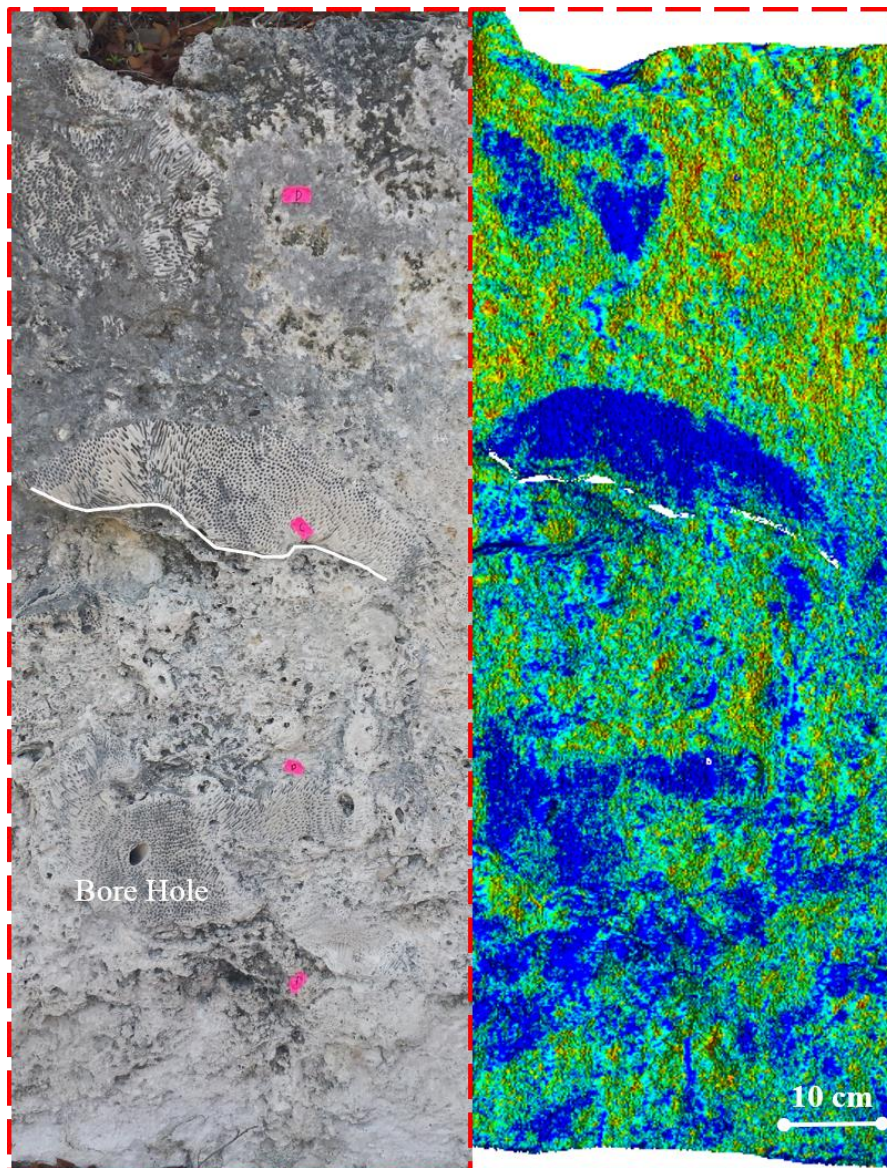


**Figure 45: iPhoto image on the left and LIDAR reflectance on the right. The large, broken in half, *M. annularis* in the middle is mainly aragonitic and coated by a high Mg calcite (light blue) rim/surface. The wall becomes more low Mg calcite rich above the discontinuity surface but there is no change in species diversity: there are *M. annularis* above and below the surface. *M. annularis* thrive in low energy environments; thus, if there were a sea level change *M. annularis* would not continue to grow in the same place as before.**

## 4.2 Diagenesis

Diagenesis refers to any physical or chemical change to a sedimentary rock that occurs after deposition (Scholle and Ulmer-Scholle, 2003). Diagenesis includes processes such as cementation to produce limestone and dissolution to form cave systems. It also aids in the development of microporosity and changes in trace element and isotopic signatures (Tucker and Wright, 1990). The key minerals that compose a carbonate rock are calcite, aragonite, dolomite and high Mg calcite. Carbonates in marine pelagic oozes and some lacustrine environments are mainly composed of calcite, where carbonates in shallow marine and/or tropical environments are composed of high Mg calcite. High Mg calcite is precipitated by calcareous skeletons, cements, and some ooids (Tucker et al., 1990).

During the time of coral growth in the Sangamon, the sea was supersaturated with respect to aragonite. In other words, this was a time of an aragonitic sea, so any low Mg calcite present in the rock record formed diagenetically. Aragonite can transition into calcite by inversion or cementation (Elmore, 2015). Inversion is the replacement of one polymorph of a mineral by another (Scholle et al., 2003), in this case, aragonite inverting to calcite. Cementation is the filling of open pore space with newly precipitated materials (Scholle et al., 2003), which is also known as solution reprecipitation (Elmore, 2015).

Therefore, since the aragonite in Windley Key Quarry is both pristine and in some cases inverting to calcite without isopachous cement, the quarry was likely not subjected to a fresh water phreatic zone, but only a marine and then a fresh water vadose zone. Sediments exposed to a phreatic zone, also known as the saturated zone,

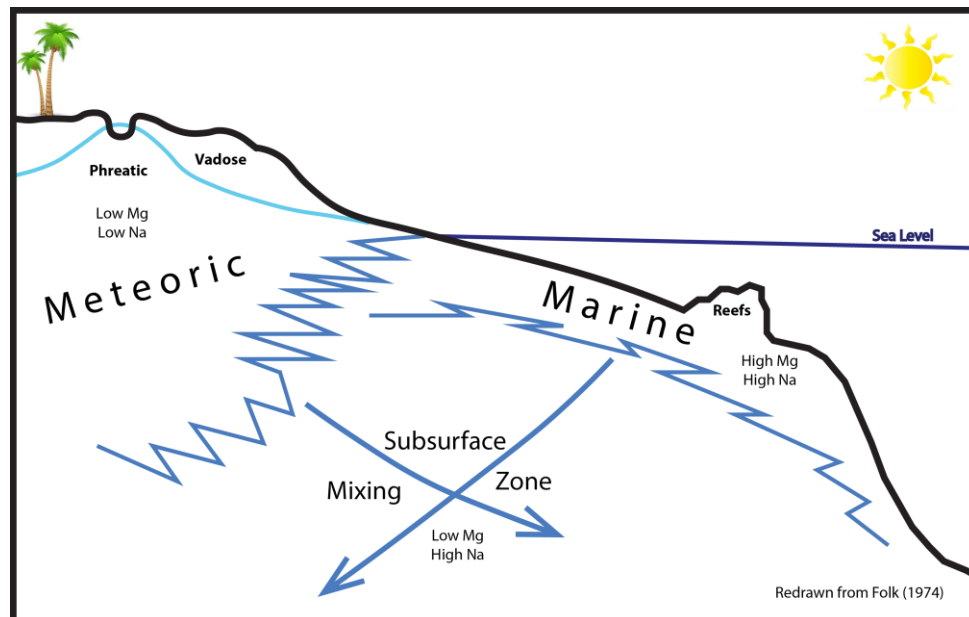


**Figure 46: Cartoon demonstrating the interaction of the meteoric vadose and phreatic zones with the marine zones. The Key Largo Limestone grew on the marine shelf until a super storm ripped it up and deposited it in the vadose zone where it was diagenetically altered.**

would form isopachous calcite cement (Folk, 1974), which is not seen in Windley Key Quarry. The vadose zone, also known as the unsaturated zone, lies closest to the surface (Figure 46) where pore spaces are filled with air and fresh water (Folk, 1974). Here, dissolution features are found, such as, solution enlarged fractures, sinkholes, caves, or collapse breccias (karst features) (Scholle et al., 2003). These karst features are common in Windley Key Quarry (refer back to Figures 41 and 42), which suggests vadose zone diagenesis.

LIDAR reflectance data shows calcite and aragonite reflect light differently. This is not due to their chemistry ( $\text{CaCO}_3$ ), but instead their mineral structure. Aragonite is orthorhombic and calcite is rhombohedral (Tucker et al., 1990). Further, low Mg calcite and high Mg calcite reflect light differently. Possibly this is analogous

to Raman spectroscopy. Bischoff, Sharma and Mackenzie (1985) found Raman spectral shifts and band halfwidths increase regularly with increasing magnesium content of synthetic calcites but show much more scatter for skeletal calcites. This is due to the effects of Mg bonding with CO<sub>3</sub> groups. The substitution of Mg into the calcite lattice causes disorder (Tucker et al., 1990).

The presence of low Mg calcite surrounding preserved aragonite throughout the quarry suggests meteoric alteration, possibly due to a large storm event, which briefly exposed the coral reef to foreign solutions that escalated the inversion of aragonite to calcite. The amount of aragonite still present likely suggests the formation was rapidly buried by storm deposits and minimally exposed to fresh water.

#### **4.3 Evidence for Tempestite**

To break a *Montastraea annularis* at 10m depth (a maximum inferred depth for this Key Largo Pleistocene reef) takes considerable wave energy. To fracture these massive corals greater than 44 meganewtons/meters<sup>2</sup> is required (Chamberlain, 1978). In 1978, Chamberlain studied the mechanical properties (compressive strength, energy absorption, and fracture patterns) of common corals in the Caribbean in order to understand the effects of storms, or excessive weight, have on coral colonies. Figure 47 shows the effect of stress and strain on a *M. annularis* sample.

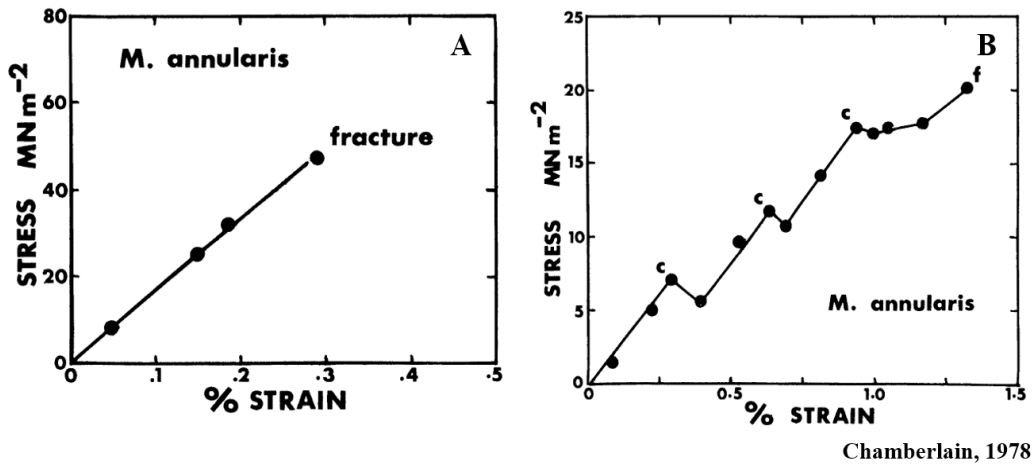


**Figure 47: Stress-strain plots for *M. annularis*. (A) If the coral does not crack, it will dislodge after being exposed to around 40 MN/m<sup>2</sup>. (B) Each small peak represents the onset of a crack which was, by itself, too small to cause dislodgment. The sharp reduction in stress after each crack is the release of stored strain energy. Stress continues to build and eventually after several cracks develop the coral is dislodged/ fractured completely.**

The calculation of the minimum wave height required to exert that much power seems trivial, but in fact it is quite complicated. There are several methods to determine paleo wave conditions, but Dupré (1984) believes the most accurate equations are those which relate wave height (H) to maximum orbital velocity ( $U_{max}$ ).

$$\text{Equation 1: } H = T \sinh(2\pi h/L) U_{max}/\pi$$

$$\text{Equation 2: } H = T \sinh(2\pi h/L) (U_{max} - \Delta U_{max}/2)/\pi$$

Equation 1 is based on Airy wave theory and Equation 2 is a modified Stokes 2<sup>nd</sup> order equation which neglects mass transport (Dupré, 1984). In order to use either equation it is necessary to know the water depth (h), wave period (T), and maximum orbital velocity ( $U_{max}$ ). In the case of this paper, only the water depth is known: 10m. One could calculate the equations many times using various wave periods and orbital velocities in hopes to identify a trend, but there are too many unknowns to make a valid hypothesis. Further work on the properties of storm waves during the Sangamon is

required; however, there is anecdotal evidence of the intensity of a storm that would be required.

The most active hurricane season recorded in the Atlantic and Gulf of Mexico occurred in 2005 which was due to higher than normal sea-surface temperatures. A post-hurricane assessment of Category 3 Hurricane Rita was made, which passed near East Flower Garden Banks, a coral reef in the northwestern Gulf of Mexico (NOAA, 2015). The passage of Hurricane Rita caused water temperatures to drop by 2-3°C that lasted about 38 days (Robbart, Deslarzes, Precht, Aronson, Zimmer, Duncan, Deis, Sinclair, Hickerson, Schmahl, and Boland, 2008). Hindcast hydrodynamic models estimated wave heights greater than 20m on the banks that left bank caps exposed at 20-30m depths (NOAA, 2015). Additional assessments by Robbart et al. (2008) record substantial mechanical impacts, sediment-scoured corals resting atop large sand flats (Figure 48), dislodged and fractured corals (Figure 49) as well as corals gouged from water-borne projectiles (Figure 50). Robbart et al. estimated Hurricane Rita removed around 1.5% of coral colonies (mostly *D. strigosa*, *P. astreoides*, and *M. annularis*) and found one dislodged coral colony that was 4m across and 2m in height. Thus, one may surmise that wave heights of 20m+ at the assumed water depths (10m) would have caused the observed discontinuity surfaces.





**Figure 48: Sediment-scoured corals atop a large sand flat at the East Flower Garden Banks. The scouring and sand removal were caused by the passage of Hurricane Rita in 2005. Photo by E. Hickerson, FGBNMS. (Robbart et al., 2008)**

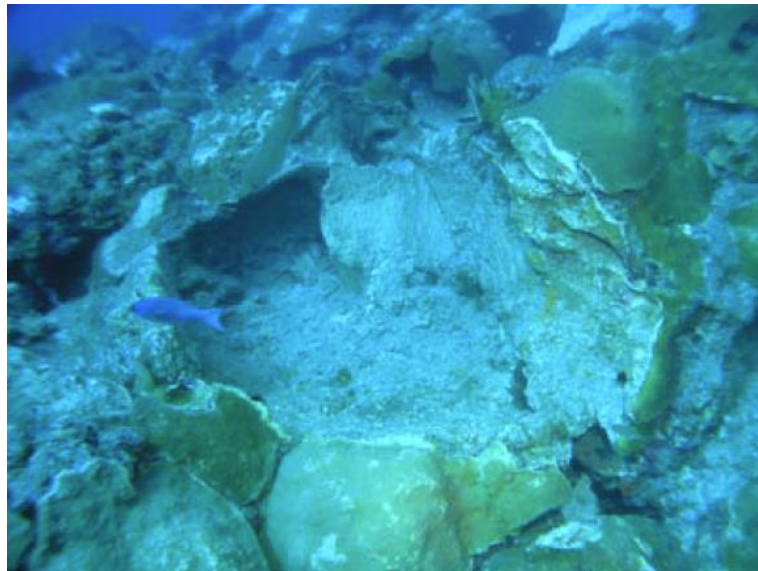


**Figure 49: This depression marks the location a coral colony used to thrive, but was dislodged during Hurricane Rita in 2005. Photo by E. Hicketson, FGBNMS. (Robbart et al., 2008)**

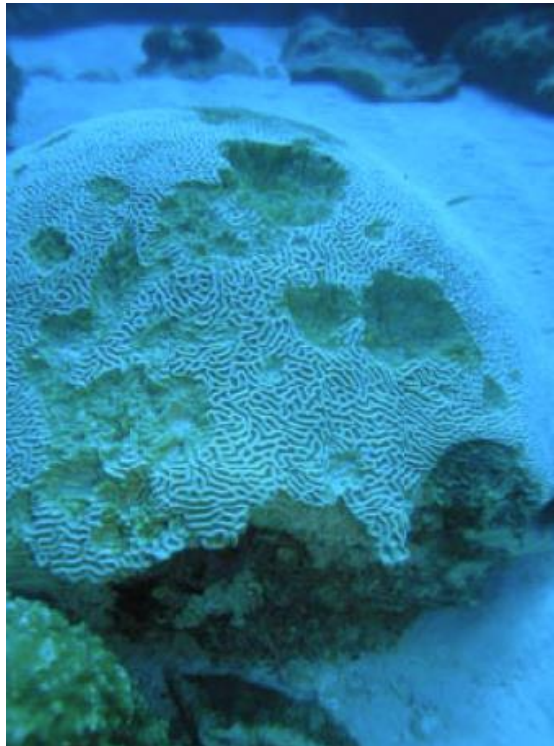
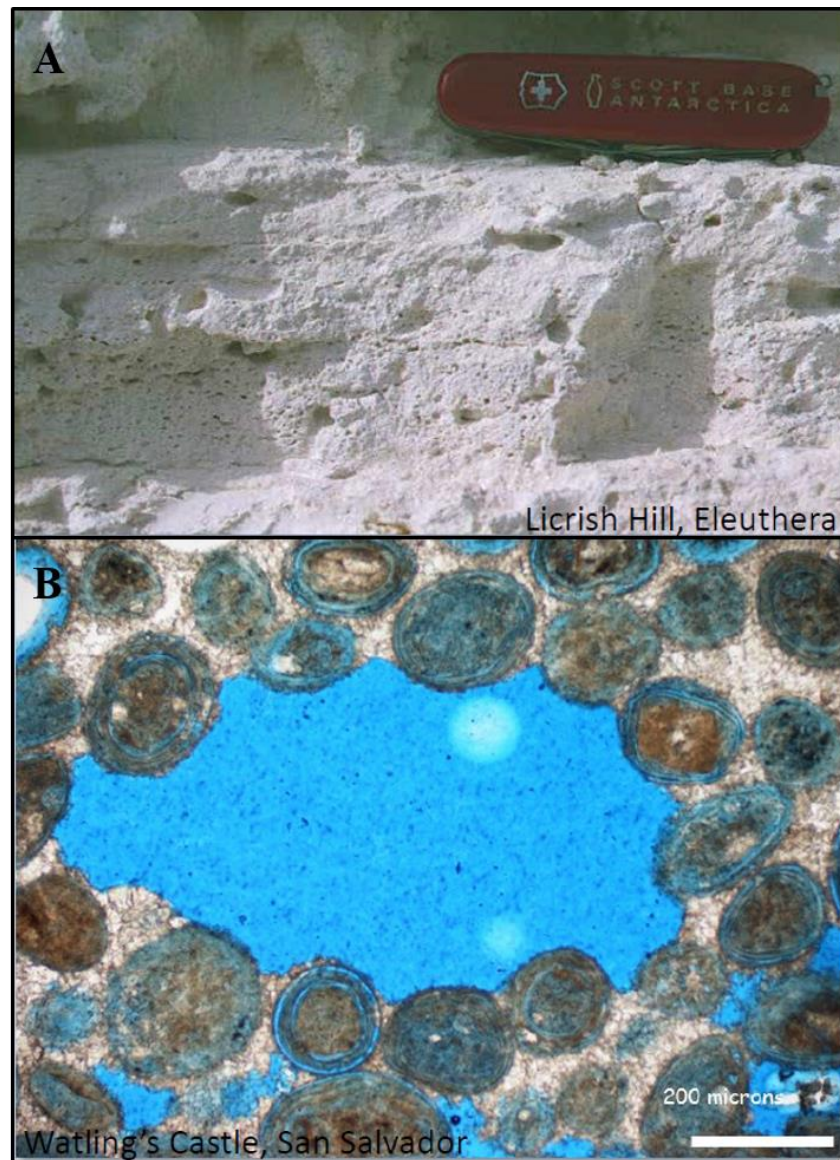


**Figure 50: *Diploria strigosa* gouged by waterborne projectiles during Hurricane Rita. Photo by E. Hickerson, FGBNMS. (Robbart et al., 2008)**

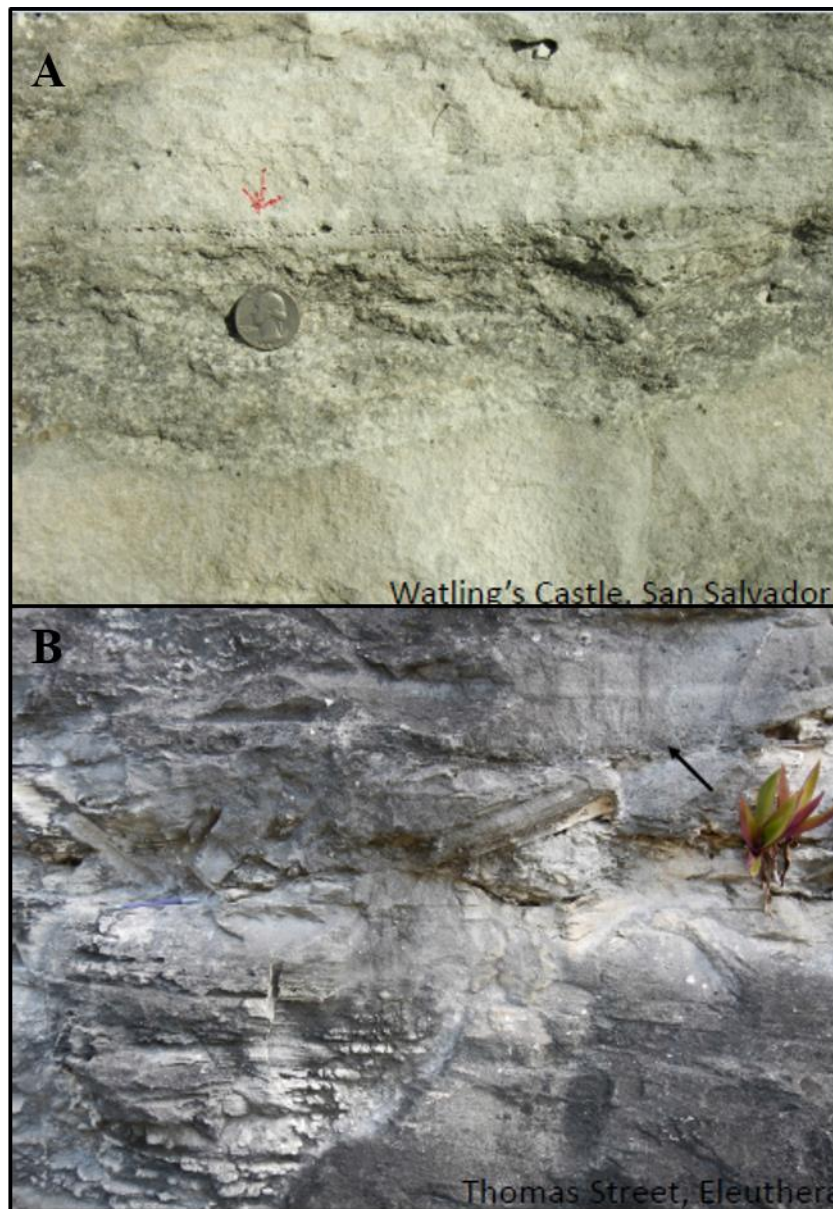
Donovan and Tormey (2015) found evidence of extreme storm activity in carbonate eolianites across the Bahama Bank. To the north, lowland dunes were run over by storm waves and reworked into storm-beach ridges with tabular, fenestrae-rich beds with minor remnants of eolian cross-beds and root structures. Fenestrae found in eolian beds at 43 m asl and other high elevation dunes suggest major storm events passed through the Caribbean as climate rapidly destabilized toward the end of the last interglacial (MIS 5e) (Donovan et al., 2015). Figure 51 shows fenestrae beds and its petrographic signature. Donovan et al. (2015) also found rip up clasts and scoured beds further south in more central Bahamas. (Figure 52).



Donovan et al. (2015)

**Figure 51: (A) Fenestrae beds in an eolian dune in northern Bahamas. These features are common near shore, but this dune is located at high elevations.**

**The fenestrae were rapidly buried and cemented because they are well preserved. Being so well preserved and observed at a high elevation suggests storm activity. (B) Thin section focused on one fenestrae bubble. Notice how cement surrounds, but does not fill the pore.**



Donovan et al. (2015)

**Figure 52: (A) Fenestrate beds with a scoured base. (B) Imbricated rip up clasts.**

White et al. (1998) used  $\delta^{18}\text{O}$  values to predict the global temperatures during the Sangamon (Figure 53). Around 125 ka, as pointed out by the red arrow, temperatures rapidly declined. This decrease caused polar ice sheets to grow and sea level to recede. As Donovan et al. (2015) mentions, this dramatic shift in temperature

would cause chaotic and extreme weather. The first stage of reef growth occurred 132-125 ka when the ice core data (Figure 53) shows global temperatures were around 4°C higher than the Holocene average, then around 126-125 ka temperatures fell 9°C, to about -5°C, which corresponds to a rapid sea level fall that terminated coral growth and led to erosion and fresh water diagenesis (White et al., 1998). Between 124-119 ka

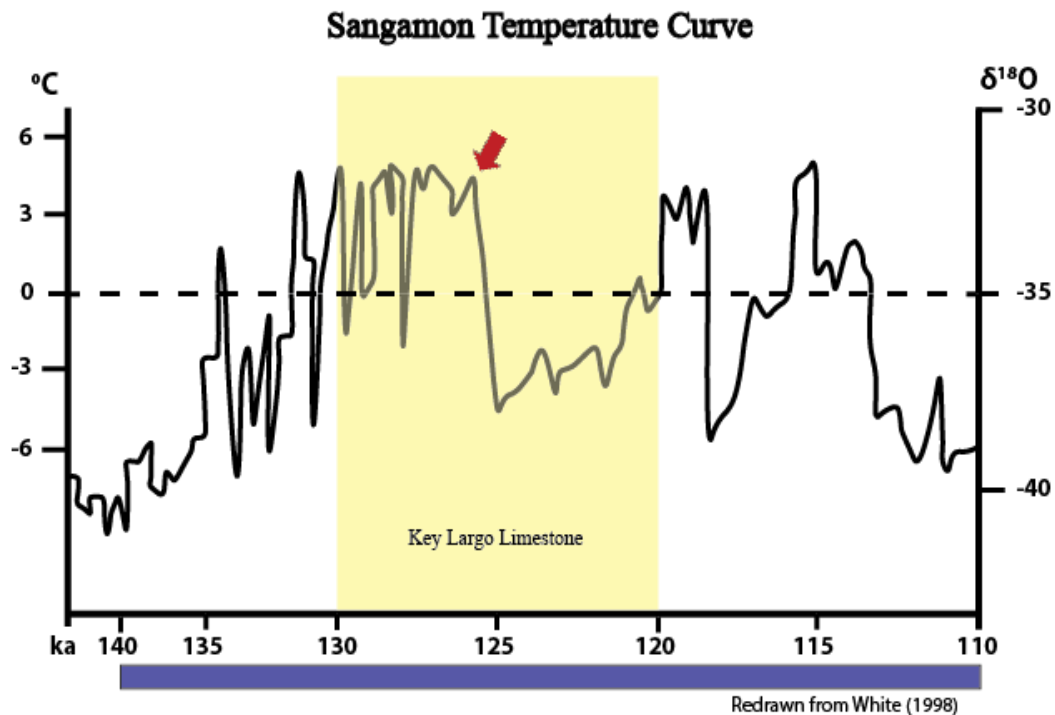


**Figure 53: Global temperature curve during the last interglacial based on oxygen isotopes from a Greenland ice core. The dashed line represents the average present day temperature. Data collected by GRIP members in 1993.**

temperatures, thus sea level, fluctuated but were gradually rising. These instabilities may have altered global meteorological patterns and invoked severe weather.

During a hurricane, wave heights, thus strength, greatly increase putting corals in danger. A hurricane is a warm-core, low-pressure system that develops over tropical or subtropical waters. A trough of low pressure draws air inward which creates very

strong winds that produce large waves (Heron, Morgan, Eakin and Skirving, 2005). These powerful waves are able to carry large boulders and debris on the sea floor to surface where they could pass through a coral reef and demolish it, as if in the way of a wrecking ball. Once exposed, abrasion from sand moving across a hardground could produce a flat surface, cutting borings and encrusts (Tucker, 1990).

#### **4.4 Evidence of a Sea Level Fall**

On the contrary, several investigators such as White et al. (1998) believes the discontinuity surfaces and abnormal features in the Key Largo Limestone are the result of a brief sea level lowstand during the last interglacial and not the product of a massive storm. White et al. (1998), as well as Fruijtier et al. (2000) (mentioned in previous work), used U-Th ages of corals in the Bahamas and related them to an erosional surface. White et al. (1998) also found younger rocks beneath an erosional surface and older ones above it (analogous to the U-Th inverse stratigraphic ages reported by Fruijtier et al., 2000), and believes this vertical juxtaposition indicates a time window for a regression-lowstand-transgression sequence in the range of 1.1 to 1.5 ka (Figure 54). Sea level fell approximately 10m to current day sea level and must have maintained this lowstand level for a long, but unknown, period of time to abrade and disrupt the coral reef and wave cut platform to their current condition (White et al., 1998). White et al. (1998) compared the U/Th isotope data (Figure 54) to GRIP member's ice core data (Figure 53) to show there was a time window of 1,500 years or less where their hypothesized rapid regression/lowstand/transgression cycle occurred.

Uranium/Thorium Ages of Corals in the Bahamas

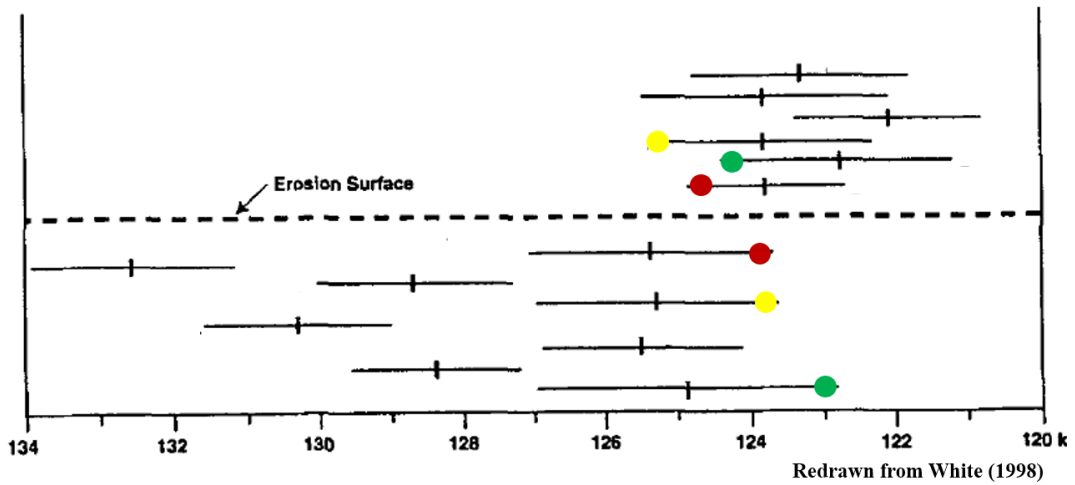


**Figure 54: Diagram showing the U/Th ages of corals in relation to an erosional surface hypothesized to have formed during the mid-Sangamon from either a sea level lowstand or a massive storm. Horizontal scale is in thousands of years (ka) and there is no vertical scale. The red, yellow and green dots are a few reference points to show that in some cases, there is a younger coral stratigraphically below an older coral. Multiple coral species were sampled.**

White et al. (1998) found corroded surfaces along the top of large coral heads of *M. annularis* and *Diploria* fossilized in growth position, which is also seen inside Windley Key Quarry. They mapped the surface around a few reefs and found the corals beneath the erosional surface were truncated with occasional lithophagid borings within the corals. In other areas the surface was bored by sponges, and these borings were encrusted by corals (White al., 1998). White et al. (1998) also found fissures, erosional channels and small caves around the Bahamas, which they claim most likely formed during the sea level lowstand and cut through both *in situ* corals and associated lithified subtidal sediments. Figures 55 and 56 show those features seen in the Bahamas are also seen in Windley Key Quarry. Similar to the features in the Bahamas, these probably

formed when sea level rose, or during a storm event, which caused an influx of sediments to fill voids between corals and in some places actually dislodge or tear apart corals.

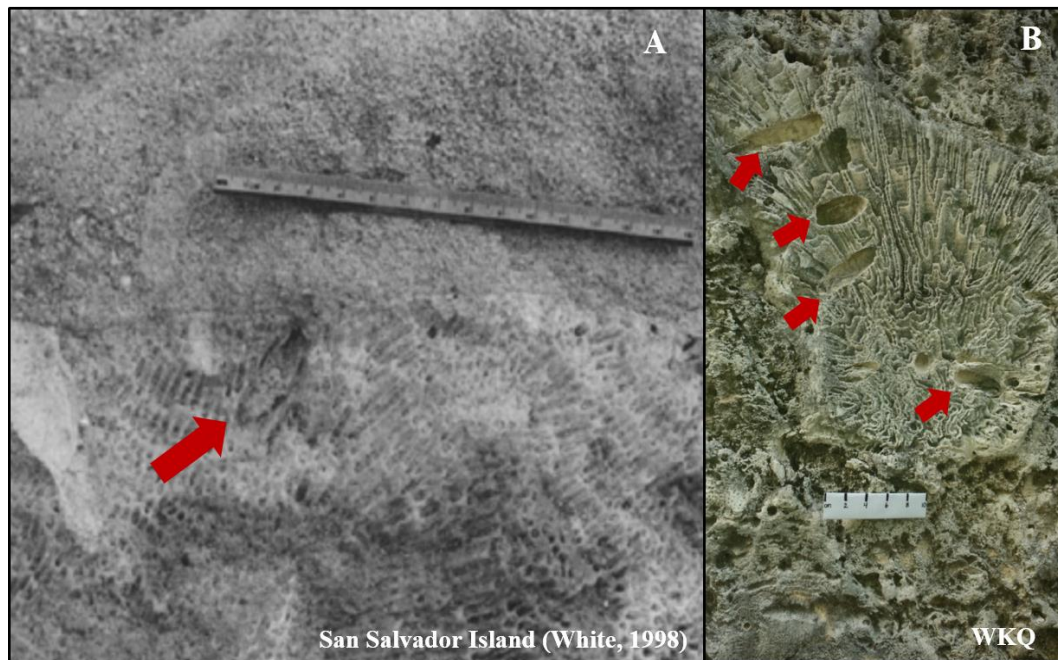


**Figure 55: (A) Truncated *M. annularis* and a lithophagid boring (red arrow) from the Bahamas. (B) Truncated *Diploria stirgosa* surrounded by a calcareous matrix with similar borings (red arrows). The scale on the right is 10cm.**

The discontinuity surfaces seen in Windley Key Quarry are not the product of a sea level fall. A gradual change in sea level would not disrupt the corals as they are now. If sea level changed during the time seen stratigraphically in Windley Key Quarry, there would be a clear change in species diversity. Throughout the quarry *M. annularis* are found at the bottom, middle and top of the walls. As mentioned earlier, *M. annularis* will only be found in quiet, low energy marine environments so even a rapid change in sea level *M. annularis* would not survive.



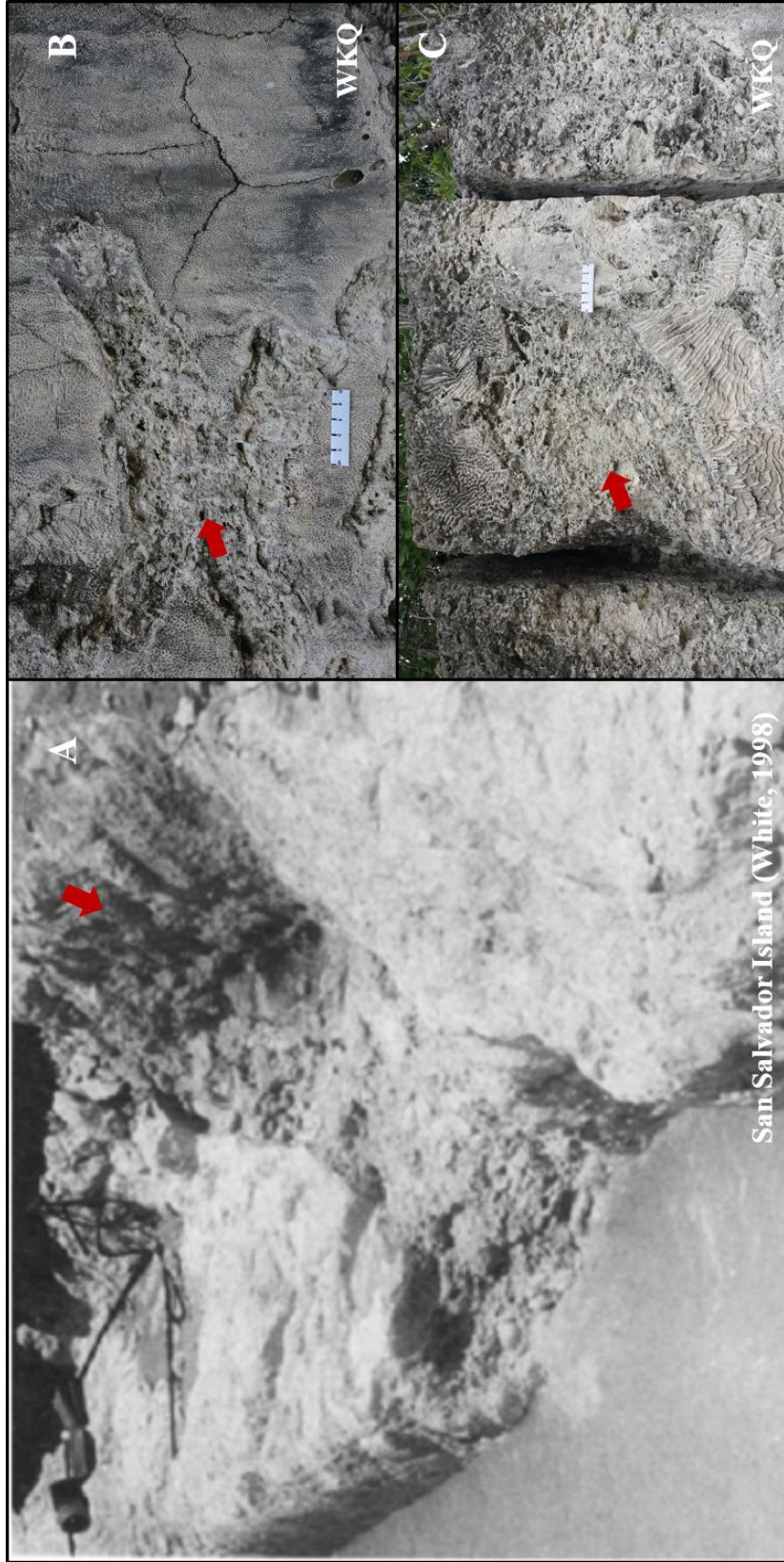


**Figure 56: (A) Sediment filled cave in the Bahamas. (B) Sediment cave in Windley Key Quarry. (C) Another possible sediment cave inside Windley Key Quarry. All three photos look very similar. The scale in (B) and (C) is 10cm.**

## Chapter 5: Conclusion

### 5.1 Conclusions

After collecting, processing, and interpreting LIDAR and XRF data of the Sangamon Key Largo Limestone Formation inside Windley Key Quarry, FL the following deductions are recognized:

1. Light Detection and Ranging (LIDAR) is an excellent supplementary outcrop investigation instrument, which allows the user to view an area in three dimensions not only in its 'true color' but also in other attributes that can pick up on features not visible to the naked eye.
2. LIDAR reflectance between 325 and 328 dB illuminates calcium carbonate rich regions.
3. Elements detected by an XRF instrument can be converted to mineralogy then used to calibrate LIDAR reflectance.
4. Scans viewed using reflectance between 325 and 328 dB will color aragonite rich areas blue, low Mg calcite areas green/yellow and high Mg calcite areas light blue. Thus, aragonite is less reflective than calcite.
5. Most discontinuity surfaces inside Windley Key Quarry are erosional which originated from a massive storm event during the Sangamon. These surfaces are coated with high Mg calcite which acts as a fluid pathway, not seal.
6. Surfaces that surround and preserve corals are diagenetic and coated with low Mg calcite preventing fluid interaction and alteration.
7. Surfaces, that are not from either of the two options above, but also cut through corals, are karst features that allowed sediment to flow through zones of

weakness. These sediment chutes are filled with coral rubble (broken corals, brachiopods, mollusk shells, and low Mg carbonate mud)

8. Coral growth occurred during a time of aragonitic seas. Thus, the Key Largo Limestone, if unaltered, should be 100% aragonite. This is not the case which means at some time, during and/or after deposition, the formation transitioned from a marine to freshwater environment and was altered by vadose zone diagenesis.
9. There were definitely sea level fluctuations during the Pleistocene but none of which would be powerful enough to dislodge, fracture and burry corals fast enough to preserve their initial aragonite composition.
10. Fluctuations in temperature and sea level during reef formation in the Sangamon destabilized the climate which led to rare, massive and destructive storm events.
11. Either a large storm wave crashed on the reef and dislodged corals itself, or a storm wave carried an object through the water which came into contact with a coral and broke it like a hammer to a nail.

## **5.2 Recommendations for Future Work**

As one of Dr. John Pigott's first students to use LIDAR and investigate it with XRF, and as it is a novel approach, it took a long time to learn how to operate the scanner and the computer program RiscanPro. Now, being very confident with LIDAR's operations, I realize there is a lot more that could be done to strengthen future similar investigations. I recommend the following:

- Increase the study area. Scan the walls of channels leading seaward and other Key Largo Limestone outcrops to identify trends such as species diversity and discontinuity surface continuity.
- Import data into another computer program that is able to interpolate between the partial surfaces currently drawn to extract a 3D surface. With a 3D surface one would be able to see the lateral extent of a discontinuity surface which could infer its origin.
- Calculate the wave height, or the velocity of a traveling object through water, necessary to exert 50 meganewtons at 10m water depth. With the answer to this difficult problem, one could infer the type of super storm: a tsunami, hurricane, etc.
- Drill a core through discontinuity surfaces inside Windley Key Quarry, or elsewhere, and make thin sections to study the petrographic characteristics.

## References

- Antonioli, F., Kershaw, S., Renda, P., Rust, D., Bellomini, G., Cerasoli, M., Radtke, U., Silenzi, S., 2006, Elevation of the last interglacial highstand in Sicily (Italy): A benchmark of coastal tectonics: *Quaternary International*, v. 145-146, p. 3-18.
- Berggren, W. A., Kent, D. V., Swisher, C. C., and Aubury, M. P., 1995, Geochronology time scales and global stratigraphic correlation: *Society of Economic Paleontologists and Mineralogist Special Publication*, v. 54, p. 129-212.
- Bischoff, W. D., Sharma, S. K., and Mackenzie, F. T., 1985, Carbonate ion disorder in synthetic and biogenic magnesian calcites A Raman spectral study: *American Mineralogist* v. 70, p. 581-589.
- Burton, D., Dunlap, D. B., Wood, L. J., and Flaig, P. P., 2011, Lidar Intensity as a Remote Sensor of Rock Properties: *Journal of Sedimentary Research*, v. 81, no. 5, p. 339-347.
- Chamberlain, J., 1978, Mechanical properties of coral skeleton: compressive strength and its adaptive significance: *Paleobiology*, v. 4, no. 4, p. 419-435.
- Clari, P. A., Pierre, F. D., and Martire, L., 1995, Discontinuities in carbonate successions: identification, interpretation and classification of some Italian examples: *Sedimentary Geology*, v. 100, no. 1-4, p. 97-121.
- Dodd, R. J., Hattin, D.E., and Liebe, R.M., 1973, Possible Living Analog of the Pleistocene Key Largo Reefs of Florida: *Geological Society of America Bulletin*, v. 84, p. 3995-4000.
- Donovan, B. G., and Tormey, B. R., 2015, Sedimentary structures in carbonate eolinites as indicators of climate instability and intense storms during the last interglacial; Eleuthera Island, Bahamas *The Geological Society of America* v. 47, no. 7, p. 181.
- Dupre, W. R., 1984, Reconstruction of paleo-wave conditions during the late Pleistocene from marine terrace deposits, Monterey Bay, California: *Marine Geology*, v. 60, p. 435-454.
- Elmore, R.D., 2014, GEOL 5003: Diagenesis. Spring 2015. Unpublished Lecture Notes.
- Enos, P., 1977, Holocene sediment accumulations of the south Florida shelf margin, part I, in Enos, P., and Perkins, R.D., eds., *Quaternary sedimentation in south Florida: Geological Society of America Memoir*, v. 147, p. 1-130.
- Folk, R. L., 1962, Spectral subdivision of limestone types: *American Association of Petroleum Geologists* v. 1, p. 62-84.

- Folk, R. L., 1974, The natural history of crystalline calcium carbonate: effect of magnesium content and salinity *Journal of Sedimentary Petrology*, v. 44, no. 1, p. 40-53.
- Fruijtier, C., Elliot, T., and Schlager, W., 2000, Mass-spectrometric  $^{234}\text{U}/^{230}\text{Th}$  ages from the Key Largo Formation, Florida Keys, United States: Constraints on diagenetic age disturbance: *Geological Society of America Bulletin*, v. 112, no. 2, p. 267-277.
- Halley, R. B., Vacher, H.L., and Shinn, E.A., 1997, *Geology and Hydrogeology of the Florida Keys: Geology and Hydrology of Carbonate Islands, Developments in Sedimentology* v. 54.
- Harrison, R. S., and Coniglio, M., 1985, Origin of the Pleistocene Key Largo Limestone, Florida Keys: *Bulletin of Canadian Petroleum Geology*, v. 33, p. 350-358.
- Heron, S., Morgan, J., Eakin, M., and Skirving, W., 2005, Hurricanes and their Effects on Coral Reefs, p. 31-36.
- Hillgartner, H., 1998, Discontinuity surfaces on a shallow-marine carbonate platform (Berriasian, Valanginian, France and Switzerland): *Journal of Sedimentary Research*, v. 68, no. 6, p. 1093-1108.
- Hoffmeister, J. E., 1974, *Land from the sea: The geologic story of south Florida, Coral Gables: University of Miami Press.*
- Hoffmeister, J. E., Stockman, K. W., and Multer, H. G., 1967, Miami limestone of florida and its recent Bahamian counterpart: *Geological Society of America Bulletin*, v. 78, p. 175-190.
- Kaufman, A., and Broecker, W., 1965, Comparison of Th and C ages for carbonate materials from lakes Lahontan and Bonneville: *Journal of Geophysical Research*, v. 70, no. 16, p. 4039-4054.
- Manzello, D., L. and post, Buckley, Schuh and Jernigan, Inc. 2015, Algal, coral and other data collected by ROV and scuba diver videography from M.V. FLING and M.V. SPREE for post-hurricane assessment of sensitive habitats of the flower garden banks vicinity project from November 13,2005 to June 23, 2007.
- Miller, W. F. P. a. S. L., 2007, *Ecological Shifts along the Florida Reef Tract: The Past as a Key to the Future*, Springer, NY, *Geological Approaches to Coral Reef Ecology.*
- Muhs, D. R., Budahn, J., Prospero, J.M., Carey, S.N., 2007, *Geochemical evidence for*

- African dust inputs to soils of western Atlantic islands: Barbados, the Bahamas and Florida: *Journal of Geophysical Research* v. 112.
- Muhs, D. R., Simmons, K.R., Schumann, R.R., and Halley, R.B., 2011, Sea-level history of the past two interglacial periods: new evidence from U-series dating of reef corals from south Florida: *ScienceDirect*, v. 30, p. 570-590.
- Multer, H. G., and Hoffmeister, J.E., 1968, Subaerial Laminated Crusts of the Florida Keys: *Geological Society of America Bulletin*, v. 79, p. 183-192.
- Multer, H. G., Gischler, E., Lundberg, J., Simmons, K. R., and Shinn, E. A., 2002, Key Largo Limestone Revisited: Pleistocene Shelf-edge Facies, Florida Keys, USA: *ProQuest Natural Science Collection*, v. 46, p. 229-271.
- Multer, J. E. H. a. H. G., 1968, Geology and origin of the Florida Keys *Geological Society of America Bulletin*, v. 79, p. 1487-1502.
- Parker, G. E., 1945, The effect of the Pleistocene Epoch on the geology and ground water of southern Florida: *Fla. Acad. Sci.*, v. 8, p. 199-143.
- Pigott, J.D., 2013, GEOL 5363: Carbonate Geology. Fall 2013. Unpublished Lecture Notes.
- Pigott, J.D., April 2015, personal correspondence.
- Puri, H. S., and Collier, A., 1967, Role of Micro-Organisms in Formation of Limestones: *AAPG Archives*, v. 17, p. 355-367.
- RIEGL Laser Instrument Systems, 2012, RIEGL VZ-400 Technical Documentation and Users Instructions.
- Robbart, M. L., Deslarzes, K. J. P., Precht, W. F., Aronson, R. B., Zimmer, B., Duncan, L., Deis, D. R., Sinclair, J., Hickerson, E. L., Schmahl, G. P., and Boland, G. S., Post-hurricane assessment (Hurricane Rita, September 2005) and recovery at the east flower garden bank, northwestern Gulf of Mexico, *in Proceedings International Coral Reef Symposium Ft. Lauderdale, Florida 2008, Volume 18.*
- Robbin, D. M., and Stipp, J. J., 1979, Depositional rate of laminated soilstone crust, Florida Keys: *Journal of Sedimentary Petrology* v. 49.
- Service, F. P., 2012, Windley Key Fossil Reef Geological State Park, *in Protection*, D. o. E., ed.: Florida, Division of recreation and Parks.
- Stanley, M. S., 1966, Paleocology and Diagenesis of Key Largo Limestone, Florida: *Bulletin of the American Association of Petroleum Geologists*, v. 50, p. 1927-1947.

Thermo Fisher Scientific, 2010, User's Guide Version 7.0.1.

Ulmer-Scholle, P. A. S. a. D. S., 2003, A color guide to the petrography of carbonate rocks: grains, textures, porosity, diagenesis, Tulsa, OK, The American Association of Petroleum Geologists.

White, B., Curran, H. A., and Wilson, M. A., 1998, Bahamian coral reefs field evidence of a brief sea level lowstand during the last interglacial Carbonates & Evaporites v. 13, no. 1, p. 10-22.

Windley Key Fossil Reef Geological State Park [Brochure], 2009, *in* Parks, F. D. o. E. P. D. o. R. a., ed.

Wright, M. E. T. a. V. P., 1990, Carbonate Sedimentology, Blackwell Science 482



# Appendix A: Windley Key Quarry Data Collection Permit

Page 1 of \_\_

<b>Permit Number</b>
07311415

Florida Department of Environmental Protection  
 Division of Recreation and Parks  
 Florida Park Service

**SCIENTIFIC (NON-COMMERCIAL) RESEARCH / COLLECTING PERMIT**

*Park Visits Must Be Arranged A Minimum Of One Week In Advance. Failure To Make Required Arrangements Will Result In Denial Of Park Entry.  
 Permit Must Be Carried At All Times While Working In State Parks.*

<b>Permittee:</b> Emma Giddens	<b>Address, Phone, Email:</b> 401 E. Boyd Street Apt.#207 Norman OK, 73069 <a href="mailto:egiddens01@gmail.com">egiddens01@gmail.com</a> (424)247-3560	<b>Issue Date:</b> 7/31/2014
<b>Representing:</b> University of Oklahoma, Graduate Student		<b>Expiration Date:</b> 7/31/2015
<b>Additional Authorized Researchers:</b> Dr. Kulwadee Pigott Charlie Crosby Dr. John Pigott	<b>Subject:</b> Process Sedimentologic-Diagenetic Investigation of Discontinuity Surface and Reservoir Quality in the Key Largo Limestone Formation, Windley Key  <b>Permitted Activity:</b> Use of LIDAR and XRF machines to survey the quarry.	
<b>In the Following Park(s):</b> Windley Key Fossil Reef Geological State Park Mike Guarino, Park Manager-(305)664-0655	<b>Permitted Collection:</b> Using visual inspection and non-destructive equipment LIDAR and XRF scans will be taken of the quarry and will not be collecting any materials.	

**Permit Attachments:**

1. Standard Conditions
2. Special Conditions

Permit Not Valid Unless Signed By All Parties

**Issuing Office**

Approved By: (Signature and Title)

*Pat Yano*  
 Asst. Bureau Chief  
 8/14/2014  
 Date

Division of Recreation and Parks-District 5  
 13798 SE Federal Hwy  
 Hobe Sound, Florida 33455  
 772-546-0900 (phone)  
 772-223-2591 (fax)

**Permittee**

I have read this permit and all attachments listed above. I fully understand it, and will abide by all rules and regulations.

Permittee Signature:

*Emma Giddens*  
 Permittee

Date:

6 AUGUST 2014

## Appendix B: LIDAR Data Collection Controls

Day 1: December 16, 2014

Scan Position	Scan	Resolution	Length of Scan	Time of Day	Temperature (F)	Humidity	Wind Speed
1	360	0.060	2 min	10:45 am	64	81%	8mph, N
	FS 1	0.005	10 min				
	FS 2	0.005	12 min				
	FS 3	0.005	12 min				
	FS 4	0.005	6 min	12:00 pm			
	FS 5	0.005	8 min				
	FS 6	0.005	10 min	12:30 pm			
	FS 7	0.005	15 min				
2	360	0.060	2 min	1:00 pm			
	FS 1	0.005	20 min				
	FS 2	0.005	16 min				
	FS 3	0.005	18 min	1:50 pm			
	FS 4	0.005	15 min				
	FS 5	0.005	10 min				

	FS 6	0.005	11 min	2:50 pm			
	FS 7	0.005	12 min				
3	360	0.060	2 min	3:20 pm	74	52%	
	FS 1	0.005	20 min	3:40 pm			
	FS 2	0.005	30 min	4:00 pm			

Day 2: December 17, 2014

Scan Position	Scan	Resolution	Length of Scan	Time of Day	Temperature (F)	Humidity	Wind Speed
4	360	0.060	2 min	9:20 am	64	68%	3mph, N
	FS 1	0.002	20 min				
	FS 2	0.004	30 min				
	FS 3	0.004	30 min				
	FS 4	0.004	30 min				
	FS 5	0.004	33 min	12:40 pm			
	FS 6	0.004	35 min				
5	360	0.060	2 min	2:20	75	56%	5mph,

				pm			NNE
	FS 1	0.004	28 min				
	FS 2	0.004	40 min				
	FS 3	0.004	22 min				

Day 3: December 18, 2014

Scan Position	Scan	Resolution	Length of Scan	Time of Day	Temperature (F)	Humidity	Wind Speed
1	360	0.060	2 min	8:30 am	70	78%	3mph, NNE
	FS 1	0.004	50 min				
2	360	0.060	2 min	10:00 am			
	FS 1	0.004	48 min				
3	360	0.060	2 min	11:00 am			
	FS 1	0.004	55 min				
	FS 2	0.004	30 min	12:15 pm			
4	360	0.040	4 min	4:30 pm			

	FS 1	0.004	25 min				
5	360	0.040	4 min	5:20 pm			
	FS 1	0.004	23 min				

Day 4: December 19, 2014

Scan Position	Scan	Resolution	Length of Scan	Time of Day	Temperature (F)	Humidity	Wind Speed
6	360	0.060	2 min	9:20 am	64	76%	4 mph, N
	FS 1	0.004	53 min				
	FS 2	0.004	57 min				
7	360	0.060	2 min	10:40 am	70	69%	5 mph, NNE
	FS 1	0.004	30 min				
	FS 2	0.004	36 min				
	FS 3	0.004	45 min				
	FS 4	0.004	57 min				
8	360	0.060	2 min	4:00 pm	74	63%	9 mph,

							E
	FS 1	0.004	45 min				
9	360	0.060	2 min	5:15 pm	71	62%	5 mph, E
	FS 1	0.004	40 min				
	FS 2	0.004	36 min				

Day 5: December 20, 2014

Scan Position	Scan	Resolution	Length of Scan	Time of Day	Temperature (F)	Humidity	Wind Speed
10	360	0.060	2 min	7:15 am	67	82%	3 mph, ESE
	FS 1	0.004	48 min				
	FS 2	0.004	40 min				
11	360	0.060	2 min	9:00 am	71	73%	2 mph, SE
	FS 1	0.004	45 min				
	FS 2	0.004	33 min				

12	360	0.060	2 min	3:30 pm	75	74%	8 mph, SE
	FS 1	0.004	50 min				
13	360	0.060	2 min	6:00 pm	73	60%	5 mph, E
	FS 1	0.004	50 min				

Day 6: December 21, 2014

Scan Position	Scan	Resolution	Length of Scan	Time of Day	Temperature (F)	Humidity	Wind Speed
14	360	0.060	2 min	4:00 pm	75	76%	10 mph, E
15	360	0.060	2 min	4:30 pm	77	74%	12 mph, SE
	FS 1	0.004	40 min				

## Appendix C: XRF Raw Scan Results

Reading #	Sample	Sub Sample	Fe	S	Mg	Ca		Al	Sr	Si
700	1	A	754.5	6,587.5	28,289.9	129,944.1		4,390.9	1,230.3	8,913.9
701	1	B	1,020.1	1,945.5	18,809.9	313,281.7		1,002.2	963.4	1,824.8
702	1	C	407.5	2,467.4	11,948.8	260,965.0		1,713.7	3,498.4	3,089.4
703	1	D	527.0	3,116.7	13,970.7	236,923.8		1,679.5	2,913.3	4,233.0
704	2	A	332.0	2,388.9	0.0	273,927.7		1,903.3	2,096.1	3,119.0
705	2	B	328.3	2,170.0	14,906.9	285,975.0		0.0	1,133.0	2,490.4
706	2	C	327.7	2,325.0	14,131.6	269,651.2		1,532.0	998.2	3,190.4
707	2	D	319.7	3,000.8	14,351.2	319,913.6		1,246.4	4,801.3	2,848.8
708	2	E	842.4	5,114.7	32,779.8	190,162.0		3,681.9	1,732.1	6,791.5
709	3	A	249.1	1,319.9	7,454.0	346,407.1		0.0	1,722.9	1,689.9
710	3	B	627.1	2,240.7	9,862.3	306,614.3		1,284.4	5,613.0	2,402.1
714	3	C	386.2	2,377.3	9,667.3	292,176.9		781.5	5,101.7	2,336.0
715	3	D	471.9	2,874.5	12,719.0	269,017.5		1,235.9	3,686.2	3,225.0
716	3	E	410.0	3,377.6	15,140.3	269,830.7		2,042.5	2,072.3	3,825.1
717	4	A	1,127.6	2,156.3	24,168.3	300,689.3		1,526.9	5,012.5	2,911.0
718	4	B	253.7	1,489.7	11,523.2	309,036.7		0.0	1,450.2	1,884.3
719	4	C	399.3	3,074.3	13,066.0	237,438.5		1,868.7	1,323.8	4,335.6
720	4	D	278.1	2,038.9	9,235.3	323,404.8		0.0	4,763.2	1,923.3
721	4	E	275.0	2,774.3	15,701.7	284,283.5		1,521.3	1,624.0	2,797.9
722	5	A	376.9	2,922.7	18,270.2	258,253.0		1,096.2	1,343.2	3,823.2
723	5	B	266.4	1,999.1	7,612.5	303,279.8		0.0	4,686.9	2,236.0
724	5	C	235.9	2,536.6	14,956.0	279,634.8		0.0	5,216.1	2,489.9
728	5	D	423.7	4,348.9	17,524.3	232,858.4		3,727.3	4,302.6	5,716.0
729	5	E	503.5	5,011.1	21,538.5	193,671.6		2,593.9	1,040.1	6,843.0
730	5	F	404.3	4,295.0	15,179.9	212,474.4		1,513.5	2,479.9	5,063.3
731	6	A	457.3	2,725.4	11,052.3	299,405.4		695.5	5,432.2	2,265.0
732	6	B	334.1	1,997.5	0.0	319,873.1		914.7	1,782.5	2,321.7
733	6	C	418.6	4,057.4	7,516.7	236,900.5		1,490.9	1,058.3	4,038.4
734	6	D	347.5	2,728.0	13,315.8	278,272.6		0.0	1,365.2	6,115.3
735	6	E	335.1	3,004.2	24,370.0	255,345.7		1,223.5	1,466.2	4,275.1
736	6	F	719.5	6,265.0	38,961.6	175,346.7		4,303.1	667.9	8,846.1
740	7	A	278.8	2,408.3	0.0	311,135.0		0.0	1,608.4	2,993.4
741	7	B	283.7	2,362.9	11,539.5	344,557.2		1,078.9	1,243.5	1,958.7
742	7	C	285.6	2,516.3	9,745.6	308,485.4		0.0	1,419.5	2,041.6
743	7	D	299.7	2,097.6	0.0	344,499.3		0.0	2,523.1	1,871.1
744	7	E	224.3	2,456.3	13,395.2	284,742.4		0.0	1,386.0	1,964.6
745	7	F	371.1	2,707.3	17,879.1	288,533.9		2,021.9	799.2	3,480.5
746	8	A	431.8	2,954.4	11,994.4	259,775.1		1,373.0	1,385.5	3,931.0
747	8	B	365.1	3,426.8	7,751.7	207,775.0		1,317.2	1,331.9	4,248.8
748	8	C	273.3	3,217.2	8,368.7	314,725.2		956.8	3,969.8	1,794.4
749	8	D	1,283.9	4,047.9	13,728.2	245,741.4		1,294.6	4,474.0	3,923.6
750	8	E	403.8	4,131.8	12,523.0	221,191.4		1,523.5	1,992.8	3,914.4
751	8	F	370.6	1,763.2	14,295.6	329,347.9		993.0	2,436.0	2,222.2
752	9	A	491.1	3,393.6	12,461.2	242,923.9		2,193.1	1,435.7	4,899.4
753	9	B	374.7	4,006.1	19,153.5	206,919.7		0.0	1,940.0	3,509.8
754	9	C	570.3	7,714.2	30,186.4	140,847.4		4,164.4	1,072.8	10,257.9
755	9	D	326.2	2,813.2	13,833.8	335,820.0		0.0	4,255.5	3,004.3
756	9	E	509.7	2,998.4	8,991.7	267,120.6		1,095.0	1,148.3	2,680.0
757	9	F	291.1	2,312.6	11,407.2	306,851.7		0.0	4,686.9	2,385.4



A	B	C	D	E	F	G	H	I	J	K
758	10	A	303.2	1,973.2	9,866.0	287,873.0		1,170.0	1,442.9	2,842.4
759	10	B	463.8	2,551.9	8,808.4	347,159.9		997.7	2,280.7	2,576.4
760	10	C	979.4	6,529.3	18,075.6	184,289.7		3,194.9	1,645.9	9,685.8
761	10	D	546.4	3,371.4	17,892.6	226,695.6		1,607.1	1,537.3	4,243.6
762	10	E	538.1	3,364.5	13,744.5	269,087.7		1,502.5	1,328.1	3,521.8
763	10	F	890.9	3,627.1	24,313.6	224,673.5		2,261.4	1,059.6	4,608.6
767	11	A	278.6	2,273.2	23,153.1	279,308.3		1,843.5	842.9	3,282.3
768	11	B	286.0	1,575.7	9,116.1	310,630.1		751.6	1,781.8	2,243.9
769	11	C	317.8	8,481.5	17,435.5	131,582.5		1,849.7	947.5	4,300.5
770	11	D	405.1	1,999.0	13,431.2	321,612.9		0.0	4,281.0	3,171.6
771	11	E	311.9	3,381.2	13,025.4	204,655.4		1,631.6	1,197.9	3,841.1
772	11	F	248.6	2,489.9	12,493.6	326,727.1		1,186.8	4,953.9	2,233.7
822	12	A	433.9	1,986.6	0.0	299,734.2		1,042.0	1,413.6	1,881.2
823	12	B	232.6	17,471.2	0.0	221,096.3		0.0	895.1	2,761.2
824	12	C	444.0	2,632.8	17,075.7	231,436.7		0.0	934.9	2,457.6
825	12	D	465.4	2,479.3	11,637.0	277,962.1		1,137.6	651.6	2,444.5
826	12	E	471.6	3,647.4	15,961.7	293,038.8		966.7	824.7	2,022.0
827	13	A	666.9	3,281.6	13,872.8	236,776.8		1,153.8	1,002.7	3,157.7
828	13	B	576.9	2,716.9	17,125.5	290,450.7		1,210.5	1,304.7	3,458.8
829	13	C	262.7	1,261.0	0.0	359,580.7		0.0	2,435.8	1,466.3
830	13	D	397.2	1,867.3	20,613.5	339,815.3		0.0	1,676.0	2,157.8
831	13	E	320.6	1,715.4	10,781.9	348,034.4		0.0	1,970.5	1,486.5
832	14	A	484.3	2,772.4	10,207.4	275,821.0		1,138.3	1,504.0	2,340.6
833	14	B	655.8	1,556.6	9,899.1	304,724.0		1,022.1	1,851.7	1,599.2
834	14	C	1,764.7	2,055.6	6,775.2	299,035.3		1,101.0	1,545.2	2,921.9
835	14	D	844.2	2,491.5	14,914.2	302,315.3		0.0	1,196.9	2,860.8
836	14	E	1,367.0	2,855.5	7,470.3	236,176.2		1,293.4	1,546.2	3,440.6
837	15	A	342.9	1,635.5	9,357.5	330,927.1		1,484.0	1,405.7	2,222.8
838	15	B	177.4	1,135.3	5,851.7	337,623.7		0.0	1,700.3	1,668.1
839	15	C	318.2	1,708.6	0.0	326,432.9		800.4	3,661.3	2,102.8
840	15	D	1,579.6	4,580.7	21,262.7	321,183.2		1,449.4	920.1	4,013.2
841	15	E	675.0	2,953.0	19,231.5	224,430.5		2,176.7	907.6	5,148.9
842	16	A	1,281.6	4,986.9	29,386.0	188,831.3		3,747.8	2,195.9	7,003.0
843	16	B	683.9	2,684.8	10,681.2	268,314.0		2,155.7	2,109.5	4,070.2
844	16	C	480.7	2,080.4	13,416.7	275,782.5		1,280.2	1,415.0	3,275.6
845	16	D	1,414.3	2,381.9	15,681.7	228,780.7		1,503.0	1,840.0	3,324.6
1110	17	A	1,187.8	13,160.1	52,018.6	59,172.7		8,047.0	517.0	17,759.1
1111	17	B	606.3	11,375.8	14,261.4	34,797.8		1,357.0	749.0	3,066.3
1112	17	C	2,384.2	8,493.5	45,512.8	135,279.9		5,176.2	777.9	12,099.3
846	18	A	311.3	2,804.7	16,011.2	292,479.8		1,315.1	1,131.7	2,947.2
847	18	B	452.0	2,530.4	10,697.8	271,754.0		1,142.2	1,097.0	3,035.5
848	18	C	635.6	2,530.6	12,801.1	299,736.1		1,260.8	1,577.3	2,885.7
849	18	D	537.3	1,911.7	6,886.0	340,536.8		894.9	3,361.5	2,050.6
850	18	E	456.1	2,637.8	21,837.4	310,606.2		2,045.1	1,752.6	3,509.2
851	18	F	845.1	3,578.2	8,051.9	271,827.2		1,035.6	952.9	2,300.9
852	19	A	4,054.4	2,305.4	12,628.2	283,617.2		1,188.8	1,957.0	3,500.3
853	19	B	422.7	2,305.1	9,598.3	287,993.4		1,910.1	782.5	3,235.6
854	19	C	440.1	1,863.6	14,461.2	332,027.3		1,401.8	682.9	2,735.2
855	19	D	667.4	5,773.5	31,117.9	163,915.5		3,499.6	1,034.3	8,134.4
856	19	E	549.5	2,959.0	13,438.1	276,433.3		2,014.1	1,179.2	3,414.9

A	B	C	D	E	F	G	H	I	J	K
857	19	F	4,044.4	2,471.7	11,648.7	257,628.8		1,235.1	3,666.3	3,174.9
858	20	A	448.8	1,883.8	14,939.6	300,245.5		1,506.7	610.0	2,988.2
859	20	B	467.2	2,414.0	13,275.2	296,268.0		1,259.4	1,180.1	2,638.8
860	20	C	885.0	2,780.7	18,147.3	289,536.2		1,289.8	834.5	4,208.8
861	20	D	699.5	2,325.4	0.0	317,402.8		1,001.1	1,141.1	2,273.7
862	20	E	556.3	1,815.8	16,287.0	366,444.3		1,582.6	1,625.2	2,660.2
863	20	F	1,745.5	8,968.0	45,546.5	127,176.9		6,891.3	1,415.5	13,781.9
864	21	A	3,239.5	2,938.4	33,742.8	271,103.8		2,543.6	893.9	4,646.1
865	21	B	553.9	1,501.2	19,910.9	323,075.0		1,490.5	957.1	2,343.1
866	21	C	530.3	2,356.8	11,372.4	310,625.7		1,342.3	2,672.1	2,728.7
867	21	D	641.3	2,707.8	10,866.4	325,436.4		1,211.4	3,124.6	2,244.0
868	21	E	1,362.6	2,701.9	15,608.9	144,784.8		1,329.4	609.7	3,936.1
966	22	A	554.8	1,859.8	11,384.4	301,882.6		762.5	1,391.9	2,176.5
967	22	B	1,882.7	4,204.9	24,325.4	210,619.3		2,494.9	638.0	4,779.4
968	22	C	1,446.2	1,825.4	11,739.3	308,429.1		935.5	983.6	2,145.7
969	22	D	4,945.1	2,946.3	15,069.9	229,717.5		730.8	1,247.4	3,530.1
970	23	A	519.2	2,575.1	18,886.2	265,875.3		1,919.2	947.0	3,521.5
971	23	B	1,018.9	2,435.8	14,404.4	297,338.6		1,100.9	691.1	2,393.1
972	23	C	769.6	3,408.7	23,132.1	214,213.5		2,826.2	850.4	4,117.0
973	23	D	1,410.6	1,814.8	14,784.6	340,923.9		731.7	5,701.0	2,034.6
974	24	A	425.1	0.0	6,935.7	339,582.8		835.3	1,508.0	1,859.0
975	24	B	868.1	1,549.6	12,235.6	339,985.0		781.5	714.9	1,537.9
976	24	C	428.8	2,001.2	0.0	339,357.9		0.0	1,019.0	1,700.6
977	24	D	825.4	2,590.1	12,237.2	296,187.2		898.2	4,564.9	2,709.0
978	25	A	479.0	1,281.3	6,426.9	370,389.2		922.6	1,618.7	1,969.7
979	25	B	338.4	1,536.7	11,175.7	342,423.7		0.0	5,542.6	1,897.7
980	25	C	468.8	1,116.6	8,342.2	343,699.7		0.0	2,946.1	1,540.3
981	25	D	688.7	2,261.1	0.0	285,499.9		1,277.1	1,094.9	3,273.7
1081	26	A	384.9	1,339.0	10,440.4	326,747.6		1,185.0	1,487.5	2,000.3
1082	26	B	657.4	921.0	9,528.6	360,679.1		989.1	861.6	1,317.1
1083	26	C	249.3	832.3	15,732.9	381,865.3		0.0	1,250.5	1,094.3
1084	26	D	438.1	1,433.9	11,399.3	332,910.3		0.0	1,907.2	1,660.6
1085	26	E	1,055.3	1,977.7	11,000.2	330,141.1		1,015.9	5,105.8	1,916.0
1086	27	A	341.5	1,933.8	15,218.0	340,824.5		0.0	3,041.8	1,822.0
1087	27	B	441.9	931.0	15,726.0	363,240.1		0.0	993.0	1,303.5
1088	27	C	1,715.2	2,689.9	8,094.1	314,994.0		0.0	5,594.5	1,960.3
1089	27	D	962.2	4,099.0	25,131.8	233,667.3		2,540.0	3,967.9	5,158.2
1090	27	E	802.8	1,804.4	5,814.2	322,539.3		1,126.5	4,686.4	2,058.9
1091	28	A	885.9	3,790.4	28,102.5	220,276.2		1,742.5	848.4	5,535.4
1092	28	B	878.1	3,625.4	19,819.5	224,659.6		2,809.5	867.0	4,822.2
1093	28	C	710.7	4,103.9	30,577.2	228,489.8		3,447.7	829.1	5,936.4
1094	28	D	738.4	3,009.4	13,883.8	303,507.3		929.2	1,875.5	2,272.2
1095	28	E	963.1	3,320.7	0.0	276,531.8		1,139.1	4,157.5	3,044.3
1096	29	A	1,258.2	2,347.7	8,047.8	283,115.7		1,379.5	1,259.0	2,617.2
1097	29	B	584.4	1,483.1	9,499.2	335,792.3		0.0	1,044.6	1,456.2
1098	29	C	340.1	1,579.5	14,083.6	337,721.0		851.4	3,997.5	1,626.2
1099	29	D	1,938.1	2,710.6	16,194.8	284,035.6		0.0	4,390.7	2,974.3
1100	29	E	600.3	2,637.2	14,520.1	289,630.6		1,076.8	4,295.7	3,096.5
1101	30	A	393.3	1,342.2	7,704.6	324,322.3		772.3	949.8	1,762.2
1102	30	B	1,106.2	4,442.6	6,812.3	289,434.8		877.9	4,842.7	1,492.7

A	B	C	D	E	F	G	H	I	J	K
1103	30	C	867.8	2,101.8	9,349.1	320,611.5		831.0	1,099.9	1,557.8
1104	30	D	1,116.8	2,045.8	11,034.1	303,151.4		809.6	2,243.3	2,047.8
1105	30	E	788.0	4,239.8	18,417.8	211,751.5		2,662.1	1,919.4	5,615.3
869	31	A	1,127.2	3,214.0	12,389.3	264,278.8		2,692.9	931.2	4,087.9
870	31	B	551.2	2,169.7	9,962.5	310,452.6		992.9	963.6	2,579.5
871	31	C	418.4	2,706.3	8,726.7	305,207.5		1,402.3	2,795.9	2,611.8
872	31	D	850.9	3,088.3	0.0	325,986.5		1,003.3	5,444.7	2,160.3
873	31	E	825.9	3,304.5	10,038.8	300,158.6		1,208.3	4,863.7	2,454.1
874	32	A	532.2	2,862.7	9,520.0	327,923.8		1,647.1	1,175.8	1,985.6
875	32	B	242.1	1,031.4	7,627.7	377,280.3		825.4	985.8	1,396.6
876	32	C	394.0	2,669.6	10,199.4	281,916.0		1,187.9	1,408.9	3,399.4
877	32	D	597.6	2,594.3	14,034.9	307,451.5		2,257.3	1,376.7	3,050.2
878	32	E	473.4	2,006.5	8,881.9	383,726.3		1,241.4	3,016.7	2,074.1
880	33	A	368.3	1,503.6	7,678.2	333,325.2		1,698.0	1,557.8	2,228.0
881	33	B	383.5	3,473.6	20,620.5	265,503.1		997.4	863.6	3,048.8
882	33	C	552.9	3,166.5	17,725.7	275,975.0		1,696.3	1,083.3	3,663.4
883	33	C2	630.0	2,707.2	10,054.0	260,718.7		1,198.5	4,678.8	3,166.9
884	33	C3	45,288.3	4,465.8	0.0	227,075.1		4,023.7	681.8	7,974.7
885	33	C4	715.6	2,792.6	6,882.2	291,632.8		1,085.4	5,025.2	3,758.6
886	33	C5	260.5	1,456.7	13,923.2	366,022.2		0.0	1,904.8	1,512.6
887	33	C6	540.9	3,599.0	17,713.0	316,811.7		1,350.3	2,477.1	2,388.3
888	33	D	641.4	2,172.2	13,926.7	328,954.1		815.9	5,366.3	2,641.7
889	33	E	317.0	2,080.4	6,705.1	311,682.9		842.2	848.4	2,013.7
890	34	A	1,002.0	8,187.7	18,141.6	134,452.5		4,503.6	1,060.8	11,316.4
891	34	B	427.8	2,701.1	16,892.9	282,474.6		1,553.6	1,408.6	3,410.3
892	34	C	411.0	2,577.1	7,057.3	312,273.7		989.9	1,104.6	2,339.6
893	34	D	466.8	3,046.0	16,081.7	310,744.7		1,253.8	2,398.2	2,828.7
894	35	A	332.1	4,340.3	13,341.1	304,284.2		1,063.6	1,790.1	2,453.8
895	35	B	428.0	2,714.3	17,693.3	317,723.1		813.1	1,047.8	1,759.2
896	35	C	297.9	3,907.6	14,306.5	285,165.3		1,307.7	5,081.7	2,716.5
897	35	D	702.9	3,490.9	12,847.6	311,312.3		1,146.5	5,606.6	2,150.9
898	36	A	651.0	6,516.8	17,811.1	187,307.7		1,610.9	3,500.1	3,834.7
899	36	B	370.6	3,498.4	13,493.5	308,458.0		0.0	5,976.8	2,376.1
900	36	C	391.3	4,046.5	9,924.0	302,031.0		758.4	5,079.9	2,562.1
901	36	D	219.3	3,735.7	6,165.1	350,116.2		0.0	2,089.3	1,484.5
902	36	E	1,044.8	5,581.3	12,263.5	234,355.4		1,664.6	1,091.0	3,376.1
903	37	A	972.3	4,097.8	14,806.1	278,975.4		1,578.1	1,028.2	2,752.3
904	37	B	288.3	2,434.0	8,052.5	348,564.4		860.7	4,469.8	2,274.9
905	37	C	1,157.3	6,365.3	18,362.4	265,004.6		0.0	5,280.9	2,471.1
906	37	D	467.2	3,926.0	6,633.4	328,912.3		1,431.6	5,267.3	1,649.9
1021	38	A	376.6	2,843.0	0.0	276,084.2		0.0	2,003.3	2,061.3
1022	38	B	589.5	3,701.6	27,995.1	240,585.4		1,493.9	1,342.8	3,235.0
1023	38	C	740.0	3,694.8	19,304.9	264,184.3		1,626.8	898.9	2,442.4
1024	38	D	315.0	2,844.1	0.0	275,497.6		0.0	3,987.2	1,498.0
1014	39	A	388.1	1,603.8	7,457.7	325,135.9		0.0	1,246.4	1,713.2
1015	39	B	949.2	3,794.3	15,318.9	222,837.3		2,318.0	915.1	4,028.3
1016	39	C	1,220.6	3,253.2	10,671.8	236,359.7		1,404.8	1,672.0	3,175.3
1017	39	D	357.2	1,854.7	11,925.7	335,044.3		796.4	3,059.0	1,669.8
1010	40	A	280.1	1,544.4	20,802.7	312,538.8		1,275.3	422.3	2,206.2
1011	40	B	173.2	1,236.3	13,788.6	319,191.9		1,228.6	1,852.5	1,616.5

A	B	C	D	E	F	G	H	I	J	K
1012	40	C	283.6	1,394.4	9,155.6	334,207.5		891.5	1,587.0	1,427.0
1013	40	D	364.9	2,710.9	12,869.3	322,972.7		736.5	809.5	2,153.2
1006	41	A	282.9	1,845.6	9,775.5	329,242.2		1,038.2	1,247.6	1,456.0
1007	41	B	412.5	2,220.9	14,468.1	304,378.9		992.6	5,116.6	2,592.1
1008	41	C	346.0	2,433.3	23,647.5	282,287.9		1,664.9	1,051.9	3,106.8
1009	41	D	500.3	2,857.5	8,427.4	300,923.2		1,271.0	3,191.8	2,505.0
1000	42	A	409.9	2,369.9	16,224.0	347,762.3		1,443.0	997.6	2,240.2
1001	42	B	293.3	2,353.9	8,988.6	306,383.8		1,038.8	5,153.8	2,066.3
1002	42	C	227.5	1,715.2	14,613.4	318,705.7		0.0	1,319.5	1,199.5
1003	42	D	371.7	2,958.5	9,103.5	305,309.8		756.7	4,817.2	2,441.4
1004	42	E	344.4	2,572.3	0.0	357,240.6		911.0	3,569.1	1,801.3
996	43	A	534.0	2,848.5	16,992.2	271,599.0		1,697.3	2,917.1	3,458.4
997	43	B	895.9	6,417.9	37,598.6	161,493.1		4,122.1	708.8	8,624.4
998	43	C	682.4	8,763.5	26,901.6	101,165.2		3,103.6	884.9	9,928.4
999	43	D	552.4	2,605.8	8,056.0	260,006.4		832.6	4,333.6	2,275.7
982	44	A	262.5	1,662.9	13,204.7	353,758.1		934.8	807.7	2,050.3
983	44	B	308.8	2,194.6	10,989.6	285,588.7		1,804.6	986.5	3,132.2
984	44	C	398.2	2,899.4	16,650.8	300,468.8		741.0	2,337.6	2,029.8
985	44	D	411.8	2,927.6	19,155.8	269,949.8		1,751.9	1,431.0	3,250.0
991	45	A	313.4	2,172.5	10,990.2	286,022.5		1,884.3	1,006.0	2,753.2
992	45	B	462.4	2,689.3	16,411.0	291,055.5		1,414.2	4,060.0	2,600.5
993	45	C	1,102.7	4,636.7	20,685.9	219,425.7		1,636.4	1,019.9	4,001.0
994	45	D	359.9	2,502.2	14,583.7	295,452.3		1,287.0	1,035.9	2,318.5
995	45	E	385.3	2,686.2	7,159.6	346,354.6		1,155.4	881.4	2,092.0
986	46	A	174.0	1,345.3	6,998.4	343,835.7		0.0	2,385.2	1,510.3
987	46	B	188.7	2,464.2	11,627.5	354,885.1		0.0	1,539.8	1,460.5
988	46	C	343.7	1,861.8	9,230.3	355,353.3		1,227.4	1,019.3	1,705.5
989	46	D	2,355.8	4,658.7	14,663.8	190,717.5		2,092.8	1,426.2	4,282.0
990	46	E	546.5	5,641.4	27,463.5	189,440.6		2,586.1	1,821.1	6,935.1
961	47	A	194.5	1,041.3	6,808.6	344,975.3		754.5	1,572.5	1,693.0
962	47	B	264.9	1,211.5	12,035.6	317,802.8		1,072.3	1,652.7	1,645.4
963	47	C	350.3	1,488.6	14,689.4	331,189.5		1,229.0	1,113.6	2,125.4
964	47	D	330.0	2,419.7	14,800.5	298,628.1		741.3	2,126.0	2,107.8
965	47	E	342.0	2,078.0	13,387.8	337,774.5		0.0	3,339.9	1,848.7
957	48	A	211.4	1,690.0	11,783.0	342,009.3		0.0	1,502.9	1,064.7
958	48	B	277.1	1,547.9	7,957.8	340,079.0		0.0	2,059.3	1,303.8
959	48	C	254.7	1,615.9	14,423.0	297,692.7		1,194.4	1,711.0	2,215.6
960	48	D	259.9	1,831.7	7,276.2	349,581.8		0.0	4,495.3	1,503.4
954	49	A	320.9	1,605.1	17,809.1	330,449.3		752.6	1,963.7	1,944.8
955	49	B	300.9	1,392.2	9,078.3	350,652.1		0.0	5,466.4	1,581.6
956	49	C	272.4	1,543.0	15,858.1	335,465.3		0.0	1,703.8	1,614.8
950	50	A	303.4	1,619.4	19,306.1	266,646.6		788.7	765.9	1,990.1
951	50	B	236.9	1,006.9	14,853.1	355,066.9		0.0	1,523.3	1,393.7
952	50	C	216.2	2,421.0	12,999.2	270,191.0		966.6	1,241.8	2,089.7
953	50	D	314.0	2,694.7	11,722.5	318,217.4		0.0	1,304.9	1,654.1
907	51	A	285.4	2,328.5	11,297.5	341,601.9		1,017.6	5,030.0	2,205.6
908	51	B	281.7	2,086.5	14,956.1	325,402.7		742.2	5,237.8	2,441.6
909	51	C	284.8	2,462.6	9,625.3	352,911.1		0.0	5,216.9	1,979.7
910	51	D	353.5	3,688.4	9,858.6	309,836.4		939.1	4,880.1	2,482.8
911	52	A	898.9	2,825.0	16,362.9	252,068.8		1,143.8	1,621.2	2,594.5

A	B	C	D	E	F	G	H	I	J	K
912	52	B	1,312.7	2,579.4	6,359.3	325,597.9		0.0	5,024.9	1,766.2
913	52	C	2,588.2	2,109.6	11,078.2	256,030.0		923.0	1,202.5	2,520.7
914	52	D	712.5	2,487.1	7,282.8	340,795.7		1,033.4	1,613.6	1,565.5
915	53	A	317.2	1,611.9	10,037.8	355,096.4		0.0	2,929.3	1,844.7
916	53	B	226.9	1,809.9	9,687.6	354,094.7		0.0	1,493.7	1,619.6
917	53	C	283.7	2,807.9	22,545.7	277,174.4		1,624.8	675.2	3,271.8
918	53	D	286.5	1,346.5	10,542.1	363,103.8		885.2	1,598.2	1,670.2
919	53	E	401.6	4,279.4	18,192.4	212,052.7		1,953.3	943.0	3,939.3
920	54	A	550.0	3,221.2	18,576.1	219,963.4		2,761.0	1,158.5	5,130.0
921	54	B	365.2	2,601.5	14,598.5	292,400.8		0.0	646.5	2,409.9
922	54	C	407.0	1,968.7	13,739.1	339,870.9		1,231.9	5,228.3	2,151.2
923	54	D	600.4	3,203.9	16,911.7	285,950.9		1,091.4	1,329.4	2,357.0
924	55	A	598.5	3,290.0	31,135.2	204,928.2		3,349.9	1,307.1	4,512.7
925	55	B	508.5	1,763.6	14,259.8	298,146.1		0.0	1,894.9	2,269.2
926	55	C	535.0	3,400.2	19,126.5	235,183.9		2,182.4	757.5	3,821.6
927	55	D	317.5	2,296.8	10,137.7	261,883.7		881.5	1,519.6	2,585.2
928	55	E	186.5	1,136.4	0.0	315,015.8		0.0	2,759.5	922.5
929	56	A	164.1	1,349.1	6,589.4	360,232.3		0.0	1,481.3	900.2
930	56	B	393.5	4,398.4	9,813.8	236,599.5		1,454.6	2,222.7	3,393.9
931	56	C	297.1	1,923.9	14,137.7	325,495.3		0.0	3,811.9	1,598.8
932	56	D	196.4	2,005.3	13,221.9	321,566.4		0.0	5,820.2	1,923.5
933	57	A	465.3	2,581.5	15,726.6	277,629.7		1,500.1	945.3	2,874.1
934	57	B	378.5	3,714.8	8,860.0	256,338.1		839.3	830.2	2,348.7
935	57	C	708.9	3,551.0	6,246.5	318,983.3		0.0	5,743.0	2,289.7
936	57	D	380.9	2,442.3	11,049.7	267,640.4		1,353.1	1,057.1	2,267.5
937	57	E	379.5	2,419.8	10,168.9	290,815.8		1,165.1	4,080.9	1,898.7
938	58	A	297.4	3,594.9	14,488.0	150,220.1		0.0	1,188.8	1,657.2
939	58	B	200.5	1,044.1	15,942.7	373,264.2		819.1	1,197.5	1,254.3
940	58	C	669.6	3,479.8	6,239.7	317,523.7		891.6	5,110.4	2,023.1
941	58	D	378.8	2,213.3	7,890.5	300,778.3		967.1	1,346.8	2,113.9
942	59	A	127.7	924.7	11,110.6	353,352.8		0.0	660.7	1,132.5
943	59	B	370.7	1,528.5	14,010.4	293,255.9		0.0	1,022.0	2,100.7
944	59	C	848.9	2,409.0	8,985.9	323,035.9		1,069.3	2,426.9	2,211.5
946	59	D	591.4	6,087.1	10,189.0	237,345.9		833.7	1,166.0	2,115.1
1077	60	A	215.3	3,305.1	11,685.7	284,362.8		0.0	1,555.5	1,917.0
1078	60	B	285.4	3,491.9	0.0	282,362.2		0.0	1,428.2	1,960.3
1079	60	C	206.9	4,428.2	6,399.5	285,986.5		0.0	1,196.8	1,734.3
1080	60	D	300.6	7,254.2	7,290.4	310,933.8		0.0	2,175.5	1,459.0
1121	61	A	226.4	4,574.7	10,877.5	368,420.5		0.0	3,444.9	1,172.4
1122	61	B	202.6	1,131.8	18,412.7	368,791.9		0.0	1,507.9	1,291.9
1123	61	C	248.2	1,788.2	9,777.8	350,885.1		0.0	5,103.1	1,870.8
1124	61	D	384.9	2,413.5	10,086.4	289,236.4		1,548.2	2,147.3	3,180.6
1125	61	E	303.2	3,356.5	10,140.1	328,182.5		0.0	4,878.8	1,900.7
1126	62	A	327.9	3,086.7	10,459.4	284,199.8		1,332.1	1,247.0	3,149.6
1127	62	B	594.7	2,052.8	0.0	286,105.8		1,370.1	1,434.3	2,732.3
1128	62	C	560.0	2,042.2	14,999.6	316,945.8		1,681.4	836.4	2,062.0
1129	62	D	281.7	915.5	5,894.6	373,613.4		0.0	1,203.5	1,395.7
1130	62	E	887.1	3,063.3	14,309.9	247,630.6		1,634.4	505.6	3,054.8
1131	63	A	267.3	1,209.2	7,096.8	348,332.5		1,690.1	1,528.8	1,828.8
1132	63	B	261.5	1,321.4	5,866.3	361,365.3		0.0	1,492.3	1,454.9

A	B	C	D	E	F	G	H	I	J	K
1133	63	C	741.6	5,130.9	21,033.7	210,374.8		4,803.8	382.9	7,064.8
1134	63	D	321.3	1,389.2	0.0	317,582.4		0.0	915.4	1,874.8
1135	63	E	465.3	2,631.0	20,294.0	313,704.2		1,036.7	3,684.4	2,113.0
1069	64	A	539.4	2,739.0	15,727.3	251,363.9		1,733.0	2,622.3	3,544.4
1070	64	B	459.7	3,935.0	25,137.7	224,751.9		2,276.1	588.8	4,878.3
1071	64	C	320.2	1,547.4	19,358.0	292,550.6		0.0	1,103.4	2,019.9
1072	64	D	745.3	5,510.6	24,221.8	161,929.7		2,183.5	412.8	6,482.9
1073	64	E	395.0	2,195.6	6,069.9	316,829.0		0.0	5,432.8	1,669.7
1064	65	A	668.8	3,039.3	16,679.8	258,073.0		2,222.4	1,244.3	4,095.8
1065	65	B	354.5	2,547.9	22,436.3	259,278.5		0.0	1,673.1	3,058.7
1066	65	C	477.9	1,786.1	22,482.3	298,125.8		848.5	994.4	2,119.2
1067	65	D	334.8	4,864.4	12,088.8	215,032.1		1,796.7	924.7	2,770.7
1068	65	E	768.6	1,876.3	16,936.2	285,064.9		0.0	655.3	1,967.9
1059	66	A	231.2	1,446.8	0.0	353,935.6		0.0	1,134.2	1,301.9
1060	66	B	278.7	2,216.2	19,506.3	304,131.7		1,459.0	1,103.3	2,774.7
1061	66	C	343.9	2,635.4	15,265.7	240,521.5		1,489.6	645.5	2,312.6
1062	66	D	269.3	1,543.4	0.0	344,174.3		0.0	4,019.0	1,589.1
1063	66	E	493.9	1,600.5	14,849.5	327,895.1		0.0	2,759.2	2,336.6
1054	67	A	640.2	5,091.1	30,573.6	155,962.0		3,166.6	832.1	5,219.3
1055	67	B	580.0	2,898.5	21,811.1	258,877.9		1,401.3	1,029.1	2,592.0
1056	67	C	187.9	2,045.6	7,279.3	345,607.9		0.0	6,251.0	1,518.4
1057	67	D	314.8	2,650.3	17,915.8	315,577.7		0.0	4,750.2	1,636.1
1058	67	E	319.5	3,054.1	16,642.9	273,516.6		1,680.3	1,761.0	2,742.2
1049	68	A	691.7	6,504.0	56,428.2	141,792.8		4,282.1	1,450.0	9,091.3
1050	68	B	482.3	2,185.6	14,992.3	298,555.1		681.4	1,832.7	2,226.5
1051	68	C	438.6	2,497.6	12,432.0	283,959.1		978.6	1,558.8	2,080.1
1052	68	D	330.2	2,055.0	13,596.7	329,553.8		0.0	1,794.2	1,381.0
1053	68	E	188.5	4,696.3	10,879.5	307,730.6		0.0	2,278.4	1,854.0
1044	69	A	580.8	2,416.6	22,466.6	266,034.3		1,428.5	819.6	3,133.3
1045	69	B	335.3	4,002.6	31,716.9	211,864.1		1,503.3	1,041.5	3,664.0
1046	69	C	332.9	1,859.1	7,437.6	318,074.4		0.0	1,226.3	1,869.5
1047	69	D	347.1	1,473.2	13,132.3	323,031.8		0.0	1,124.4	1,412.6
1048	69	E	344.7	3,159.6	10,872.7	249,603.8		2,250.9	1,536.7	3,615.2
1039	70	A	199.8	1,564.0	17,210.7	336,324.9		0.0	1,100.4	1,229.9
1040	70	B	438.5	2,799.5	7,490.9	288,185.8		845.0	946.8	2,170.3
1041	70	C	311.1	1,814.8	7,424.8	346,512.9		0.0	1,284.6	1,249.6
1042	70	D	385.0	2,721.7	12,563.1	262,069.3		1,596.4	1,183.5	3,022.5
1043	70	E	1,059.6	2,803.5	7,833.6	259,580.0		837.7	1,525.7	2,334.4
1035	71	A	425.1	2,402.4	14,662.2	270,408.3		1,435.2	1,205.3	2,902.0
1036	71	B	378.6	1,894.2	18,570.8	292,563.1		1,437.3	1,272.8	2,769.8
1037	71	C	645.1	2,443.1	16,328.5	246,362.0		955.4	799.7	3,195.9
1038	71	D	410.4	5,955.2	20,073.8	180,000.9		1,421.2	1,310.1	3,992.8
1031	72	A	412.4	2,255.8	18,105.5	281,196.7		1,477.1	4,319.6	2,417.5
1032	72	B	348.4	2,458.3	9,334.9	251,707.6		1,084.6	4,574.0	2,550.2
1033	72	C	314.4	5,061.9	12,328.4	254,529.6		997.3	1,249.3	2,140.0
1034	72	D	403.2	2,126.9	7,800.9	322,354.5		0.0	5,893.3	1,725.0
1026	73	A	439.1	2,846.2	0.0	317,755.0		766.4	1,708.1	1,929.2
1027	73	B	351.9	2,695.2	21,546.6	281,742.2		2,874.5	4,630.4	3,151.2
1028	73	C	173.2	1,391.5	14,313.9	354,148.3		0.0	4,605.3	1,400.0
1029	73	D	405.2	2,408.6	8,371.9	300,671.0		954.0	5,344.7	1,923.2

A	B	C	D	E	F	G	H	I	J	K
1030	73	E	416.3	2,200.0	9,757.8	265,751.2		0.0	4,481.6	2,350.2
815	74	A	203.4	1,349.8	8,488.7	310,759.6		0.0	1,270.6	1,490.6
816	74	B	445.9	3,190.3	10,851.2	246,860.8		1,824.3	4,458.1	4,025.7
817	74	C	454.3	1,967.0	20,673.2	453,111.6		1,784.5	4,955.6	2,397.0
818	74	D	401.5	6,303.9	22,379.5	178,903.2		2,745.5	927.7	5,328.7
810	75	A	293.1	1,358.2	7,606.0	316,813.3		1,407.8	1,078.6	1,751.9
811	75	B	347.0	1,686.9	0.0	328,404.8		0.0	1,201.5	1,650.0
812	75	C	545.1	3,352.6	23,518.7	241,199.9		3,449.5	743.9	4,955.8
813	75	D	467.0	1,441.9	18,779.0	376,327.0		924.5	878.2	2,038.6
814	75	E	359.2	2,006.7	8,174.6	313,165.7		0.0	838.0	1,984.1
805	76	A	261.7	1,556.7	7,130.6	345,291.2		0.0	1,550.5	1,291.3
806	76	B	187.3	1,053.6	11,045.8	371,511.7		0.0	1,160.9	1,216.6
807	76	C	279.6	1,880.9	7,318.1	289,755.4		0.0	2,057.4	1,951.1
808	76	D	434.0	5,161.4	9,728.2	249,436.4		1,245.3	1,798.8	2,863.3
809	76	E	557.5	2,931.6	23,778.2	264,296.5		1,194.8	1,142.3	2,936.2
800	77	A	242.1	1,232.3	16,937.2	348,118.5		0.0	1,184.4	1,359.4
801	77	B	241.8	1,356.4	14,710.3	340,446.9		0.0	1,765.7	1,424.3
802	77	C	792.6	11,186.5	58,394.4	95,038.7		6,539.9	1,335.0	15,324.1
803	77	D	414.8	3,898.5	23,925.3	170,709.2		2,237.8	781.5	4,381.0
804	77	E	274.8	2,008.0	12,721.4	309,915.1		0.0	997.0	2,270.8
795	78	A	229.2	1,089.1	15,074.5	305,647.3		0.0	1,865.7	1,294.5
796	78	B	311.8	2,623.8	12,023.8	246,756.5		1,212.9	1,030.5	3,284.3
797	78	C	296.8	1,732.3	0.0	311,045.5		1,023.5	1,320.9	2,587.5
798	78	D	337.9	1,924.4	20,977.8	288,525.2		1,170.1	1,116.4	2,247.7
799	78	E	510.3	2,059.0	11,796.9	335,031.3		1,034.5	1,548.2	2,102.9
790	79	A	321.5	2,841.4	13,629.0	319,774.4		0.0	6,222.3	1,912.4
791	79	B	254.4	1,009.1	6,919.5	332,883.9		861.9	786.2	1,515.8
792	79	C	360.4	2,583.5	19,863.9	284,184.6		1,882.7	1,228.0	3,384.9
793	79	D	330.3	1,990.0	14,620.2	304,908.4		954.8	985.5	2,723.9
794	79	E	374.1	2,350.0	10,186.0	350,460.4		0.0	4,668.9	2,079.8
783	80	A	316.6	2,236.3	19,660.6	263,863.5		1,805.2	861.0	2,622.4
784	80	B	298.4	1,632.1	9,245.4	334,766.0		0.0	799.8	2,006.6
785	80	C	288.0	2,523.5	7,200.7	282,025.8		1,198.9	801.7	2,855.5
786	80	D	475.7	1,530.7	20,544.5	342,618.5		1,015.1	1,483.2	2,182.3
787	80	E	334.3	1,987.3	23,486.8	327,797.5		0.0	4,057.0	2,253.1
778	81	A	538.2	3,637.9	20,418.8	233,301.0		2,693.7	796.5	4,917.5
779	81	B	244.1	1,554.7	7,401.1	308,000.5		0.0	1,370.4	1,593.9
780	81	C	375.1	2,525.2	16,860.0	314,051.4		1,628.4	884.5	2,167.6
781	81	D	268.5	2,019.1	23,351.6	328,160.8		1,093.3	5,332.1	2,481.3
782	81	E	308.1	1,201.6	0.0	346,423.0		0.0	4,050.7	1,656.3
773	82	A	246.2	1,433.5	17,774.6	316,761.8		817.7	807.5	2,072.0
774	82	B	297.2	4,890.3	13,369.4	184,508.3		2,077.1	750.9	4,769.3
775	82	C	361.3	2,098.4	17,098.8	298,372.0		860.2	860.5	2,861.2
776	82	D	324.5	1,532.5	6,222.1	348,909.2		856.2	1,550.0	1,504.7
777	82	E	400.6	1,504.0	5,695.5	326,770.4		816.9	1,148.2	1,523.4
1136	83	A	2,259.5	4,167.1	27,431.1	209,880.6		2,704.5	978.0	4,770.5
1137	83	B	200,171.8	2,157.0	13,790.4	39,811.3		976.6	244.9	1,706.0
1138	83	C	1,906.2	2,919.6	24,439.1	242,216.6		1,850.8	1,477.3	4,032.8
1139	83	D	1,655.2	2,686.7	13,745.8	98,119.1		994.5	628.0	2,615.6
1140	83	E	364.6	2,682.3	9,904.5	302,700.0		1,027.0	2,282.8	2,027.3

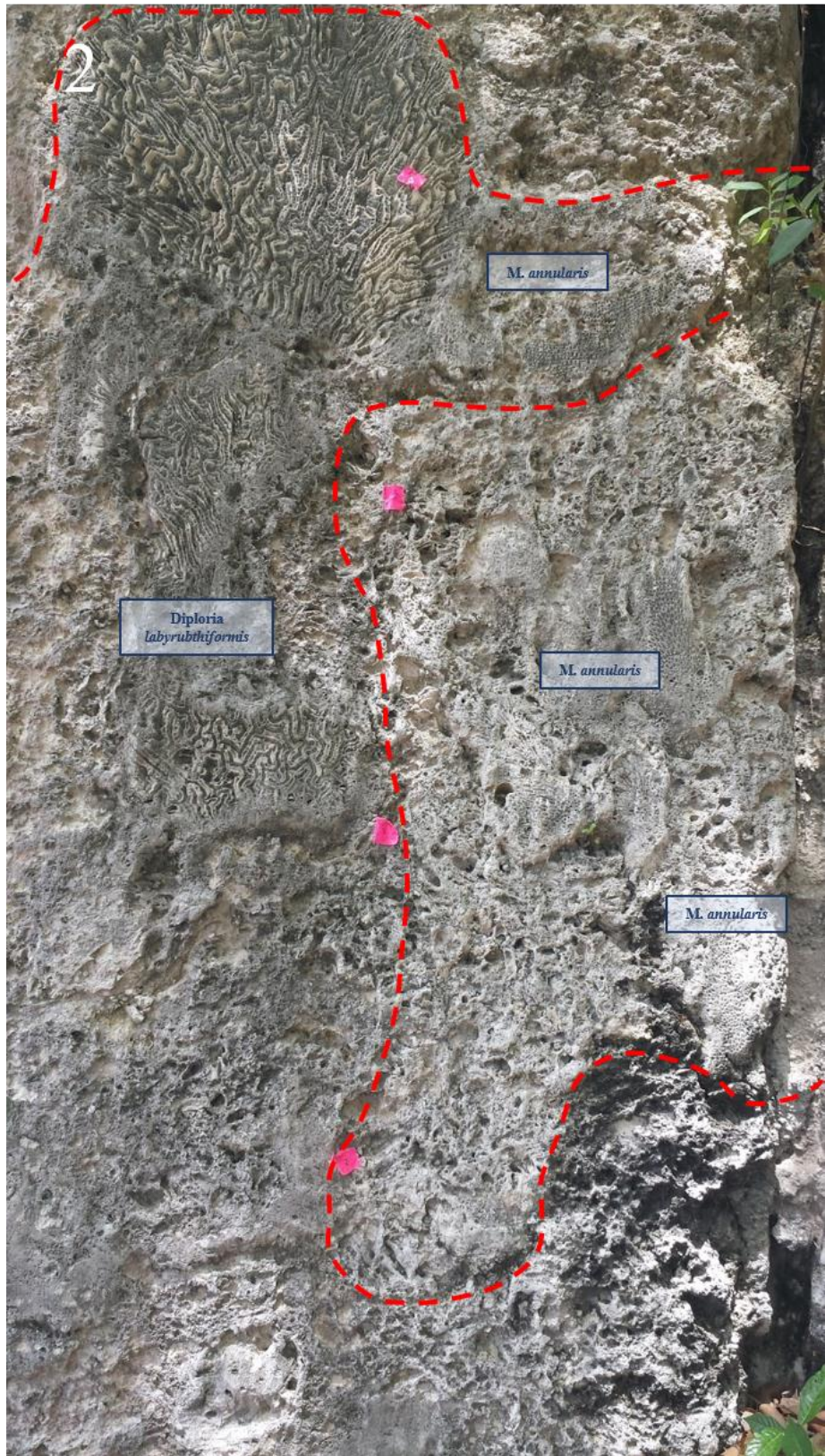
A	B	C	D	E	F	G	H	I	J	K
1113	84	A	435.9	4,126.8	5,961.8	303,064.0		869.2	1,774.8	1,902.2
1114	85	A	423.9	3,568.1	10,622.1	285,092.3		1,516.9	5,185.2	2,704.8
1115	86	A	416.2	3,929.0	8,485.9	275,378.4		1,293.7	4,996.7	2,660.8
1116	87	A	1,996.6	3,406.1	18,624.6	289,675.8		1,047.6	999.0	1,959.3
1117	88	A	3,390.9	3,738.5	20,979.4	240,479.0		2,303.0	744.4	3,836.0
1106	89	A	335.8	2,976.0	11,170.4	209,976.1		0.0	2,981.5	2,051.9
1107	89	B	444.5	3,203.2	10,936.9	300,182.9		720.7	5,009.6	1,888.0
1108	90	A	494.7	2,747.6	8,302.3	271,345.9		1,607.3	4,710.7	3,258.3
1109	90	B	206.3	1,824.0	8,705.1	335,046.3		0.0	1,679.5	1,508.4
1119	91	A	368.7	2,034.6	17,106.2	263,707.3		859.7	1,362.2	1,902.5
1120	91	B	476.9	1,724.3	9,735.8	321,143.9		0.0	1,237.3	2,192.4
1118	92	A	183.1	1,147.5	8,729.5	357,575.9		0.0	798.5	1,440.6

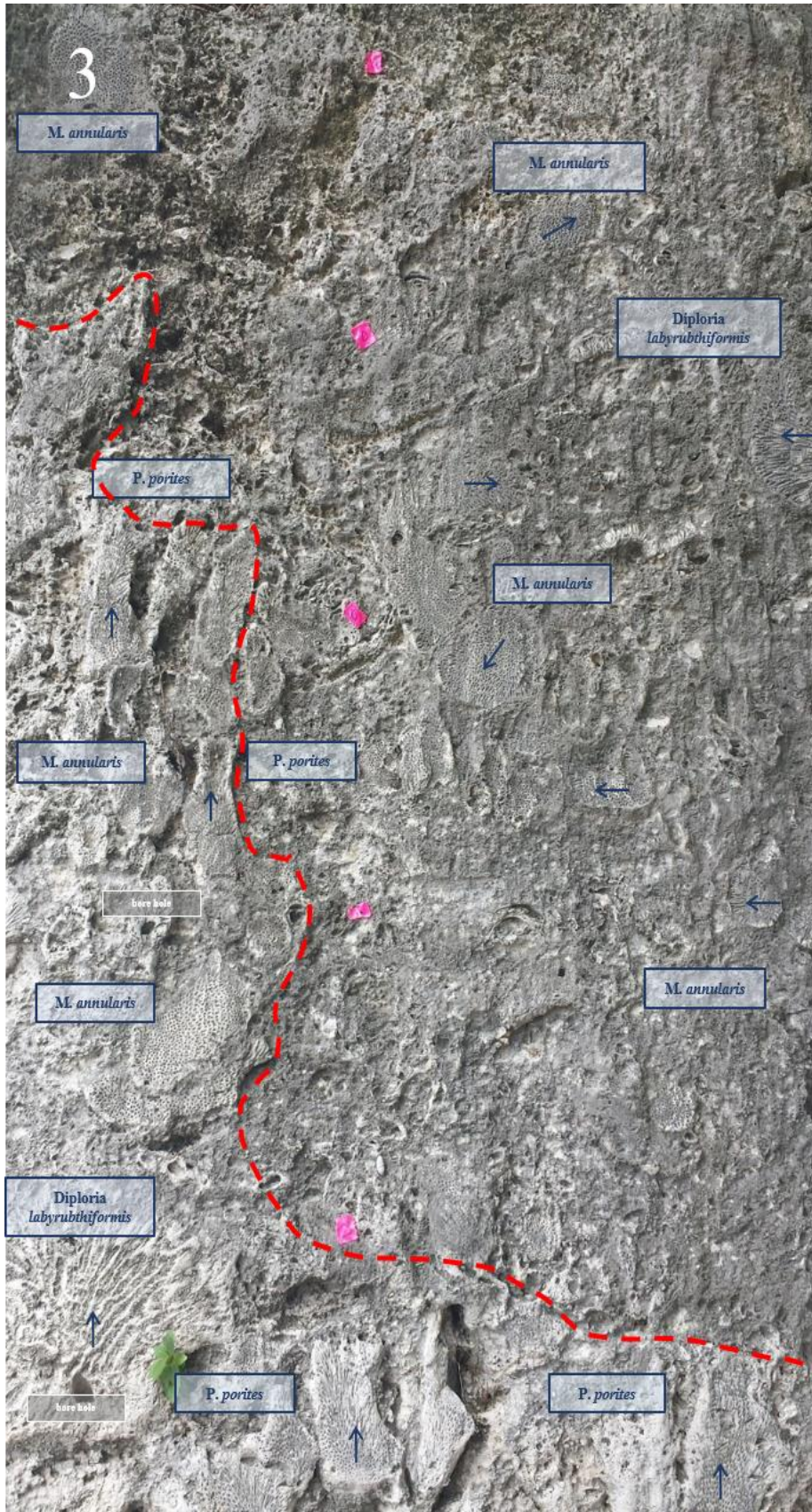


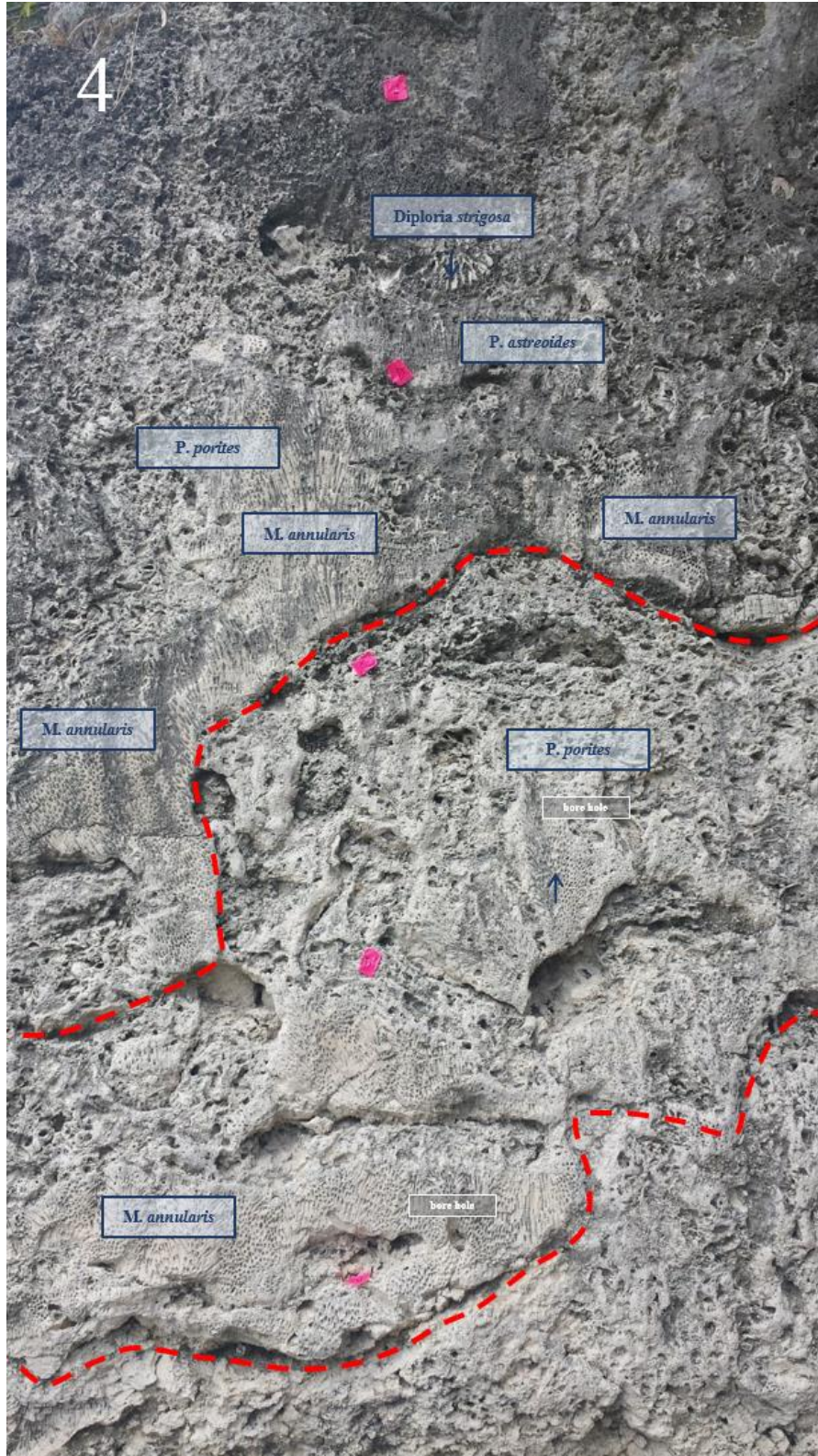
## Appendix D: Windley Key Quarry XRF Station Photo's with Coral and Discontinuity Surface Identification

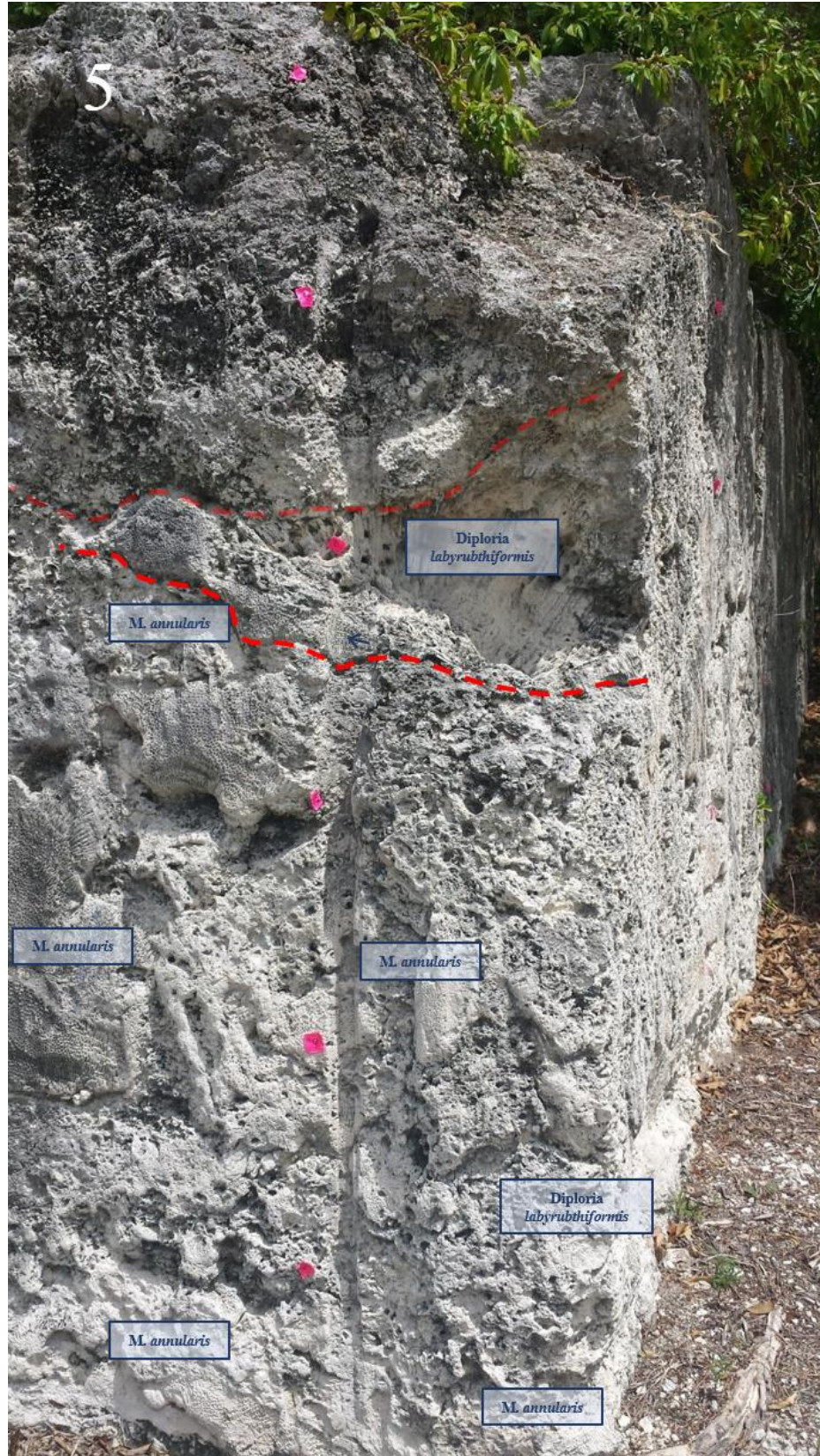
\*Refer back to page 40 for a map of each station's location\*



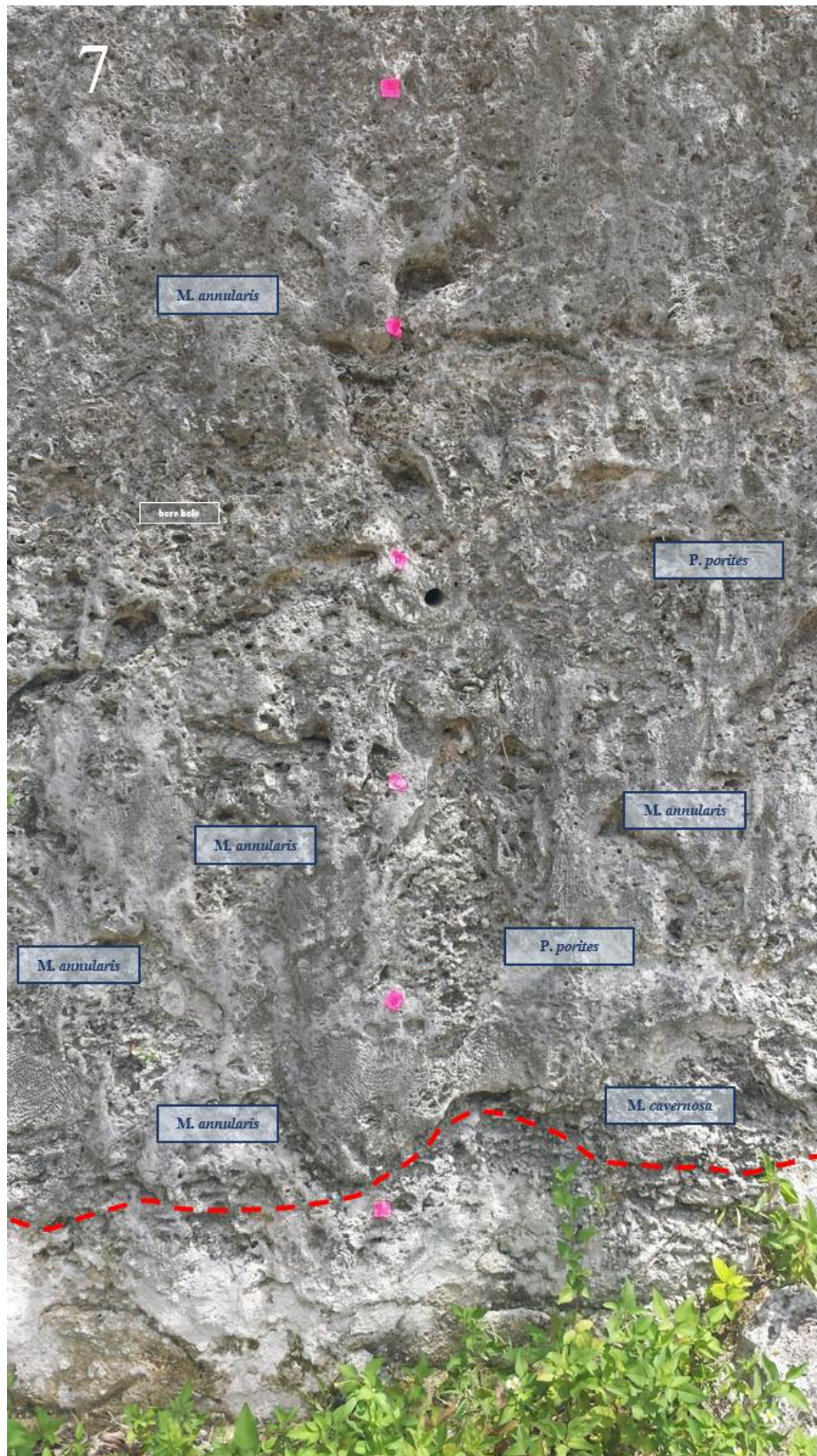






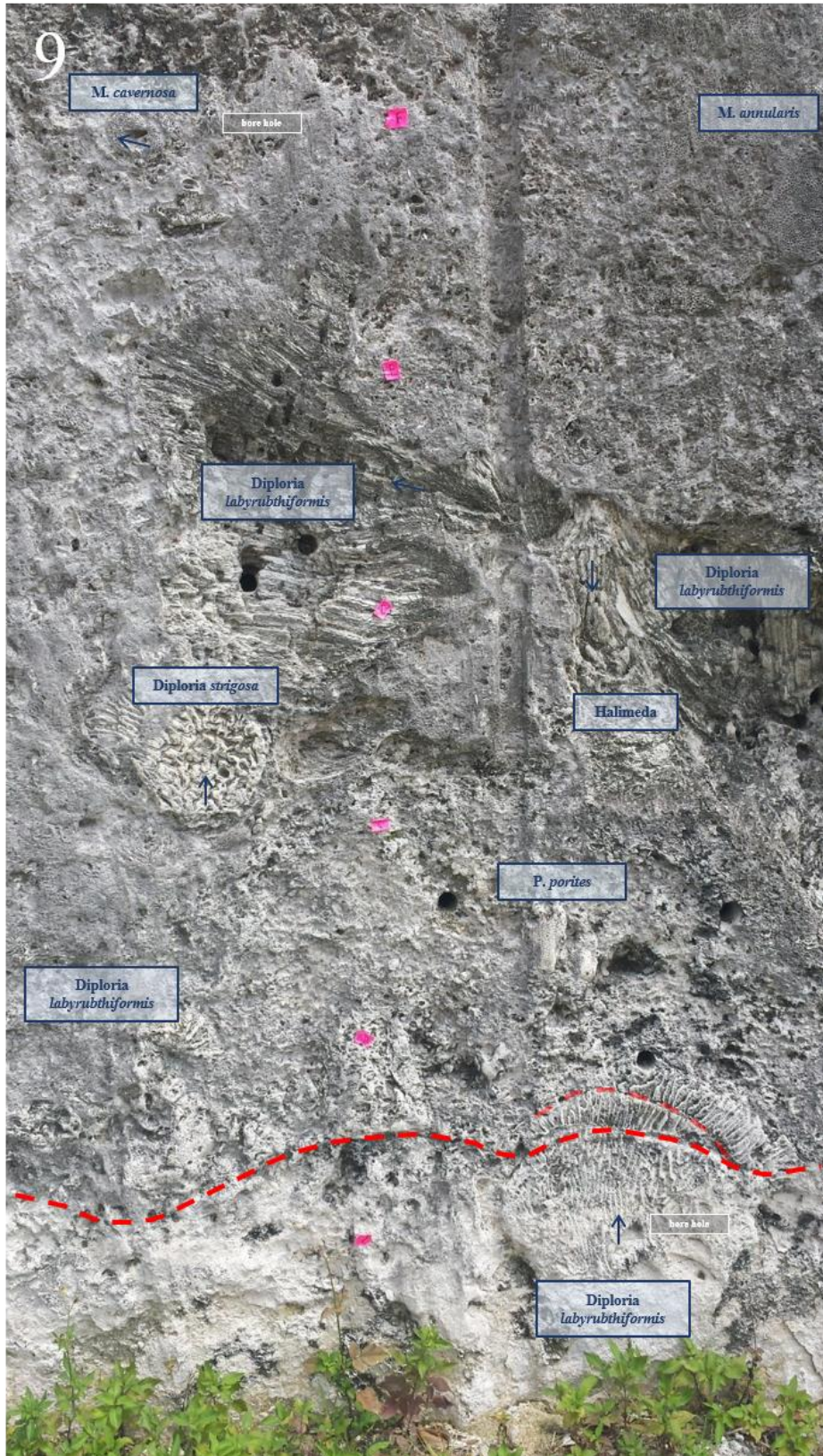


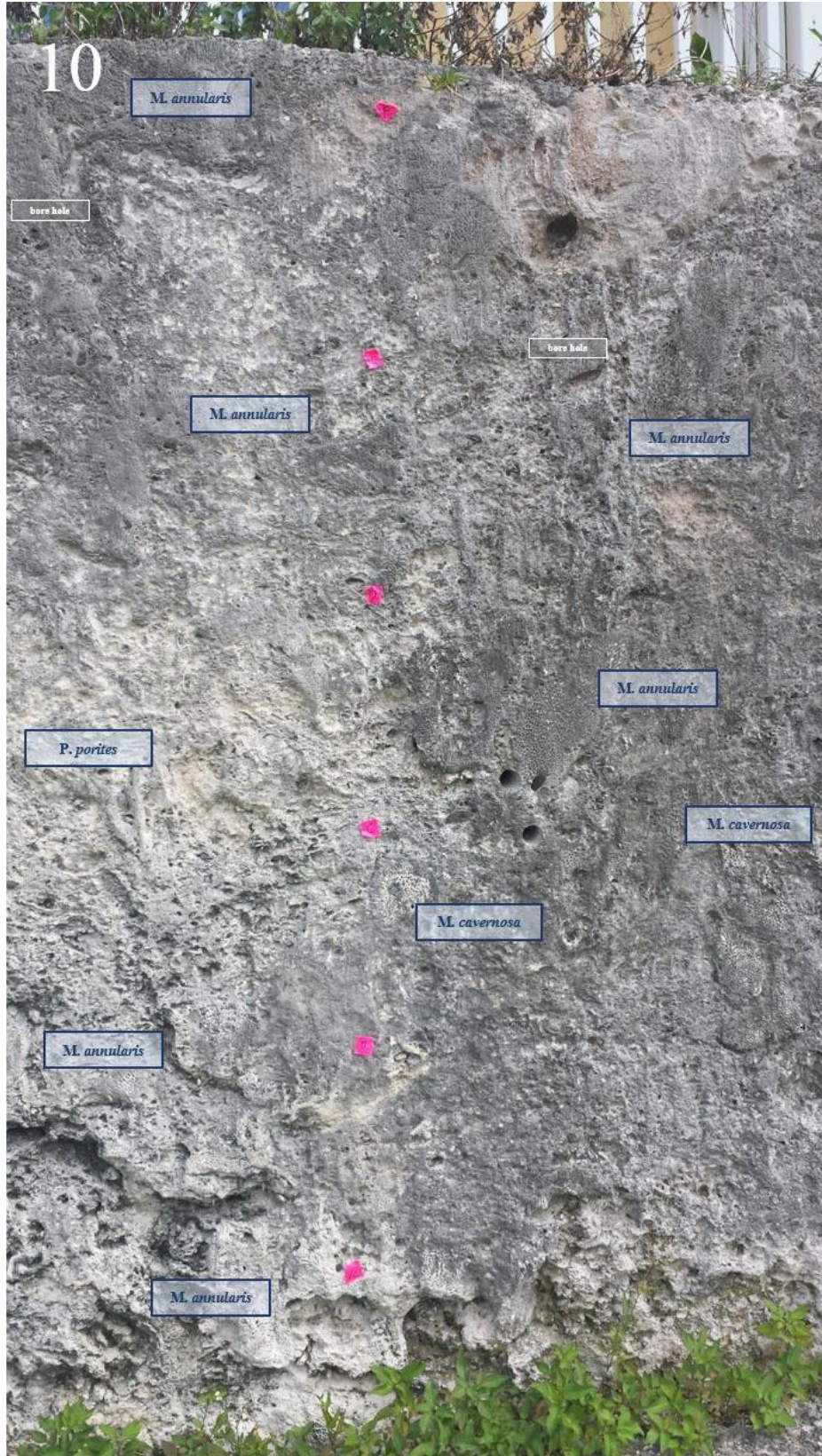


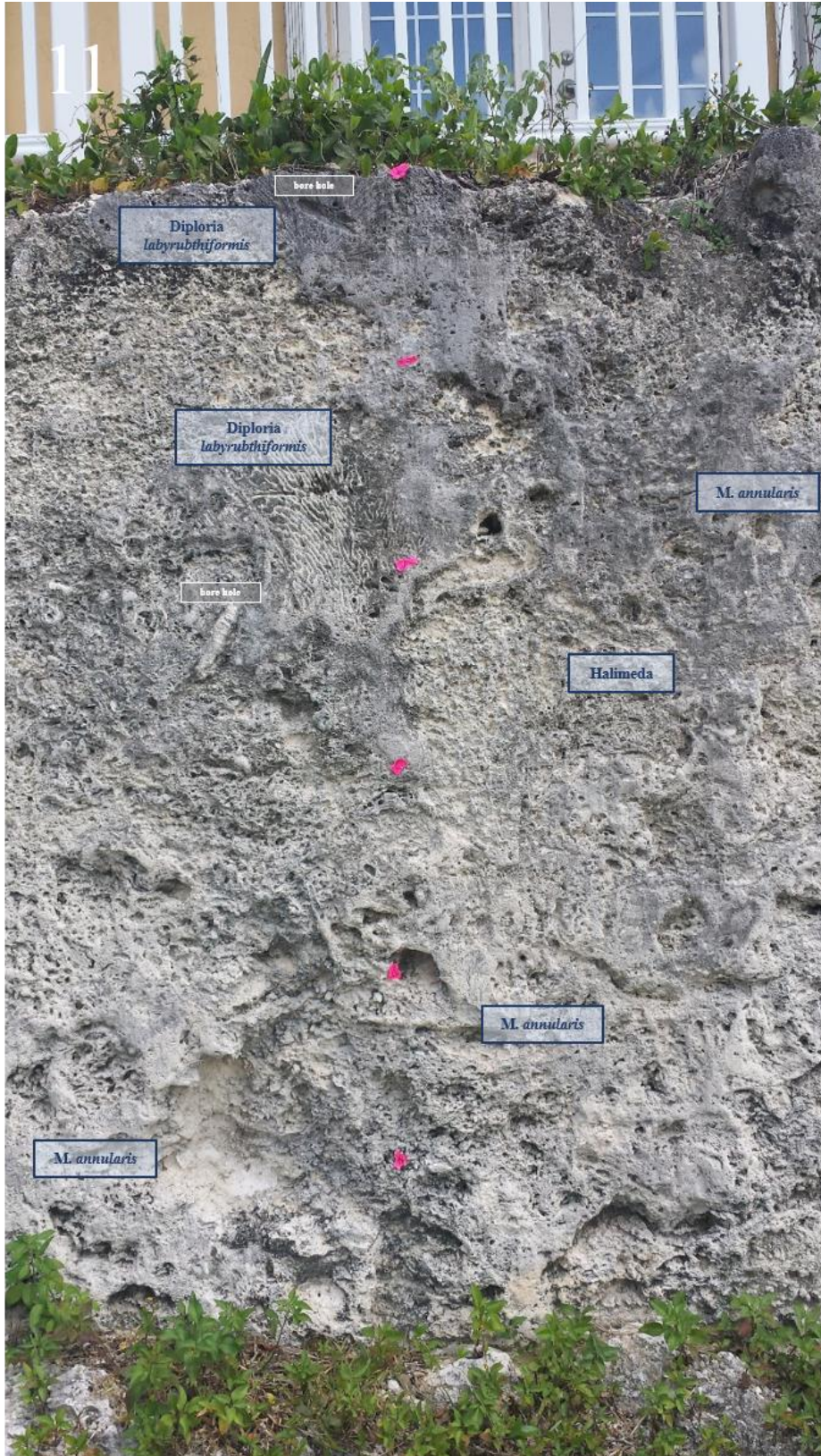


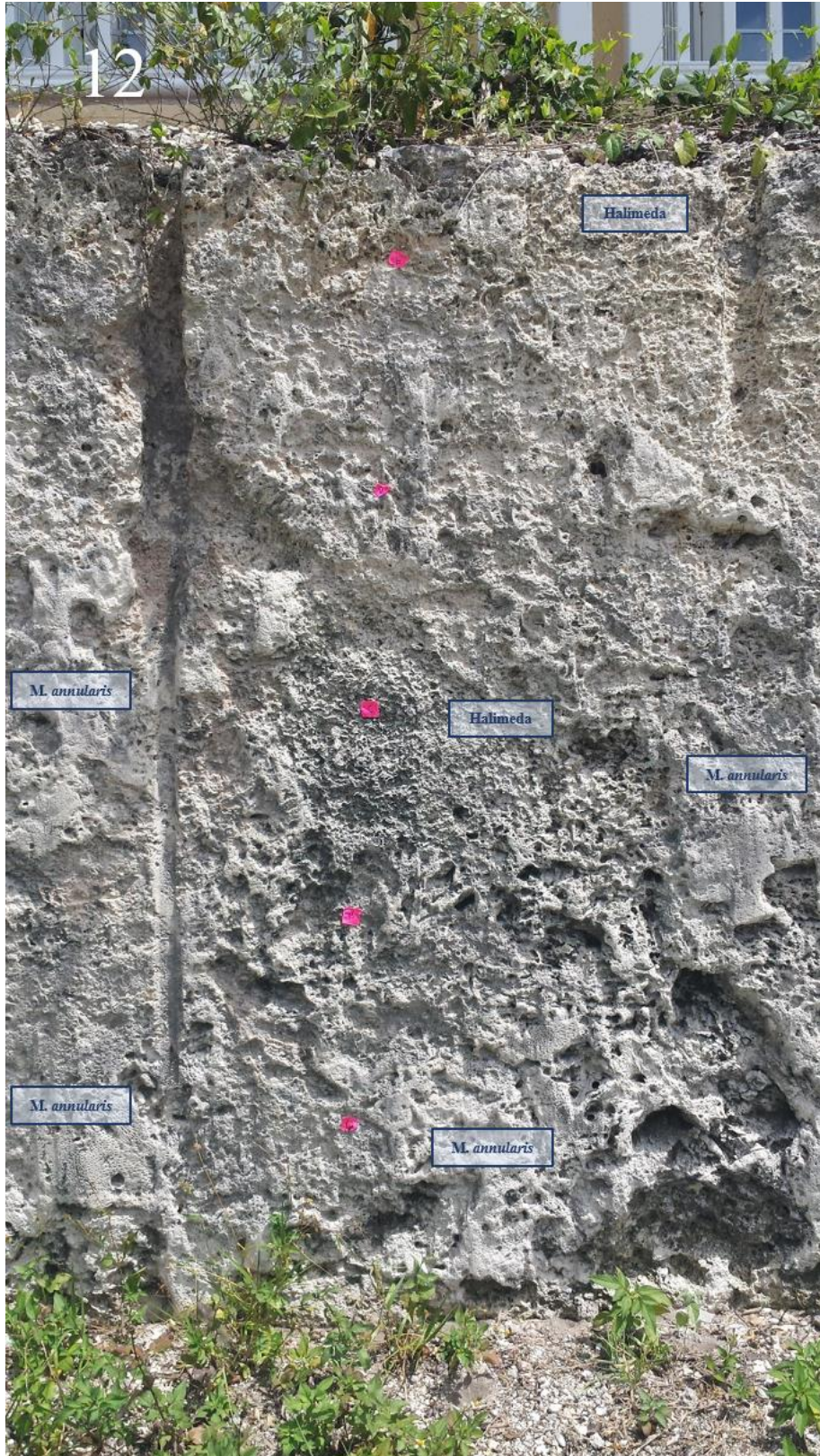


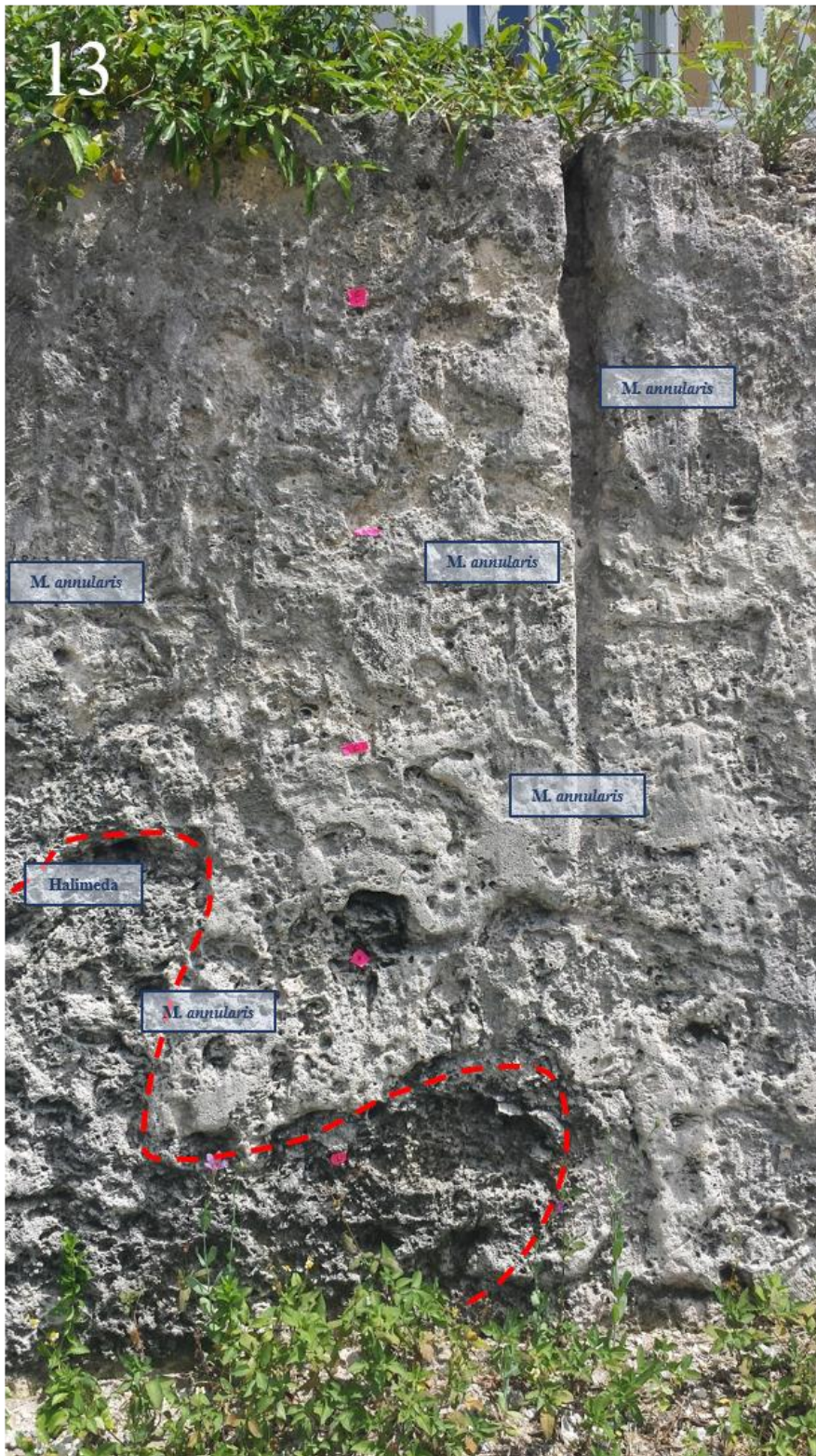


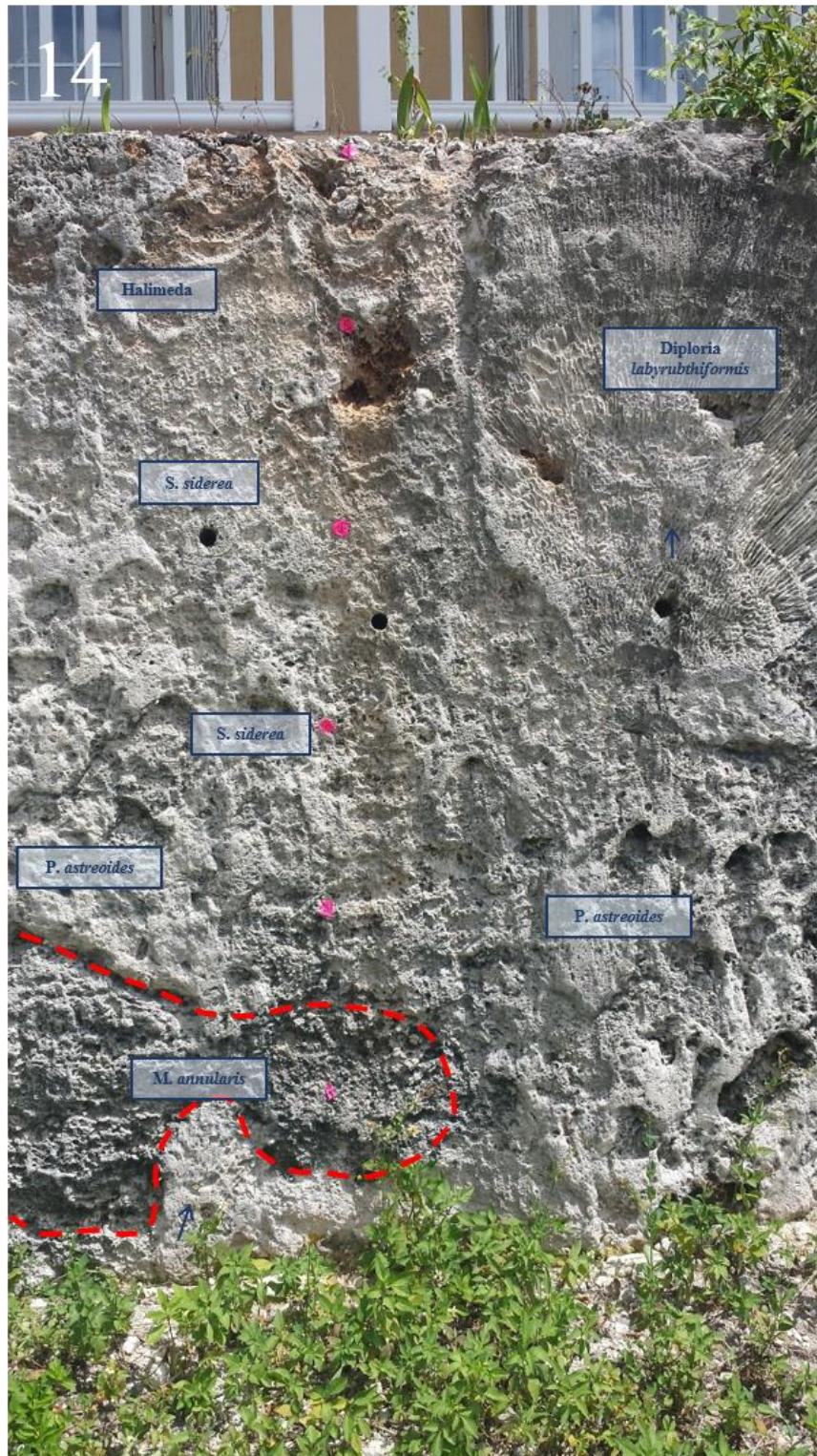


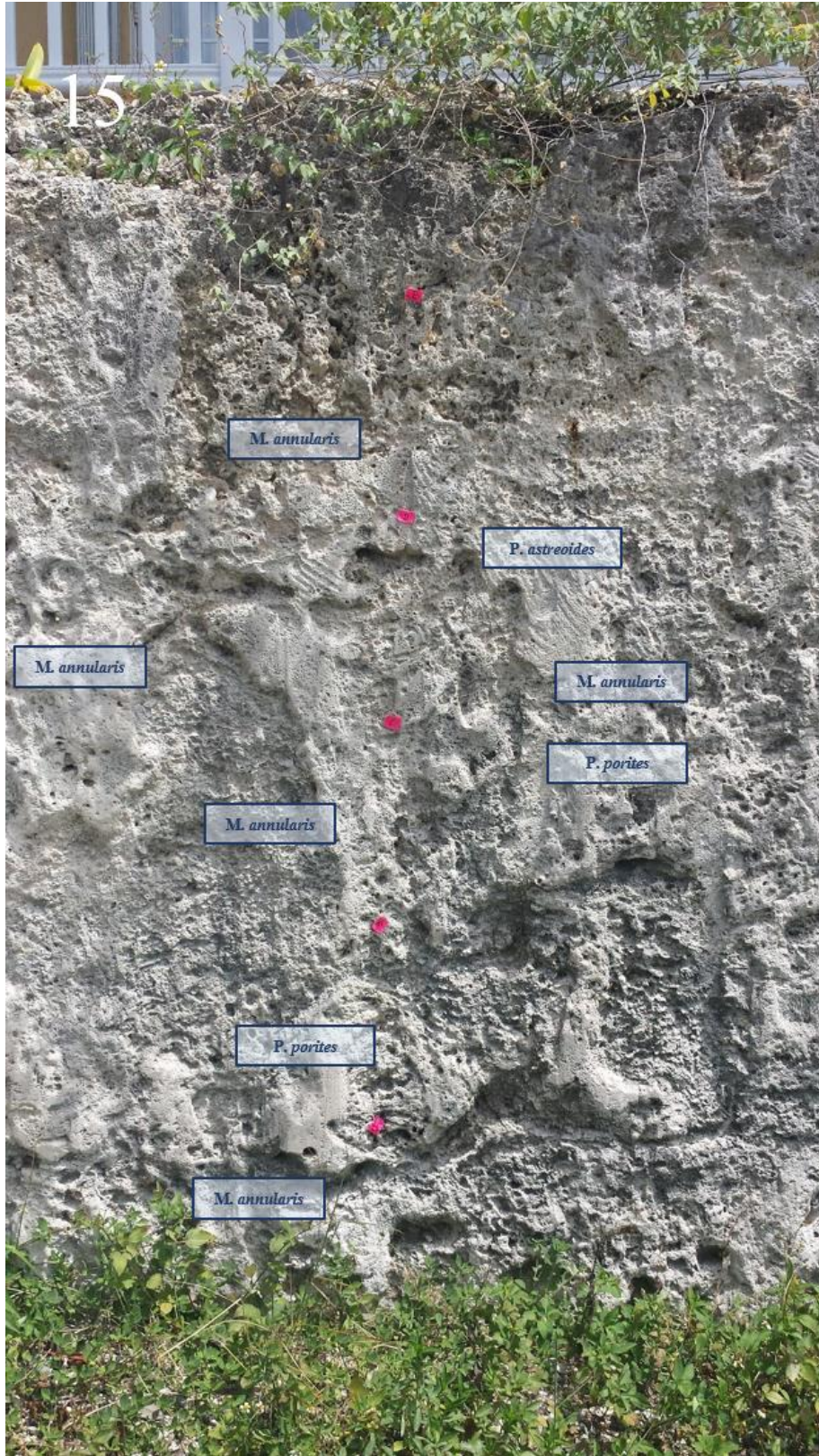




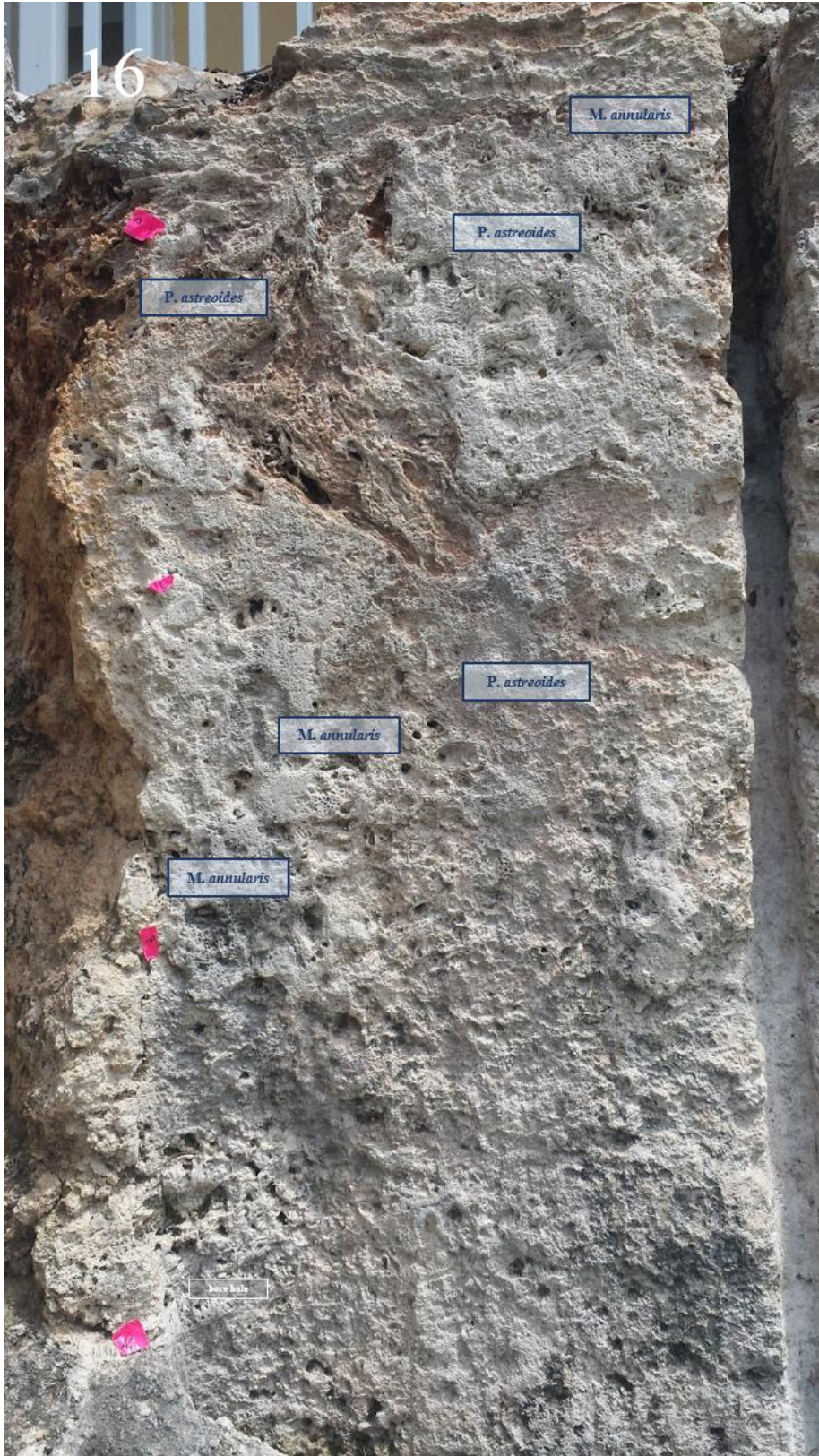






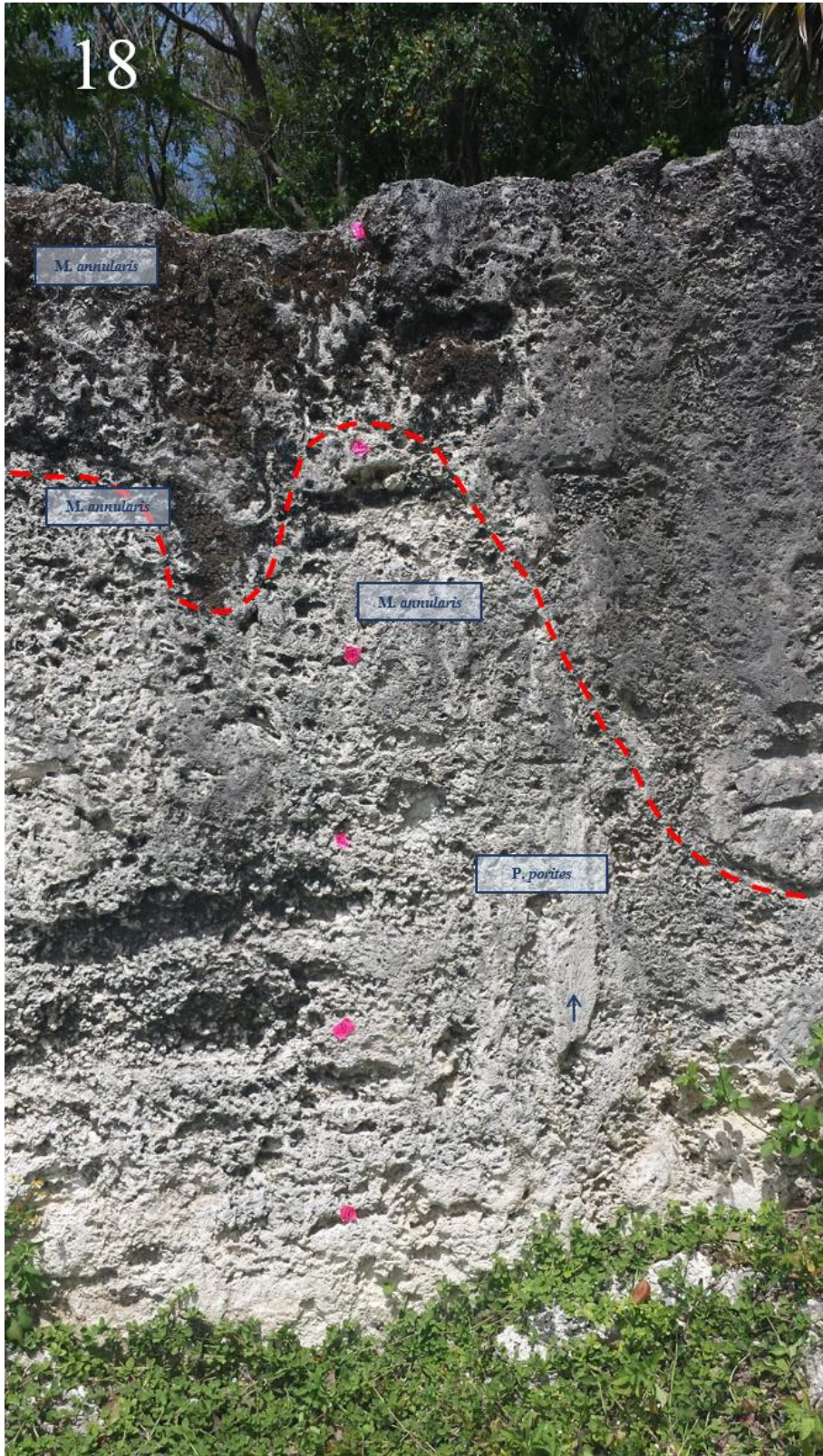


16

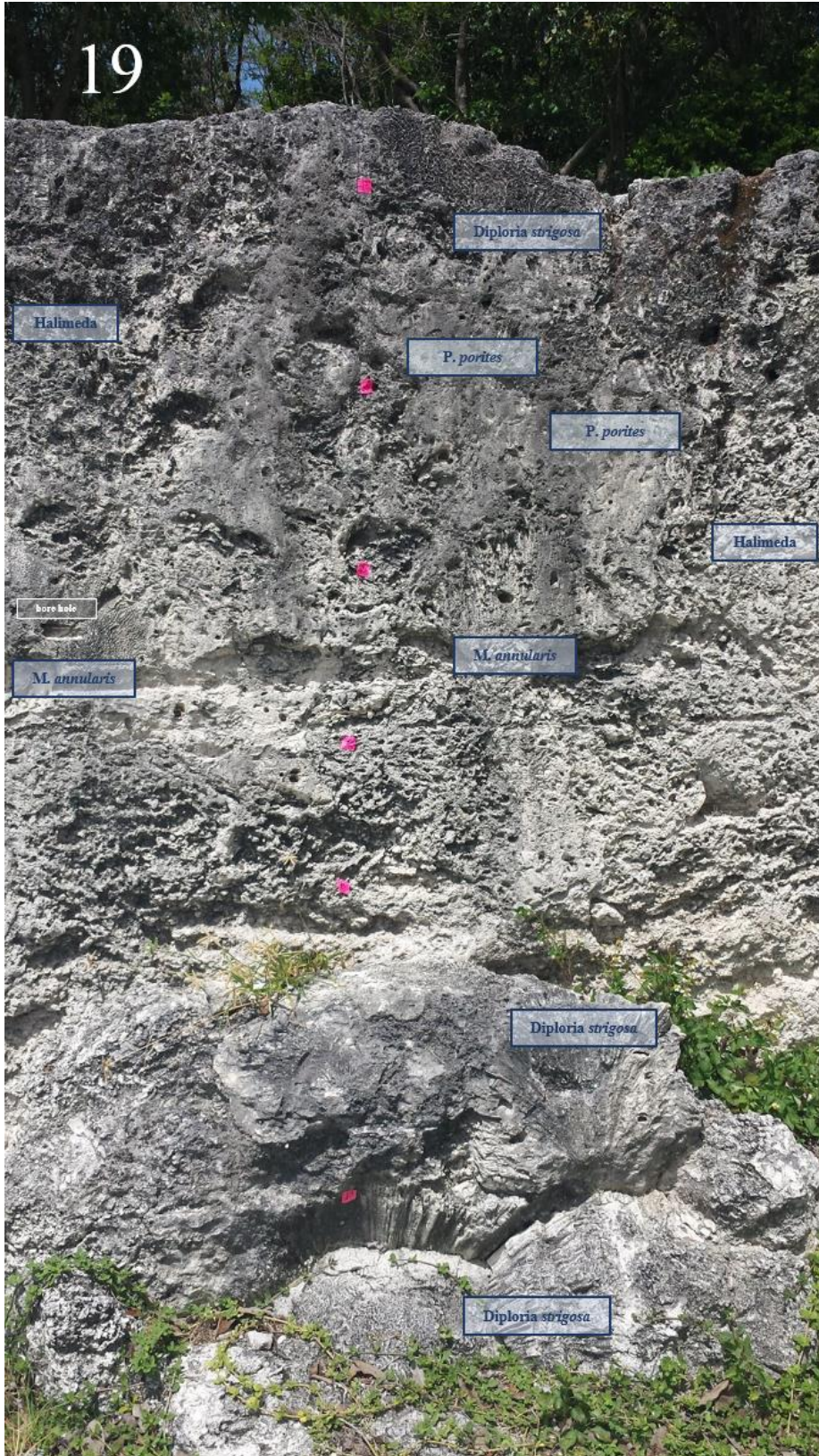


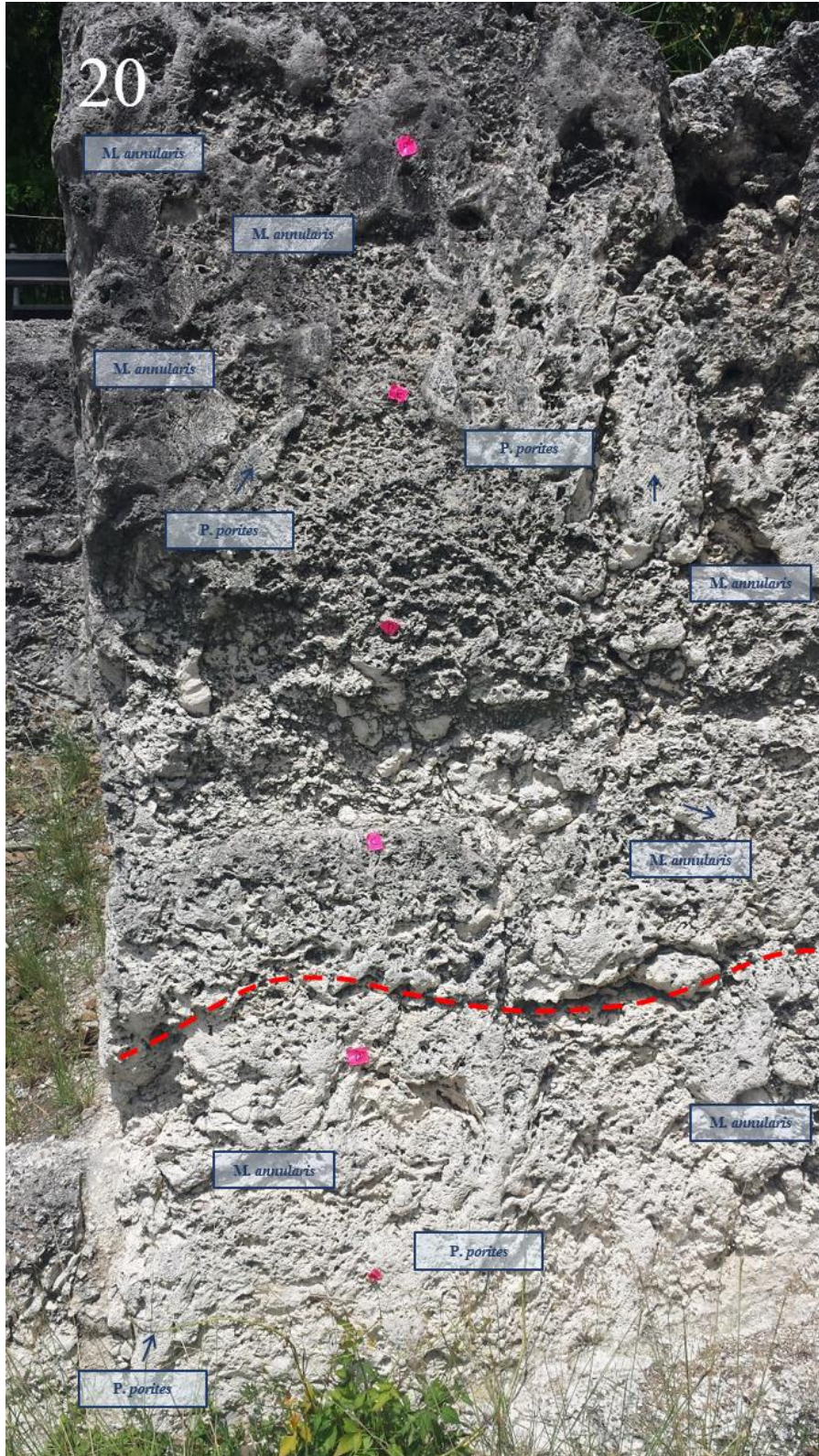


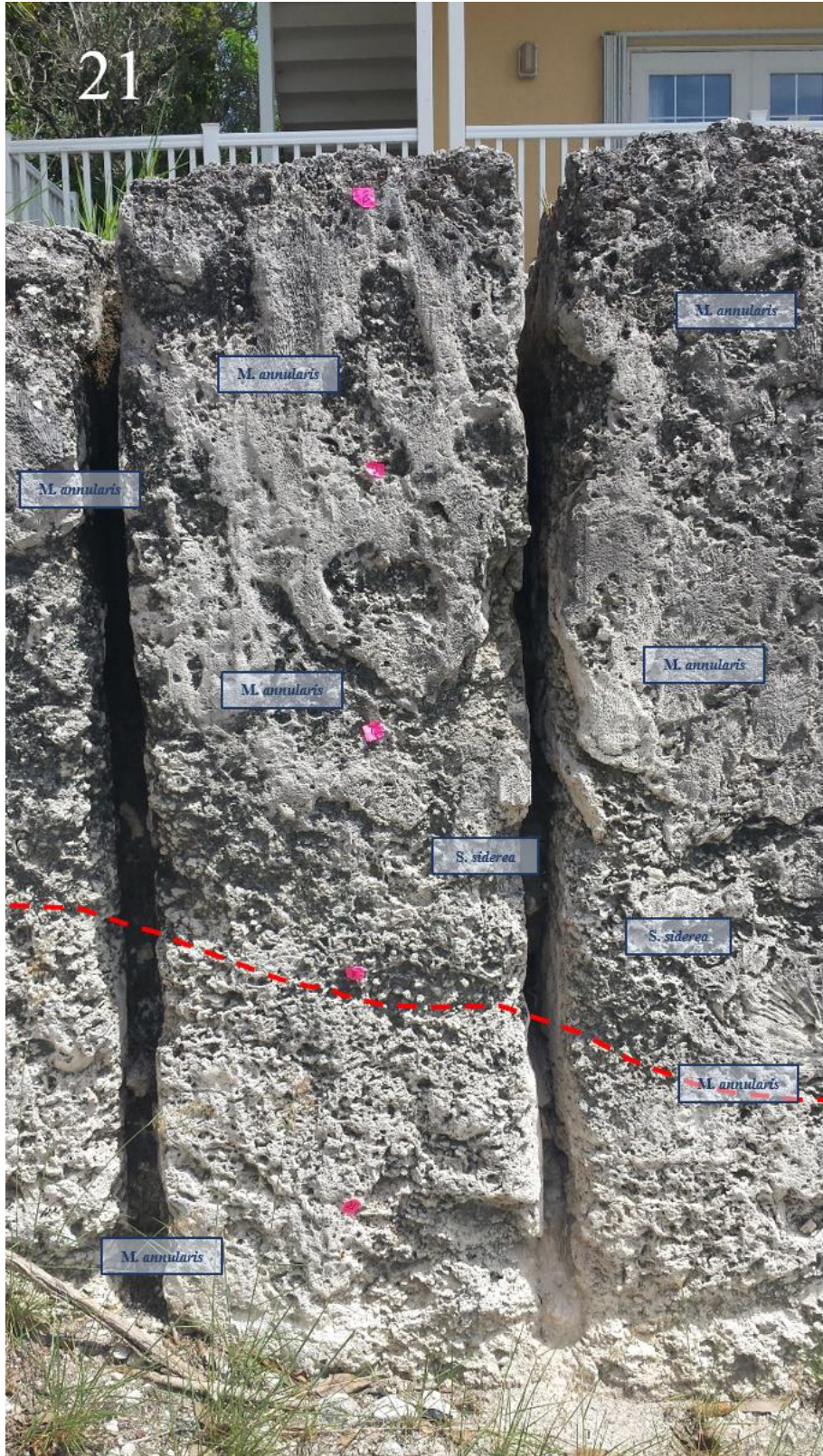




19

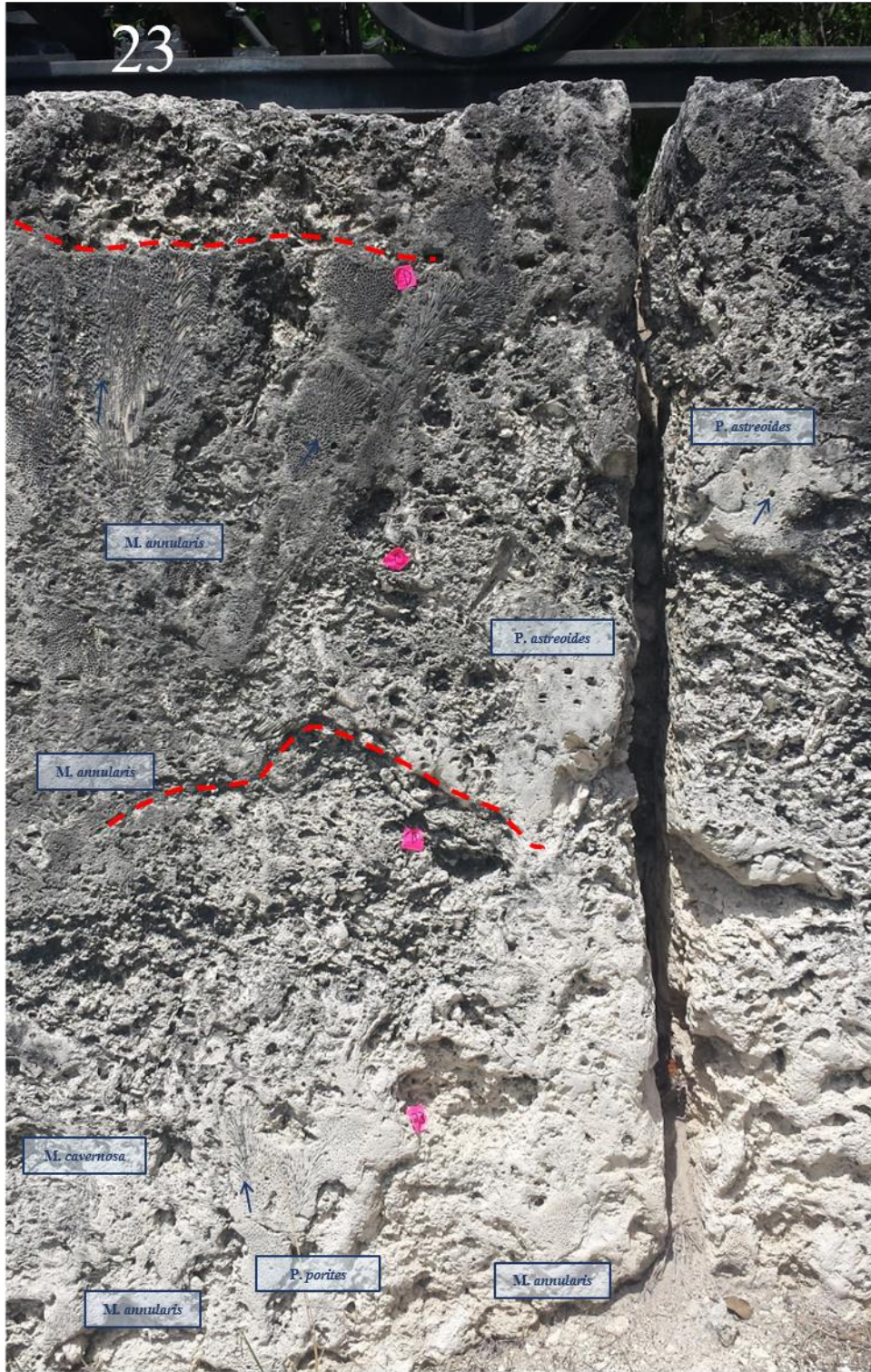








23

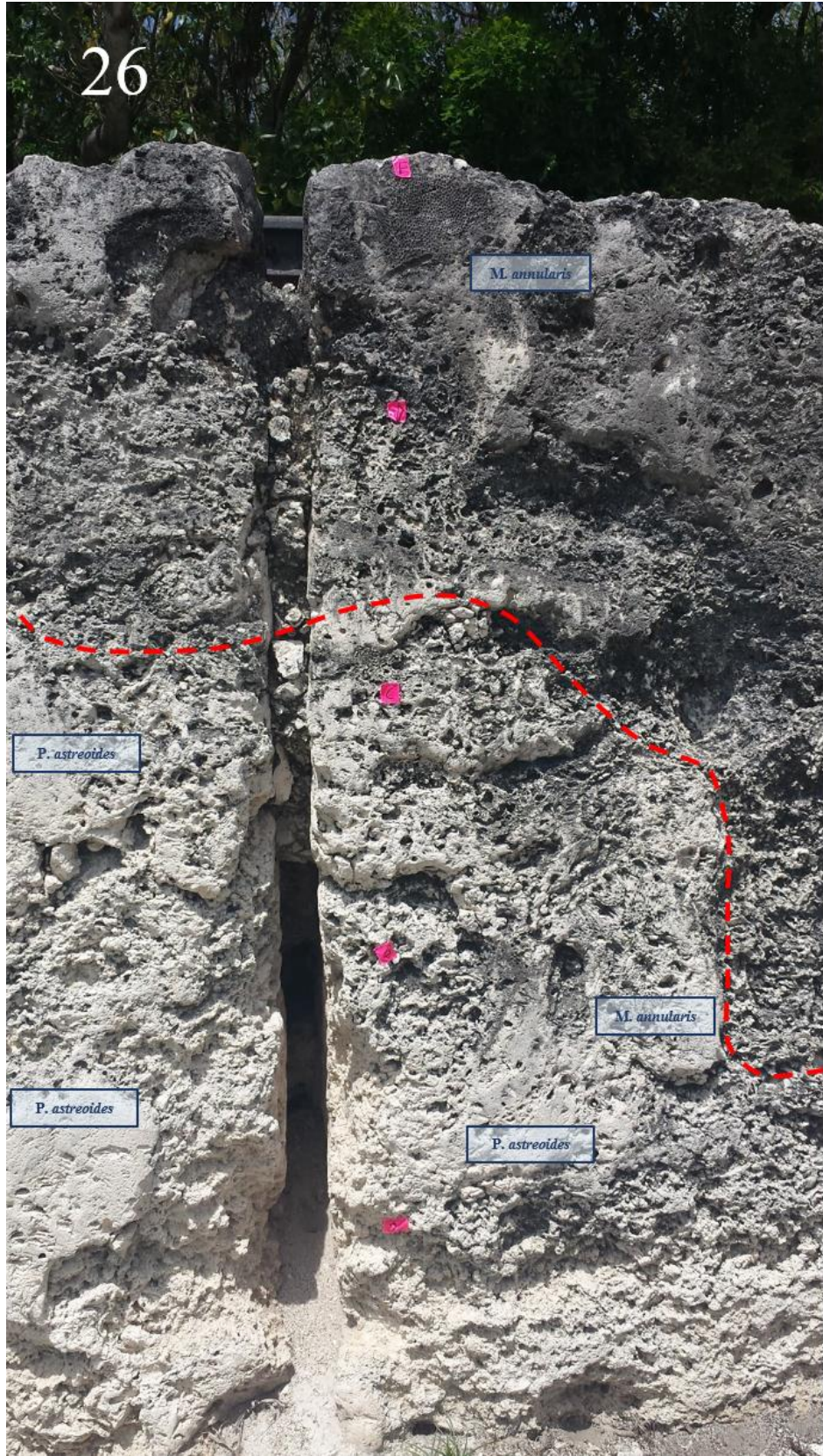




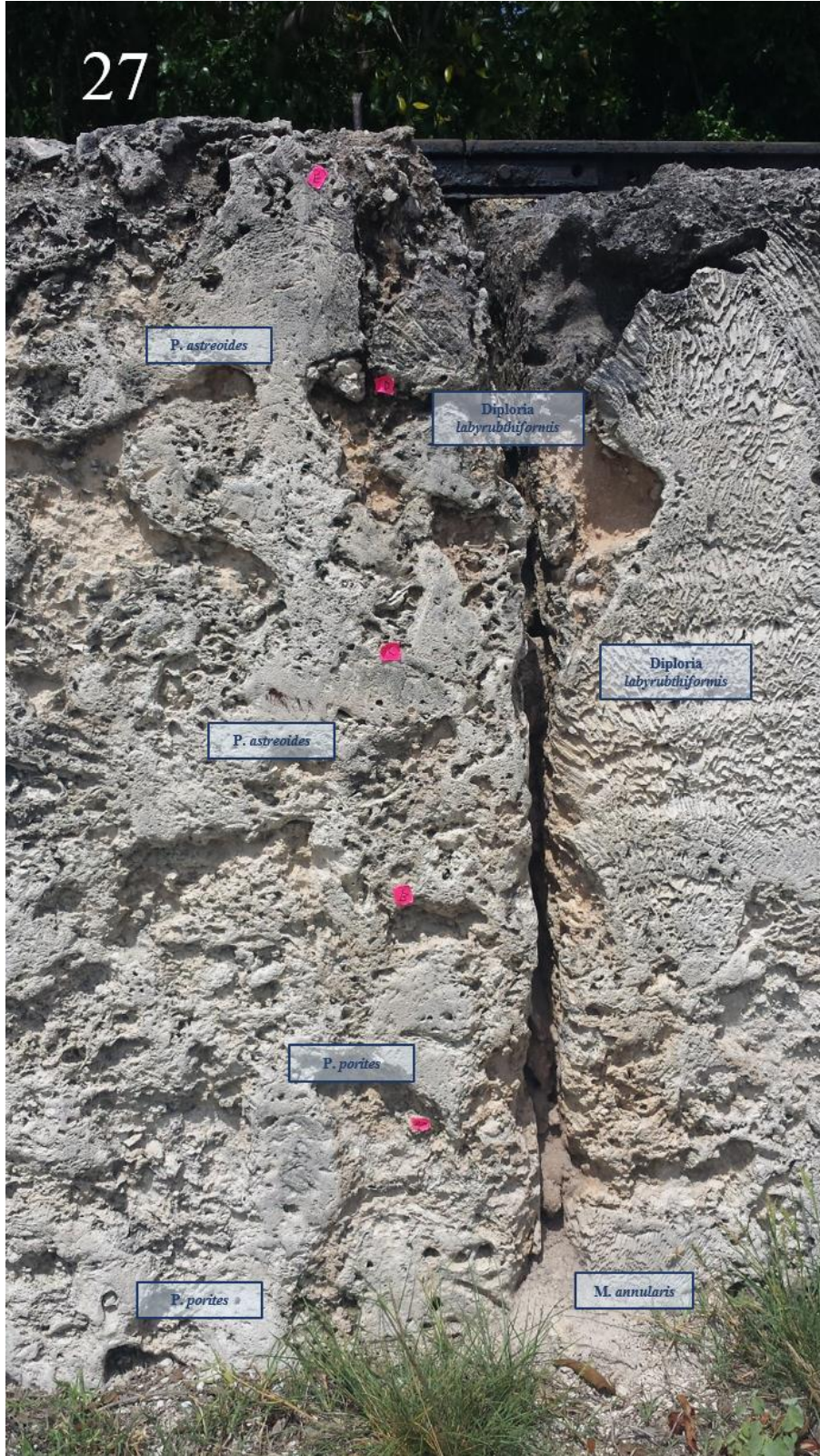
\*no station 25\*

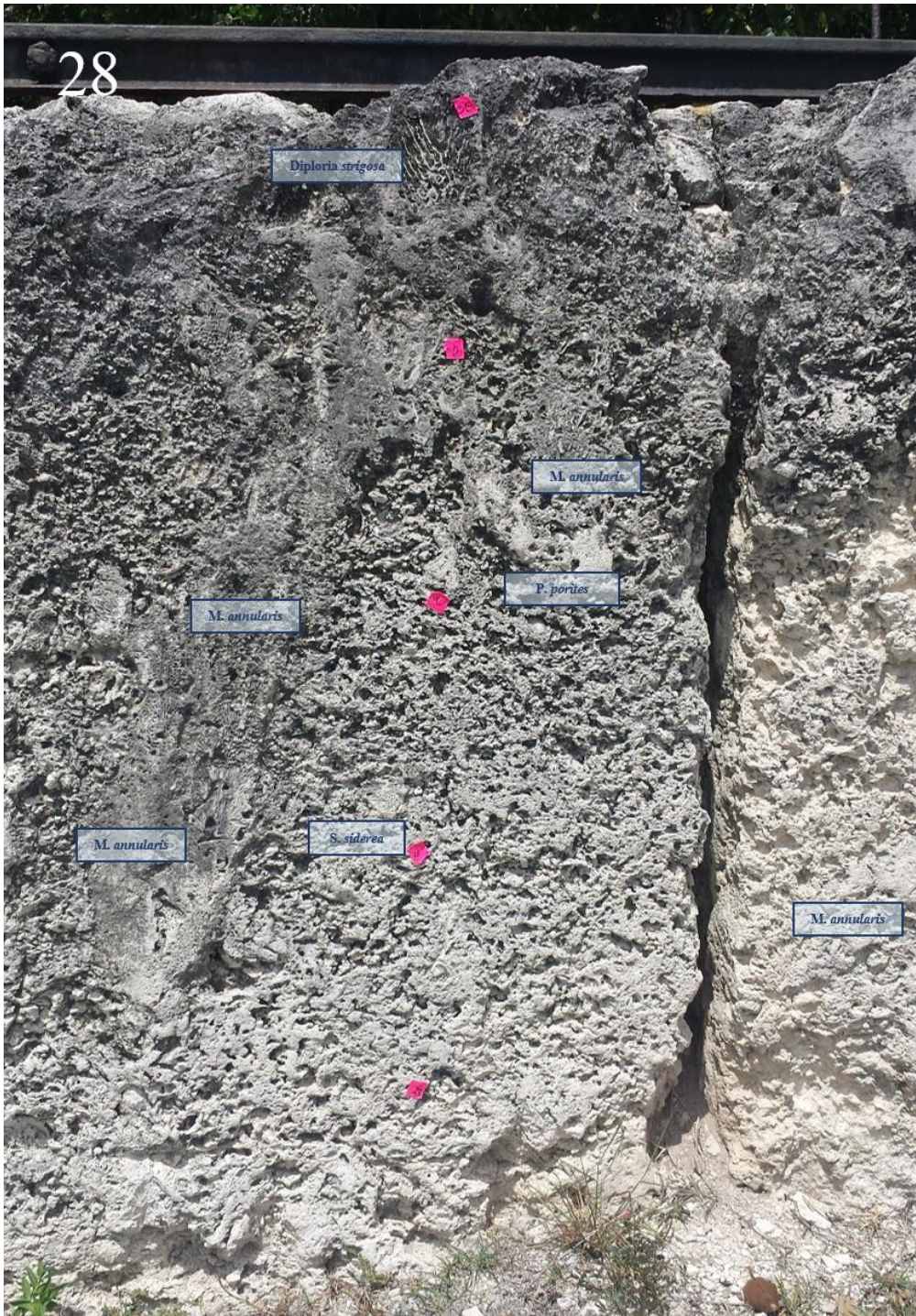


26



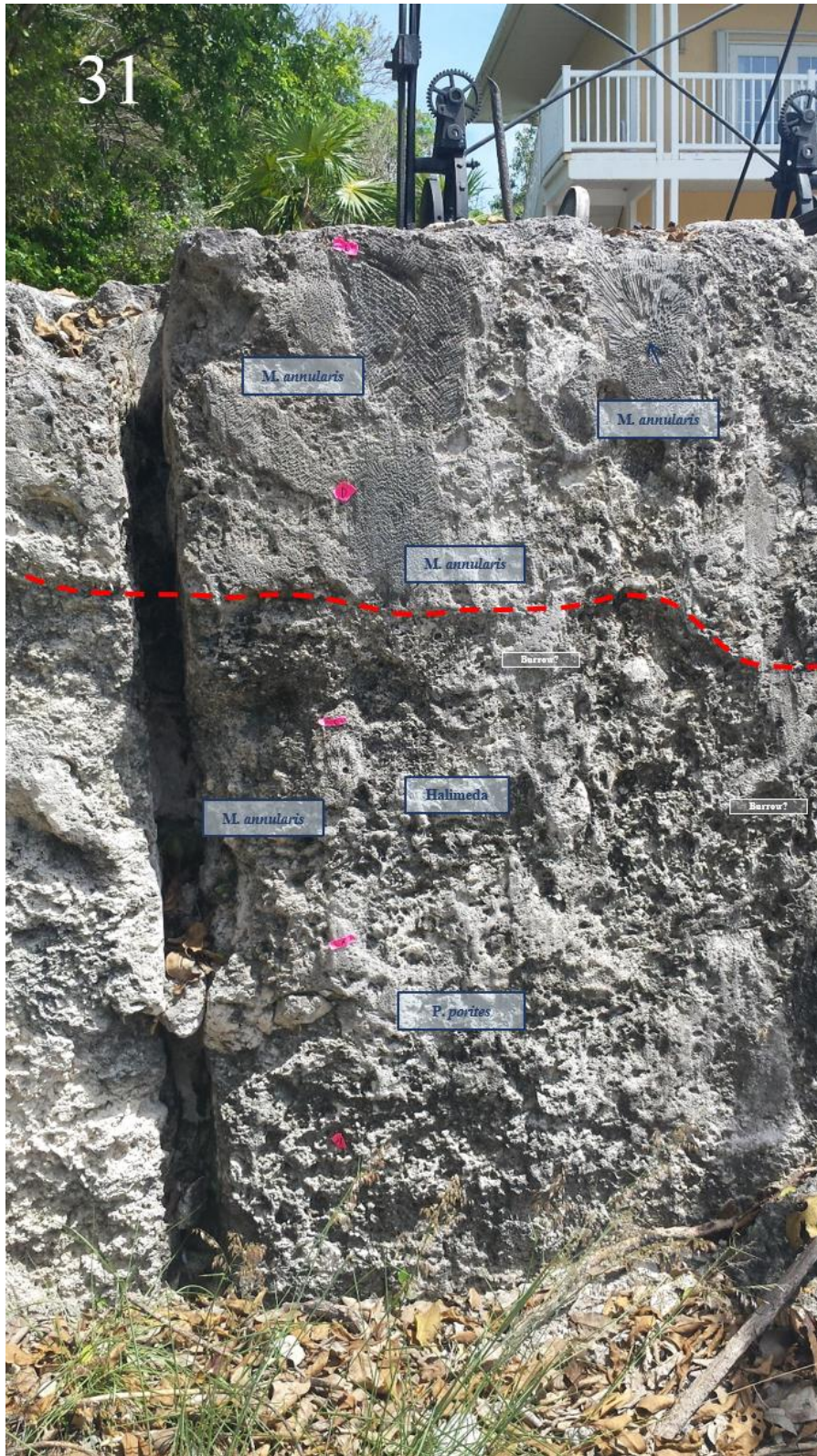
27

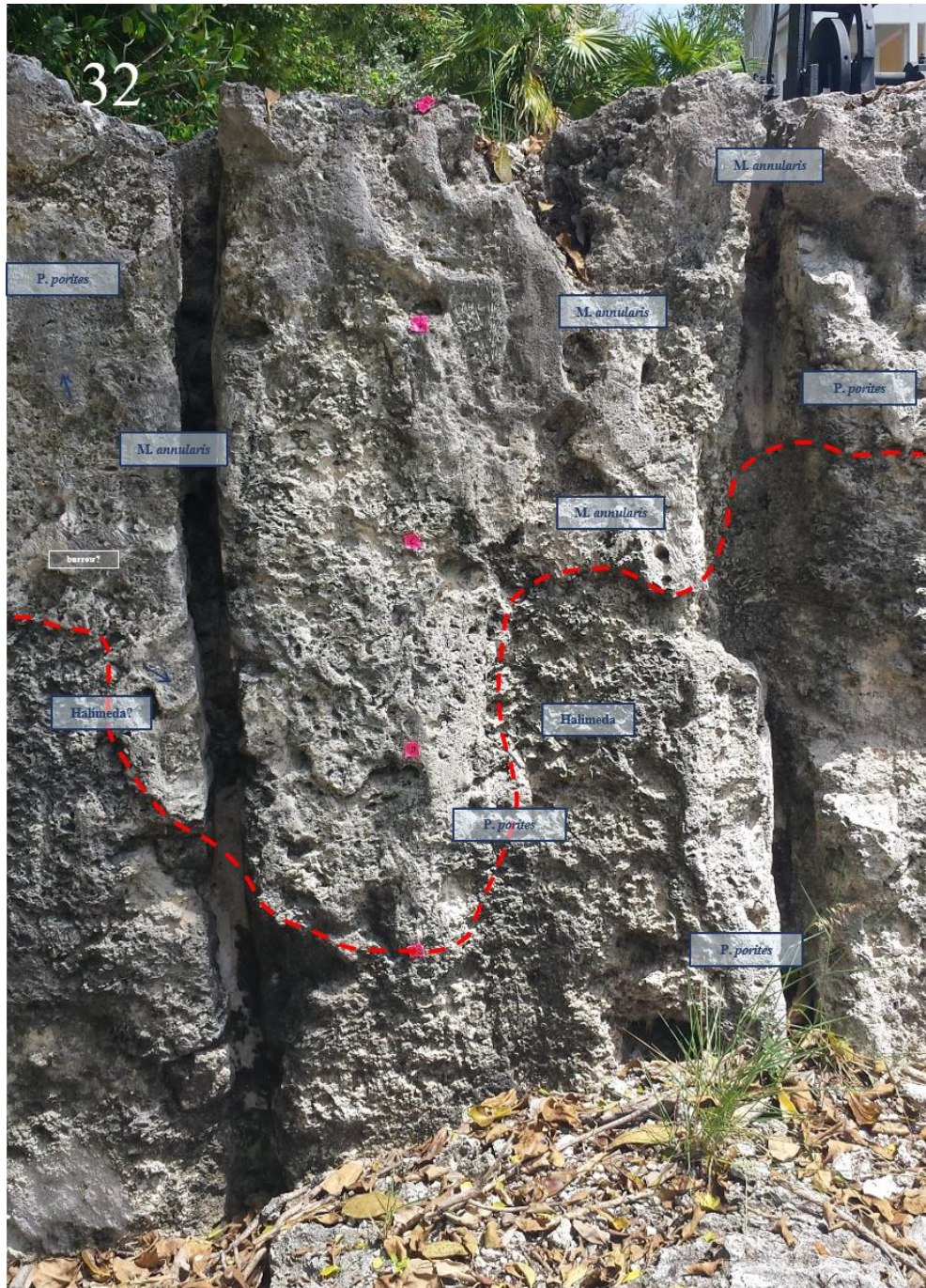












33











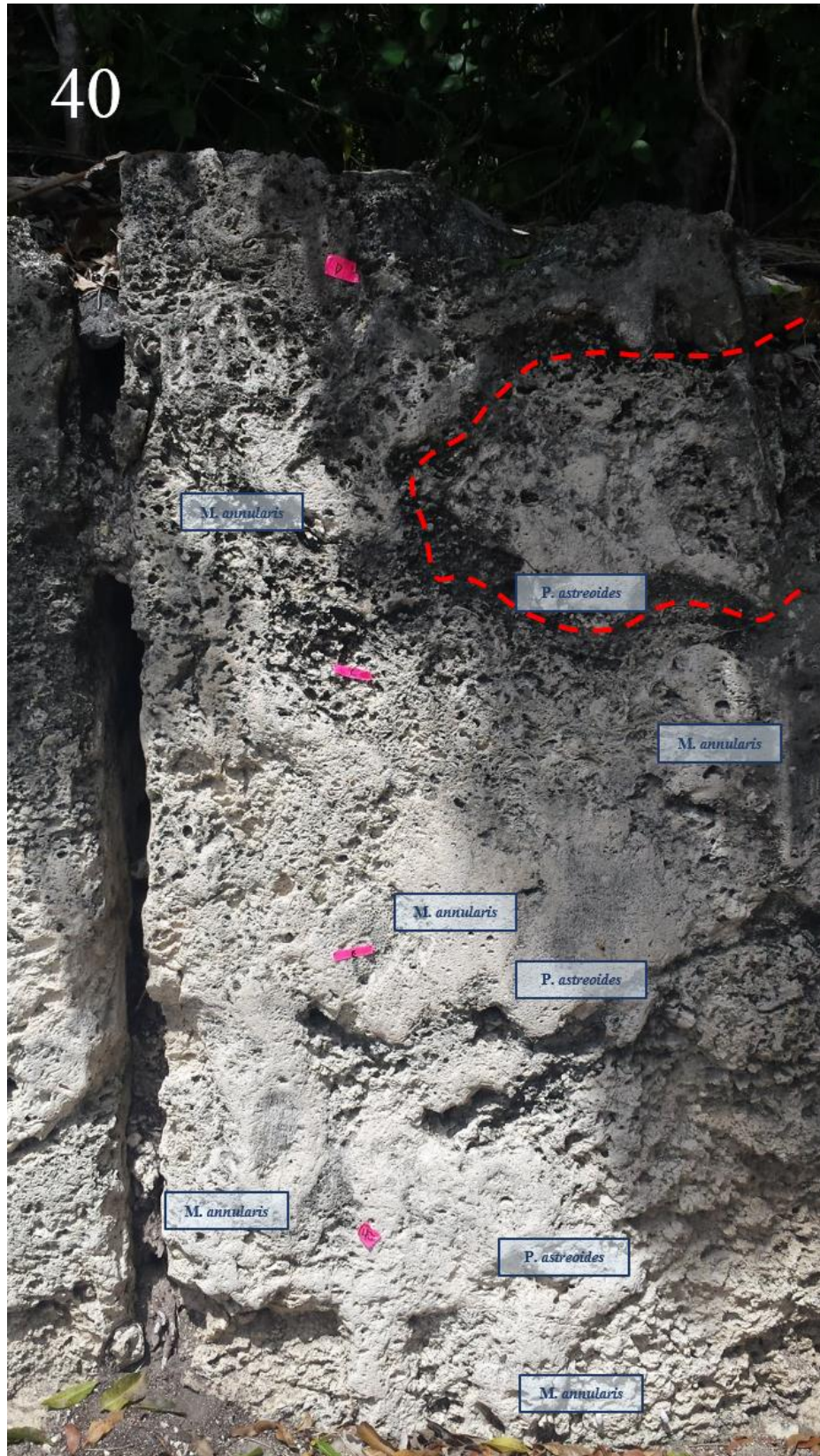




39



40

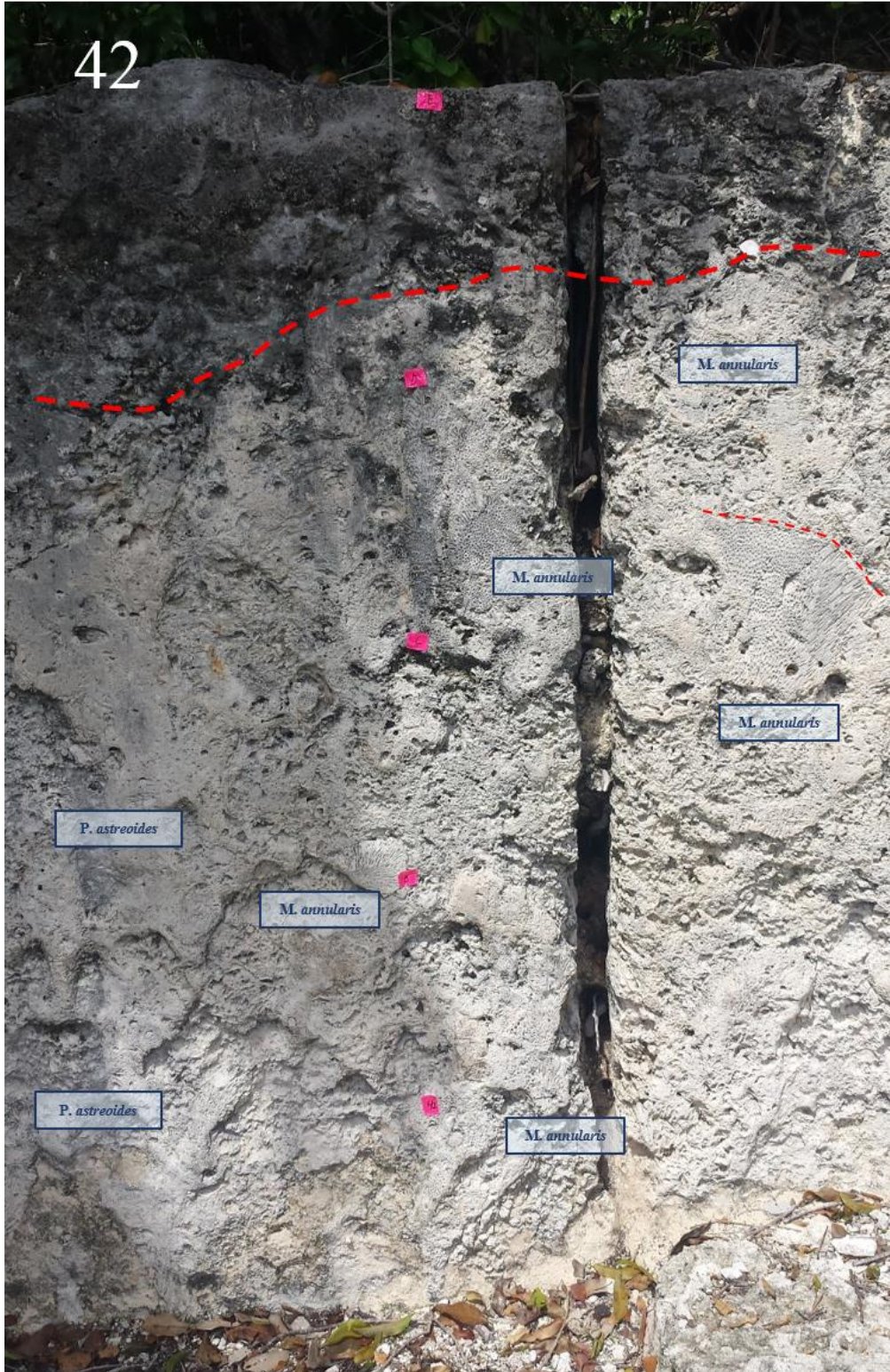


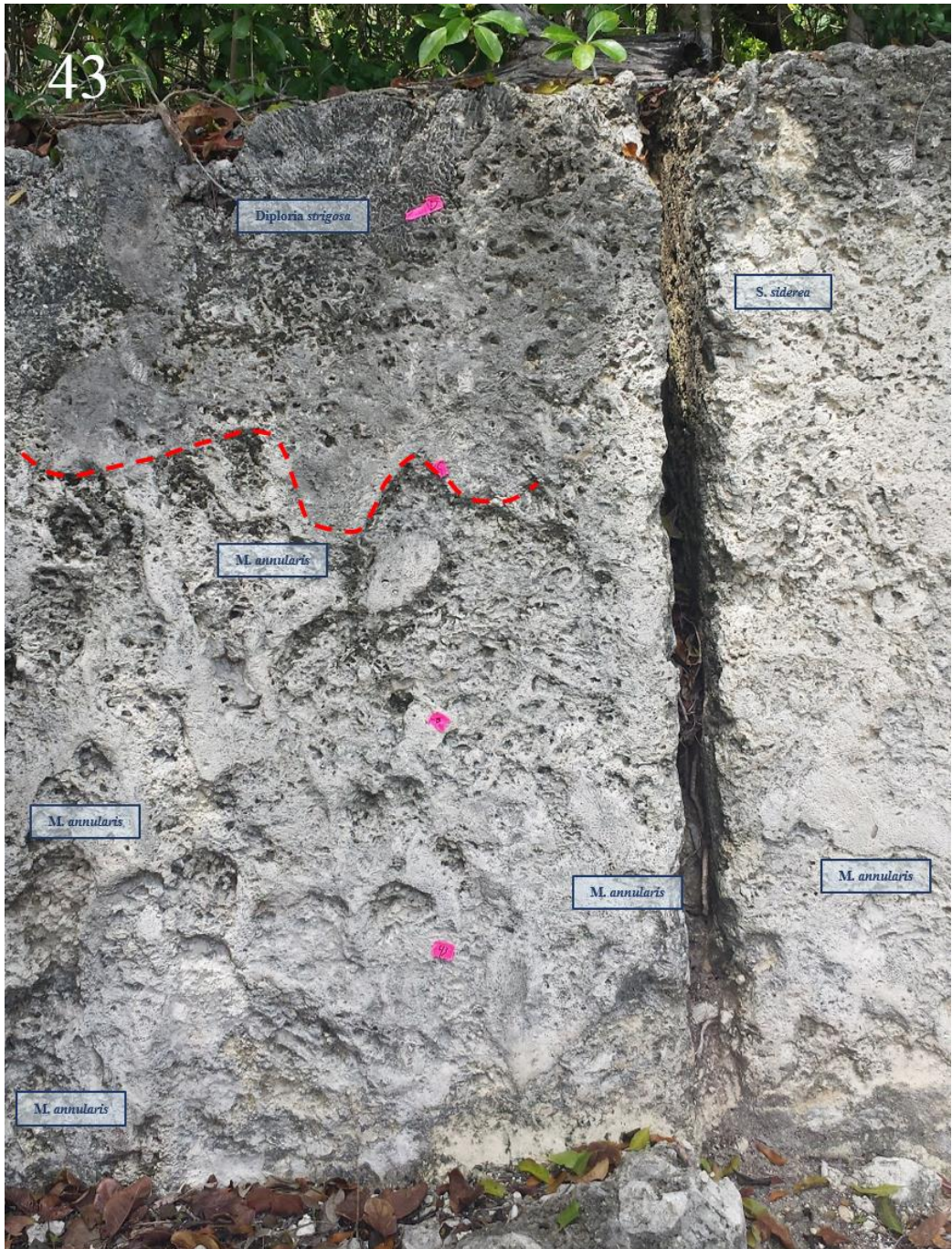
41



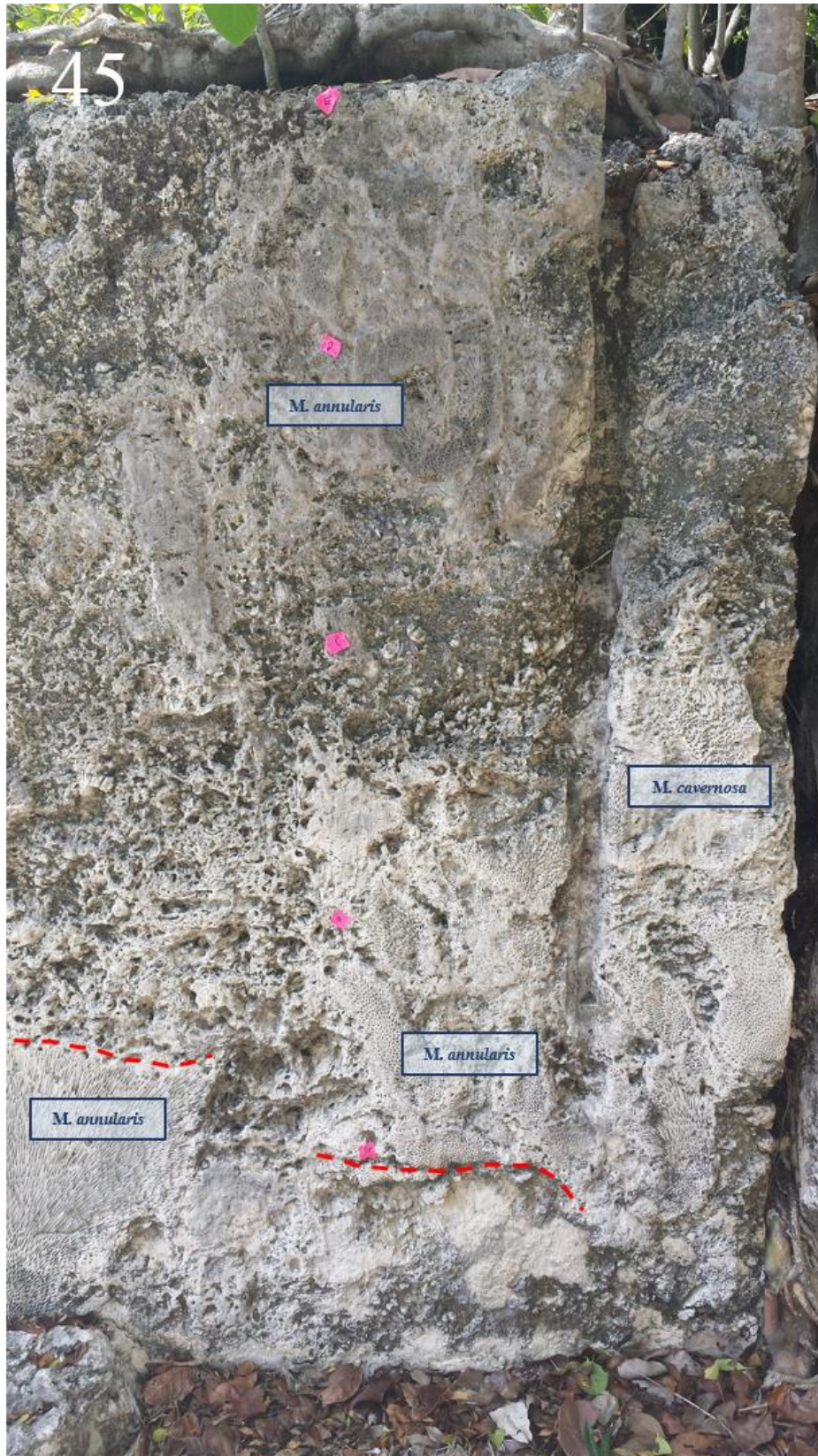


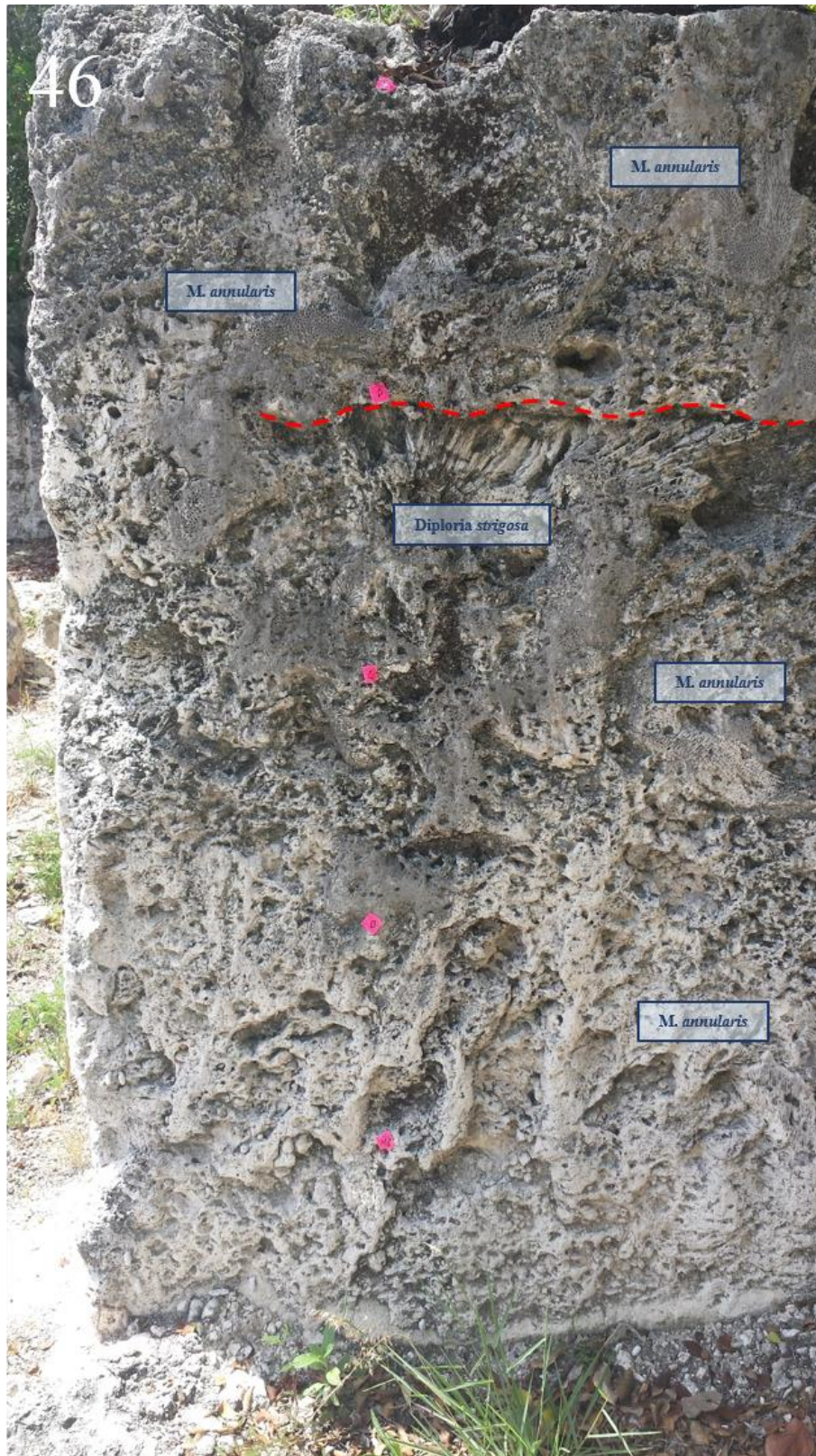
42









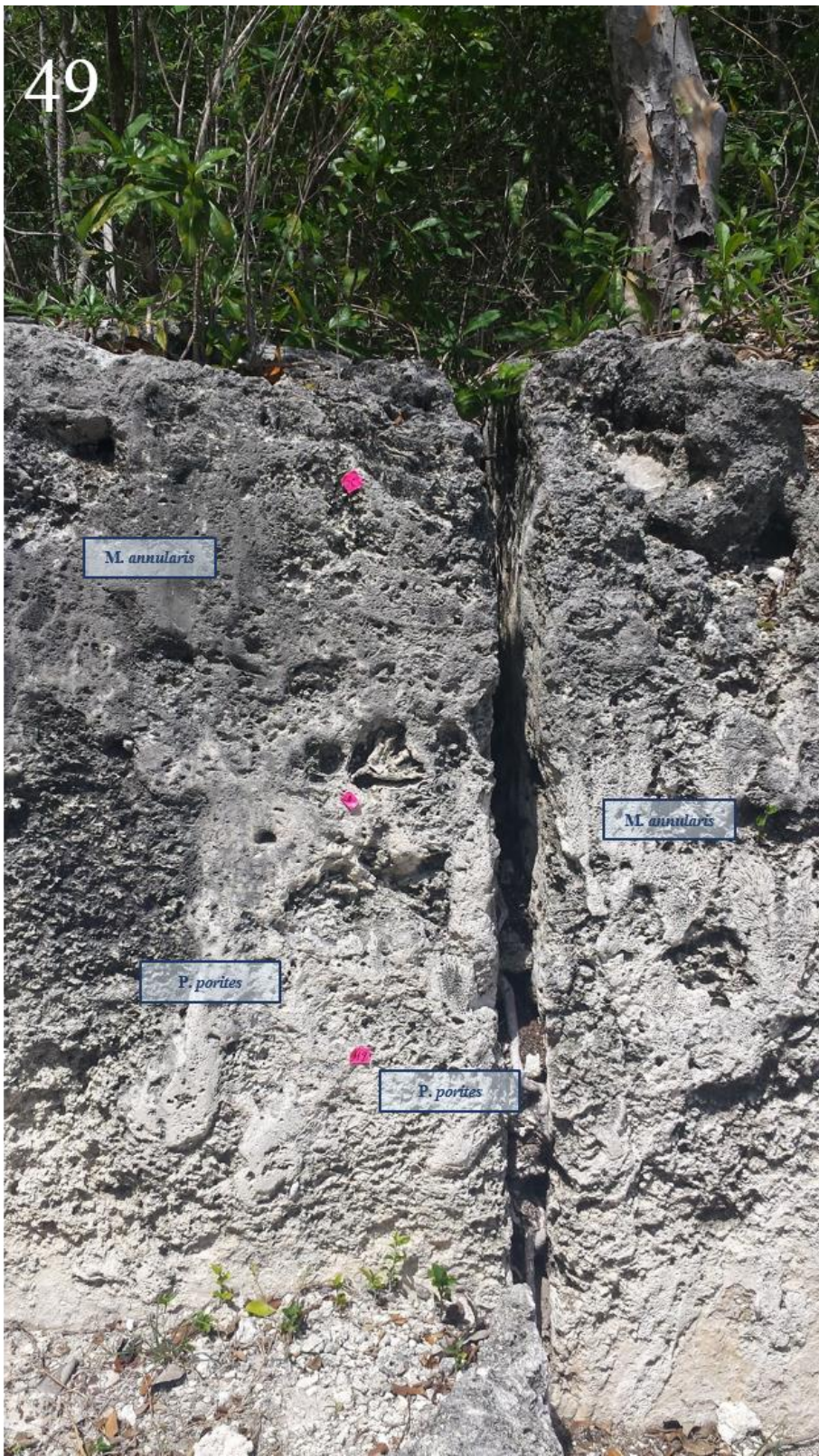




48

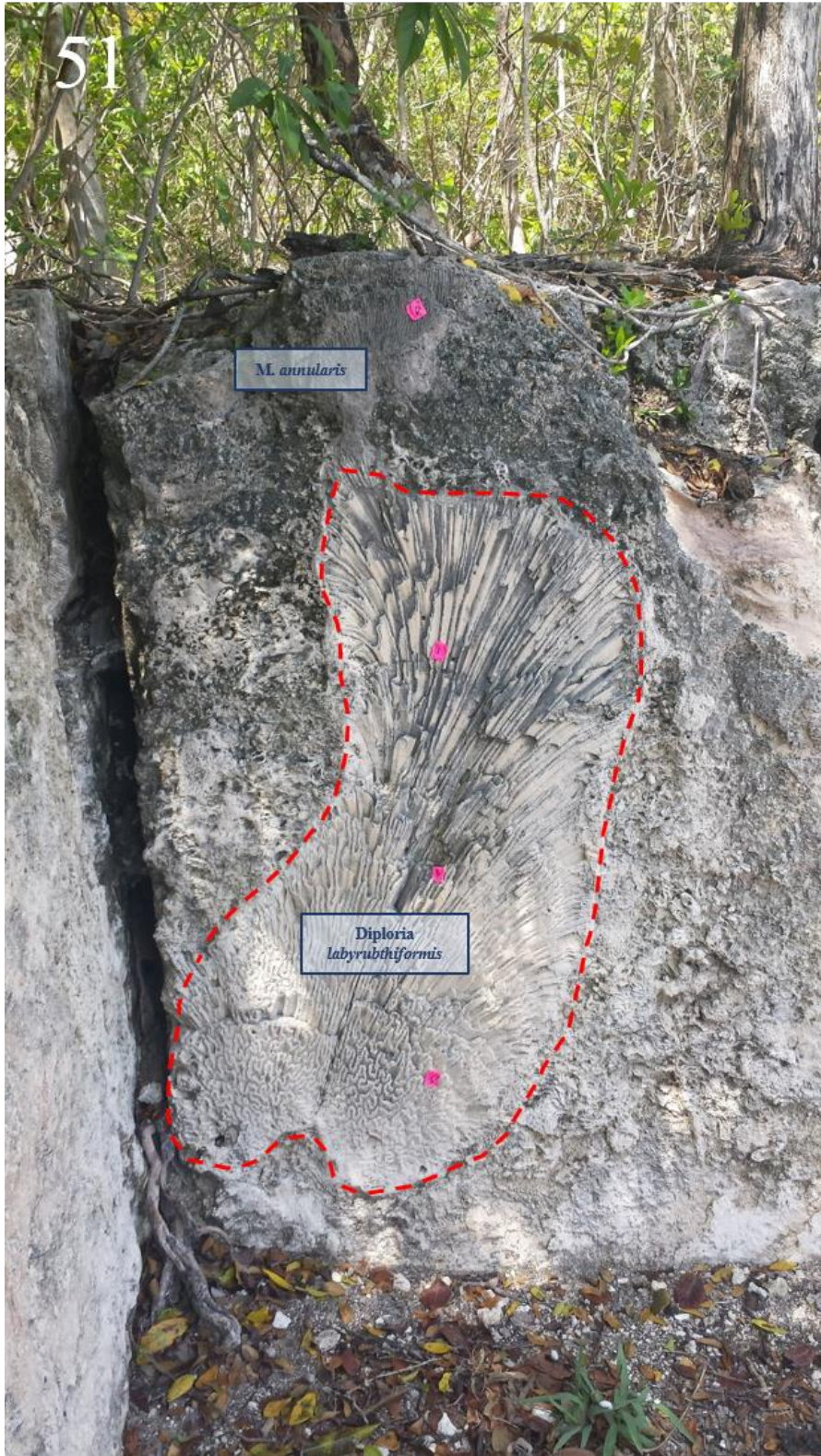


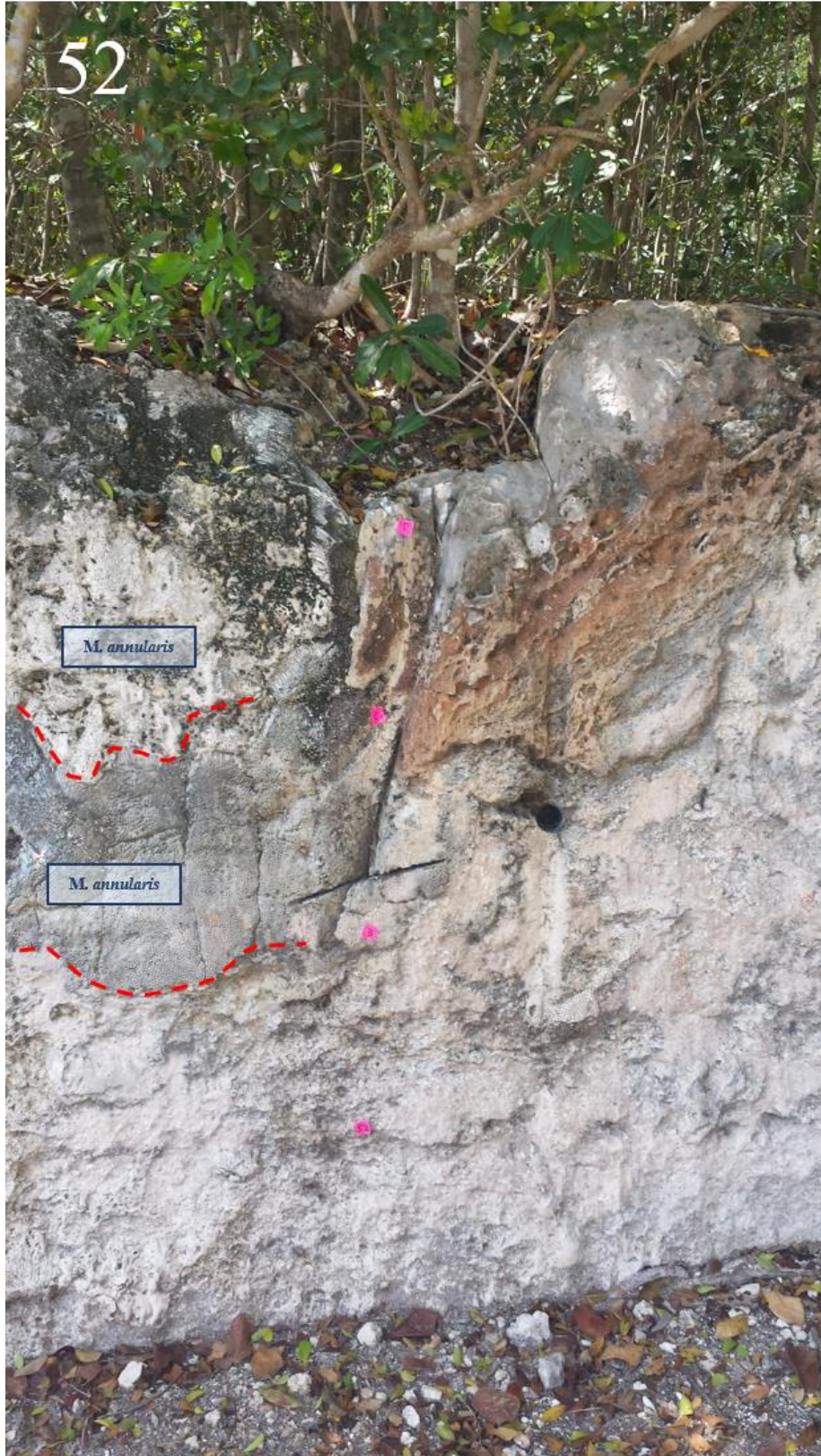
49

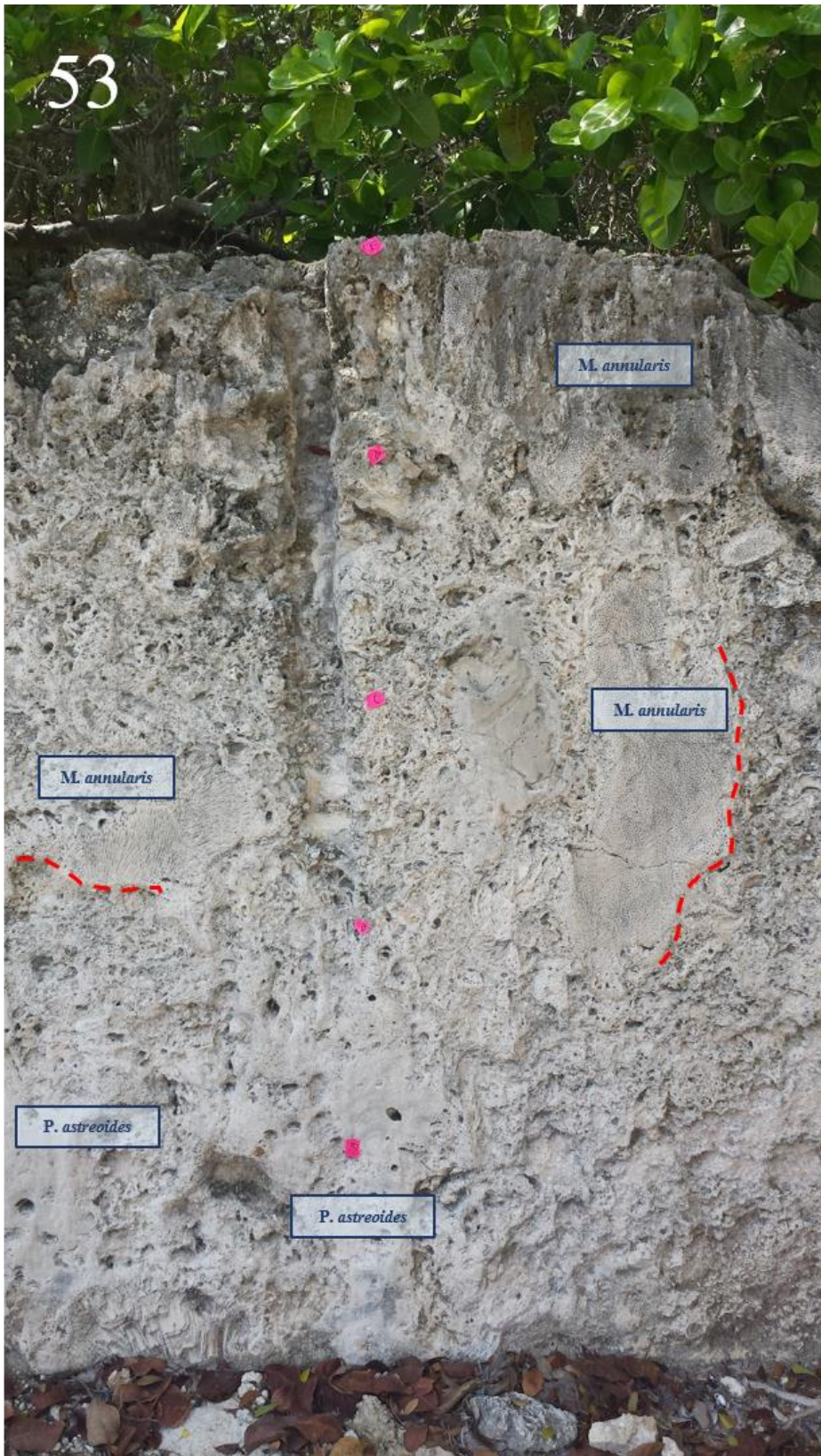






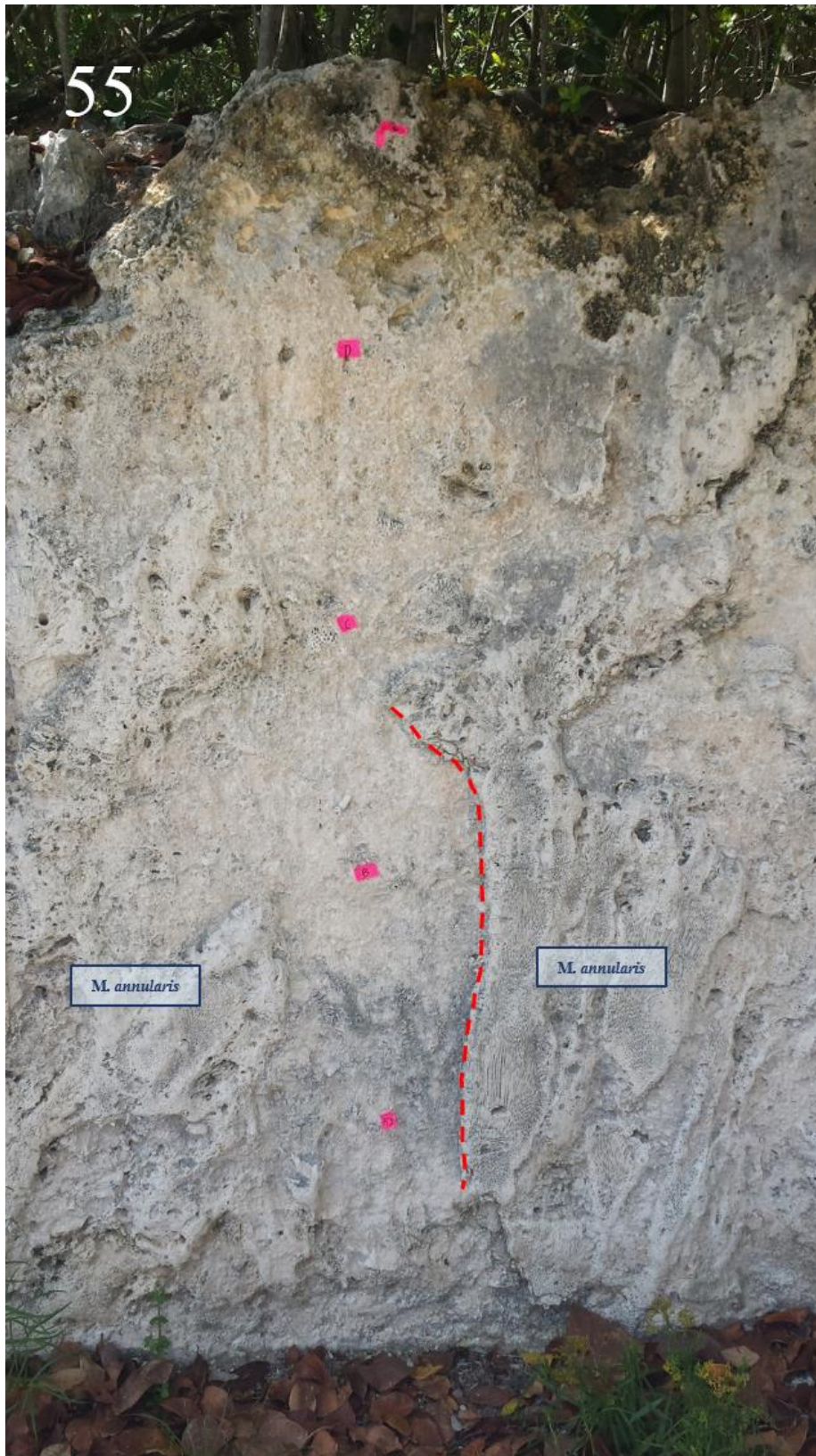




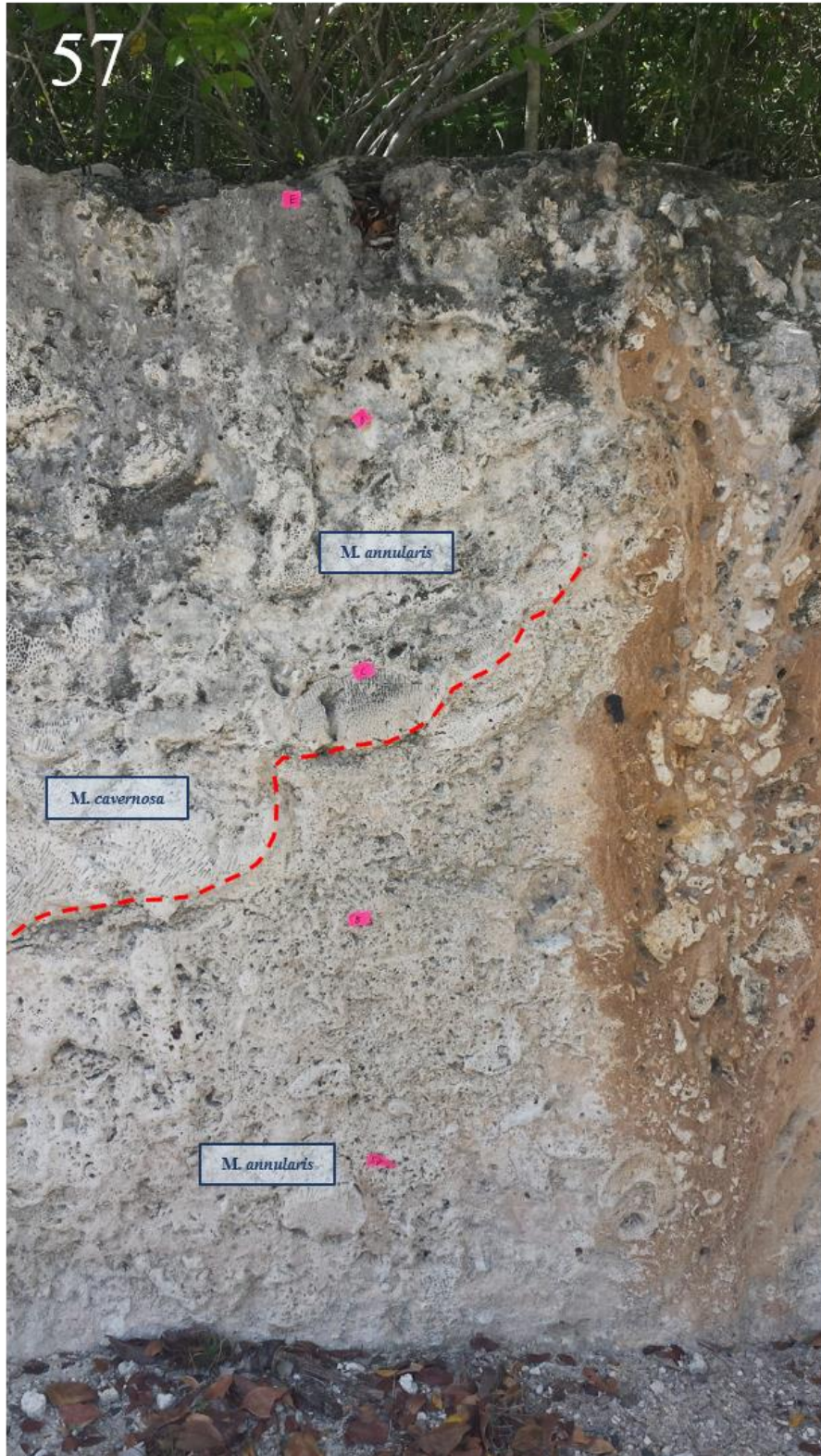


54

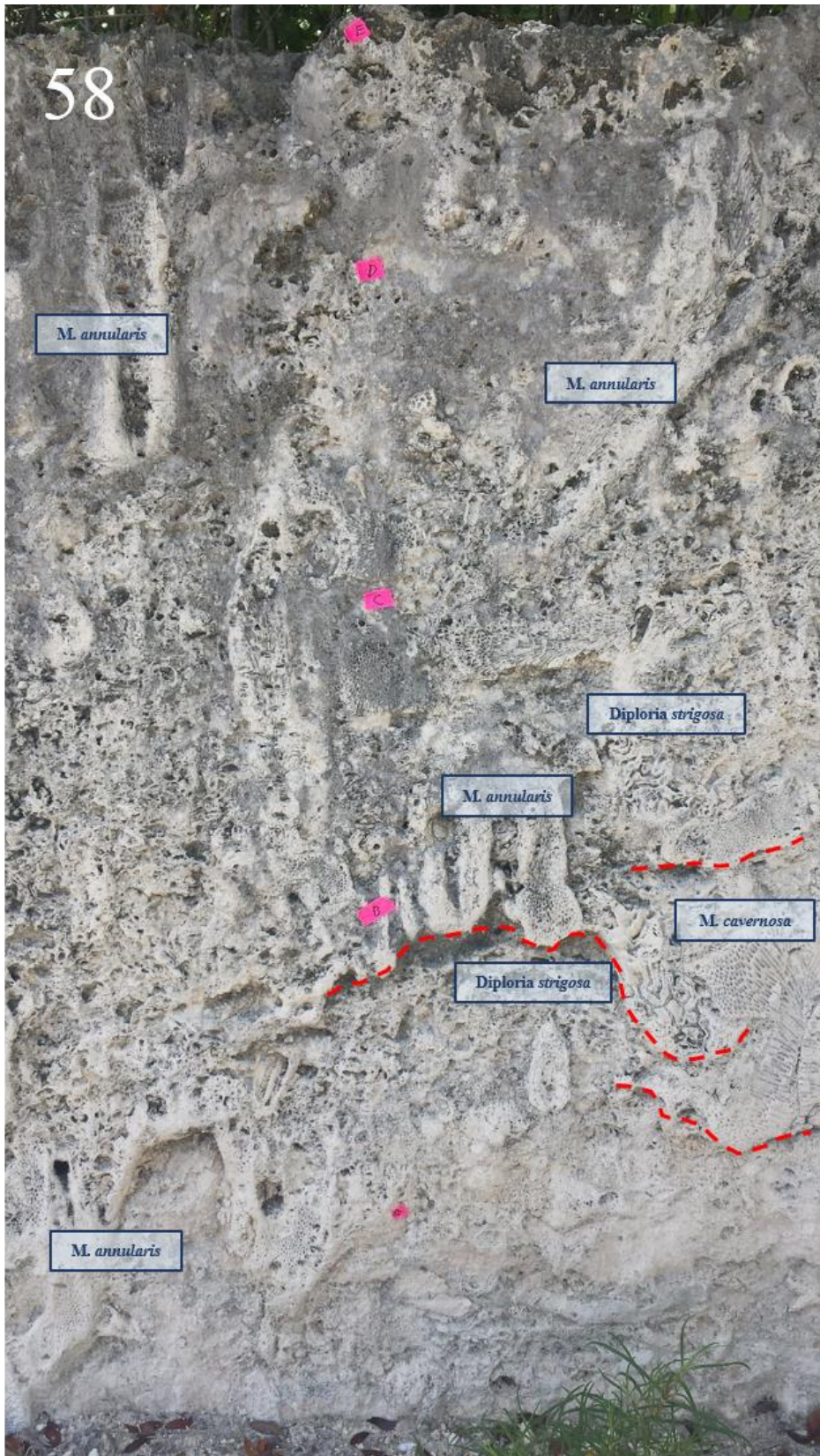




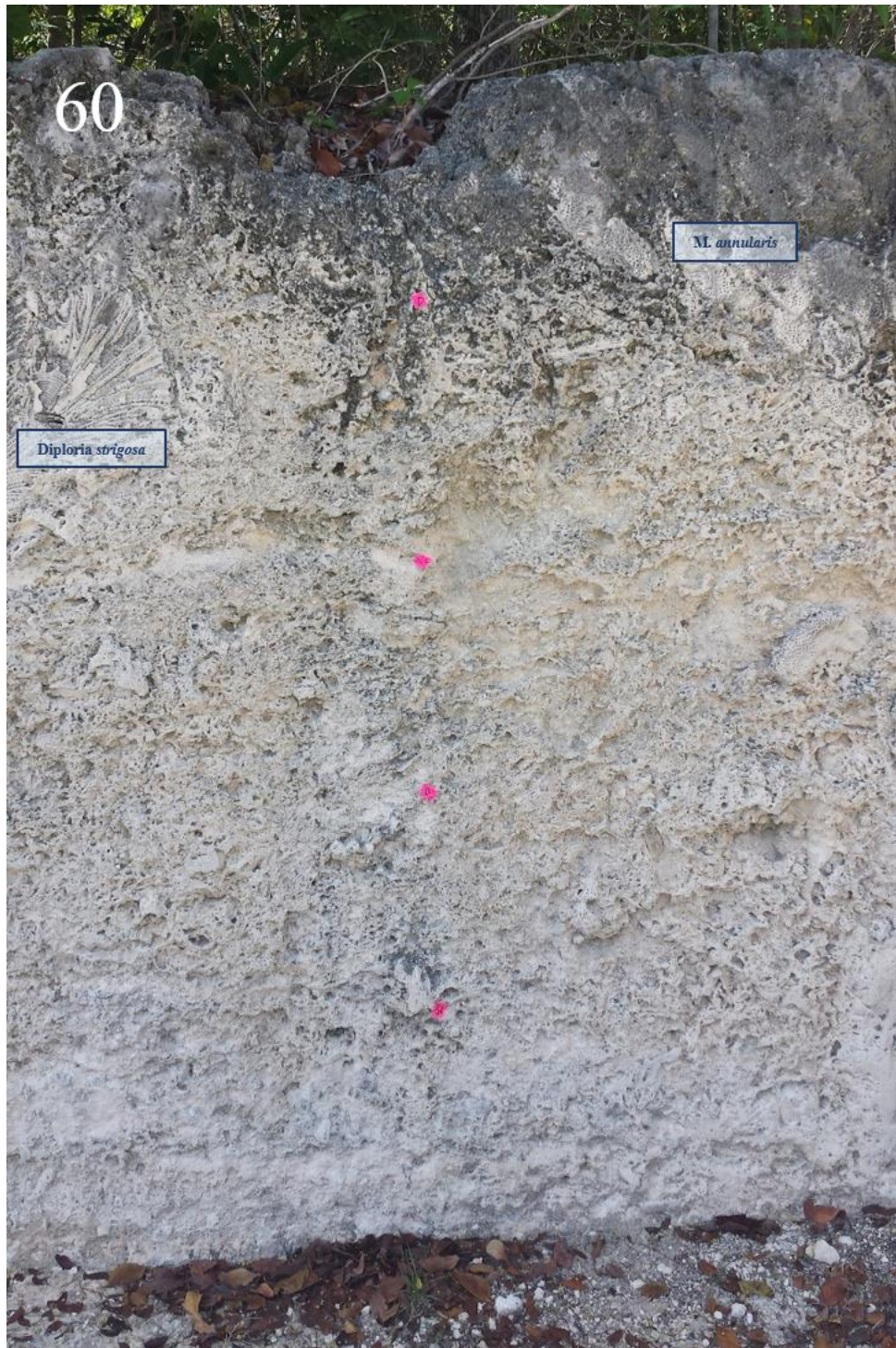






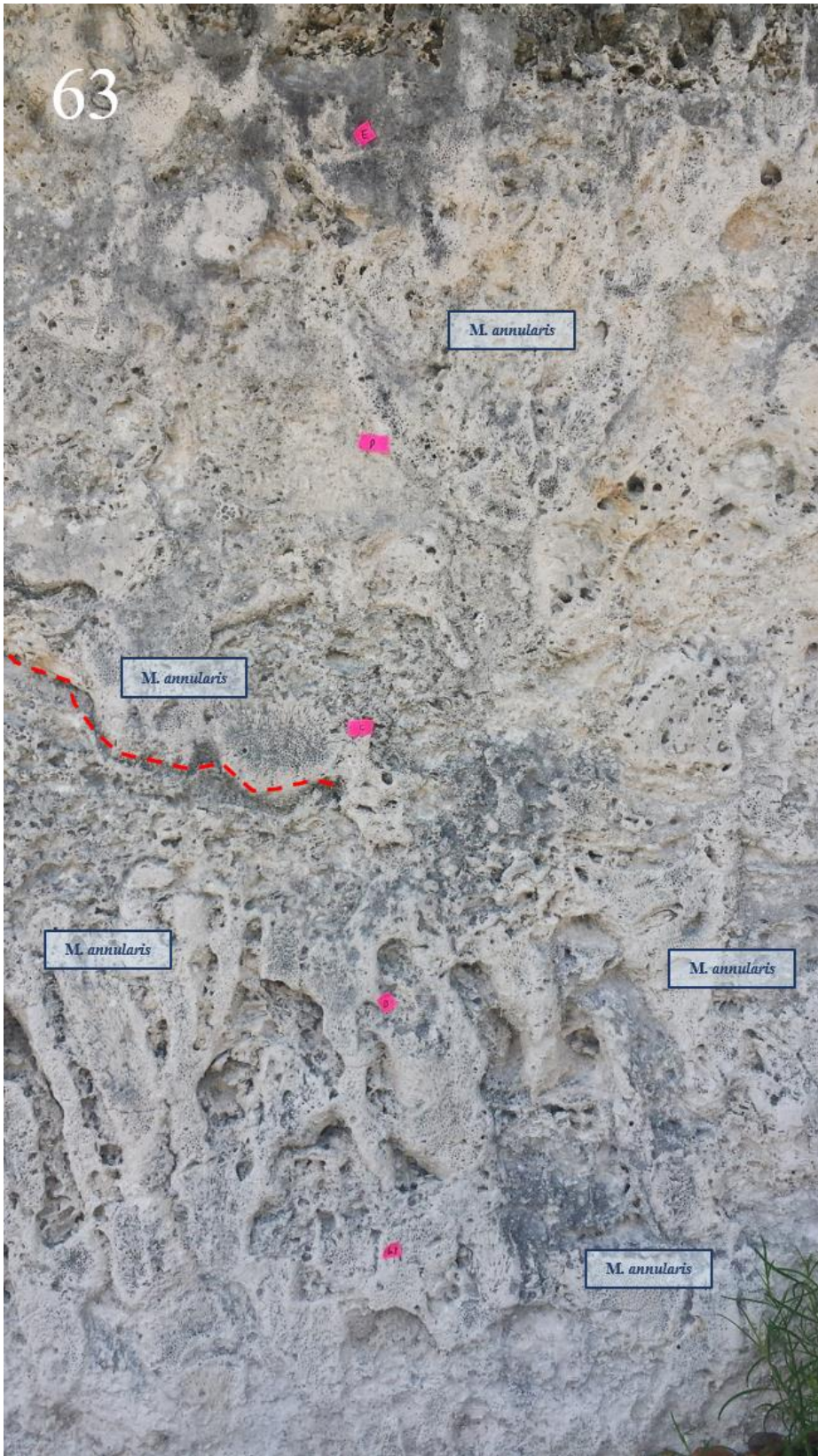


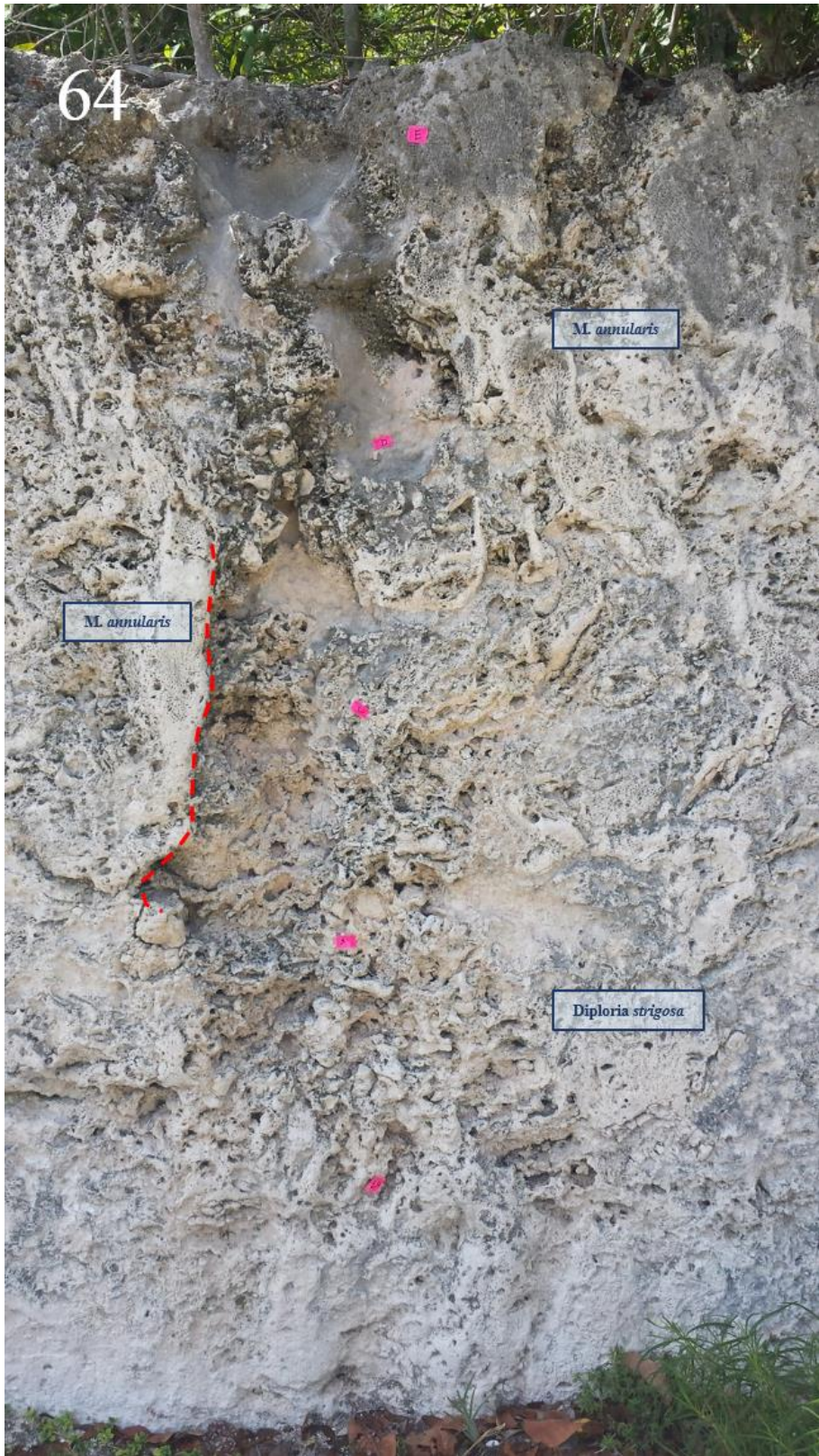






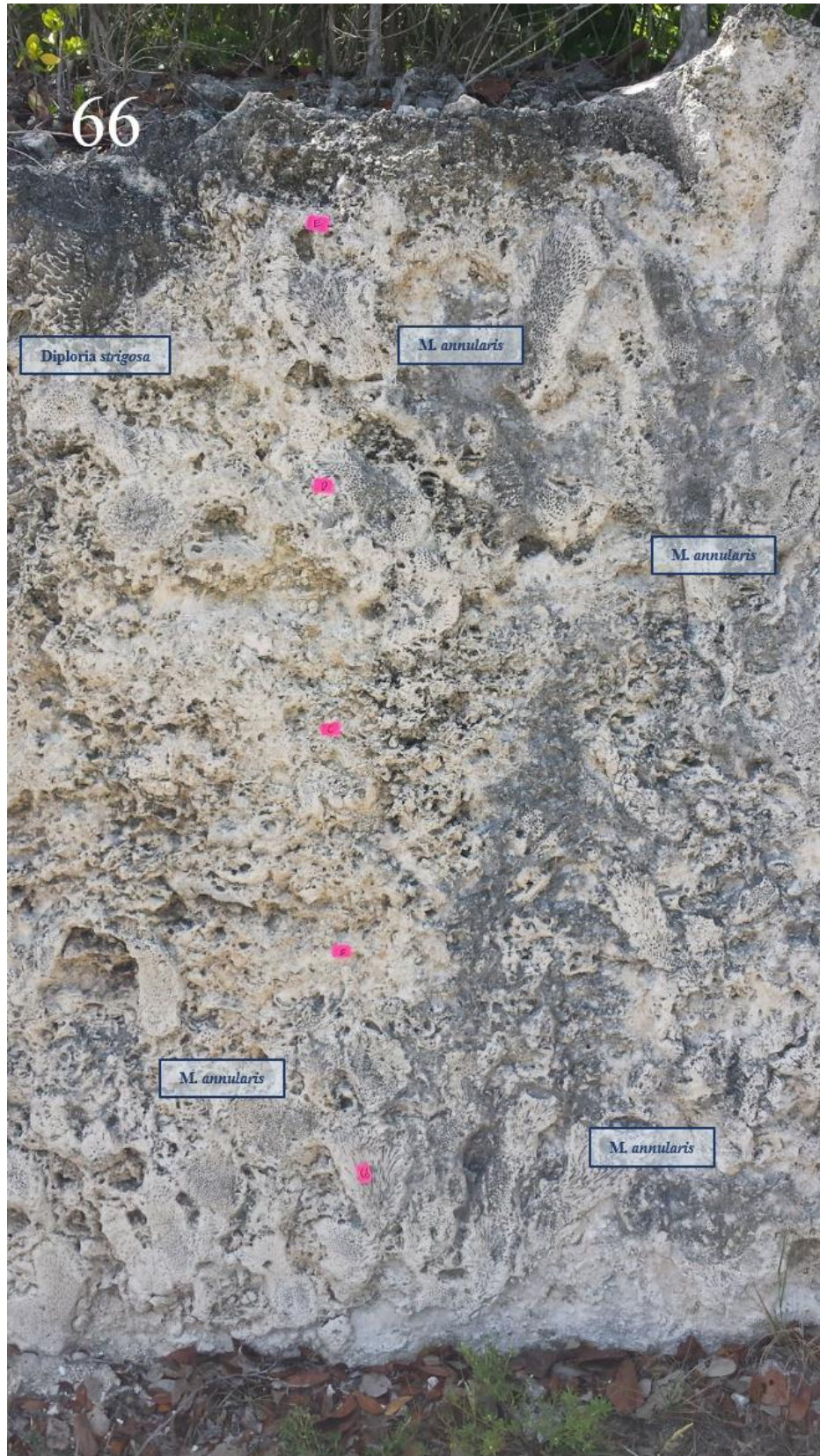










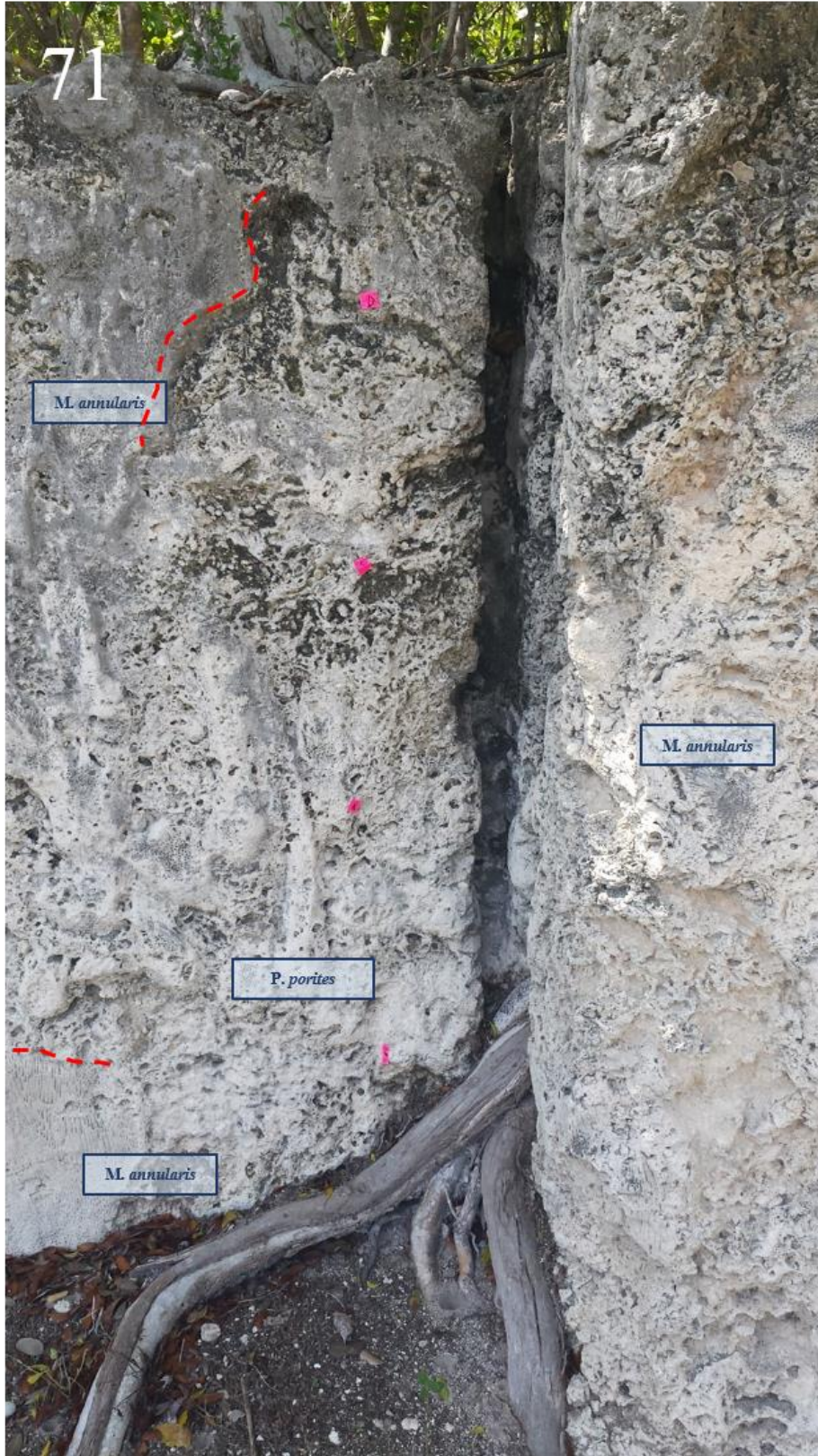


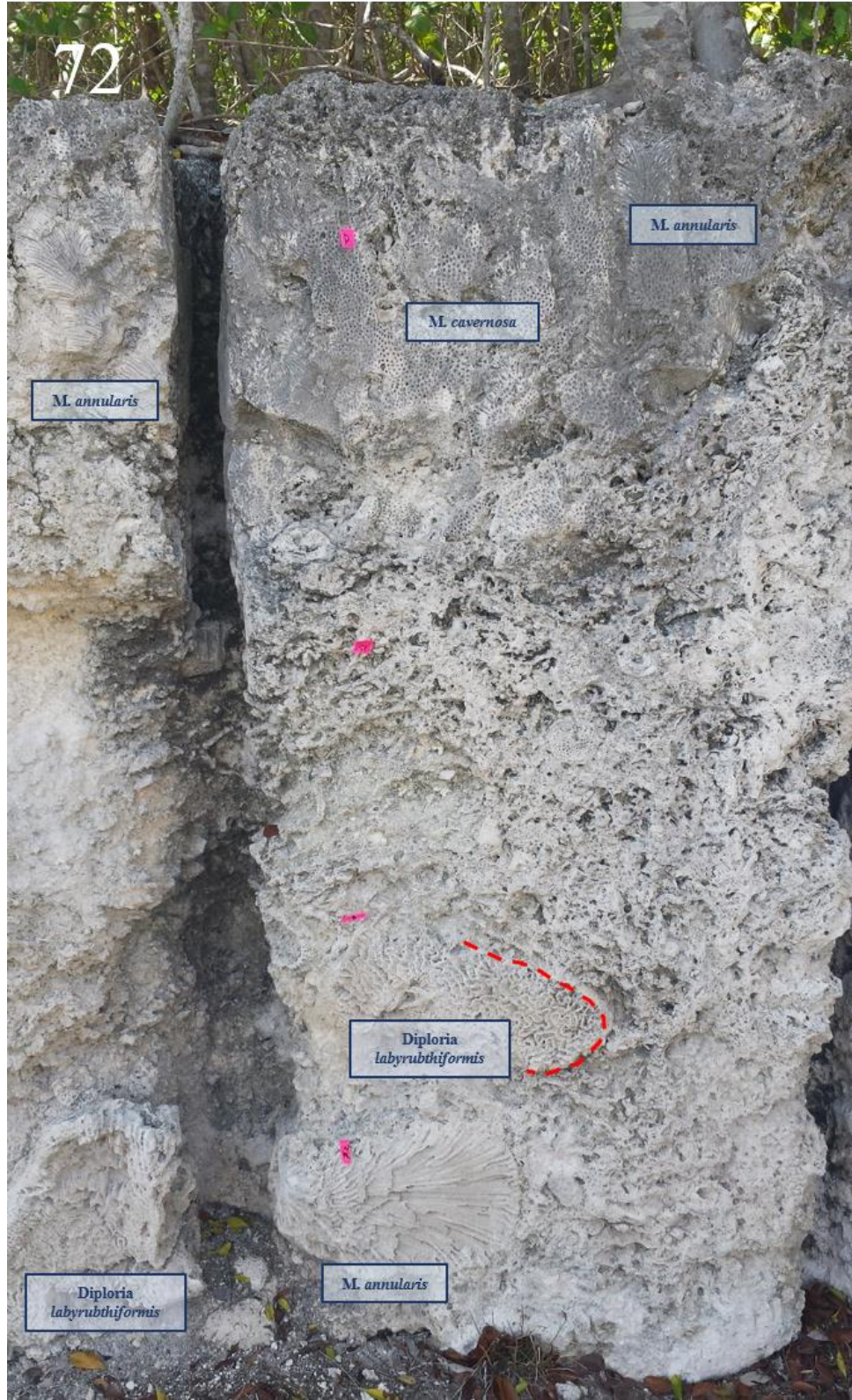








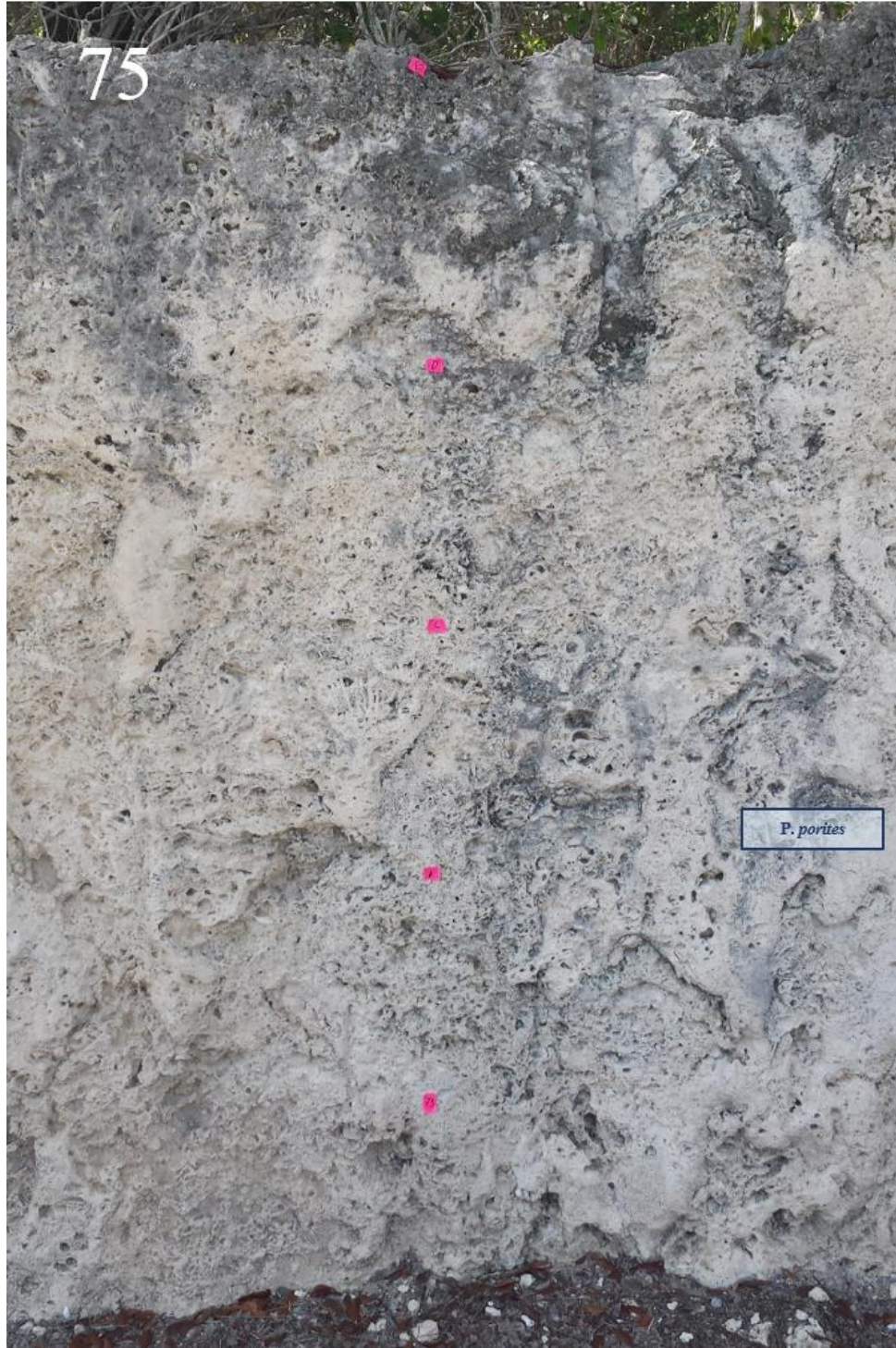


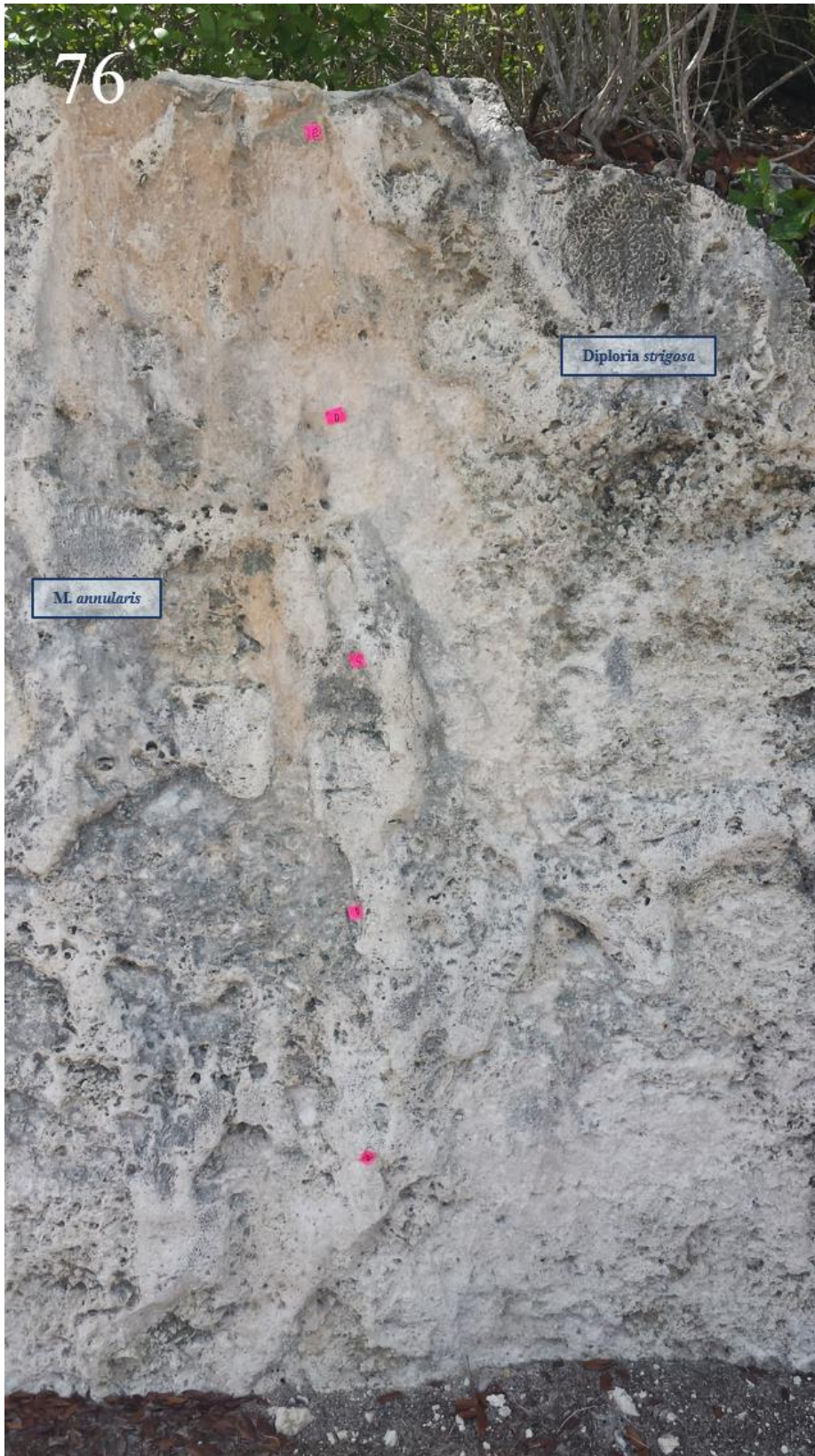


























## Appendix E: XRF Mineralogy Results

Sample	Sub Sample	%ARAG	%HIMGCAILOVMGCA	%PYRITE	%GYPSUM	%CLAY	QTZ-CHEF	SUM		
1	A	28.66	58.59	0.00	0.34	3.24	9.18	0.00	100.00	Wall 1
1	B	15.90	27.41	54.71	0.33	0.17	1.48	0.00	100.00	
1	C	60.62	14.47	21.29	0.14	0.82	2.66	0.00	100.00	
1	D	54.73	20.04	21.01	0.19	1.11	2.83	0.08	100.00	
2	A	40.13	0.00	55.56	0.12	0.92	3.27	0.00	100.00	
2	B	20.68	23.52	54.07	0.12	0.78	0.00	0.82	100.00	
2	C	19.03	23.39	53.95	0.12	0.89	2.62	0.00	100.00	
2	D	67.28	13.42	16.75	0.09	0.90	1.57	0.00	100.00	
2	E	32.95	55.00	3.59	0.31	1.86	6.29	0.00	100.00	
3	A	27.60	8.91	62.54	0.08	0.39	0.00	0.49	100.00	
3	B	80.52	6.91	10.26	0.17	0.47	1.65	0.00	100.00	
3	C	77.85	7.67	12.46	0.11	0.70	1.07	0.13	100.00	
3	D	61.93	14.99	20.05	0.15	0.93	1.86	0.09	100.00	
3	E	36.57	21.85	36.96	0.14	1.24	3.23	0.00	100.00	
4	A	68.33	25.18	4.17	0.30	0.16	1.87	0.00	100.00	
4	B	25.16	16.52	57.15	0.09	0.49	0.00	0.59	100.00	
4	C	27.37	22.83	44.87	0.16	1.30	3.47	0.00	100.00	
4	D	69.32	7.11	22.38	0.08	0.60	0.00	0.51	100.00	
4	E	28.35	23.12	45.01	0.09	1.05	2.38	0.00	100.00	
<b>AVERAGE</b>		<b>44.37</b>	<b>20.58</b>	<b>31.41</b>	<b>0.16</b>	<b>0.95</b>	<b>2.39</b>	<b>0.14</b>		
<b>STD DEV</b>		21.72	14.83	21.24	0.09	0.69	2.25	0.26		

Sample	Sub Sample	%ARAG	%HIMG	%CALO	%VMGC	%PYRITE	%GYPSUM	%CLAY	QTZ-CHEF	SUM
5	A	25.16	29.65	41.68	0.14	1.12	1.84	0.41	100.00	
5	B	72.42	5.33	20.92	0.08	0.63	0.00	0.63	100.00	
5	C	79.18	14.91	4.31	0.07	0.84	0.00	0.69	100.00	
5	D	71.37	21.37	0.00	0.14	1.57	5.55	0.00	100.00	
5	E	22.92	42.02	27.07	0.21	2.39	5.13	0.27	100.00	
5	F	50.71	24.76	19.12	0.16	1.92	2.78	0.54	100.00	
6	A	79.64	8.87	9.52	0.13	0.76	0.92	0.16	100.00	
6	B	31.12	0.00	66.63	0.11	0.66	1.43	0.05	100.00	
6	C	23.52	13.62	57.57	0.18	1.94	2.97	0.20	100.00	
6	D	25.14	20.70	50.97	0.12	1.03	0.00	2.04	100.00	
6	E	26.16	38.10	32.09	0.12	1.14	1.96	0.44	100.00	
6	F	13.23	70.16	6.07	0.28	2.62	7.65	0.00	100.00	
7	A	29.23	0.00	68.77	0.10	0.92	0.00	0.99	100.00	
7	B	19.65	15.32	62.63	0.09	0.78	1.53	0.00	100.00	
7	C	24.96	13.91	59.45	0.10	0.93	0.00	0.65	100.00	
7	D	39.83	0.00	58.88	0.09	0.66	0.00	0.54	100.00	
7	E	25.37	20.68	52.22	0.08	0.99	0.00	0.65	100.00	
7	F	14.05	27.91	53.76	0.13	0.96	3.19	0.00	100.00	
8	A	27.06	19.54	49.45	0.16	1.15	2.41	0.23	100.00	
8	B	32.28	14.87	47.56	0.17	1.78	2.86	0.49	100.00	
8	C	60.78	7.19	29.55	0.08	1.09	1.31	0.00	100.00	
8	D	75.87	15.69	4.87	0.42	0.91	1.97	0.26	100.00	
8	E	41.99	21.14	31.82	0.16	1.89	2.88	0.11	100.00	
8	F	37.21	17.31	43.54	0.11	0.47	1.36	0.00	100.00	
9	A	28.94	20.96	44.58	0.19	1.36	3.97	0.00	100.00	
9	B	41.16	34.34	21.13	0.15	1.86	0.00	1.35	100.00	
9	C	24.72	62.25	0.00	0.25	4.03	8.61	0.14	100.00	
9	D	59.60	13.33	25.39	0.09	0.83	0.00	0.76	100.00	
9	E	22.96	14.83	58.88	0.20	1.14	1.96	0.03	100.00	
9	F	69.99	10.38	18.19	0.08	0.71	0.00	0.65	100.00	
10	A	26.52	14.70	56.01	0.11	0.71	1.93	0.02	100.00	
10	B	34.79	9.74	53.19	0.14	0.72	1.37	0.06	100.00	
10	C	36.40	34.09	19.07	0.42	2.85	6.34	0.83	100.00	
10	D	31.20	31.11	33.07	0.21	1.32	2.93	0.15	100.00	
10	E	24.93	21.89	49.23	0.20	1.22	2.53	0.00	100.00	
10	F	20.84	42.51	31.18	0.34	1.14	3.99	0.00	100.00	
11	A	14.62	35.93	45.66	0.09	0.82	2.87	0.00	100.00	
11	B	30.59	12.10	55.42	0.10	0.50	1.16	0.14	100.00	
11	C	28.38	46.01	14.34	0.18	6.11	4.97	0.00	100.00	
11	D	62.01	13.22	23.31	0.11	0.51	0.00	0.83	100.00	
11	E	28.04	25.98	40.67	0.14	1.74	3.43	0.00	100.00	
11	F	68.85	10.77	18.09	0.07	0.75	1.48	0.00	100.00	
12	A	26.73	0.00	70.70	0.16	0.64	1.77	0.00	100.00	
12	B	22.22	0.00	65.59	0.11	10.83	0.00	1.24	100.00	
12	C	20.01	32.18	45.60	0.18	1.07	0.00	0.95	100.00	
12	D	12.70	19.94	64.31	0.18	0.88	1.99	0.00	100.00	
12	E	14.72	25.16	57.07	0.16	1.34	1.55	0.00	100.00	
13	A	21.28	25.53	49.33	0.27	1.23	2.20	0.16	100.00	
13	B	22.60	25.64	48.69	0.19	0.82	1.88	0.18	100.00	
13	C	37.37	0.00	61.81	0.08	0.34	0.00	0.41	100.00	
13	D	24.99	26.44	47.39	0.11	0.48	0.00	0.58	100.00	
13	E	30.38	13.02	55.60	0.10	0.48	0.00	0.42	100.00	
14	A	28.42	15.62	52.87	0.18	0.98	1.93	0.00	100.00	
14	B	31.90	13.30	52.75	0.22	0.25	1.58	0.00	100.00	
14	C	27.96	9.18	60.36	0.62	0.00	1.79	0.10	100.00	
14	D	20.78	22.29	55.21	0.28	0.54	0.00	0.90	100.00	
14	E	33.65	12.43	50.24	0.58	0.44	2.53	0.14	100.00	
15	A	23.05	12.40	61.79	0.11	0.47	2.18	0.00	100.00	
15	B	28.20	6.80	64.07	0.06	0.37	0.00	0.50	100.00	
15	C	56.21	0.00	42.06	0.09	0.48	1.10	0.05	100.00	
15	D	14.47	29.74	52.22	0.48	0.88	2.05	0.16	100.00	
15	E	18.90	35.49	40.24	0.27	1.03	4.07	0.00	100.00	
16	A	41.97	48.61	1.03	0.47	1.49	6.43	0.00	100.00	
16	B	38.60	15.08	41.76	0.24	0.77	3.54	0.00	100.00	
16	C	26.15	20.87	49.97	0.17	0.64	2.12	0.08	100.00	
16	D	37.36	26.52	32.70	0.56	0.13	2.74	0.00	100.00	
17	A	8.19	75.40	0.00	0.36	4.59	11.44	0.00	100.00	
17	B	31.11	52.27	0.00	0.49	11.08	5.06	0.00	100.00	
17	C	14.01	74.54	0.00	0.83	2.25	8.37	0.00	100.00	
<b>AVERAGE</b>		<b>33.58</b>	<b>22.55</b>	<b>39.55</b>	<b>0.20</b>	<b>1.48</b>	<b>2.34</b>	<b>0.29</b>		
<b>STD DEV</b>		<b>17.54</b>	<b>17.12</b>	<b>20.68</b>	<b>0.15</b>	<b>1.93</b>	<b>2.36</b>	<b>0.40</b>		

Wall 2

Sample	Sub Sample	%ARAG	%HIMGCAILOVMGCA	%PYRITE	%GYPSUM	%CLAY	QTZ-CHEF	SUM	
18	A	19.83	24.37	52.58	0.11	1.04	2.07	100.00	
18	B	21.37	17.59	57.84	0.17	0.92	2.00	100.00	
18	C	27.18	18.27	51.70	0.21	0.69	1.95	100.00	
18	D	50.42	5.68	42.12	0.16	0.42	1.20	100.00	
18	E	27.03	29.01	40.22	0.14	0.77	2.83	100.00	
18	F	19.15	13.46	64.02	0.33	1.18	1.87	100.00	
19	A	33.98	17.63	44.96	1.36	0.00	1.85	100.00	
19	B	14.75	15.56	65.51	0.15	0.80	3.23	100.00	
19	C	11.16	20.95	65.19	0.14	0.50	2.06	100.00	
19	D	22.66	61.14	6.38	0.28	2.66	6.88	100.00	
19	E	21.73	21.19	52.55	0.20	1.00	3.33	100.00	
19	F	63.09	13.68	19.91	1.35	0.00	1.91	100.00	
20	A	10.83	23.64	62.43	0.15	0.55	2.40	100.00	
20	B	20.88	20.07	56.12	0.16	0.77	2.00	100.00	
20	C	14.68	28.33	53.63	0.30	0.65	2.04	100.00	
20	D	20.89	0.00	76.62	0.25	0.59	1.64	100.00	
20	E	23.15	19.63	54.69	0.15	0.35	2.02	100.00	
20	F	22.39	64.74	0.00	0.53	2.55	9.78	100.00	
<b>AVERAGE</b>		<b>24.73</b>	<b>23.05</b>	<b>48.14</b>	<b>0.34</b>	<b>0.86</b>	<b>2.84</b>	<b>0.04</b>	
<b>STD DEV</b>		13.11	16.15	20.45	0.38	0.71	2.12	0.10	
Wall 3									
21	A	14.36	48.88	32.09	1.01	0.00	3.67	100.00	
21	B	15.20	28.01	54.22	0.17	0.27	2.12	100.00	
21	C	42.83	13.55	40.89	0.16	0.64	1.93	100.00	
21	D	47.54	11.63	38.32	0.19	0.68	1.65	100.00	
21	E	18.70	42.73	33.16	0.81	0.51	3.66	100.00	
22	A	24.52	16.63	56.87	0.19	0.46	1.21	100.00	
22	B	13.37	45.99	34.45	0.76	0.73	4.69	100.00	
22	C	17.29	17.71	63.03	0.49	0.00	1.48	100.00	
22	D	25.85	26.83	43.30	1.99	0.00	1.36	100.00	
<b>AVERAGE</b>		<b>24.41</b>	<b>28.00</b>	<b>44.04</b>	<b>0.64</b>	<b>0.36</b>	<b>2.42</b>	<b>0.14</b>	
<b>STD DEV</b>		12.59	14.54	11.32	0.60	0.30	1.26	0.25	
Wall 4									
23	A	17.49	30.84	47.46	0.19	0.84	3.18	100.00	
23	B	12.43	22.95	62.07	0.36	0.41	1.78	100.00	
23	C	17.50	42.58	33.21	0.31	1.18	5.22	100.00	
23	D	74.06	12.07	12.59	0.36	0.00	0.85	100.00	
24	A	24.74	8.61	65.29	0.14	0.00	1.23	100.00	
24	B	11.73	17.62	69.12	0.28	0.10	1.15	100.00	
24	C	17.90	0.00	80.81	0.15	0.61	0.00	100.00	
24	D	69.35	11.86	16.65	0.24	0.52	1.22	100.00	
25	A	24.55	7.12	66.71	0.14	0.22	1.26	100.00	
25	B	74.18	8.14	16.78	0.09	0.35	0.00	100.00	
25	C	44.68	8.26	46.34	0.14	0.16	0.00	100.00	
25	D	21.99	0.00	74.73	0.27	0.63	2.30	100.00	
26	A	24.49	13.99	59.33	0.12	0.32	1.75	100.00	
26	B	13.56	12.80	72.05	0.20	0.00	1.40	100.00	
26	C	17.89	19.39	62.21	0.07	0.17	0.00	100.00	
26	D	30.47	14.48	54.12	0.14	0.31	0.00	100.00	
26	E	70.84	8.68	18.80	0.28	0.14	1.26	100.00	
27	A	44.16	17.01	37.72	0.10	0.53	0.00	100.00	
27	B	14.97	20.73	63.71	0.13	0.10	0.00	100.00	
27	C	80.55	4.61	13.82	0.48	0.04	0.00	100.00	
27	D	63.01	32.00	0.00	0.30	1.07	3.62	100.00	
27	E	69.41	2.65	25.99	0.23	0.22	1.50	100.00	
28	A	16.64	49.58	28.66	0.34	1.23	3.07	100.00	
28	B	17.75	36.07	39.47	0.35	1.20	5.16	100.00	
28	C	15.19	50.52	26.95	0.25	1.42	5.67	100.00	
28	D	31.39	19.04	47.10	0.24	0.81	1.40	100.00	
28	E	69.56	0.00	27.52	0.31	0.80	1.71	100.00	
<b>AVERAGE</b>		<b>36.68</b>	<b>17.47</b>	<b>43.30</b>	<b>0.23</b>	<b>0.49</b>	<b>1.66</b>	<b>0.17</b>	
<b>STD DEV</b>		24.44	14.38	22.65	0.10	0.43	1.68	0.21	
Wall 5									

Sample	Sub Sample	%ARAG	%HIMGCAILOVMGCA	%PYRITE	%GYPSUM	%CLAY	QTZ-CHEF	SUM	
29	A	23.95	12.29	60.72	0.46	0.22	2.35	0.00	100.00
29	B	17.51	13.35	68.24	0.19	0.26	0.00	0.44	100.00
29	C	56.22	13.98	28.25	0.09	0.38	1.07	0.00	100.00
29	D	67.73	17.88	12.98	0.58	0.00	0.00	0.83	100.00
29	E	65.93	15.53	16.05	0.18	0.68	1.48	0.15	100.00
30	A	16.59	11.15	70.58	0.13	0.33	1.21	0.00	100.00
30	B	76.40	4.09	16.81	0.34	1.12	1.24	0.00	100.00
30	C	18.98	13.43	65.66	0.29	0.35	1.29	0.00	100.00
30	D	37.81	14.27	46.14	0.36	0.16	1.22	0.04	100.00
30	E	38.94	31.50	22.82	0.31	1.58	4.85	0.00	100.00
31	A	17.96	20.67	55.54	0.42	0.74	4.66	0.00	100.00
31	B	17.08	14.98	65.50	0.19	0.60	1.58	0.07	100.00
31	C	45.93	9.72	41.28	0.13	0.87	2.07	0.00	100.00
31	D	75.63	0.00	22.25	0.23	0.64	1.25	0.00	100.00
31	E	72.98	8.33	16.03	0.24	0.79	1.63	0.00	100.00
32	A	19.53	13.09	63.88	0.17	0.87	2.46	0.00	100.00
32	B	15.05	9.59	73.90	0.07	0.26	1.13	0.00	100.00
32	C	26.23	15.51	54.96	0.14	0.98	1.98	0.19	100.00
32	D	22.92	19.80	53.00	0.19	0.72	3.37	0.00	100.00
32	E	41.03	8.01	48.87	0.12	0.45	1.52	0.00	100.00
33	A	25.43	9.62	61.95	0.12	0.39	2.49	0.00	100.00
33	B	16.00	34.01	46.61	0.14	1.37	1.66	0.23	100.00
33	C	19.52	27.98	48.49	0.19	1.07	2.74	0.00	100.00
33	C2	78.03	9.52	9.62	0.20	0.75	1.79	0.09	100.00
33	C3	11.68	0.00	67.09	15.04	0.00	6.19	0.00	100.00
33	C4	77.93	3.90	15.43	0.22	0.68	1.51	0.33	100.00
33	C5	27.70	16.56	54.87	0.07	0.39	0.00	0.40	100.00
33	C6	37.73	22.01	37.18	0.16	1.08	1.85	0.00	100.00
33	D	72.63	11.85	13.77	0.17	0.42	0.99	0.17	100.00
33	E	15.51	10.12	72.12	0.11	0.75	1.38	0.00	100.00
34	A	28.74	43.13	11.76	0.53	4.61	10.95	0.29	100.00
34	B	24.75	25.49	46.24	0.15	0.92	2.45	0.00	100.00
34	C	19.76	10.14	67.47	0.14	0.89	1.59	0.00	100.00
34	D	37.69	20.44	39.02	0.14	0.94	1.77	0.00	100.00
35	A	30.01	18.34	48.30	0.11	1.64	1.60	0.00	100.00
35	B	17.18	25.45	55.17	0.14	0.86	1.20	0.00	100.00
35	C	75.90	13.92	7.02	0.09	1.32	1.75	0.00	100.00
35	D	78.16	10.56	8.78	0.19	0.86	1.43	0.00	100.00
36	A	67.64	26.59	0.00	0.24	2.73	2.79	0.00	100.00
36	B	82.95	10.95	4.36	0.10	1.04	0.00	0.60	100.00
36	C	75.43	7.84	14.09	0.11	1.31	1.01	0.20	100.00
36	D	32.75	6.42	58.99	0.07	1.36	0.00	0.42	100.00
36	E	23.22	22.30	48.70	0.43	2.17	3.18	0.00	100.00
37	A	18.85	23.60	53.38	0.35	1.23	2.60	0.00	100.00
37	B	62.29	5.60	30.18	0.08	0.71	1.08	0.06	100.00
37	C	78.15	19.11	0.00	0.33	1.74	0.00	0.66	100.00
37	D	74.08	2.96	19.88	0.13	1.15	1.81	0.00	100.00
<b>AVERAGE</b>		<b>42.22</b>	<b>15.01</b>	<b>39.23</b>	<b>0.52</b>	<b>0.94</b>	<b>1.96</b>	<b>0.11</b>	
<b>STD DEV</b>		<b>24.72</b>	<b>8.89</b>	<b>22.89</b>	<b>2.17</b>	<b>0.77</b>	<b>1.82</b>	<b>0.20</b>	

Wall 6

Sample	Sub Sample	%ARAG	%HIMGCAILOVMGCA	%PYRITE	%GYPSUM	%CLAY	QTZ-CHEF	SUM	
38	A	39.32	0.00	58.67	0.14	1.14	0.00	0.73	100.00
38	B	24.39	45.05	26.61	0.21	1.30	2.44	0.00	100.00
38	C	16.71	31.82	47.26	0.27	1.22	2.71	0.00	100.00
38	D	68.62	0.00	29.77	0.11	1.04	0.00	0.47	100.00
39	A	21.57	10.26	67.05	0.13	0.45	0.00	0.54	100.00
39	B	19.74	28.97	45.10	0.40	1.30	4.49	0.00	100.00
39	C	34.98	17.92	43.22	0.49	0.75	2.64	0.00	100.00
39	D	45.66	12.94	39.73	0.10	0.50	1.07	0.00	100.00
40	A	7.05	31.47	59.01	0.09	0.48	1.91	0.00	100.00
40	B	29.83	18.21	49.73	0.05	0.40	1.78	0.00	100.00
40	C	25.86	11.79	60.56	0.09	0.40	1.30	0.00	100.00
40	D	13.71	19.06	64.93	0.12	0.93	1.12	0.12	100.00
41	A	20.77	13.43	63.55	0.09	0.60	1.55	0.00	100.00
41	B	73.46	13.56	10.94	0.11	0.59	1.28	0.06	100.00
41	C	17.89	35.74	42.88	0.11	0.83	2.54	0.00	100.00
41	D	52.20	8.73	36.17	0.16	0.88	1.87	0.00	100.00
42	A	15.26	21.72	60.24	0.12	0.68	1.98	0.00	100.00
42	B	76.08	6.44	15.30	0.08	0.72	1.38	0.00	100.00
42	C	22.00	20.79	56.19	0.07	0.58	0.00	0.36	100.00
42	D	72.36	7.10	18.32	0.11	0.92	1.02	0.17	100.00
42	E	51.18	0.00	46.80	0.10	0.75	1.17	0.00	100.00
43	A	48.74	22.47	25.20	0.17	0.87	2.55	0.00	100.00
43	B	14.85	71.51	2.82	0.36	2.71	7.75	0.00	100.00
43	C	23.08	62.96	0.00	0.34	5.14	7.27	1.20	100.00
43	D	75.19	7.16	15.29	0.19	0.78	1.30	0.09	100.00
<b>AVERAGE</b>		<b>36.42</b>	<b>20.76</b>	<b>39.41</b>	<b>0.17</b>	<b>1.04</b>	<b>2.04</b>	<b>0.15</b>	
<b>STD DEV</b>		<b>22.31</b>	<b>18.11</b>	<b>20.39</b>	<b>0.11</b>	<b>0.97</b>	<b>1.94</b>	<b>0.30</b>	
Wall 7									
Sample	Sub Sample	%ARAG	%HIMGCAILOVMGCA	%PYRITE	%GYPSUM	%CLAY	QTZ-CHEF	SUM	
44	A	12.64	18.09	67.38	0.08	0.51	1.31	0.00	100.00
44	B	18.34	17.45	60.26	0.11	0.82	3.01	0.00	100.00
44	C	37.91	22.01	37.85	0.13	0.95	1.08	0.08	100.00
44	D	25.46	29.49	41.06	0.14	1.05	2.80	0.00	100.00
45	A	18.64	17.36	59.95	0.11	0.80	3.13	0.00	100.00
45	B	61.79	18.33	17.04	0.14	0.77	1.93	0.00	100.00
45	C	21.27	38.17	35.44	0.45	1.58	3.06	0.04	100.00
45	D	18.31	22.38	56.26	0.12	0.88	2.04	0.00	100.00
45	E	14.51	9.77	73.00	0.12	0.88	1.71	0.00	100.00
46	A	37.41	7.27	54.40	0.05	0.43	0.00	0.43	100.00
46	B	23.65	14.67	60.36	0.06	0.85	0.00	0.41	100.00
46	C	16.08	12.21	69.33	0.11	0.54	1.74	0.00	100.00
46	D	33.55	29.25	31.05	1.07	0.66	4.42	0.00	100.00
46	E	36.67	48.21	7.48	0.21	2.47	4.67	0.28	100.00
<b>AVERAGE</b>		<b>26.87</b>	<b>21.76</b>	<b>47.92</b>	<b>0.21</b>	<b>0.94</b>	<b>2.21</b>	<b>0.09</b>	
<b>STD DEV</b>		<b>13.37</b>	<b>11.24</b>	<b>20.01</b>	<b>0.27</b>	<b>0.52</b>	<b>1.41</b>	<b>0.16</b>	
Wall 8									
Sample	Sub Sample	%ARAG	%HIMGCAILOVMGCA	%PYRITE	%GYPSUM	%CLAY	QTZ-CHEF	SUM	
47	A	25.43	8.22	64.88	0.06	0.31	1.10	0.00	100.00
47	B	27.36	16.29	54.32	0.08	0.34	1.59	0.00	100.00
47	C	17.90	20.42	59.40	0.11	0.39	1.77	0.00	100.00
47	D	35.48	20.08	42.30	0.11	0.82	1.11	0.10	100.00
47	E	48.74	14.31	35.78	0.10	0.58	0.00	0.49	100.00
48	A	23.90	15.46	59.72	0.07	0.56	0.00	0.31	100.00
48	B	32.89	9.21	56.97	0.09	0.46	0.00	0.38	100.00
48	C	29.18	20.46	47.91	0.08	0.54	1.83	0.00	100.00
48	D	63.28	4.62	31.12	0.07	0.52	0.00	0.38	100.00
49	A	29.96	22.78	45.65	0.09	0.44	1.03	0.04	100.00
49	B	73.09	5.62	20.51	0.08	0.32	0.00	0.38	100.00
49	C	26.50	20.73	51.79	0.08	0.45	0.00	0.46	100.00
50	A	14.51	32.62	50.82	0.11	0.56	1.34	0.04	100.00
50	B	22.99	18.92	57.39	0.07	0.25	0.00	0.38	100.00
50	C	23.75	21.12	52.36	0.08	1.02	1.66	0.00	100.00
50	D	22.18	16.69	59.56	0.10	0.96	0.00	0.51	100.00
51	A	68.16	8.92	20.95	0.07	0.66	1.24	0.00	100.00
51	B	71.45	13.37	13.46	0.07	0.58	0.91	0.17	100.00
51	C	69.70	6.55	22.51	0.07	0.69	0.00	0.48	100.00
51	D	71.81	7.91	17.70	0.10	1.18	1.24	0.07	100.00
<b>AVERAGE</b>		<b>39.91</b>	<b>15.22</b>	<b>43.26</b>	<b>0.09</b>	<b>0.58</b>	<b>0.74</b>	<b>0.21</b>	
<b>STD DEV</b>		<b>21.15</b>	<b>7.19</b>	<b>16.55</b>	<b>0.02</b>	<b>0.25</b>	<b>0.73</b>	<b>0.20</b>	
Wall 9									

Sample	Sub Sample	%ARAG	%HIMG	%CALO	%VMGC	%PYRITE	%GYPSUM	%CLAY	QTZ-CHEF	SUM
52	A	31.03	26.52	39.43	0.33	0.72	1.96	0.00	0.00	100.00
52	B	73.22	2.97	22.76	0.37	0.22	0.00	0.47	0.00	100.00
52	C	24.25	18.76	54.20	1.01	0.00	1.67	0.12	0.00	100.00
52	D	26.05	8.86	62.79	0.22	0.58	1.50	0.00	0.00	100.00
53	A	42.76	10.26	45.98	0.09	0.42	0.00	0.49	0.00	100.00
53	B	23.35	12.19	63.34	0.07	0.58	0.00	0.46	0.00	100.00
53	C	11.97	35.94	48.34	0.10	1.08	2.58	0.00	0.00	100.00
53	D	24.05	12.80	61.53	0.08	0.35	1.20	0.00	0.00	100.00
53	E	20.62	35.12	38.21	0.17	2.05	3.83	0.00	0.00	100.00
54	A	23.96	33.61	35.82	0.22	1.26	5.12	0.00	0.00	100.00
54	B	11.92	23.91	62.27	0.13	0.96	0.00	0.81	0.00	100.00
54	C	69.43	11.54	17.01	0.10	0.46	1.47	0.00	0.00	100.00
54	D	23.38	25.65	48.02	0.20	1.03	1.72	0.00	0.00	100.00
55	A	24.96	52.93	14.99	0.22	1.16	5.74	0.00	0.00	100.00
55	B	32.37	20.00	46.32	0.17	0.43	0.00	0.70	0.00	100.00
55	C	15.37	34.63	44.46	0.21	1.34	3.98	0.00	0.00	100.00
55	D	30.04	16.20	50.98	0.12	0.92	1.56	0.17	0.00	100.00
55	E	46.48	0.00	52.81	0.06	0.37	0.00	0.28	0.00	100.00
56	A	23.38	7.81	68.06	0.05	0.44	0.00	0.26	0.00	100.00
56	B	45.10	14.93	35.20	0.15	1.97	2.65	0.00	0.00	100.00
56	C	55.84	14.85	28.25	0.08	0.55	0.00	0.42	0.00	100.00
56	D	79.47	10.59	8.81	0.05	0.59	0.00	0.48	0.00	100.00
57	A	17.43	25.42	53.62	0.17	0.88	2.48	0.00	0.00	100.00
57	B	17.57	15.95	62.90	0.16	1.70	1.59	0.13	0.00	100.00
57	C	82.18	1.98	14.15	0.20	0.91	0.00	0.59	0.00	100.00
57	D	20.79	18.46	57.29	0.15	0.94	2.39	0.00	0.00	100.00
57	E	64.99	9.98	22.50	0.12	0.75	1.67	0.00	0.00	100.00
58	A	35.23	36.91	24.42	0.17	2.38	0.00	0.89	0.00	100.00
58	B	17.33	19.96	61.31	0.06	0.27	1.06	0.00	0.00	100.00
58	C	74.97	2.73	20.02	0.19	0.92	1.17	0.00	0.00	100.00
58	D	24.44	11.34	61.75	0.13	0.76	1.57	0.00	0.00	100.00
59	A	10.69	15.77	72.87	0.04	0.30	0.00	0.33	0.00	100.00
59	B	18.57	22.06	58.10	0.13	0.45	0.00	0.69	0.00	100.00
59	C	38.94	10.33	48.47	0.26	0.46	1.54	0.00	0.00	100.00
59	D	25.28	18.45	51.48	0.25	2.87	1.62	0.05	0.00	100.00
<b>AVERAGE</b>		<b>34.50</b>	<b>18.27</b>	<b>44.53</b>	<b>0.18</b>	<b>0.89</b>	<b>1.43</b>	<b>0.21</b>		
<b>STD DEV</b>		<b>20.95</b>	<b>11.63</b>	<b>17.64</b>	<b>0.16</b>	<b>0.64</b>	<b>1.50</b>	<b>0.28</b>		

Wall 10a

Sample	Sub Sample	%ARAG	%HIMGCAILOVMGCA	%PYRITE	%GYPSUM	%CLAY	QTZ-CHEF	SUM	
60	A	28.58	17.62	51.69	0.08	1.40	0.00	0.64	100.00
60	B	28.65	0.00	68.96	0.11	1.57	0.00	0.71	100.00
60	C	23.25	9.70	64.32	0.08	2.04	0.00	0.61	100.00
60	D	36.93	8.60	50.97	0.10	2.94	0.00	0.45	100.00
61	A	47.39	10.19	40.58	0.06	1.48	0.00	0.29	100.00
61	B	21.58	22.66	55.06	0.06	0.30	0.00	0.34	100.00
61	C	68.81	6.92	23.26	0.06	0.49	0.00	0.46	100.00
61	D	37.56	13.41	45.65	0.13	0.82	2.43	0.00	100.00
61	E	69.36	8.01	21.01	0.08	1.05	0.00	0.49	100.00
62	A	23.18	16.17	57.08	0.12	1.23	2.22	0.00	100.00
62	B	28.04	0.00	68.76	0.23	0.58	2.40	0.00	100.00
62	C	13.99	22.07	60.72	0.18	0.51	2.52	0.00	100.00
62	D	18.70	7.02	73.60	0.08	0.19	0.00	0.39	100.00
62	E	10.57	26.77	58.32	0.36	0.92	3.06	0.00	100.00
63	A	24.19	8.51	64.49	0.08	0.33	2.40	0.00	100.00
63	B	23.56	6.75	68.83	0.08	0.37	0.00	0.42	100.00
63	C	8.03	40.05	40.44	0.30	2.14	9.04	0.00	100.00
63	D	17.23	0.00	81.58	0.12	0.43	0.00	0.64	100.00
63	E	53.07	22.92	21.84	0.13	0.71	1.34	0.00	100.00
64	A	47.40	22.61	26.10	0.19	0.89	2.81	0.00	100.00
64	B	11.80	45.58	36.69	0.18	1.66	4.10	0.00	100.00
64	C	19.21	29.61	49.96	0.11	0.47	0.00	0.64	100.00
64	D	10.43	55.65	25.20	0.36	2.83	4.95	0.59	100.00
64	E	79.57	2.14	17.14	0.11	0.60	0.00	0.44	100.00
65	A	23.39	27.14	44.50	0.24	0.97	3.75	0.00	100.00
65	B	30.09	34.92	32.94	0.12	0.92	0.00	1.00	100.00
65	C	16.64	33.42	48.03	0.15	0.45	1.27	0.03	100.00
65	D	21.28	24.03	48.27	0.15	2.56	3.71	0.00	100.00
65	E	12.14	28.02	58.56	0.28	0.34	0.00	0.66	100.00
66	A	19.07	0.00	79.99	0.08	0.47	0.00	0.40	100.00
66	B	18.29	28.42	50.27	0.09	0.76	2.17	0.00	100.00
66	C	13.62	28.67	53.61	0.14	1.14	2.82	0.00	100.00
66	D	58.48	0.00	40.60	0.08	0.42	0.00	0.42	100.00
66	E	41.85	17.58	39.45	0.15	0.33	0.00	0.64	100.00
67	A	19.26	63.79	7.65	0.29	2.43	6.58	0.00	100.00
67	B	19.01	35.72	41.79	0.21	0.95	2.32	0.00	100.00
67	C	82.67	2.58	13.75	0.05	0.59	0.00	0.36	100.00
67	D	66.72	18.12	13.88	0.09	0.78	0.00	0.42	100.00
67	E	31.11	24.75	40.21	0.11	1.16	2.66	0.00	100.00
68	A	20.48	71.94	0.00	0.19	1.97	5.43	0.00	100.00
68	B	31.02	21.04	45.94	0.16	0.63	1.03	0.19	100.00
68	C	28.28	18.65	50.48	0.15	0.85	1.59	0.00	100.00
68	D	28.62	17.82	52.43	0.10	0.63	0.00	0.40	100.00
68	E	37.98	13.83	45.70	0.06	1.87	0.00	0.56	100.00
69	A	14.94	36.63	45.17	0.21	0.72	2.34	0.00	100.00
69	B	20.28	55.41	19.80	0.13	1.74	2.63	0.03	100.00
69	C	21.64	10.45	66.58	0.11	0.61	0.00	0.60	100.00
69	D	18.91	18.93	61.20	0.11	0.41	0.00	0.43	100.00
69	E	30.56	17.61	46.34	0.13	1.34	4.02	0.00	100.00
70	A	17.42	23.80	57.85	0.06	0.51	0.00	0.35	100.00
70	B	18.28	11.94	67.05	0.16	1.05	1.46	0.06	100.00
70	C	21.01	9.60	68.35	0.10	0.56	0.00	0.37	100.00
70	D	23.09	20.84	52.07	0.15	1.06	2.79	0.00	100.00
70	E	30.98	12.31	54.02	0.42	0.62	1.53	0.12	100.00
<b>AVERAGE</b>		<b>29.41</b>	<b>20.94</b>	<b>46.64</b>	<b>0.15</b>	<b>1.01</b>	<b>1.58</b>	<b>0.26</b>	
<b>STD DEV</b>		<b>17.79</b>	<b>16.11</b>	<b>18.62</b>	<b>0.08</b>	<b>0.68</b>	<b>1.98</b>	<b>0.27</b>	

Wall 10b



Sample	Sub Sample	%ARAG	%HIMG	%CALO	%VMGC	%PYRITE	%GYPSUM	%CLAY	QTZ-CHEF	SUM
71	A	22.60	23.63	50.36	0.15	0.84	2.41	0.00	100.00	
71	B	21.73	27.58	47.79	0.13	0.58	2.20	0.00	100.00	
71	C	16.36	29.57	50.95	0.26	0.77	1.75	0.34	100.00	
71	D	30.83	41.22	21.30	0.19	3.20	3.00	0.26	100.00	
72	A	65.78	20.42	11.03	0.12	0.63	2.02	0.00	100.00	
72	B	79.19	8.87	9.28	0.12	0.85	1.69	0.00	100.00	
72	C	25.01	20.86	49.87	0.12	2.34	1.79	0.00	100.00	
72	D	82.73	3.80	12.38	0.11	0.54	0.00	0.44	100.00	
73	A	30.15	0.00	67.47	0.15	0.98	1.21	0.03	100.00	
73	B	66.67	23.53	5.19	0.10	0.79	3.71	0.00	100.00	
73	C	61.40	12.92	24.92	0.04	0.38	0.00	0.34	100.00	
73	D	79.68	5.44	12.81	0.12	0.68	1.28	0.00	100.00	
73	E	75.62	9.42	13.43	0.14	0.68	0.00	0.72	100.00	
74	A	22.69	12.25	64.02	0.07	0.47	0.00	0.48	100.00	
74	B	76.77	11.38	7.78	0.15	1.11	2.82	0.00	100.00	
74	C	51.88	16.01	30.01	0.09	0.34	1.68	0.00	100.00	
74	D	21.42	46.03	23.33	0.18	3.35	5.69	0.00	100.00	
75	A	18.93	10.87	67.47	0.10	0.41	2.22	0.00	100.00	
75	B	21.50	0.00	77.31	0.12	0.53	0.00	0.54	100.00	
75	C	13.99	39.73	39.05	0.20	1.21	5.82	0.00	100.00	
75	D	12.55	23.79	62.07	0.13	0.27	1.19	0.00	100.00	
75	E	15.20	12.52	70.82	0.13	0.68	0.00	0.65	100.00	
76	A	25.18	8.76	65.11	0.08	0.48	0.00	0.38	100.00	
76	B	17.57	14.08	67.67	0.05	0.30	0.00	0.33	100.00	
76	C	37.61	9.47	51.49	0.10	0.68	0.00	0.65	100.00	
76	D	36.05	15.23	44.00	0.17	2.30	2.24	0.00	100.00	
76	E	20.41	37.62	38.88	0.19	0.95	1.92	0.03	100.00	
77	A	18.19	22.61	58.41	0.07	0.34	0.00	0.38	100.00	
77	B	27.29	18.89	52.96	0.07	0.39	0.00	0.40	100.00	
77	C	17.86	70.68	0.00	0.21	3.41	7.85	0.00	100.00	
77	D	18.83	51.72	22.41	0.19	2.01	4.84	0.00	100.00	
77	E	17.46	19.22	61.79	0.09	0.71	0.00	0.72	100.00	
78	A	31.25	20.91	47.06	0.07	0.32	0.00	0.39	100.00	
78	B	21.50	21.50	53.30	0.13	1.15	2.27	0.15	100.00	
78	C	24.34	0.00	73.21	0.11	0.60	1.69	0.05	100.00	
78	D	19.15	31.73	46.58	0.11	0.62	1.80	0.00	100.00	
78	E	24.68	15.46	57.70	0.16	0.52	1.48	0.00	100.00	
79	A	83.61	10.52	4.52	0.08	0.81	0.00	0.47	100.00	
79	B	13.61	10.01	74.68	0.09	0.28	1.34	0.00	100.00	
79	C	21.10	29.87	45.10	0.12	0.89	2.90	0.00	100.00	
79	D	17.10	22.10	58.40	0.11	0.66	1.49	0.14	100.00	
79	E	63.87	7.98	26.91	0.10	0.62	0.00	0.52	100.00	
80	A	16.02	32.51	47.51	0.11	0.83	3.01	0.00	100.00	
80	B	13.61	13.47	71.69	0.10	0.51	0.00	0.62	100.00	
80	C	15.86	11.93	68.92	0.11	1.05	2.13	0.00	100.00	
80	D	22.01	26.44	49.75	0.14	0.31	1.35	0.00	100.00	
80	E	55.22	25.27	18.35	0.09	0.51	0.00	0.56	100.00	
81	A	15.89	36.35	41.29	0.21	1.44	4.82	0.00	100.00	
81	B	24.72	10.43	63.69	0.09	0.55	0.00	0.52	100.00	
81	C	14.67	24.67	57.28	0.12	0.83	2.42	0.00	100.00	
81	D	68.54	22.46	7.15	0.07	0.53	1.26	0.00	100.00	
81	E	58.57	0.00	40.64	0.09	0.27	0.00	0.43	100.00	
82	A	13.45	26.28	58.48	0.08	0.45	1.22	0.04	100.00	
82	B	19.25	30.14	42.79	0.15	2.90	4.78	0.00	100.00	
82	C	15.02	26.38	56.18	0.12	0.69	1.35	0.26	100.00	
82	D	24.89	7.32	66.03	0.10	0.43	1.23	0.00	100.00	
82	E	20.01	7.63	70.55	0.14	0.40	1.28	0.00	100.00	
<b>AVERAGE</b>		<b>32.76</b>	<b>19.99</b>	<b>44.37</b>	<b>0.12</b>	<b>0.90</b>	<b>1.67</b>	<b>0.19</b>		
<b>STD DEV</b>		<b>22.21</b>	<b>13.60</b>	<b>22.02</b>	<b>0.04</b>	<b>0.78</b>	<b>1.74</b>	<b>0.24</b>		

Wall 11

Sample	Sub Sample	%ARAG	%HIMG	%CAILO	%MGC	%PYRITE	%GYPSUM	%CLAY	QTZ-CHEF	SUM
83	A	19.51	48.99	25.40	0.87	0.39	4.84	0.00	100.00	Extra Scans
83	B	2.69	13.75	40.05	42.55	0.00	0.96	0.00	100.00	
83	C	27.16	39.36	29.72	0.68	0.02	3.05	0.00	100.00	
83	D	25.92	50.35	18.34	1.32	0.20	3.68	0.18	100.00	
83	E	38.60	12.50	46.30	0.12	0.92	1.56	0.00	100.00	
84	A	31.66	7.40	57.82	0.15	1.58	1.39	0.00	100.00	
85	A	78.79	8.88	9.00	0.12	1.13	2.07	0.00	100.00	
86	A	79.72	6.41	10.55	0.13	1.34	1.85	0.00	100.00	
87	A	17.47	28.70	51.34	0.68	0.18	1.64	0.00	100.00	
88	A	14.50	36.57	43.63	1.28	0.00	4.02	0.00	100.00	
89	A	63.63	17.14	16.95	0.14	1.34	0.00	0.79	100.00	
89	B	74.73	9.35	13.82	0.13	0.96	0.96	0.05	100.00	
90	A	76.89	6.64	13.13	0.16	0.83	2.35	0.00	100.00	
90	B	27.48	11.04	60.33	0.07	0.63	0.00	0.45	100.00	
91	A	25.58	27.68	44.44	0.13	0.71	1.45	0.00	100.00	
91	B	21.26	13.81	63.66	0.16	0.44	0.00	0.68	100.00	
92	A	12.89	12.02	74.25	0.06	0.36	0.00	0.42	100.00	

# Appendix F: Solid Mineral Sample XRF Standards in Parts Per Million (ppm)

MEASURED STANDARDS				PROGRAM OPERATIONAL PROCEDURE:				ASSUMPTIONS: MAJOR MINERALS, LINEAR RESPONSE, COLITE SR PROXY, MATRIX EFFECT CONSTANT
FE	S	MG	CA	AL	SI	SI		
394219.3	534376.00							
534376.00	239664.19							
239664.19		249555.56						
		82820.48						
		263886.34						
		6311.56		<LOD>	1807.03	7638.3		
		7843		492763.03				
				85113.64	202738.59			
					421143.19			